NASA Conference Publication 2124

An Assessment of Ground-Based Techniques for Detecting Other Planetary Systems Volume II: Position Papers

March 1980

National Aeronautics and
Space Administration

1. Report No.	2. Government Accession No.	3. Recipient's Catalog No.
NASA CP-2124, Volume II		

4. Title and Subtitle	5. Report Date
AN ASSESSMENT OF GROUND-BASED TECHNIQUES FOR DETECTING OTHER PLANETARY SYSTEMS. VOLUME II: POSITION PAPERS	6. Performing Organization Code

7. Author(s)	8. Performing Organization Report No.
Edited by David C. Black and William E. Brunk*	A-8114
	10. Work Unit No. 196-41-68-01
9. Performing Organization Name and Address	11. Contract or Grant No.
Ames Research Center, NASA, Moffett Field, Calif. and *NASA Headquarters, Washington, D.C.	13. Type of Report and Period Covered Conference Publication
12. Sponsoring Agency Name and Address	14. Sponsoring Agency Code
National Aeronautics and Space Administration Washington, D.C. 20546	

15. Supplementary Notes

16. Abstract

One of the oldest unanswered questions in astronomy is "how did the solar system form?" Recent studies of the solar system using telescopes and spacecraft have provided exciting new discoveries as well as valuable information on the present state and evolution of planets in the solar system. However, the processes involved in planetary evolution tend to obscure vital clues as to how the planets formed, and even if we could unravel the natural record to reveal how Earth and her sister planets formed, it remains unclear whether we would understand how the solar system itself formed. One way to obtain valuable and probably essential data for an understanding of the origin of the solar system is to discover and study planetary systems revolving around stars other than the Sun: there is currently no unequivocal observational evidence for other planetary systems.

In an attempt to examine whether it is feasible to use ground-based astronomical techniques to search for other planetary systems, two scientific workshops were held during the interval October 1978 to January 1979. The workshop participants, experts in various branches of astronomy and instrumentation, addressed the questions of whether the accuracy of existing techniques (e.g., astrometry and spectroscopy) could be improved to the level required for such a demanding observational effort, what the factors are that limit the achievable accuracy, and whether the achievable accuracies were sufficiently good to permit strong scientific interferences in the presence of negative results from a search. Volume I of this report is an overview of the workshop findings; volume II contains technical position papers authored by workshop members on major aspects of the workshop deliberations.

17. Key Words (Suggested by Author(s))	18. Distribution Statement
Origin of solar system Detection of planetary systems Astronomical techniques	Unlimited STAR Category - 89

19. Security Classif. (of this report)	20. Security Classif. (of this page)	21. No. of Pages
Unclassified	Unclassified	253

*For sale by the National Technical Information Service, Springfield, Virginia 22161

☆ U.S. GOVERNMENT PRINTING OFFICE: 1980 - 695-104/227

NASA Conference Publication 2124

An Assessment of Ground-Based Techniques for Detecting Other Planetary Systems
Volume II: Position Papers

Edited by
David C. Black, Ames Research Center, Moffett Field, California
William E. Brunk, NASA Headquarters, Washington, D.C.

National Aeronautics and
Space Administration

Ames Research Center
Moffett Field, California 94035

10

PREFACE

The material contained in Volume I of this document is an overview of the Workshop deliberations and findings. The general scientific and technical basis that underlies the High-Priority Program outlined in that Volume is presented in Chapter 3.

We felt that many readers of these proceedings would have no desire to plumb the more detailed considerations that were developed by the Workshop members and their collaborators in support of the general discussion given in Chapter 3. However, recognizing that some readers may wish to examine these details, and that it would be useful to have these wide-ranging considerations localized in a single document, we provide in this volume ten position papers concerning key elements to the Workshop study. These papers are referred to in Volume I as P1, P2, etc. We extend our thanks to the authors for their efforts.

David C. Black
Ames Research Center

William E. Brunk
NASA Headquarters

TABLE OF CONTENTS

	Page
Preface	iii
Paper 1 - Using Small Aperture Interferometry to Detect Planets in Nearby Binary Star Systems - Douglas G. Currie, Harold A. McAlister, Timothy J. Schneeberger, and Simon P. Worden	1
Paper 2 - Limit Posed for Astrometry by Earth's Atmosphere - C. KenKnight	55
Paper 3 - A Proposed Ground-Based Narrow Field Astrometric System - Pierre Connes	61
Paper 4 - On the Astrometric Detection of Neighboring Planetary Systems, II - George Gatewood, Lee Breakiron, Ronald Goebel, Steven Kipp, Jane Russell, and John Stein	77
Paper 5 - Detection of Extra Solar Planets Using Optical Amplitude Interferometry - Douglas G. Currie	119
Paper 6 - Optical Interferometers in Astrometry - Michael Shao	127
Paper 7 - Precision Stellar Catalogs and the Role of Anomalous Refraction - Douglas G. Currie	143
Paper 8 - The University of Arizona Radial Velocity Spectrometer - K. Serkowski, J. E. Frecker, W. D. Heacox, and E. H. Roland	175
Paper 9 - A Proposed System for Spectroscopic Detection of Dark Companions - Pierre Connes	197
Paper 10 - Sites for Future Dedicated Telescopes - M. F. Walker	239

PAPER 1

USING SMALL APERTURE INTERFEROMETRY TO DETECT PLANETS IN NEARBY BINARY STAR SYSTEMS

Douglas G. Currie
Dept. of Physics and Astronomy
The University of Maryland, College Park, MD 20742

Harold A. McAlister
Dept. of Physics
Georgia State University, University Plaza, Atlanta, GA 30303

Timothy J. Schneeberger and Simon P. Worden
Air Force Geophysics Laboratory
Sacramento Peak Observatory, Sunspot, NM 88349

ABSTRACT

If suitably accurate binary star orbits can be observed, the effects of planets in the binary star system may be detectable in the reflex motion of the component binary stars. We show that interferometric measurements of binary star systems will provide this information. We discuss the effects of the atmosphere on degrading images and how interferometry will remove these effects to provide very accurate binary star positions relative to the other components in the binary system. Two systems, amplitude interferometry and speckle interferometry, can accomplish this using existing telescopes and techniques. With these methods, mearly accuracies of 2×10^{-5} arc second are possible for binaries of 1 arc second separation and 10^{-4} arc second for a 5 arc second binary. These accuracies are more than enough to detect planets in orbits like Jupiter's out to over 20 pc. There are 188 observable systems within 20 pc, in most of which it is possible to have stable planetary orbits similar to solar system orbits. With advanced data recording systems it is possible to observe binary systems where the components are as faint as +16 stellar magnitudes. A dedicated 2-meter interferometric telescope to monitor binary stars could be built for about 1.4 million dollars.

I. INTRODUCTION

Low mass and non-luminous companions of nearby stars may be detected in several ways. Among the most promising methods are indirect methods; that is detecting the effects of an invisible object on its visible companion. Spectroscopic methods may be used to observe radial velocity fluctuations in the visible star caused by the orbital reflex motion relative to the invisible companion. Astrometric detection involves observing the positional perturbation caused by the orbit of the unseen object. Astrometry therefore requires establishing the position of the center of light in a stellar image and referencing this center to a fixed frame.

Astrometry is limited by the ability to establish the center of a star image and uncertainties in the reference frame. Star images, perturbed by seeing, are roughly gaussian. The accuracy for finding the center of the gaussian is obviously dependent on the stability of the gaussian profile. Long exposures are therefore used to: 1) collect enough photons to accurately define the center of each star image and 2) to average out seeing for image motion. The reference frame of these measurements may in principle be established by the centers of three or more other star images. Since the proper motions of these stars may influence the coordinate frame, the reference stars are chosen to be distant background stars. The Earth's atmosphere can also distort the reference frame as a function of atmospheric conditions and colors of the reference stars. These uncertainties may be reduced by using a relatively large number of reference stars in conjunction with sophisticated mathematical error

analysis schemes. In spite of such difficulties conventional astrometry may now reach positional accuracies of ± ".05 for a single exposure, this may be improved to better than ± ".001 (Gatewood, 1976) for the results of one year's observation.

Astrometric accuracy could be improved by getting smaller star images. The problem of finding a star image center is clearly easier the smaller the image is. If images were improved to the diffraction limit the increase is substantial. The task of finding the center of a 2 meter telescope diffraction limited spot of ".05 may be done with much higher precision than finding the center of a 1 arc-second seeing disk with the same number of photons. We can also increase accuracy by removing the atmospheric effects on the reference frame. Both things are possible using some form of interferometry.

Stellar interferometry, first demonstrated by Michelson (1920), makes it possible to approach the full theoretical (diffraction limited) resolving power of large optical systems. Large baseline (hundreds of meters) instruments like the intensity interferometer (Hanbury-Brown 1968) have been demonstrated. Smaller scale instruments have recently been perfected to adapt existing telescopes into diffraction limited systems using techniques known as Amplitude Interferometry (Currie, 1967; Currier et al., 1974) and Speckle Interferometry (Gezari et al., 1972). These techniques were extensively reviewed by Dainty (1974), Worden (1977) and Labeyrie (1978). Long baseline interferometers have been proposed which would convert the image scale to the full diffraction limit and remove atmospheric effects on the reference frame. Such systems are ideal for detecting small scale astrometric perturbations due to planetary

mass objects. However these instruments are costly and have yet to be completely demonstrated in the field. On the other hand, Amplitude and Speckle Interferometry have already demonstrated the ability to make conventional telescopes diffraction limited.

Both Amplitude and Speckle Interferometry are limited by the so-called isoplanatic problem. This is shown schematically in Figure 1. To remove atmospheric effects using these interferometry methods it is necessary that light from all objects to be studied pass through the same column of turbulent atmosphere. Thus a program star and its reference star must lie within an angle known as the isoplanatic angle so that the light from both passes through essentially the same atmosphere. The precise value of the isoplanatic angle depends upon conditions in the atmosphere, the definition, and the observing instrument, but is probably less than 10 arc-seconds (Hubbard et al., 1979).

Binary stars are suitable candidates for planetary searches. McAlister (1978) has used speckle interferometry in a systematic program to determine binary star separations to accuracies of a few thousands of an arc-second, using relatively simple detectors and calibration methods. If a planet orbits one component of a binary star system, then the orbit of that component about the other star will "wobble". For the nearby stars this may be a modulation of up to ".01 for Jovian type planets. Harrington (1977) has shown that most binary star systems have stable planetary orbits. Interferometric searches for planetary perturbations of binary star orbits are therefore important. Indeed, interferometric searches of small separation binaries is almost the only way to search these systems.

Binary star interferometry is therefore important to assure a complete search for low mass stellar companions through all nearby stars and all types of stellar systems.

In this document we discuss interferometric methods to search binary star systems for planets. This suggestion was presented in some detail by McAlister (1977). We briefly discuss the physics behind atmospheric degradation of images and the interferometric instruments and techniques to remove this degradation. We address the accuracies and limitations of these techniques. A discussion of the sample of nearby binary star systems follows. Finally we provide information on the costs and features of possible dedicated telescopes for an interferometric binary star search.

II. ATMOSPHERIC IMAGE DEGRADATION

Small scale temperature inhomogeneities in the Earth's atmosphere produce index of refraction changes. These refractive index changes cause phase delays along an incoming plane wave, which may be light from a stellar point source. This is represented schematically in Figure 2. Without the phase errors optical systems produce the image in Figure 2a which is said to be "diffraction limited", where a point source image is the classical Airy disc for a circular telescope aperture. The size of this image is inversely proportional to the telescope diameter. With any phase errors, telescope resolution is degraded to that appropriate for an optical system only as large as the scale over which some phase coherence (i.e the phase is the same) exists. Since the atmosphere breaks an incoming plane wave into about 10 cm fragments, all telescopes produce images with resolution no better than a 10 cm telescope, namely one arc-second. This process is shown in Figure 2b.

In 1970, Labeyrie (1970) proposed a method to recover some information down to large telescope diffraction limits. He pointed out that short exposure ($\Delta \tau \lesssim .01$ sec) photographs "freeze" the turbulence in the atmosphere. Although the phase coherence size in this "frozen" system is still only 10 cm there will be some 10 cm patches scattered over the entire aperture which are at the same phase. These portions act in concert as a form of "multiple aperture interferometer which provides some information down to the

diffraction limit of the entire telescope aperture. As shown in Figure 2c, the image of a point source seen through a multiple aperture interferometer is a series of nearly diffraction limited images modulated by a one arc-second seeing disk. This process is known as speckle interferometry since the short exposure photos, shown in Figure 3, look like laser speckle photos.

As alternate approach to steller interferometry, suggested by Currie (1967) Currie et al. (1974), is similar to Michelson's interferometry. Known as Amplitude Interferometry, this technique uses a device like that shown in Figure 4. The individual collection apertures are smaller than the 10 cm coherence length along a stellar wavefront in order to reduce the correction due to atmospheric degradation to a negligible level. As the atmosphere modulates the relative phase shifts between these two apertures, the coherence properties (and thus angular size) of the object as it appears outside the atmosphere can be learned. To obtain complete two-dimensional size and shape information the observer varies the separation and position angle for the two apertures. Currie has proposed and built a multiple aperture amplitude interferometer system, so that the full telescope aperture may be covered simultaneously and all Fourier components sampled simultaneously. The efficiency of such a system should be comparable to a speckle interferometry system.

III. INTERFEROMETRIC INSTRUMENTS AND DATA REDUCTION

In this section we describe interferometric data recording systems and data reduction techniques.

A diagram of the Kitt Peak photographic speckle interferometer is shown in Figure 5. There are about six similar systems in use at the present time. The Kitt Peak camera was designed by Lynds (Lynds et al., 1975; Breckinridge et al., 1978). As shown in the figure light from the telescope passes through a shutter and focuses at the telescope image plane. The shutter is necessary to insure exposures shorter than the atmospheric change time, typically 20 milli-seconds. The telescope image is relayed and magnified by a microscope objective. The magnification is set to provide a pixel resolution oversampling the telescope diffraction spot size by at least a factor of 4. For the Kitt Peak 4-meter telescope this provides a final image scale of .2 arc-sec/mm Atmospheric dispersion blurs speckle image pattern in the sense that the "red" portion of an image focuses at a slightly different portion than the "blue" portion. Since this may be significant for even 200 Å bandpass photos a set of rotating atmospheric compensating prisms are included to counteract the dispersion. Since there are about 20 orders of optical interference across a narrow band ($\Delta \lambda \gtrsim 200$ Å), an interference filter is used to preserve coherence across the entire speckle photo. If this were not included the "speckles" near the edge of the photos would be elongated. A three stage image tube

intensifies the image enough to allow photographic data recording. A transfer lens relays the intensified image to a data recording system, in this case a 35 mm film camera.

The speckle photos in Figure 3 were taken with the Kitt Peak System. The different character of these photos is readily apparent. This is understandable from the analogy to a multiple aperture interferometer. Each speckle should be a diffraction limited image of the object. Indeed, the binary star (α Aur) speckles are double, the point source speckles roughly diffraction spots, and the resolved star (α Ori) speckles somewhat larger. This aspect led Lynds et al (1975) to a direct speckle image reconstruction scheme whereby individual speckles were identified and co-added to produce a nearly diffraction limited image for the special case of stars like α Ori.

A number of methods exist to reduce speckle interferometry data. Labeyrie's original method is widely used; in particular for binary star measurements. Individual speckle photos are Fourier transformed either optically or digitally and the Fourier modulus computed. If the speckle image is represented in one dimension as $i(x)$, and its transform as $I(s)$ this process is mathematically represented by:

$$I(s) = \int_{-\infty}^{\infty} i(x) e^{-2\pi i x s} dx \qquad (1)$$

The modulus or power spectrum, $|I(s)|^2$, of this transform contains the diffraction limited information in an easily extractable form. Examples of the mean power spectra for several binary star systems are shown in Figure 6. In the case of the binaries, power spectra show banding which represents the binary separation, the wider the bands are apart, the closer the binary separation. The orientation of these bands represents the position angle of the binary system. Superimposed in this signal is a background attributable to the residual effects of seeing. For stars brighter than about +7 visual magnitudes about fifty individual speckle snapshots are transformed to produce a mean power spectrum. A least square fit to the spacing and orientation angle of the bands in this power spectrum yield the binary separation and position angle; All accomplished from less than 1 second actual exposure time at the telescope!

The residual effects of the seeing must be removed to yield the maximum accuracy. Even though the bands (fringes) are readily visible in raw speckle power spectra, their spacing is effected by the residual seeing effects. Labeyrie's method uses observation of point source stars to determine these seeing effects and remove them. If $P_i(x)$ are point source speckle photos with a mean power spectrum $\langle|P(s)|^2\rangle$, and $\langle|I(s)|^2\rangle$ the mean power spectrum of the object speckle photos $i_i(x)$ then the diffraction limited power spectrum of the object is given by:

$$|O(s)|^2 = \frac{\langle |I(s)|^2 \rangle}{\langle |P(s)|^2 \rangle} \qquad (2)$$

Point source data is usually derived from speckle observations of point source stars situated near on the sky to the program objects. Since these point source objects are not in general observed within the same isoplanatic angle and not at the same time their power spectrum can only represent the residual seeing effects in a statistical sence. Worden et al. (1977) have developed a method to calibrate for residual seeing effects using the same set of speckle photos as used to study the program objects.

We illustrate the Worden et al. (1977) method in Figure 7. The method proceeds as follows: the mean autocorrelation function of a series of speckle, $i_i(x)$ photos is computed.

$$\langle AC(\Delta x) \rangle = \left\langle \int_{-\infty}^{\infty} i_i(x) \cdot i_i(x-\Delta x)dx \right\rangle$$

$$= \langle i_i(x) * i_i(x) \rangle \qquad (3)$$

(The autocorrelation is the Fourier transform of the power spectrum - see Bracewell 1965 for details). As we see in Figure 7, the mean autocorrelations are dominated by the seeing background. This background may be accurately removed by computing and subtracting the mean cross-correlation between consecutive speckle photos of the same set of data used to compute the auto-

correlation. The cross calculation between the $i^{\underline{th}}$ and $i^{\underline{th}} + 1$ speckle photo is given by

$$<XC(\Delta x)> = <\int_{-\infty}^{\infty} i_i(x) \cdot i_{i+1}(x-\Delta x)dx>$$

$$= <i_i(x) * i_{i+1}(x)> \qquad (4)$$

Welter and Worden (1978) showed that the resulting subtraction in the object autocorrelation as it would appear with virtually all seeing effects removed.

Current photographic speckle cameras are generally limited to objects brighter than +7. Thus the photographic recording systems are being replaced with high quantum efficiency digital recording systems. These systems record individual photon events. The University of Arizona speckle camera uses a CID (Charge Injected Device) television system to record photon arrivals. This system simply replaces the photographic emulsion and it can record data for objects faint enough so that only a few photons arrive in a 20 milli sec exposure. In Figure 8 we show data from this system for Saturn's moon Rhea which is a $10^{\underline{th}}$ magnitude object. For faint objects like this, only the few hundred photon locations are recorded, rather than the entire frame. This allows such systems to run at the maximum speckle data rate of one speckle frame every 20 ms. This form of data is ideal for the correlation data reduction method described above, since the correlation functions are simply

the sum of vector differences between photon locations. Consequently a direct computer interface may compute the results in real time at the telescope. The limiting requirement for this method is that at least two photons arrive in a 20 ms exposure. This translates to about a +16 stellar magnitude limit. Although angular diameters are more difficult to derive than binary separations, we have used this system to derive angular diameters for $13^{\underline{th}}$ magnitude objects accurate to ± 5% with less than 5 minutes total observing time.

The Amplitude Interferometer obtains the high angular resolution information in a somewhat different fashion than the Speckle Interferometer. In this case, the light is sampled at the entrance aperture of the telescope where the effect of the atmosphere has been to introduce only an error in the phase delay. The light from two separate apertures on opposite sides of the telescope is then interferometrically combined. Such a combination is illustrated in Figure 9.

By appropriate choice of the size of the interferometric aperture, one component of the atmospheric correction becomes negligible. The magnitude of the combined coherence function appears as the magnitude of the fringes in the combination of the interferometer two beams. In the case of high coherence one gets a varying signal as indicated in Figure 10. The fluctuations in this signal are caused by the motion of the wind. These fluctuations, or, more precisely, the autocorrelations and cross correlations of individual photo-electrons are used to elevate the fringe visibility.

The currently operating Amplitude Interferometer is illustrated in Figure 4. The light from the telescope is sampled for two apertures which have a diameter of 4 centimeters. This has been used in a regular program to measure star diameters down to about 6th magnitude (Currie et al., 1974, Currie et al., 1976, Braunstein, 1977). Although some work has been done on binary stars (Braunstein, 1978) most of the work has been on stellar diameters. In order to illustrate the current performance of the Amplitude Interferometer on the telescope we consider Figure 11, which shows a typical set of data for a resolved star and for an unresolved star which is used as a reference or check. This shows the visability of the fringes. From this measure, the diameter of the star is derived.

Taking successive measurements on different nights, we have seen a high degree of stability, even though there have been significant changes in the atmosphere. This illustrates the general validity of the atmospheric model and amplitude interferometric parameters in assuring independence of atmospheric fluctuations.

In order to permit the observation of fainter objects, we wish to simultaneously use all the light entering the telescope aperture, i.e. the data from many thousands of pairs of apertures. (i.e. a Multiple Aperture Amplitude Interferometer or MAAI). This may be done by replacing each of the two photomultipliers with a "television camera" in which each resolution element acts as a separate channel interferometer.

The light then operates as shown in Figure 12. When an array detector is used, an inverting prism is required which causes every separation to be sampled. The overall design of this instrument is indicated in Figure 13.

The description of such an instrument, as might be used on a space telescope, has been given by Currie (1974) while a more detailed discussion of certain aspects appears in (Braunstein, 1978). A photograph of the MAAI is shown in Figure 14.

IV. ACCURACY

McAlister has had a substantial speckle program to derive binary star parameters underway at Kitt Peak for the last several years. This program's results provide preliminary information with which to estimate the precision possible with speckle interferometry (McAlister 1978).

Internal errors in speckle interferometry are divided into the basic uncertainty in the data itself, and the error due to uncertain calibration of the image scale. Based on 46 pairs of binary star observations for 5 stars, each pair separated in time by one day to one month, McAlister has computed errors. One observation is defined as the result from a single fifty frame set of speckle photos. For this data (with binary separations of 0.2" to 3".25) McAlister concludes that the error due to basic uncertainty in the data is ± .3% in separation and ± 0°.2 in position angle for each fifty frame data set. If the calibration errors are included the angular separation measurement reduces to ± .6%.

Calibrations of image scale and position angle are made by placing a double slit with known slit separations over the telescope aperture. Since the telescope is then effectively a two-slit interferometer, the fringe spacing and position angle in power spectra of data taken through this slit provides accurate calibrations of angular separations and position angles. Calibrations are generally made only several times per night. If a set of built-in

calibration double slits were used to calibrate each star after every observation, calibration errors could be reduced to much less than the inherent error in the data. For binaries with separations less than 1", accuracies of ± ".002 are already obtainable and accuracies of ± ".1 are obainable for stars of 5" separation, in single observations.

A similar level of accuracy has been obtained using the Amplitude Interferometer for the measurement of stellar diameters (Currie, 1976). Although such measurements are not identical to the binary measurements this does provide an evaluation of the general ability of the amplitude interferometer to obtain high accuracy. The reproductivity in angular diameters from one year to the next on the stable stars is of the order of one to two milliarcseconds. Most of this error may be related to aspects of the current Amplitude Interferometer with a single pair of apertures and would not occur in the Multi-Aperture Amplitude Interferometer (MAAI). The MAAI has been used to resolve of stellar diameters as small as 10 milliarcseconds, and is expected to provide 5 milliarcseconds on the 5-meter telescope or 33 milliarcseconds on a 60-inch telescope.

McAlister ahs computed possible external errors in his results by comparing binary orbits he has derived from speckle interferometry with high quality published orbits. He concludes that speckle orbits match the published orbits to within the accuracies of these orbits, this result precludes large systematic errors in speckle binary star measurements.

The above analysis for speckle interferometry is based on photographic data recording systems. An advanced photoelectric data acquisition system

has several advantages. Since the new systems run at essentially television rates (60 frames per second), a single fifty frame sample takes less than 1 second to obtain! McAlister observes about 150 stars per night with several minutes spent on each star. We might expect that fifty observations of five minutes duration would be possible in an observing session with a dedicated telescope. If we assume errors may be reduced as the square root of observing time then the over 10^4 fifty frame data sets obtained per year would refine the accuracies a factor of 10^2 over the McAlister's values. This corresponds to 2×10^{-5} arc second per year on binaries with separations smaller than 1 arc second and 10^{-4} arc second per year on a binary with five arc seconds separation. The higher quantum efficiency and linearity of the digital system should indicate that these numbers apply to stars brighter than about +9, as compared to McAlister's limit of +7. The accuracies on binaries near the faint limit at +14 would probably be a factor of ten worse for the same observing time.

The isoplanatic angle is another limitation. Conventional wisdom, not based on many real observations, places the isoplanatic angle at about 3 arc-seconds, meaning interferometry of binary stars with separations much larger than this would be impossible. However, recent measurements by McAlister (1979) and Hubbard et al (1979) of binary stars with larger separations places this angle closer to 6 arc-seconds and perhaps as large as 10 arc-seconds. It may therefore be possible to use as a reference star an unrelated background star rather than the other binary component. This may extend interferometric position determinations to wider binaries and some single stars.

Photographic speckle systems have been limited to binary stars where the two components are within five magnitudes of each other. Photoelectric systems may extend this limit to 7 or 8 magnitudes. However, the requirement of two photons in each exposure may practically limit one to systems where both stars are brighter than + 16 magnitudes.

The maximum size of the detector array is another possible limitation. Since we desire to oversample the telescope diffraction spot size by at least a factor of four and to cover 10" on the sky we would need a 700 x 700 element array for a 2 meter aperture telescope (diffraction limit ".06). However, 800 x 800 element arrays are to become available soon, so detector size should not limit speckle interferometry.

V. SUITABLE TARGET BINARY SYSTEMS

In this section we examine a set of possible program binary systems and discuss detection probability. As a data source we have used Gliese's Catalogue of Nearby Stars (1969) which includes all stars with known parallaxes equal to, or greater than ".045, plus borderline cases.

There is some conjecture that binary star formation inhibits planet formation. However, definitive models for planetary formation are not available. At present, there is absolutely no reason to, a priori, dismiss binary systems as possible planetary systems. It is of particular interest to study the frequency of these occurances and mass distribution of companions in order to further illuminate the physical processes of star formation and of planetary system formation. Moreover, the extensive satellite systems of Jupiter and Saturn point strongly to the hiarchial formation of such systems. There are, however, dynamical constraints on possible planetary orbits in binary systems. Harrington (1977) has examined dynamical stability of a planetary third body in a binary system in terms of the restricted three body problem. He concludes that stable planetary orbits are possible in two classes of binary systems: Those in which the planetary orbit is large compared to the binary orbit, and those in which it is small. In both cases the planetary orbit must be a factor of three to four larger (or smaller) than the maximum (or minimum) binary separation. Since there are no detectable effects of a planet in the case where the

binary separation is small compared to the planetary orbit we restrict our discussion to the opposite case. If we use Jupiter's orbit at approximately 5 AU radius as a benchmark we can examine which binaries may have a stable Jovian orbit. Table I lists the separations for a stable Jovian orbit as a function of parallax.

Table I

Angular Size of Binary Orbits for a Stable Jovian Orbit

Parallax (")	Size of Jovian Orbit (")	Minimum Binary Orbit Size for Stable Jovian Orbit (")
.2	1.000	4.000
.1	.500	2.00
.075	.375	1.500
.050	.250	1.00

Table II shows the effects of a Jovian planet ($m = 10^{-3}M_{\odot}$) in a Jovian orbit (5 AU) and a large terestrial planet ($m = 10^{-5}M_{\odot} = 3M_{\oplus}$) at 1 AU. These effects are shown as a function of the reflex motion on a solar type primary ($1\ M_{\odot}$) and a late type M dwarf ($.15\ M_{\odot}$).

Table II

Effects of Planets on the Primary Star
Orbital Amplitude as a Function of Distance

Parallax (")	$10^{-3}M_\odot$ Effect on $1M_\odot$ (")	$10^{-3}M_\odot$ Effect on $.15M_\odot$ (")	$10^{-5}M_\odot$ Effect on $1M_\odot$ (")	$10^{-5}M_\odot$ Effect on $.15M_\odot$ (")
.2	2×10^{-3}	1.3×10^{-2}	2×10^{-6}	2.6×10^{-5}
.1	1×10^{-3}	6.7×10^{-3}	1×10^{-6}	1.3×10^{-5}
.075	7.7×10^{-4}	5×10^{-3}	7.5×10^{-7}	9.7×10^{-6}
.050	5×10^{-4}	3.3×10^{-3}	5×10^{-7}	6.5×10^{-6}

Based on the calculations of 10^{-4} arc-second accuracy in section IV. We see that Jovian planets are detectable for all binary separations out to 20 pc. In the special case of nearby M dwarf stars it may even be possible to detect large terrestrial planets.

In the Gliese (1969) catalog there are 248 star systems with binary separations between ".2 and 15".0. 188 of these systems lie north of -30°. In Table III we list the binary separation distributions for these 188 star systems.

Table III

Binary Separations of Stars North of -30° in the Gliese Catalog

Separation (")	Number of Systems
.2 - .5	23
.5 - 2.0	64
2.0 - 6.0	64
6.0 - 10.0	19
10.0 - 15.0	18

Table IV lists the parallax distributions of these 188 systems.

Table IV

Parallaxes of Northern Binary Stars with Separations Less Than 15" in the Gliese Catalog

Parallax (")	Number of Systems
> .200	9
.200 - .100	24
.100 - .075	21
.075 - .050	76
< .050	58

Using Harringtons stability criterion we find that roughly half of the 188 systems would have a stable Jovian orbit, while almost all of them would have a stable terrestrial orbit. The sample therefore permits large numbers of planetary orbits at distances similar to those in the solar system.

For the 182 systems which list magnitudes for both components we report the following magnitude differencies between the two components.

Table V

Magnitude Differences for 182 Northern Binary Systems in the Gliese Catalog

Δm	Number of Systems
0 - 1	74
1 - 3	48
3 - 5	28
> 5	32

Almost half of the systems have nearly equal magnitudes, while 82% have less than the 5 magnitude difference needed for the present photographic system. These magnitude differences should be about 1 magnitude less if observations were made around 8000Å, since the secondary is almost invariably redder than the primary. The magnitudes for 375 of the component stars are in Table VI.

Table VI

Magnitudes of Component Stars in Northern Gliese Catalog Binary Stars

Apparent V Magnetude	Number of Stars
0 - 5	35
5 - 7	79
7 - 9	68
9 - 11	90
11 - 13	74
> 13	29

50% are brighter than +9, the magnitude limit for the maximum accuracy. 251 of these stars have spectral classification which are catalogued in Table VII.

Table VII

Spectral Types of Northern Gliese Catalog Binary Stars

Spectral Type	Number of Stars
A	10
F	40
G	43
K	59
M	99

As may be expected, the spectral types, which are generally for the primary component only, are weighted heavily toward M types. The secondary components should be weighted even more heavily towards later spectral types. Almost all of these stars are main sequence (Luminosity Class V), 16 are subgiants (Luminosity Class IV), 2 are giants (Luminosity Class III).

We conclude that there are a sizeable sample of binary candidates for planetary detection. Even if we apply the restrictive requirements that one component be brighter than +9, that the system have a stable Jovian orbit, that the magnitude difference be less than $\Delta m = 5$, and that the separation be less than 6", we have nearly fourty candidate systems.

We hasten to note that the results of a systematic long term search of these systems would be extremely valuable in their astrophysical importance. Orbits derived from the binary orbits which would be a by-product of a planetary search allow a very accurate calibration of lower main sequence masses, and solar neighborhood distance scale. The program should also turn up large numbers of low mass, but not planetary, stellar components. This data will be essential for calibrating binary star mass functions.

VI. A DEDICATED INTERFEROMETRIC TELESCOPE

To study over 100 binary systems to the accuracy desired requires substantial time on a large telescope. In this section we discuss the possibilities for a low cost telescope which could serve as a dedicated interferometric instrument. Such an instrument may also be usable for other aspects of a planetary detection program, such as certain radial velocity programs.

With the advent of computer controlled telescopes and lightweight optics, telescope costs may be substantially reduced. The University of Wyoming recently constructed a computer controlled 92" telescope for 1.8 million dollars. We include here a design proposed by the Kitt Peak National Observatory for a low cost 2-meter telescope which serves as an example of an instrument which could serve as a dedicated interferometric telescope. We provide the preliminary discussion of this instrument in Appendix A. Telescope drawings are shown in Figure 15. The Nasmyth foci are particularly appealing since they eliminate flexure changes in the instrument as the telescope moves to different positions on the sky. This feature is desirable for both interferometric and spectroscopic instruments. The design shown has several features which are not needed for a planetary detection telescope, such as a chopping secondary or prime focus capability. These items could be eliminated to save costs. Kitt Peak's cost estimates are shown in Table VIII. The estimates for constructing a digital speckle camera are based on an Air Force Geophysics Laboratory program to construct such a device at the University of Arizona.

It is recommended that the detached telescope be used with both a multi-aperture amplitude interferometer and a speckle interferometer. While there are unique advantages and classes of separation which may be done with each separately, there is a large domain which they may confirm each other and detect systematic errors which occur with both. The speckle interferometer is less expensive and less complicated to operate. On the other hand, the multi-aperture amplitude interferometer has a resolution which is almost a factor of 2 larger, it is less affected by atmospheric phenomena, and has a much simpler data reduction. However, it may not work in as bad seeing as the speckle interferometer. The data obtained by the two techniques are significantly independent. The question of ultimate sensitivity and limiting magnitude will primarily involve the modes of implementation but the ultimate sensitivity and accuracy of the two systems should be comparable.

The construction costs for a dedicated interferometric facility should be less than 1.4 million dollars. Operating costs may be estimated based on costs for the Sacramento Peak Observatories operation of a dedicated photometric 48" telescope in Cloudcroft, New Mexico. The annual operating costs for this instrument are $170,000 per year. Operating costs for a dedicated interferometric telescope, including observers, data reduction personnel, and maintainance personnel should be similar.

SUMMARY

We have shown that a small aperture stellar interferometry can obtain accuracies of better than 10^{-4} arc-seconds per year on binary star orbits. There are 188 accessable binary star systems within 20 pc of the sun. About half of these systems should have stable orbits for a Jovian type planet which would be easily detectable with the accuracies possible. We have discussed a possible interferometric system for observing these binaries. A dedicated interferometry telescope could be contructed for 1.4 million dollars and operated for $170,000 per year.

We conclude that stellar interferometry is a viable option for detecting extra-solar planets, and it is an option which could be easily implemented. In fact, interferometry is ideal for precisely those systems which conventional astrometry has some difficulty, the close binary systems.

Table VIII

Estimated Costs for A Low Cost
Dedicated Interferometry Facility

I. Telescope and Building (Kitt Peak Estimates)

	Budget Estimates ($1000 units)
Optics	200
Optics Support	50
Secondary Assembly	60
Tube, Altitude Bearings	100
Azimuth Yoke and Bearings	200
Drives	250
Telescope Controls (including computer which may also be used for data reduction)	100
Dome and Building	170
Miscellaneous (instrumentation, auxilliary equipment, etc.)	120
TOTAL	1250

II. Interferometer (speckle) and Data Reduction Equipment (Based on AFGL Estimates for University of Arizona Speckle System)

	Budget Estimates ($1000 units)
Optical and Mechanical Components	30
Image Intensification	20

Table VIII (continued)

Estimated Costs for A Low Cost
Dedicated Interferometry Facility

II. Interferometer (speckle) and Data Reduction Equipment (continued)

	Budget Estimates ($1000 units)
Photoelectric Array and Interface	50
Two-Dimensional Array Processor and Computer Interface	50
TOTAL	150

III. Interferometer (Amplitude) and Data Reduction Equipment (Based Upon Projections from the Current Instrument)

	Budget Estimates ($1000 Units)
Optical and Mechanical Components	80
Photodetectors	65
Two Dimensional Memory, Electronics and Computer Interface	60
TOTAL	210

Table VIII (continued)

Estimated Costs for A Low Cost

Dedicated Interferometry Facility

IV. Annual Operation and Maintainance (Based on Sacramento Peak Estimates for a Dedicated 48" Photometric Telescope)

	Budget Estimates ($1000 units)
Personnel	
2 Observers	30
1 Maintainance (electronics)	15
1 Maintainance (facility)	15
1 Astronomer	20
Overhead on Personnel	40
Utilities	25
Computer Maintainance	15
Miscellaneous Equipment	10
TOTAL	170

REFERENCES

Bracewell, R. (1965) The Fourier Transform and its Application, New York, McGraw-Hill.

Braunstein, R., (June 1978) The Analysis of Amplitude Interferometry Data and the Testing of the Intensified Charge Coupled Device, University of Maryland Ph.D. Thesis.

Breckinridge, J. B. (1975) J. Opt. Soc. Am., 65, 7.

Breckinridge, R. B.,McAlister, H. A., and Robinson, W. G. (1978) Applied Optics, in press.

Currie, D. G. (1968) On a Detection Scheme for an Amplitude Interferometer, NAS-NRC, Woods Hole Summer Study on Synthetic Aperture Optics.

Currie, D. G. (1968) On the Atmospheric Properties Affecting an Amplitude Interferometer, NAS-NRC, Woods Hole Summer Study on Synthetic Aperture Optics.

Currie, D. G., (April 1977) Amplitude Interferometry on the Large Space Telescope submitted as a part of a proposal to the National Aeronautics and Space Administration, 23 February 1973, University of Maryland Technical Report #77-056, April 1977.

Currier, D. G., Knapp, S. L., and Liewer, K. M. (1974) Four Stellar Diameter Measurements by a New Technique: Amplitude Interferometry, Ap. J., 187, 131.

Currier, D. G., Knapp, S. L., Liewer, K. M., and Braunstein, R. H. (June 1976) Stellar Disk Diameter Measurements by Amplitude Interferometry 1972-1976, University of Maryland Technical Report #76-125, June 1976

Dainty, J. C. (1976) Laser Speckle and Related Phenomena, Berlin, Springer-Verlag.

Gatewood, G. (1976) Icarus, 27, 1.

Gezari, D. Y., Labeyrie, A., and Stachnik, R. V. (1972), Ap. J., 173, L1.

Gliese, W. (1969) Catalogue of Nearby Stars, Veroff des Astron. Rechen-Institut, Heidelberg, 22.

Hanbury-Brown, R. (1968), Ann. Rev. Astr. Ap., 6, 13.

Harrington, R. S. (1977), A. J., 82, 753.

Hubbard, J., Strittmatter, P. A., Woolf, N. J., Hege, K., Reed, M., and Worden, S. P. (1979) in preparation.

Labeyrie, A. (1978), Ann. Rev. Astro. Ap., 16, 77.

Lynds, C. R., Worden, S. P., and Harvey, J. W. (1976), Ap. J., 207, 174.

McAlister, H. A. (1978), Proceeding of IAU Cooloquium #48, Modern Astrometry, Vienna, Austria, Sept. 1978.

McAlister, H. A. (1979) in preparation.

Michelson, A. A. (1920), Ap. J., 51, 257.

Welter, G. W., and Worden, S. P. (1978) J. Opt. Soc. Am., in press.

Worden, S. P. (1977) in Vistas in Astronomy (ed. A. Beer) 20, 301.

Worden, S. P., Stein, M. K., Schmidt, G., and Angel, J. R. P. (1977) Icarus, 32, 450.

APPENDIX A

Kitt Peak National Observatory
Functional Requirement and General Specifications
For New Generation 2-M Telescope

Preliminary December 1, 1978

I. TELESCOPE

A. Introduction

The general concept is that of a low-cost, highly efficient telescope, which does not require frequent instrument changes. The telescope will be carefully optimized for O/IR photometry and spectrometry. It will provide a powerful research tool for attacking many key astronomical problems.

A number of design features are directly related to aspects of the Next Generation Telescope (NGT)program studies, and hence, much valuable information will be gained in support of this program.

B. Mounting

1. The telescope shall utilize an altitude-azimuth mount configuration. (See attached concept sketch).
2. The telescope should be contained in an approximately 32-foot diameter dome.

C. Focus Positions

The telescope shall provide for two 3-mirror Nasmyth foci, two 3-mirror bent Cassegrain foci (90° from the Nasmyth and not a fixed gravity position), a 2-mirror Cassegrain, all parfocal, and a prime focus (future).

D. Instrumentation Potential

1. Nasmyth - major fixed instruments: moderate-resolution optical spectrometer, infrared echelle spectrograph.
2. Cassegrain - lightweight instruments for O/IR photometry and spectrophotometry.
3. Prime - cooled solid-state detector arrays.
4. Provision for acquisition TV's should be provided for all foci.
5. Field rotation compensation by instrument rotation will be included at Cassegrain and prime focus. The optical Nasmyth position will have instrumentation or field rotation as part of the instrument package.

E. Optics

1. The design shall incorporate a primary mirror of at least 2-m diameter and provide the following nominal focal ratios:

Prime	f/1.5 with 10' (9 mm) field of view. Scale 15 μ/1".
Nasmyth, Cassgrain	f/15 with 5' (44 mm) field of view. Scale 145 μ/1".

2. The design of the upper structures of the tube will provide for easy interchangeability of several specialized structures. These will include:
   a) f/15 chopping secondary with or without sky baffles
   b) prime focus structure
   c) other Cassegrain/Nasmyth secondaries, fixed or chopping, f/15 or slower

Only the f/15 chopping secondary shall be provided with the initial telescope facility.

3. The f/15 secondary mirror shall be undersized, using a diameter of (TBD) cm of the primary mirror, thereby providing a 2.5 cm-wide low-emissivity ring around the main part of the primary.
4. For infrared observations, the secondary shall be physically larger in diameter than its associated supporting structure.
5. For optical observations, easily removable sky baffles around the secondary shall be provided. Provision for baffling elsewhere may be required.
6. The telescope design shall provide for easy checking and alignment of the optical axis of the various foci.
7. The telescope design shall provide for easy washing and cleaning of the optical components.
8. Provision for easy removal of the tertiary for use of the 2-mirror Cassegrain shall be provided. Future tertiaries with internal fused silica prisms for visual work are possible and should be allowed for.

F. Environment

The telescope must be fully functional with no degradation of specifications under typical ambient conditions found on Kitt Peak: 10-90° F, 2-99% RH, 0-25 mph wind (shutdown at 40 mph).

II. PERFORMANCE SPECIFICATIONS

A. Optical Quality

At the Cassegrain/Nasmyth foci, 90% of the light from (TBD) cm diameter shall fall within a circle of $0\overset{\frown}{.}6$ in diameter at a wavelength of 0.5 μ for zenith angles less than 60°. Neglecting diffraction and obscuration, 99.5% of the light shall fall within a circle of diameter $1\overset{\frown}{.}0$. For a zenith angle of 80°, image quality shall not degrade to more than twice the above specifications.

B. Sky Coverage

1. No structure shall vignette the telescope above 10° from the horizontal in any direction.
2. Azimuth rotation of $+270^{\circ}$ from the south shall be allowed for.
3. Electrical limit switches and mechanical stops shall be provided as necessary for telescope protection.

C. Absolute Pointing Accuracy

The absolute pointing error goal shall be $0\overset{\frown}{.}5$ rms for zenith angles less than 60°. The 24-hour repeatability shall be better than 1".

D. Tracking

The goal shall be tracking an object to within $0\overset{\frown}{.}1$ rms for periods of time up to 2 hours for zenith angles less than 60°.

E. Motions

1. The slewing speeds shall be at least 2°/second.
2. Tracking speeds shall be at least 0°.5/second.
3. Setups on a new object within 90° should be possible within a time of 2 minutes.

F. Cone of Avoidance at the Zenith

The telscope shall operate as specified to within 5° of the zenith.

G. Chopping Secondary Characteristics

1. Chopping direction: Remotely adjustable 270° from the center position and should include the capability for automatic field rotation compensation.
2. Amplitude: Remotely adjustable continuously from zero to 3'.
3. Frequency: 0 to 40 Hz.
4. Performance: For a chopping amplitude of 20". the 10-90% rise time will be < 3 msec with < 1% overshoot.

H. Nasmyth Platforms

Size (TBD, at least 5 feet long beyond focus, 8 feet is preferable); instrument weight limits (TBD); location of best focus (TBD, at least 18 inches beyond bearing); instrumentation, electrical, vacuum, displays, controls, and other needs (TBD).

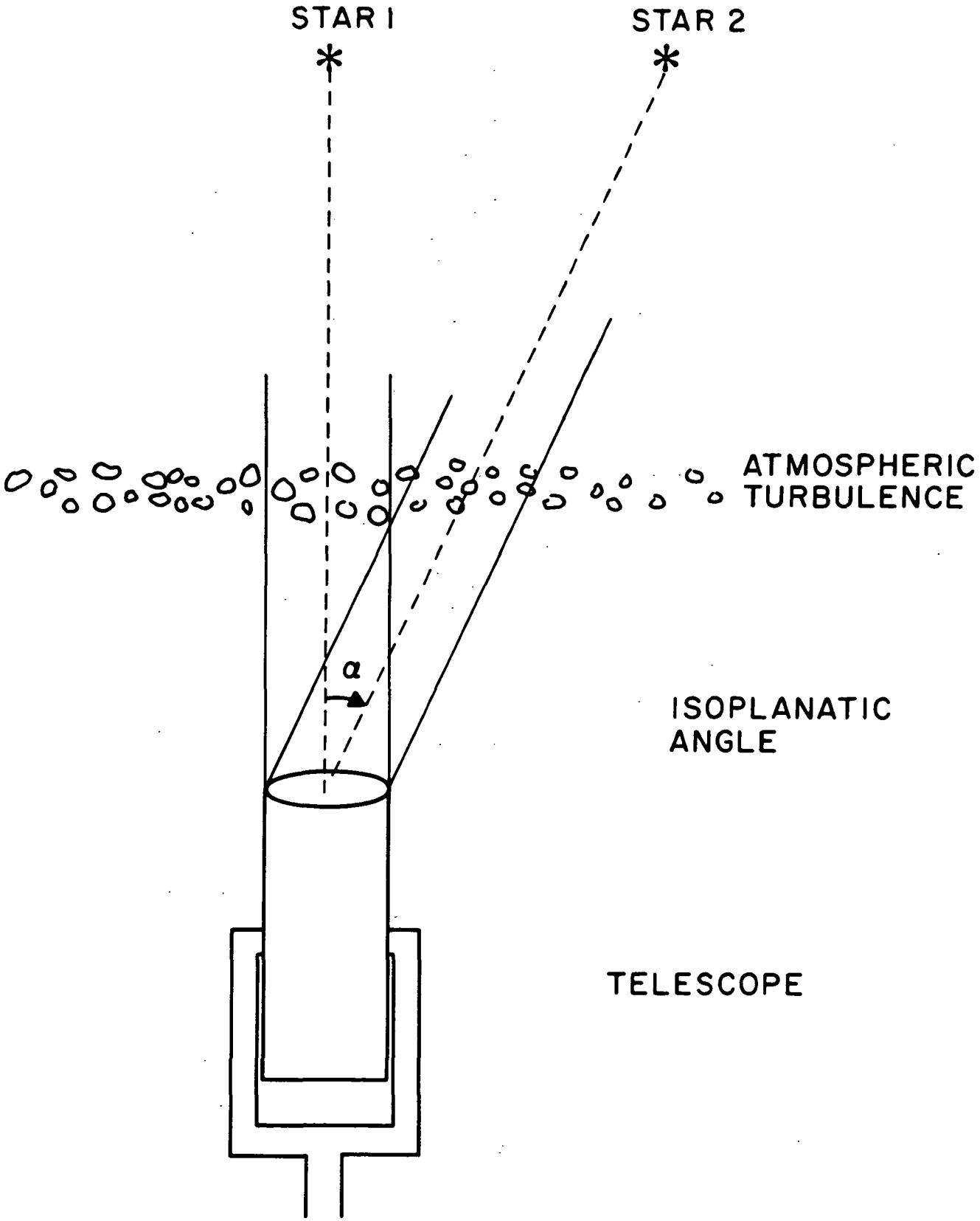

Figure 1.- The isoplanatic angle - the maximum angle separating two objects so that light from the two objects passes through the same column of turbulent atmosphere.

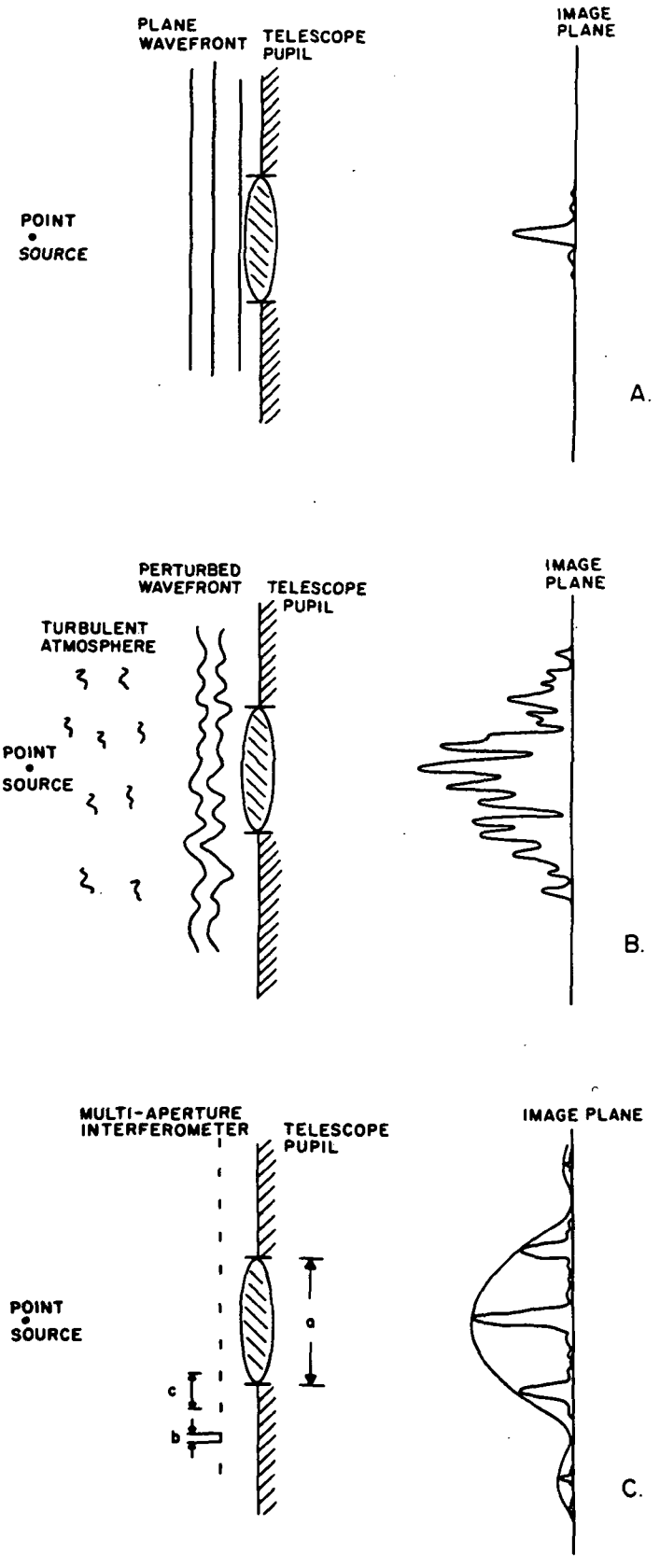

Figure 2.- Schematic diagram of image formation through a turbulent atmosphere. (a) Image formation outside the atmosphere; the image is diffraction limited.

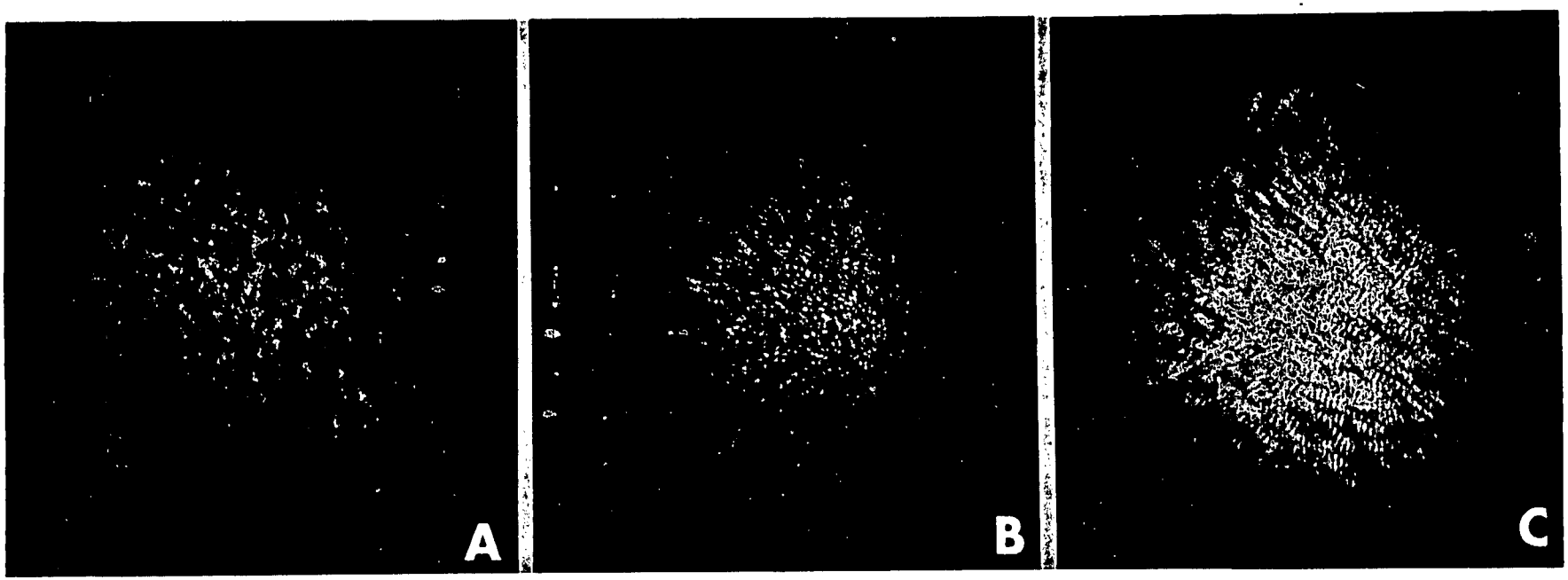

Figure 3.- Speckle photographs for three stars from the Kitt Peak 4-m telescope. Note the different character for the three objects. (a) The resolved supergiant star α Orionis (Betelgeuse), (b) a point source star γ Orionis (Bellatrix), (c) a close double star, separation ".05 α Auriga (Capella).

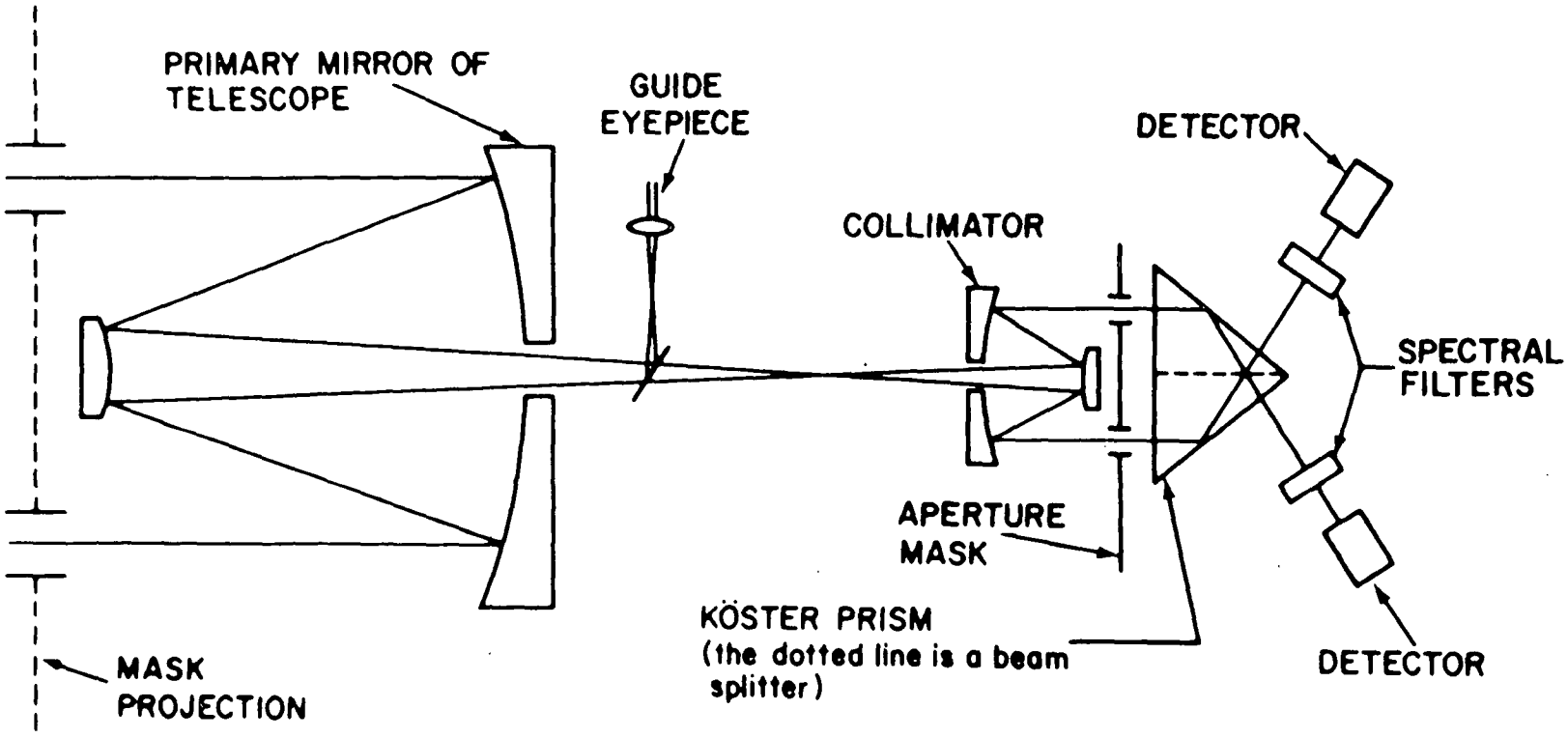

Figure 4.- A diagram of Currie's amplitude interferometer.

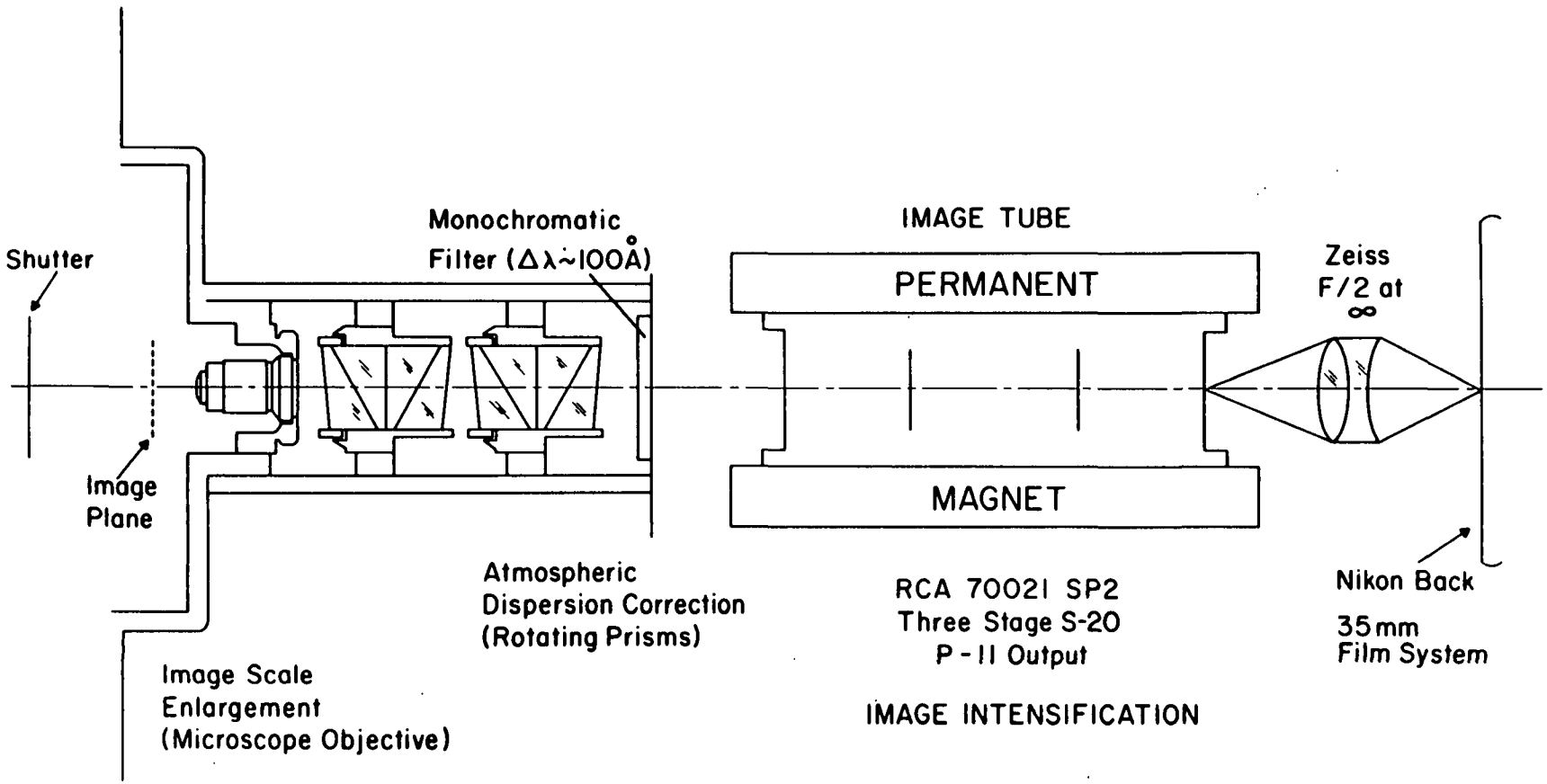

Figure 5.- A diagram of Kitt Peak's photographic speckle interferometry camera.

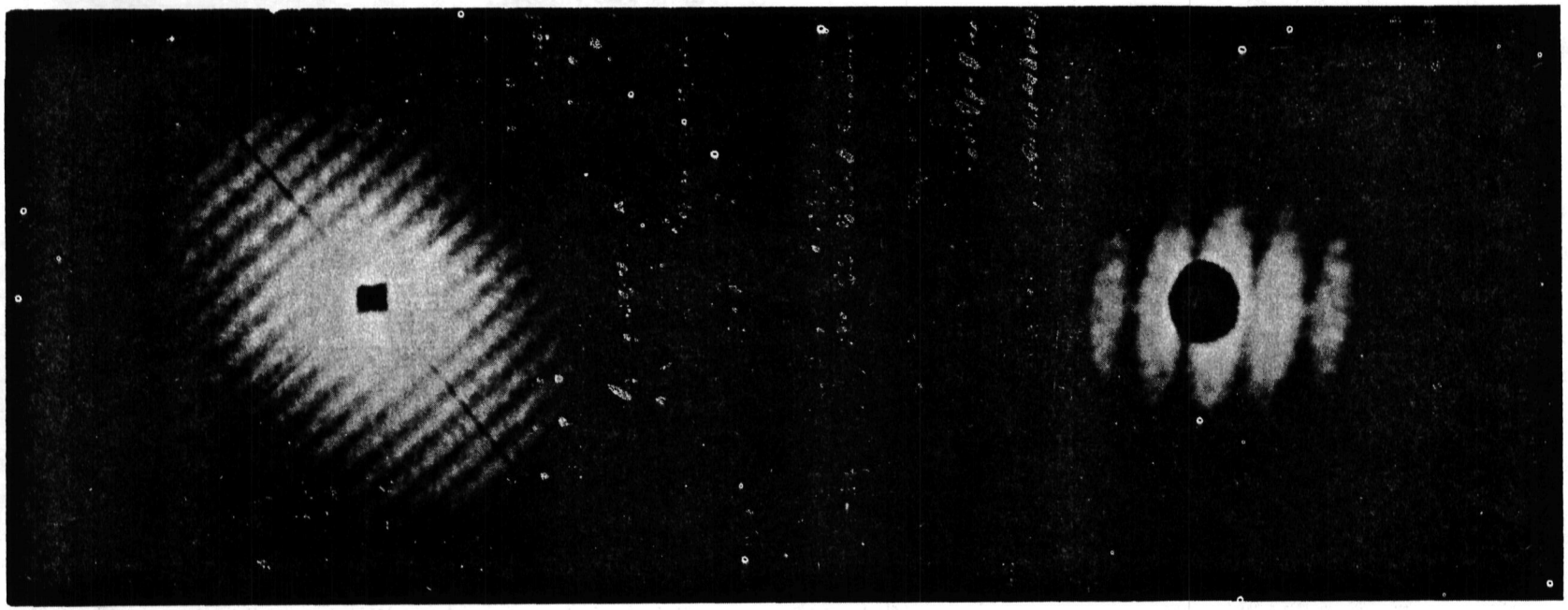

Figure 6.- Mean speckle power spectra for two binary stars. The larger separated fringes are for i Serpertis (separation ".1), the smaller β Cephei (separation ".25).

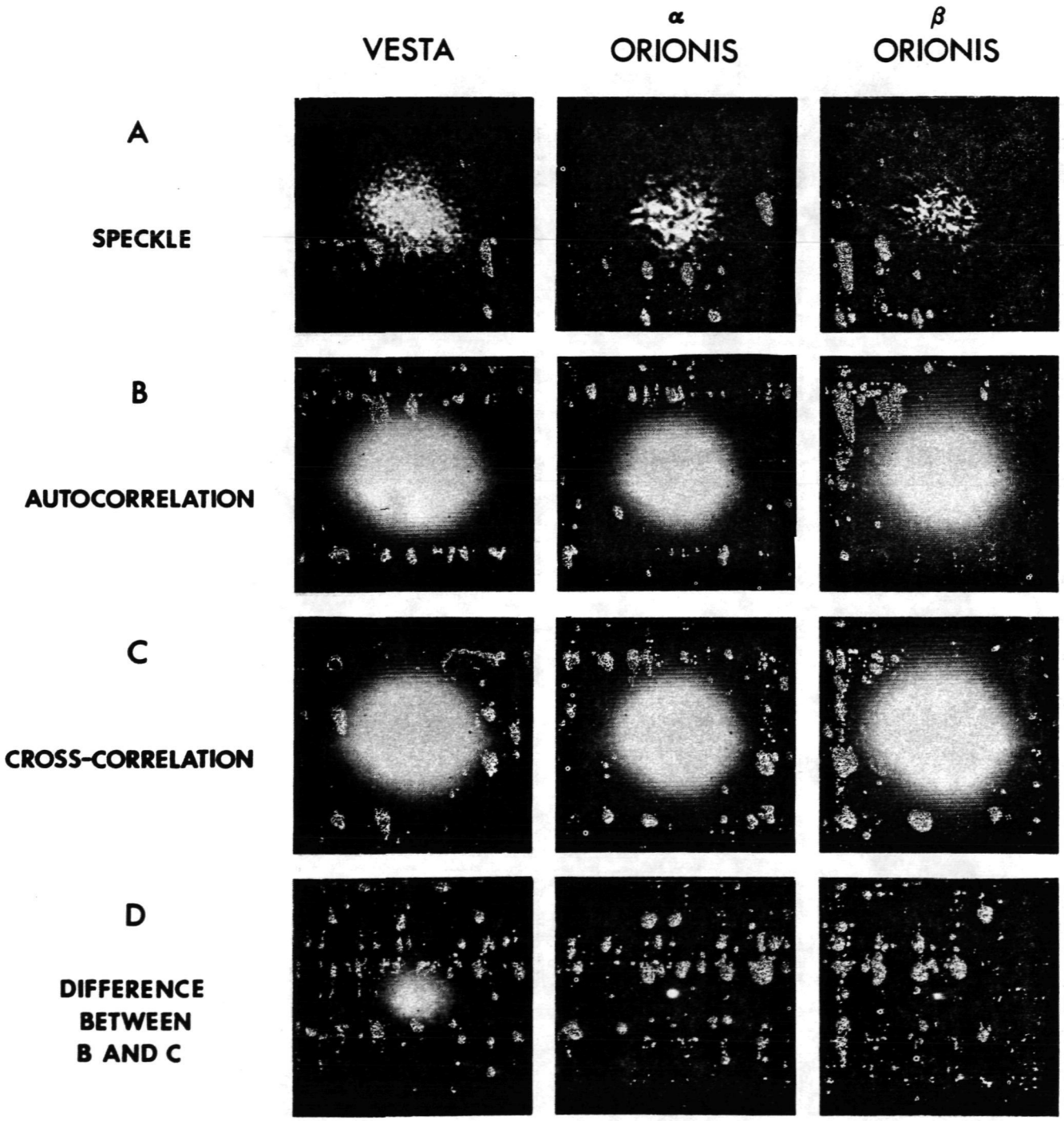

Figure 7.- Schematic representation of Worden et al. (1977) method for reducing the effects of seeing in final speckle interferometry results.

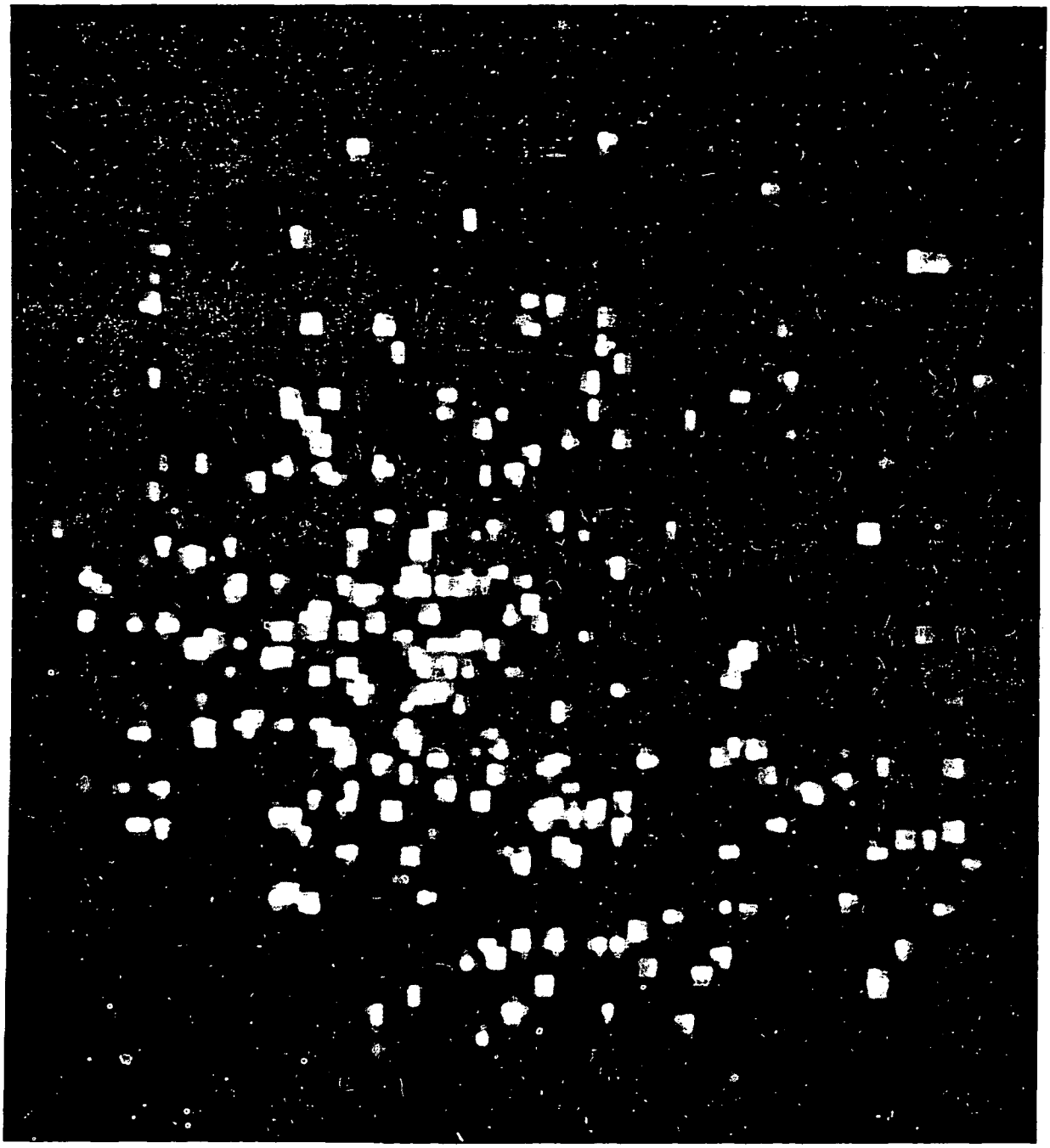

Figure 8.- Speckle data showing individual photons for Saturn's moon Rhea ($M_V \approx 10$) taken with University of Arizona CID speckle camera.

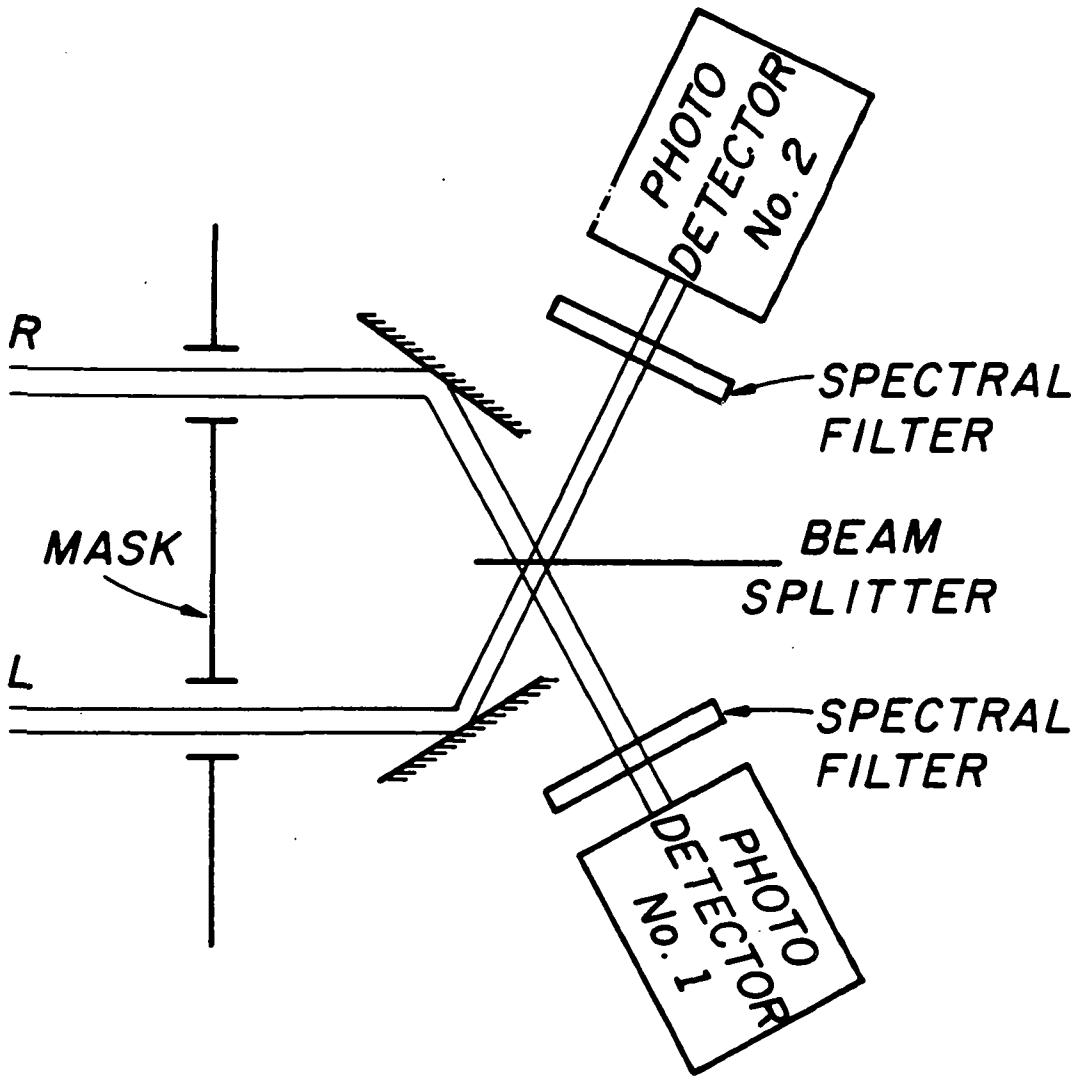

Figure 9.- Combination of the starlight from the separate apertures for an Amplitude Interferometer.

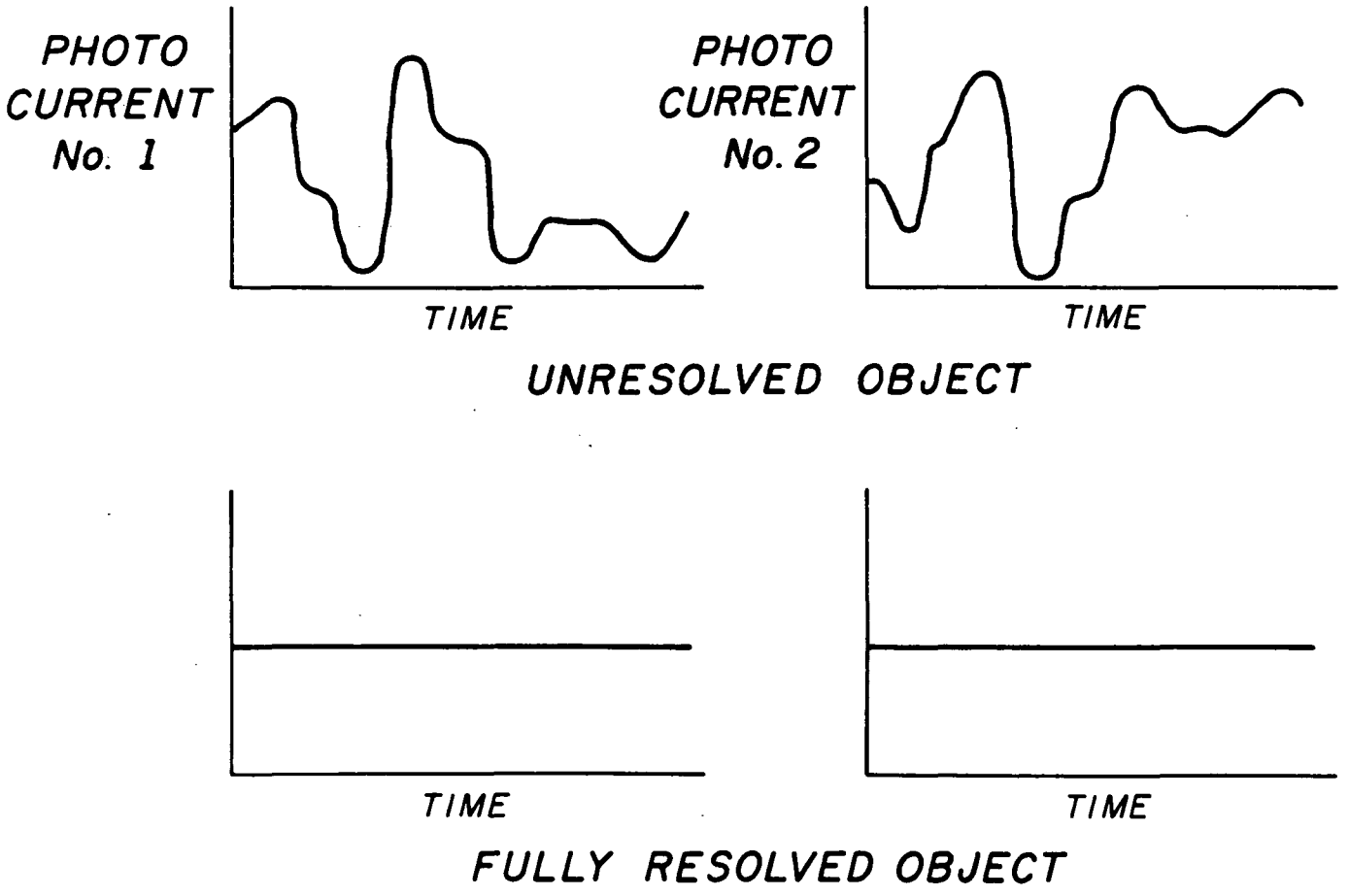

Figure 10.- Variation of photomultiplier outputs for a bright source with high coherency and low coherency in a two-beam Amplitude Interferometer.

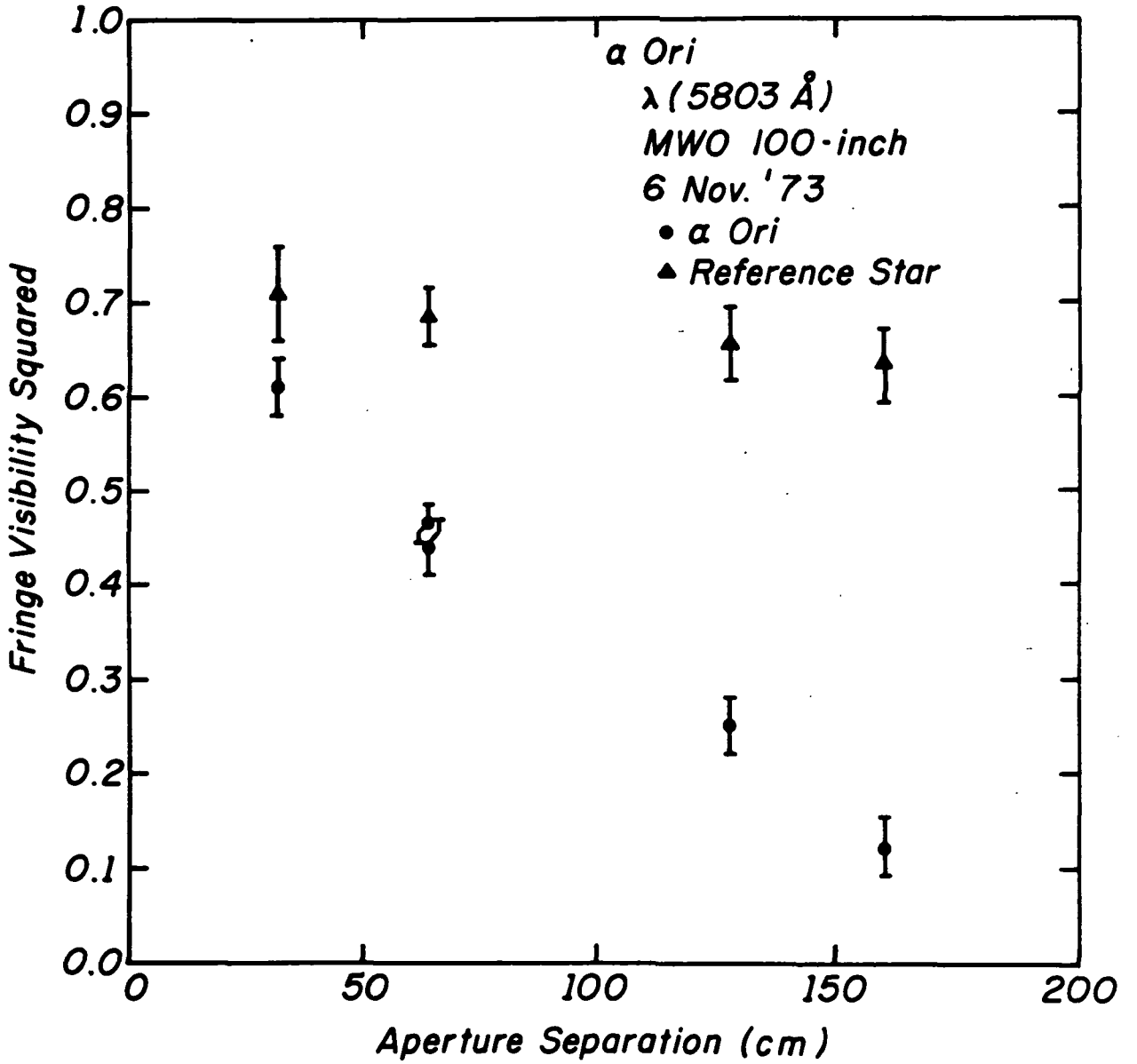

Figure 11.- Amplitude Interferometer outputs for a resolved star (α Orionis) and an unresolved star.

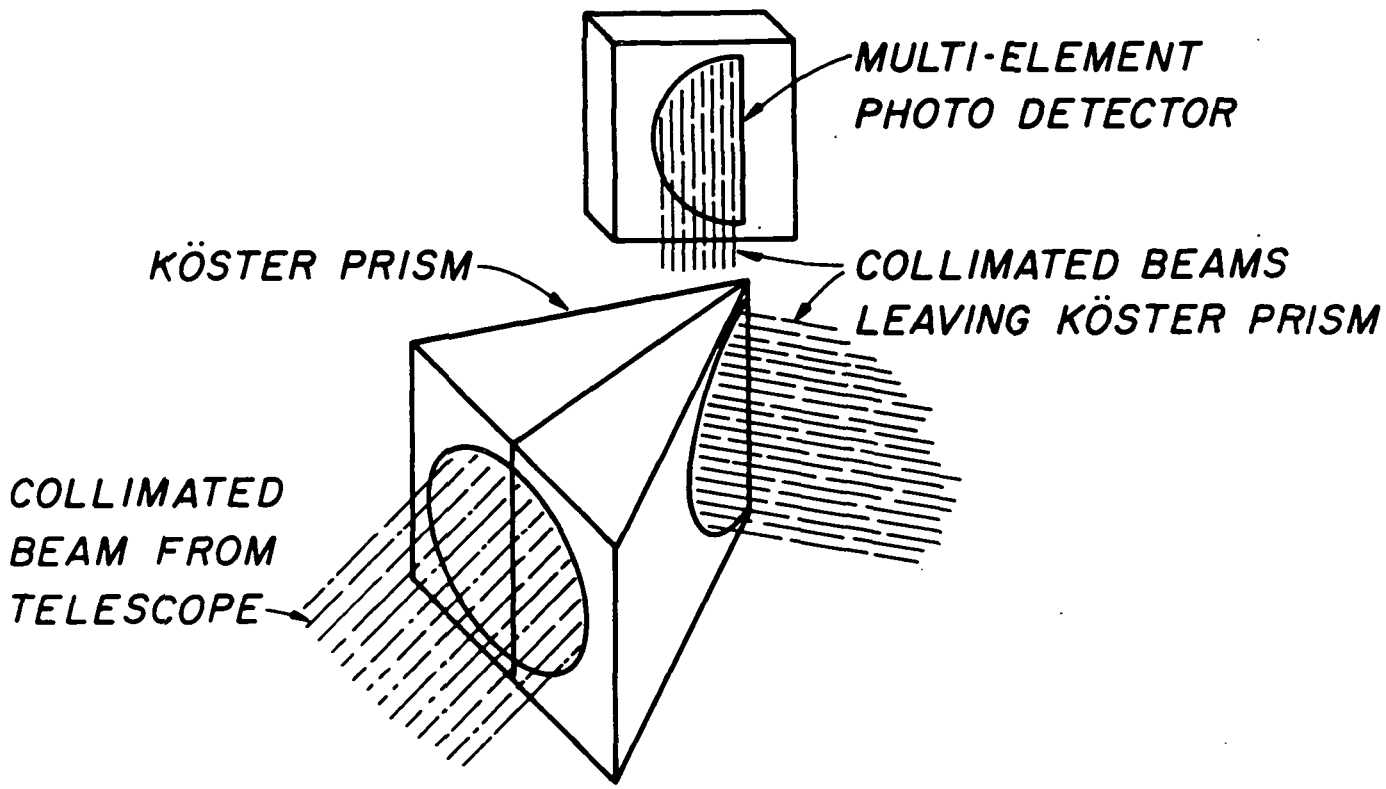

Figure 12.- Multi-element detector scheme for a Multiple Aperture Amplitude Interferometer.

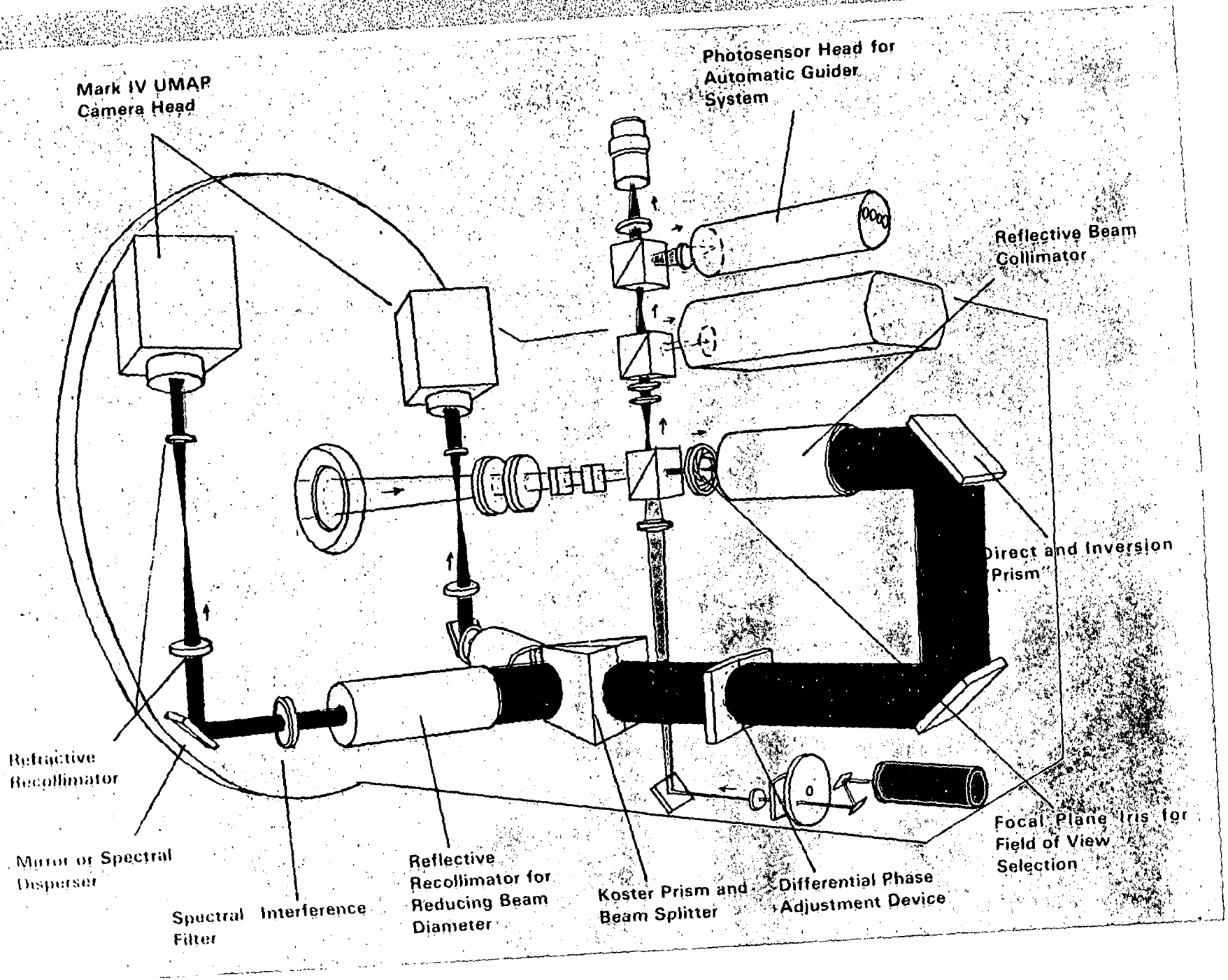

Figure 13.- Multiple aperture interferometer design.

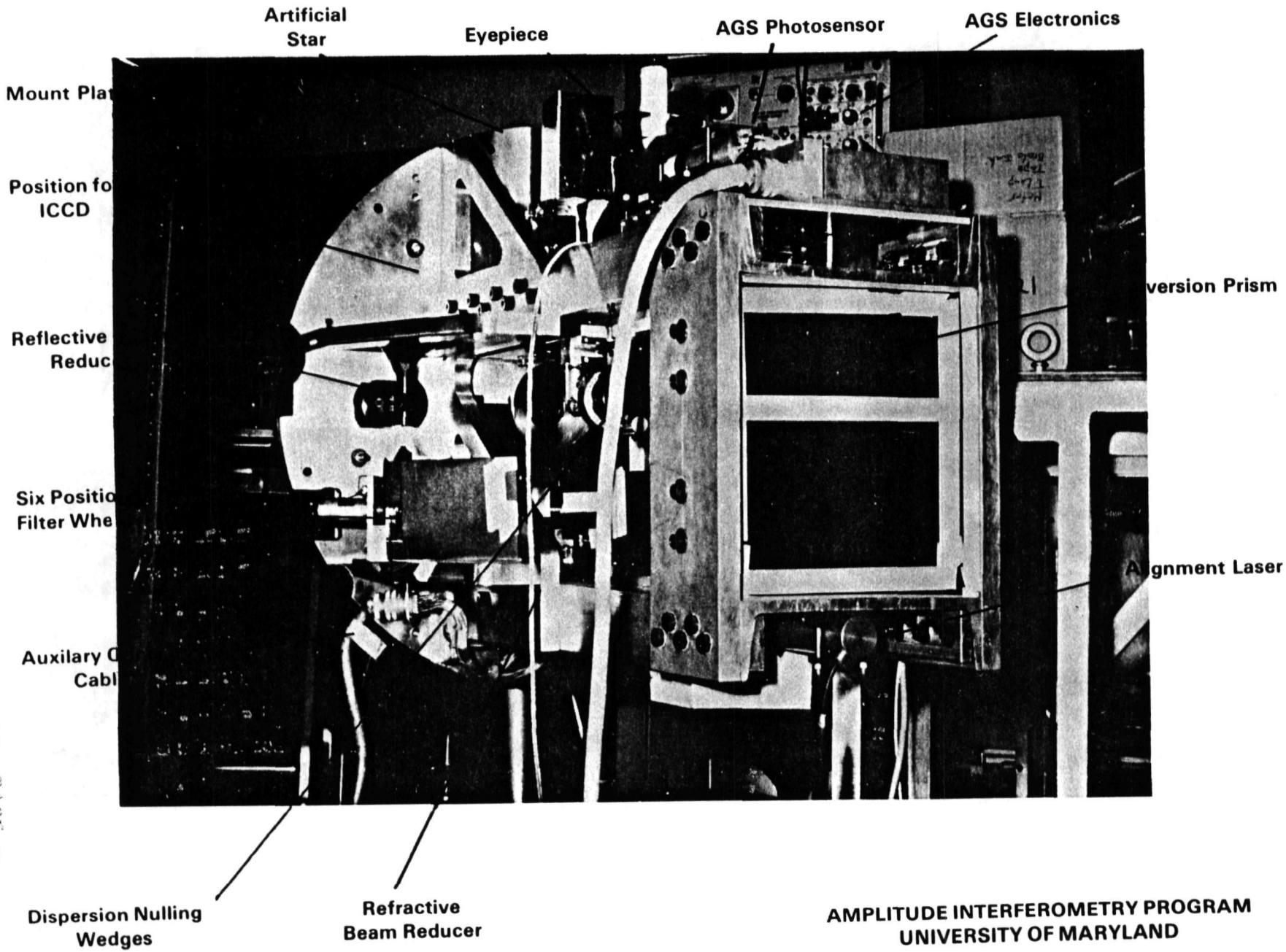

Figure 14.- Photograph of a multiple aperture amplitude interferometer, as may be used in a space telescope.

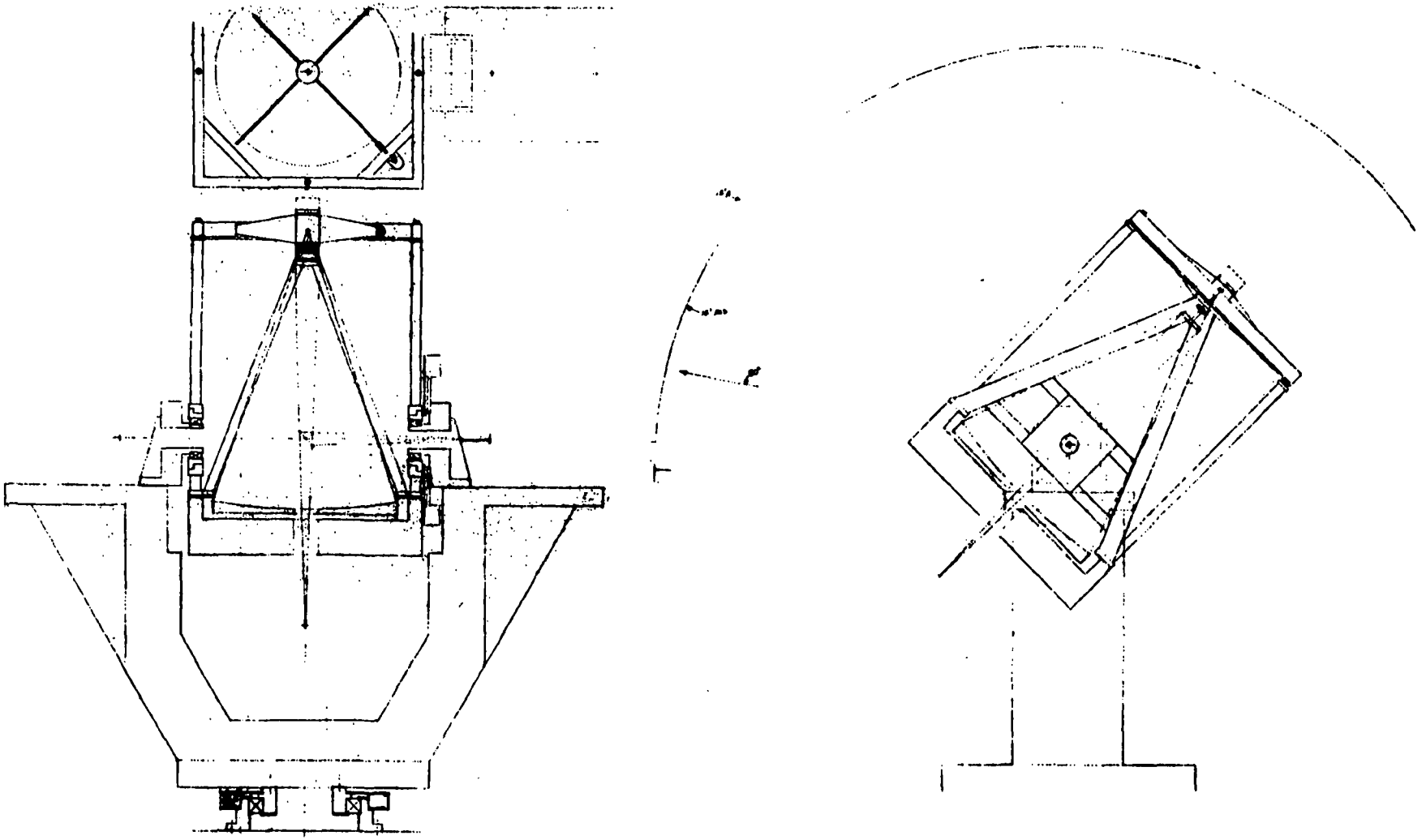

Figure 15.- Preliminary Kitt Peak National Observatory design for a low-cost 2-meter telescope.

PAPER 2

LIMIT POSED FOR ASTROMETRY BY EARTH'S ATMOSPHERE

C. KenKnight

University of Arizona

Current knowledge about the atmosphere as an optical element affecting astrometry is fairly complete in outline. The atmospheric density declines exponentially upward with a scale height of about 8 km. Starlight entering the atmosphere at an angle z with the local vertical is refracted by the air of changing density so that the optical path becomes more vertical. The effect is of the order of 3×10^{-4} radian at 45° to the vertical and increases nearly as $\tan z$ with zenith angle z. As in refraction by a wedge, the air refraction depends on wavelength λ. Thus an accurate theory of refraction and angular position measured at two wavelengths, in blue and red light, allows the correction for most of the refraction effect during data analysis. For a typical field of view (10^{-2} radian at $z = 45°$), the scale of the field is compressed in the vertical direction by 6 μrad. If the dependence on wavelength allows correction for 99.9% of this scale change, a residual accidental error of a few nanoradians remains for the observation of one night.

Another optical effect of the atmosphere arising in the turbulent lower 20 km of it heated by the warm Earth surface has been called "accidental refraction" and "seeing." The density changes caused by heat waves convecting about in the lower atmosphere are random in direction, not just vertical. The largest turbulent elements are strongest in their optical effect. The turbulent elements range from a not well-known largest size, L_0, of the order of 100 m to a small size, L_1, of the order of several millimeters. Energy is injected by the momentum transfer between air layers or between the air and the ground whenever viscous shear causes heated air to turn over. The energy cascades to smaller parcels of air in a random process that eventually distributes the energy uniformly in the smallest eddies where heat conduction becomes effective enough to even out the density differences.

The optical path difference for light that has traversed the whole atmosphere has an average difference that is zero for two points on a wave front separated by a distance B, but the rms path difference, L_2, is nonzero and calculable. The path difference L_2 increases with the separation of two rays proportional to $B^{5/6}$ at small separation but becomes constant at about 10 μm for $B \geqslant L_0$. Because the path difference L_2 increases nearly as B, the wave-front deformation due to turbulence is nearly a pure tilt of the wave front. Thus a telescope of aperture up to about 1 m in diameter exhibits an image that moves about in the focal plane by an angle of 5 μrad under low turbulence conditions. The image is also broadened slightly by wave-front deformations more complicated than tilt so that the full width of the star images is also 5 μrad at those atmospheric conditions. The width is measured where the intensity declines to $1/e = 0.37$ of the central image brightness.

By comparison, diffraction of light by the telescope aperture would have allowed a stellar image to be confined to a focal plane spot of size $\lambda/D = 0.5$ μrad at $D = 1$ m.

For larger telescopes, the wave-front deformations become so large that the star images break up into many maxima. The image size does not decrease as λ/D as diffraction would predict, but only according to L_2/B, which is proportional to $B^{-1/6}$. The effective average separation, B, of ray pairs for a circular telescope of diameter D is about 0.3 D. This extremely slow change of angle noise for baseline B also holds for two optical elements separated by a large distance B (less than L_0) when the optical elements approximate two small parts of a huge lens. An increase in B by a factor of 100 that does not reach L_0 can improve angle measures only by a factor of 2. At larger B the improvement increases directly with B, but the poorly known L_0 is of the order of 100 m, so such devices are very large.

Because the centroid of the stellar image is moving around with finite speed, there is a characteristic time during which the position of the star may be obtained essentially only once. Any method that can find the position more rapidly than this is giving positions so highly correlated that they are not independent.

One characteristic frequency affecting stellar image motion is

$$\omega_0 = \frac{2\pi v}{L_0}$$

where v is the wind velocity component perpendicular to the line of sight. From power spectra of the position fluctuations in the north-south direction of a star trail on a photographic plate obtained with a stationary telescope, this frequency has been measured to be about 1 Hz. The power spectrum is nearly flat to 1 Hz and then drops abruptly as $f^{-5/6}$ at higher frequencies as predicted by turbulence theory. For a west wind of about 10 m/sec, this points to $L_0 \approx 60$ m.

If we supposed that all correlations ceased after time ω_0^{-1}, we could predict that, in an observation period of T seconds, the uncertainty in the centroid would decrease by a factor $(\omega_0 T)^{1/2}$ below the standard error L_2/B in one "oscillation." The angle L_2/B is about 2 μrad in good conditions, so an observation lasting 1000 sec might have a mean that is uncertain only by 63 nrad (13 marcsec). An experiment on a 20-sec trailed plate showed, however, that the uncertainty in the mean declined only as $(\omega_0 T)^{1/3}$. This reveals that significant structures in the atmosphere are larger than 60 m in wavelength so that a spectrum of correlations extend beyond the time ω_0^{-1}.

For a telescope in the 1-m range using an angular field 10^{-2} rad wide, a feature with a half-wavelength of 50 m would have to be 5 km from the telescope to be easily detected in relative astrometry as a phase-perturbing object, and proportionately farther away if the field were smaller or if its wavelength were larger. The scale height of the variance in atmospheric density perturbations due to turbulence is about half the scale height of density

itself because the variance is a second-order statistic. Thus turbulence strength falls off as exp(-h/4 km) on the average. There are many narrow regions of turbulence revealed by vertical balloon flights, but both the peaks of the turbulence strength and the weaker regions between them tend to fall off with the 4-km scale height.

These facts suggest that, when many star positions are measured with a modest-aperture telescope, the data on relative star positions in a small field of view can be processed as a time series so that most of the slower fluctuations can be recognized as phase-perturbing objects being convected past the telescope at a definite wind speed. When this was done, and it seems important to do so in general, the accidental errors in star positions declined as $(\omega_0 T)^{1/2}$. The use of relative astrometry immediately assures another factor of 2 improvement in the separation angle within a 5 mrad angular field because the relative star motions have at least a correlation of 75% in such a field for a modest-aperture telescope. Note that a telescope synthesized from two widely separated apertures is not apt to be able to use an analysis that uses the steady wind convection to decrease the effects of passing heat waves unless the positional information from each aperture is used in addition to the interferences arranged between the apertures. There is not enough information about the waves. It would help to augment the optical data by placing additional small telescopes near the large system that simultaneously record relative star positions in the same star field. A simultaneous computer solution for all the data would triangulate for many phase objects continuously, in a manner analogous to x-ray tomography as used in medical practice.

So far, we predict standard errors in relative star positions of about 30 nrad per night, caused by heat waves in the atmosphere. To do better than this, we should note that "accidental refraction," like the larger refraction by the layered atmosphere, depends on wavelength. In all photoelectric astrometry systems, it is easy to detect the star positions in blue and red light simultaneously. The dispersion angle by an air wedge is about 50 times smaller than the deflection angle between red and blue light. Thus, at $z = 45°$ the 300-μrad deflection by the atmosphere is a 6-μrad dispersion between the red and blue images. The 2-μrad deflection by seeing is a dispersion by 40 nrad. To see that this small dispersion can be used to correct for most of the seeing deflection, we must consider a specific system.

Consider a 1-m telescope with a sinusoidal amplitude grating of period d corresponding to angle $8\ L_2/B$. Suppose further that the grating moves in the focal plane and that detectors in the pupil count an average of 4×10^4 electrons/sec in blue and red passbands when they view a 10th-magnitude star. A grating spacing large in comparison to the star image will cause a modulation of at least 80% of that possible without atmospheric phase perturbations. It can be shown that the uncertainty in star position relative to the grating due to quantum noise in the detection process is $\Delta x = d/(4\pi N^{1/2})$ after counting N electrons in one or more modulation cycles of 100%. For 80% modulation, Δx will be slightly more. If we insert $d = 16$ μrad and an integration time of 1/16 sec for one or more cycles, $\Delta x = 25$ nrad. As this is smaller than the dispersion due to the deflections of the centroid by seeing on a 1-sec time

scale, we conclude that, for at least 10th-magnitude stars on a 1-m telescope, a large portion of the "accidental refractions" for each star in the angular field can be removed by providing at least two detectors per star.

In a computer simulation of the above system using highly realistic light waves (proper statistics of both phase and amplitude perturbations), a problem was found in centroid definition of the noisy and asymmetric star image. The following estimators of the star image centroid were computed: (a) an array of evenly spaced, linear detectors in the focal plane for which the mean position is $\Sigma I_j \vec{x}_j / \Sigma I_j$ for intensities I_j at detector j located at $\vec{x}_j$, (b) a quadrant photomultiplier arranged to split the focal plane light equally between the four detectors to give a median position, (c) the sinusoidal amplitude grating described above, (d) a detector in the entrance pupil giving the continuous phase function and the scintillation modulated intensity at each point of the phase function and giving the intensity-weighted tilt of the phase in the pupil. None of the estimators was identical to another. The median estimator was poorest among these by a factor of 2 in the standard error. The other estimators agreed to with $\lambda/2D$ in an rms sense. But such an angle is 250 nrad for blue light and a 1-m telescope, which is far greater than the $\Delta x = 25$ nrad obtained above.

The noise in blue and red estimators of the centroid is highly correlated for the focal plane grating, on the basis of comparison of the position estimates for $d = 8L_2/B$ and $d = 4L_2/B$, which corresponds to changing λ from 0.5 to 1.0 μm. But at the telescope, the red and blue light passes through slightly different volumes of air because of refraction. Also red light is generally more sensitive to any composition (water vapor) gradients in real air; thus it must be left to experimental proof that, for the modest-aperture single telescope, the two-color measures can remove the 98% of the seeing-caused centroid motion suggested above. The worst case for this technique would be a precision of 250 nrad/sec and, using the time series analysis to remove slow heat waves blown through the beam, a precision of about 8 nrad per night due to the atmosphere. Such a limit (1.6 marcsec) is completely adequate for a planet search, assuming 40 nights/yr on each star field.

The synthetic telescope with widely separated apertures (Michelson-type interferometer) has no such centroid definition problem. The fringe of greatest modulation is the centroid. The envelope of modulation of the fringes is not deformed by the phase deformations of the atmosphere if the effective detector size projected on the entrance pupil is small in comparison to the light beam separation (10 cm) for which the path difference L_2 is λ/π. Thus, interferometers of large baseline can take full advantage of two-color corrections.

The single-aperture telescope with a grating in or near the focal plane is also an interferometer, one of the achromatic type associated with the name of Ronchi in optics testing. Thus, it can be provided with several detectors per exit pupil and the data can be analyzed to reveal wave-front deformations such as defocus, coma, astigmatism, and so on. All interferometers are self-calibrating with respect to telescope optic errors. Thus, one source of systematic error can be monitored and removed.

All interferometers are multipliers of atmospheric scintillation noise. But a small-B interferometer, such as the single-aperture telescope with focal plane grating, is far less troubled by scintillation noise than a large-B interferometer. All interferometers cause some transverse shear in the system and then make two wave fronts interfere. But the atmosphere is part of the system and it causes the small shears that generate the amplitude modulations of scintillation. The small-B interferometer takes advantage of the fact that scintillation intensity is highly correlated over transverse distance on the order of a few centimeters. But the large-B interferometer interferes two wave fronts that are completely uncorrelated in their intensity fluctuations. The resultant intensity modulation masquerades as a phase modulation and makes the recognition of fringes very difficult in the large-B device.

Very generally, a large-B interferometer "sees" the atmosphere in an essential way while the small-B interferometer is almost "blind" to the atmosphere. If there is any possibility of obtaining the required positional data with a small-B interferometer, then there is no reason to choose a device whose greatest ability is to detect the very noise source most deleterious to astrometry. A case in point is that scintillation can be greatly decreased in the signal of the small-B interferometer just because a detector can receive all the blue or red light of one star from, say, one-fourth of the whole telescope aperture for integration times on the order of 1 sec. The modulation is nearly synchronous over that large area of the exit pupil because the phase perturbations of the atmosphere are all small in the small-B interferometer. Nonetheless, some experiments on large-B interferometers need to continue because of their unique ability to study the two-color compensation problem.

PAPER 3

A PROPOSED GROUND-BASED NARROW FIELD ASTROMETRIC SYSTEM

Pierre Connes
Service d'Aéronomie du Centre National de la Recherche Scientifique
91370 Verrières le Buisson, France.

ABSTRACT

A study of atmosphere induced errors on relative stellar positions within a narrow field implies that accuracy of present results is limited mainly by instrumental factors and not by atmospheric ones. Thus a potentially large improvement may be realized from the ground in the classical problems of long focus astrometry.

We propose a photoelectric technique which makes use of a custom mask for each sky region. It is fully specific in the sense that displacements not positions, are directly measured ; hopefully an easily computed photon noise limit might be reached. A specially designed reflecting telescope, immersed in helium, should eliminate the usual telescope errors (arising from coma, flexure, temperature variations and aging) and also atmospheric dispersion. However the technique is still a slow star by star affair, and there is little competition with the proposed Astrometric Satellite. It might lead to an order of magnitude accuracy increase in parallax or astrometric binaries work for a limited number of previously selected stars and seems especially worthwhile in view of the present interest in dark companion detection.

INTRODUCTION

All astrometric measurements are in principle more accurate outside the atmosphere and should indeed be made in space some time in the next century. However a fairer comparison or rather a more relevant one in the 1978 context, is between the presently planned Astrometric Satellite (AS) and the best performance that might be achieved from the ground now at reasonable cost and effort.

For general sky mapping at a few m arc sec accuracy, AS is clearly unbeatable by virtue of atmospheric refraction elimination and completely uniform sky coverage. No ground-based program, no matter the cost, is likely to do the same even in a much longer time. As an automatic by-product, proper motions and parallaxes will be provided with the same kind of accuracy for all the recorded stars. Does this necessarily kill all ground-based astrometry? We think not.

Colloquium on European Satellite Astrometry, Padova 5-7 June 1978

Neglecting all causes for systematic errors which may or may not be serious - our purpose is not to discuss them - one still has a fundamental limitation in the number of photons collected. The proposed telescope is small (20 cm ?) and scans the whole sky at a uniform rate, thus spending little time on each star. The total number of passes per star is also rather small for a projected 2 years lifetime. This results in an easily computable angular position RMS error for a given star per pass, and in overall position and parallax accuracies (after the whole program is completed) which may also be estimated. Consequently in so-called Version A, one considers useful information will be collected up to mag 14, and up to mag 11 for Version B (1). For still fainter stars, accuracy decreases markedly while data handling and confusion problems get more difficult.

Then periodic proper motions due to dark companions cannot be handled and the system is not suitable for the study of astrometric binaries. For long periods - more than a few years - the observing program is too short to disentangle periodic from linear terms in proper motions ; for shorter ones the number of passes i.e. of independent observations is too small to separate fully parallax from periodic motion (and the parallax solution may be perturbed as a result).

From the ground there is no difficulty at all in using much larger telescopes, nor in spending longer and more numerous observing periods on a limited number of pre-selected interesting objects. Consequently present programs aimed at faint stars parallaxes or detection of dark companions will not be made obsolete by AS and it is perfectly reasonable to speculate on possible improvements of ground-based narrow field astrometry, the traditional tool through which such programs are pursued. Indead it seems wiser to do so before freezing the program of AS in order to better define its field of applications.

Surprisingly enough narrow field astrometry has remained up to now completely untouched by modern technology. The photographic plate is still the only detecting device ; image tubes are not adaptable and no suitable photoelectric micrometer has been built. Many of the observations are still done with century-old refractors, some even built for visual use. No overall analysis of error causes has been published ; reading the literature leaves the impression that authors do not know whether the worst ones are instrumental or atmospheric. The problem of accurate setting on a stellar turbulence patch photocenter attracts relatively little interest. Of course we do have studies of anomalous refraction and we also have several efficient photoelectric micrometers adapted to meridian circles ; however both of these efforts tend to improve so-called "absolute" astrometry but have no bearing so far on "differential" techniques.

We have recently proposed (2) a new ground-based narrow field astrometric technique. There are four parts in the discussion : First a study of anomalous refraction effects within a narrow field. The second describes a special purpose astrometric telescope, and the third a purely photoelectric detection technique. Finally possible programs are discussed. Since this proposal is rather detailed and lengthy only the essential points will be given here.

II - ATMOSPHERIC LIMITATIONS

The phenomenon we are considering here is not seeing (an instantaneous image spread which does not affect photocenter position) nor normal refraction (fully computable from atmospheric models) but anomalous refraction i.e. a small random and unpredictable photocenter shift. Furthermore we are only interested in the differential effect (within a field of the order of 1°) and solely in the very low frequency terms : this is because an ideal narrow field technique should first have the capability of complete insensitivity to angular shifts affecting the whole field, whether arising from fluctuating refraction or telescope vibrations ; second it should be able to integrate over time, thus to give the mean photocenter position during the observation (lasting a few minutes at least).

To a limited extent only, classical photographic astrometry has these capabilities, as first shown by Schlesinger (who also proved that anomalous refraction is strongly correlated over small angular distances). However the limited linear range of photographic processes means time integration is far from perfect ; photographic pattern CG does not coincide with mean image photocenter position, being a function - for instance - of stellar magnitude and exposure whenever the image is asymetrical. Since there are also other errors (from the telescope) long focus photography is simply not accurate enough to prove (or disprove) the existence of an anomalous low frequency distortion within a small field.

So we must start from estimates of anomalous refraction by such tools as photographic zenith tubes, meridian circles and Danjon's astrolabes (3). If we knew the actual atmospheric structure i.e. how much of the ray deviation arises at each level we might compute the true differential effect. Since we don't, the best we can do is to assume the whole ray deviation takes place within a thin layer at altitude h. By a first integration over the telescope pupil we get the instantaneous turbulence patch photocenter displacement (relative to the normally refracted image). Then the layer is broken into Fourier components with different spatial frequencies f and assumed to move at constant horizontal velocity V (frozen flow hypothesis) ; by integrating over time we obtain the mean photocenter deviation. We next pass to the differential effect between two stars, and finally to the apparent fluctuation in the angular distance between the one in the center of the field ("program" star), and the CG of a set of background stars more or less uniformly distributed over the field (because this is precisely what an ideal differential technique will do). Last we look for a worst case by varying h, f and V.

Only the conclusions need be given here. For any plausible combination of altitude and wind speed the residuals are negligible - or at least considerably smaller than the hypothetical 10 m arc sec "night error" of Land (4). A perturbing layer close to the ground may produce slow deviations but these affect in a similar manner all stars in the field. A high altitude one does produce differential effects - easily seen within a small field - but these are purely at high frequencies : it is impossible for such a layer to remain fixed with respect to the ground and even the lowest plausible horizontal velocity cancels the mean effect if the observations last a few minutes or more ; the only requirement is moderate zenithal distance ($z < 45°$). We again stress that an ideal technique should provide correct time integration.

Finally we have refraction effects inside the dome or tube but these are really instrumental and will be dealt with in II. The general conclusion is that present day long focus astrometry is quite far from reaching any kind of "natural" atmospheric accuracy limit ; the way is open to sizeable improvements in parallax or astrometric binaries programs.

III - TELESCOPE -

A complete discussion is found in (2) and the telescope has been separately described in (5) ; only a summary will be given here.

The classical long focus refractor has negligible spherical aberration, distortion and astigmatism and small residual coma, but appreciable secondary chromatic aberration. Flexure of the tube is very large, flexure and temperature distortion of the lens appreciable. Aging effects may exist but are not well studied ; indeed facilities for checking telescope stability are non-existent. Considerable changes have been noticed after dissassembling and remounting the lens, which are troublesome for very long term programs.

Two special purpose reflecting telescopes have been built from the design of Strand. Extreme simplicity is their main feature : an f/10 parabolic primary plus a plane secondary eliminate alignment problems. Spherical aberration is zero ; coma is relatively large but highly stable. Flexure is small and accurate means for checking the optical axis are incorporated. While chromatic aberration is zero, atmospheric dispersion is still there and usable spectral range is not markedly increased: a filter has to be placed in front of the photographic plate just as with refractors.

An ideal astrometric telescope should eliminate coma, temperature flexure and aging effects, and also compensate for atmospheric dispersion. Our proposed design fulfills all these conditions at the same time. It is simply a plateless Schmidt i.e. a spherical mirror with a circular stop in the center of curvature plane. The focal ratio is in the range of f/12 to f/16 which means negligible spherical aberration and small easily tolerated field curvature while keeping a field of the order of 1°. There is no axis at all and zero coma ; the images are circular and uniform over the whole field.

The main advantage arises from the following property : small deformations of quasi plane surfaces placed in or close to the central plane produce zero distorsion ; while images are no longer perfectly circular they stay uniform over the field. Angular distances between their photocenters are not affected. Consequently, the telescope may be fixed, enclosed behind a plane window and fed by a moving flat siderostat. The telescope itself is at constant temperature and gravity, and any residual effects on the outside flat are negligible. Then, if the telescope is immersed in helium and the window suitably tilted with respect to the axis, atmospheric dispersion is reduced more than 100 times. The spectral range 4000 to 9000 Å accessible to Ga-AS photocathodes may be used. Helium immersion plus constant temperature eliminate all internal refraction problems and absence of a dome the so-called dome effects.

Another essential feature of our proposal arises from use of the siderostat flat in autocollimation. In this way the entire telescope may be checked in an extremely accurate manner without looking at the sky. The various tests (2) make use of the photoelectric detection scheme to be described next. All the telescope parameters are referred to the mask itself and telescope aging eliminated for all practical purposes. Perfect mask stability is ultimately the only requirement, and may in turn be absolutely checked (if necessary) in a standard manner with a two coordinates laser controled measuring engine. Altogether we believe the proposal represents the most practical solution to the difficult problem of accurate measurements of small angles.

IV - PHOTOELECTRIC DETECTION AND CUSTOM MASK SYSTEM -

The basic improvements to be expected from a photoelectric detection scheme are improved quantum efficiency, perfect linearity and elimination of emulsion shifts. A secondary but still important issue is labor reduction in analysing the large number of plates taken in parallax or proper motion studies.

Clearly no existing or contemplated image tube is suitable. A grid system (AMAS, (6)) has been proposed for the LST ; it has the capability of giving the positions of a few randomly located stars i.e. works for any field. We believe a better approach for the particular problem treated here is realized by making full use of a priori information i.e. the (approximate) positions of all useful stars in the field. From the fundamental viewpoint of photon statistics limitations, it may be shown this is a far more efficient technique. The essence of the method is not trying to get more accurate positions, but detecting the motion directly relative to a special purpose mask, custom built for each field. The basic idea is derived from the proposal by Fellgett for measuring radial velocities by correlation (7), that has led to the radial velocity photometer of Griffin. Actually a first partly successful attempt at measuring parallaxes has been made by Van Altena (8); the mask was simply a high contrast positive of the stellar field. We believe a more spphisticated approach is needed.

Our solution is shown on Fig. 1. Light from all background stars such as B1, B2 passes through a mask M which is generally opaque except for small transparent regions (to be described in Fig. 2) around each wanted star. The field is divided in two halves and a split lens L1 L2 collects the flux and sends it to a pair of "background" photomultipliers PM_{B1}, PM_{B2}. The central portion of the mask has been cut out and is supported by a carriage with two interferometrically controled XY motions. Maximum displacement is equal to the largest expected proper motion ; if we want to follow Barnard's star for fifty years the displacement will be 25 mm for f = 10 m (while the mask diameter would be of the order of 20 cm). The mobile mask position plays the role of a tracking micrometer. Light of the central star falls on a separate photomultiplier PMc ; two error signals in X and Y are produced and the carriage is continually servoed to follow the image. Simultaneously the entire telescope is guided to null the background error signals sum while their difference controls field rotation.

Even if guiding on the background stars is perfect, carriage position nevertheless continually fluctuates because of photon noise on the one hand, and of the rapid atmospheric distorsions discussed in II (mostly from high altitude layers). Our contention is that atmosphere induced fluctuations will very nearly average out to zero for a run of a few minutes or more, due to the absence of predictable low frequency differential terms. Photon noise will of course impose the basic limitation to setting accuracy. The true mean carriage position is derived by sampling the X and Y coordinates and calculating the mean digitally.

Production of the error signals shall be explained next. A plane parallel plate P in front of the focal plane is periodically titled by a small angle. All stellar images (central or background) follow identical closed trajectories in the focal plane ; they are position modulated. Small identical variable density patterns are imprinted on the mask, the center of each coinciding with the expected undeviated position of each star image. All stars produce intensity modulated outputs ; after suitable demodulation, X and Y error signals are generated.

Several different scan trajectories and associated transmission patterns may be tried. A nearly ideal solution is given by the combination of a circular uniform scan $\theta = \omega t$ (easiest to implement accurately, through uniform rotation of P around the telescope axis) with a $T = \cos^2\alpha$ transmission law (fig. 2). Demodulation means multiplication by cos θ and sin θ , which is also very simple with a sine-cosine potentiometer. One shows the two products, when integrated over one period of rotation are <u>proportional</u> to the positional errors ΔX, ΔY of the <u>mean</u> photocenter irrespective of image shape, or even shape fluctuations.

This <u>linearity</u> of the error signals is a cardinal feature of the proposal. First it means the carriage will follow <u>linearly</u> the central star image (a few other conditions, such as frictionless support must also be met, but a large servo bandpass is not needed ; the carriage does <u>not</u> have to follow the fastest image motions). Second the background stars error signals do not have to be <u>individually</u> brought out. Global error signals may be used ; they give mask displacement relative to the <u>optical</u> center of gravity of the reference star configuration (i.e. weighted by individual star luminosities).

For a complete discussion of custom mask system refer to (2) ; only the main results need be given here. An essential property of classical plate reduction procedures used in photographic astrometry is to ability to separate out scale changes, plate tilt etc... provided at least three reasonably located background stars are available. An identical result is obtained here <u>in real time</u> provided each stellar image stays within the small $\cos^2\alpha$ pattern (a few arc sec in diameter). This condition is easily met in practice, and even allows the background stars small relative proper motions.

Mask fabrication is not particularly difficult. Thanks again to error signal linearity the positioning accuracy required for each pattern is rather low (of the order of 1 arc sec). Nor is it time consuming. With a very simple copying engine (2), the mask is produced from a sky plate in

one operation rather comparable to crude measurement of one plate while a regular astrometric program normally involves accurate measurements of many plates.

Altogether off-sky labor is much reduced, which reacts on the whole project by making practical the use of several hundred background stars (versus 5 to 10 as usually done so far). This means a further reduction of observational or astronomical errors. First photon noise from the background star reference set is reduced, and optimal compensation of atmospheric or instrumental distorsions approached. Second fainter stars may be used which are expected to have smaller parallaxes of their own. Actually it may be feasible to use compact galaxies as references with specially designed masks.

The performance of an ideal photoelectric detection scheme is easily predicted from the averaged seeing pattern, which is Gaussian with half width ε (the fine speckle structure is irrelevant here), and from the number of photoelectrons. Assuming $\varepsilon = 2$ arc sec (i.e. 50 % of the energy within 2 arc sec, or average - to poor conditions), a 1 m telescope, 30 % instrumental transmission, a Ga-As photocathode and 1000 s observing time the results are summarized by fig. 3. How closely our proposed mask system might approach these predictions may only be shown by actual tests.

A fully interferometric approach to the same problem (i.e. central star motion relative to a background star configuration) has been carefully considered, and rejected as definitely too complex for a ground based instrument - having to deal with seeing. In space the answer might be different. The comparison is detailed in (2).

V - APPLICATIONS -

We want to make order of magnitude predictions for the results that might be achieved through a determined attempt. We suppose a 1 m diameter telescope is fully available to the program with 2000 h/year observing time. Half is devoted to parallax (the morning and evening hours) and the rest to a search for dark companions (actually the separation would not be so schematic).

a) Parallaxes

We start with the angular setting error given in Fig. 3 for 1000 s of observing time. However the actual length of each observing run is irrelevant here : only the total time per star matters. We may for instance divide the available 1000 h among 200 stars and devote 5 hours to each. All 5 hours do not have to be in the same year ; our choice only means 200 parallaxes/year will be produced. We have some freedom in trading number of stars for accuracy ; however because of lost time in re-pointing, changing masks, etc... the system is clearly not suited to produce thousands of parallaxes per year. Fig.4 summarizes the predictions and compares them with those of the AS proposals. The only limitations considered in both cases are the fundamental ones of photon statistics, and diffraction disk or seeing disk diameters.

Such a limit may possibly be reached for the very faintest stars considered in each program ; it will certainly not be achieved in practice for brighter stars because of systematic errors we are not able to predict accurately. The figure also presents the estimated accuracies of some already known parallaxes - definitely not photon noise limited.

Should both AS and our proposal be implemented our program would be limited to a relatively small number (a few thousands at most) of stars selected either because they are too faint for AS or for increased accuracy. Of course, some cross checking between these two altogether different techniques would be very valuable. Inversely one should consider carefully the possible accuracy and limitations of ground-based observations before defining the programs of versions A and B of AS. Lastly AS cannot observe directly compact galaxies while this is feasible with our device. Tying in just a few of the AS observed stars to galaxies would give absolute rotation of the entire AS system of stars.

For a more detailed discussion of parallax problems - including the important one of relative to absolute parallax correction, refer again to (2).

b) Astrometric binaries, or Detection of Dark Companions -

We still have about 1000 h/year of observing time divided between an arbitrary number of stars to be kept under watch. These might include a few known astrometric binaries for cross checking with older techniques, but the bulk would be made of nearby solar or later type stars for which the existence of low mass dark companions is considered possible. So far only 30 astrometric binaries are known, while extrapolated estimates give far greater number of stars with dark companions (Fig. 5) (9, 10). A systematic search, if done with increased sensivity, has a high probability of turning out actual results.

Let us consider a program stretching over 30 years and aimed at detecting periodic proper motions with $T \leq 30$ years. We may for instance look at 1000 stars with 30 hours observing time per star ; of course equal times do not have to be spent on all stars and we may again trade number of stars for accuracy. Somewhat arbitrarily we consider a one solar mass star, and a Jupiter-like companion (same orbit radius). We may then plot, again with the assumptions of Fig. 3 the mass of the dark companion which would produce a just detectable perturbation as a function of distance in pc for various stellar types (Fig. 6). No doubt these predictions (based on the photon statistics - seeing disk limitation alone) are very optimistic since they suppose complete elimination of all systematic errors. Nevertheless they do show what might be achieved from the ground by optimal techniques.

We must recall that in one case only (Barnard's star) photographic astrometry may have detected a Jupiter sized companion (11) but the result is still controversial ; obviously no mere accumulation of plates beyond the many thousands already taken in this quest is going to solve the problem in an unambiguous manner. A change of technique is needed. Finally hypothetical planets are not the only possible subjects for a study : there is a small number of cases in which collapsed companions might induce in the visible star an orbit within range of our proposal. For instance, β Lyrae is a spectros-

copic binary with 19 days period ; the (computed) angular radius for the visible star orbit is about 1 m arc sec, not much below the sensitivity of present day astrometry.

VI - PROPOSALS AND CONCLUSION -

Let us try to define a test program for the suggestions of this paper.

The mask system should first be tested in the laboratory on simulated star fields. This test is definitely the most critical - and painstaking - one in the whole program, but inexpensive since no large optics or beyond the state of the art elements are needed. The points which will be fully checked are setting accuracy for a given photon flux and cancellation of the various optical system errors (guiding, tilt, scale, focusing etc...). To some degree the effect of seeing may be tried, but anomalous refraction can probably not be realistically simulated in the laboratory.

One might then consider taking the device to the focal plane of an existing reflector or refractor. However adapting the entire system to a moving focus means considerable extra work ; what is worse, the test might not be conclusive since it would be very difficult to extricate possible atmosphere induced errors from telescope ones. Nevertheless cancellation by the mask system of anomalous refraction distorsions (an essential point) might be checked with a fixed polar telescope. This would be of the type discussed in III, but without siderostat, window or helium immersion ; only the primary spherical mirror is needed (it might be later incorporated into the final telescope version). The system would be restricted to one stellar field, which does not matter. The proposed experiment is short term (a few months) : one does not need to actually measure a parallax or proper motion, but merely to demonstrate overall system performance in diverse atmospheric conditions.

The biggest expense is of course for the construction of the complete telescope. Several optical components are needed (versus just two in the Strand type reflector) but none of them is difficult. Also the dome and equatorial mounting are eliminated. One may consider a range of diameters from perhaps 50 to 150 cm. Beyond 150 cm window fabrication becomes a problem, while at 50 cm - but not much below - the improvement over present photographic programs due to increased Q.E. and spectral range is still worthwile. Any sensible decision on telescope size should involve a detailed program study - which means in particular up to date information on AS prospects, a comparison between capital expenses and running costs, etc... ; so far this has not been done. In any case the project is small scale compared to a space venture with similar aims.

One might believe LST will solve once for all an age-old problem : actually getting the diffraction limited resolving power of a large telescope. Nevertheless right at the same time a sizeable effort - both theoretical and experimental - is being done to achieve the same through the atmosphere, lately with marked success (12, 13, 14). It is puzzling to see long focus astrometry plodding on with the same old tools and attracting no interest either from opticians or atmosphere specialists. The probable explanation is that diffraction limited resolving power is a well-known - and challenging -

concept. The one of photon statistics limited setting error on an image photocenter, while straightforward is less classical, and the rewards for achieving it not quite so obvious. But they might prove just as large in practice. And the photoelectric mask technique we propose here is much less elaborate than building and operating adjustable figure mirrors.

For dark companions detection different non astrometric methods should also be considered, but this is beyond the scope of our paper (we have independantly proposed a program for single line spectroscopic binaries). Astrometric detection may seem dreadfully slow compared to direct imaging, with LST for instance. But even if this approach were to prove feasible (which seems doubtful when brightness ratios comparable to the Sun - Jupiter one are considered), the - essential - orbit determination will be slow in any case. Actually the two techniques should collaborate, not compete . Availability of LST undoubtedly means we shall be able to see much fainter close companions ; a simultaneous capacity for improved photocenter orbit estimation should be welcome. But as far as astrometry is concerned, we conclude it would be mistake to go to Space right away (for detecting small perturbations) without having first tried out simple proposals - such as ours - from the ground, in the belief insuperable atmospheric difficulties exist. Nothing - in Nature or litterature- justifies this viewpoint.

REFERENCES

(1) ESRO OP/PS 76, 11 (1976)

(2) P. CONNES, A proposed ground based technique for measuring parallaxes and detecting dack companions, Orsay (1977)

(3) E. HOG, Zeits Astrophys. 69, 213 (1908)

(4) G. LAND, Astron. Jour., 51, 25 (1944)

(5) P. CONNES, Proc. ESO Conf. on optical telescopes of the future, 351 (1978).

(6) L.W. FREDERICK et al., ESRO SP 108, 49 (1974)

(7) P. FELLGETT, Opt. Acta 2, 9 (1955)

(8) W.F. VAN ALTENA IAU Symp. 61, 311 (1974)

(9) P. VAN DE KAMP, Ann. Rev. As. Astrophys. 13, 295 (1975)

(10) H.A. ABT, S.G. LEVY, Astrophys. Jour. 30, 173 (1976)

(11) P. VAN DE KAMP, Astron. Jour. 80, 658 (1975)

(12) A. LABEYRIE Progr. in Optics 14, 47 (1976)

(13) A. BUFFINGTON et al., Science, 200, 489 (1978)

(14) J.W. HARDY, Proc.ESO Conf. on optical telescopes of the future, 455 (1978)

(15) P. VAN DE KAMP, Principles of Astrometry, Freeman and Co (1967)

(16) K.A. STRAND et al., Pub. USNO, XX (1971) and private communication.

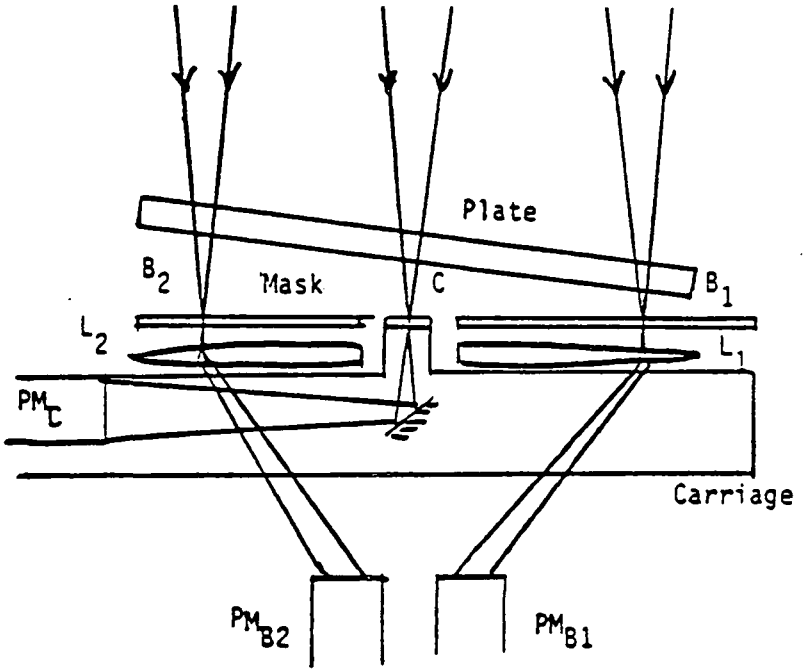

Figure 1.- Custom mask system.

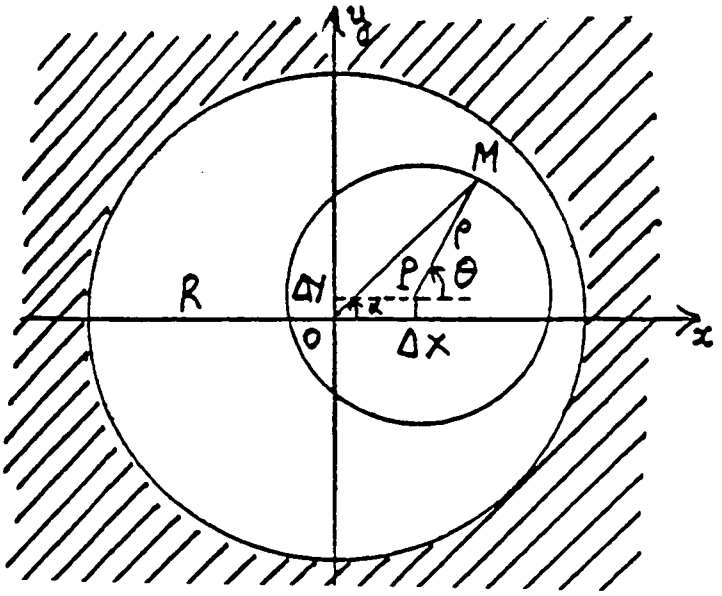

Figure 2.- Generation of error signals through spatial modulation. Stellar image photocenter M moves on a circle with radius ρ (defined by tilt of plane parallel plate) at uniform speed. Center P of the circle is displaced from center 0 of the pattern by all error causes (mask distortions, guiding, telescope misadjustments, refraction aberration, and proper motions). One wants to derive error signals proportional to Δx and Δy. Within circle of radius R, transmission is $T = \cos^2\alpha$, i.e., ϕ on 0x, 0.5 on both diagonals and 0 on 0y.

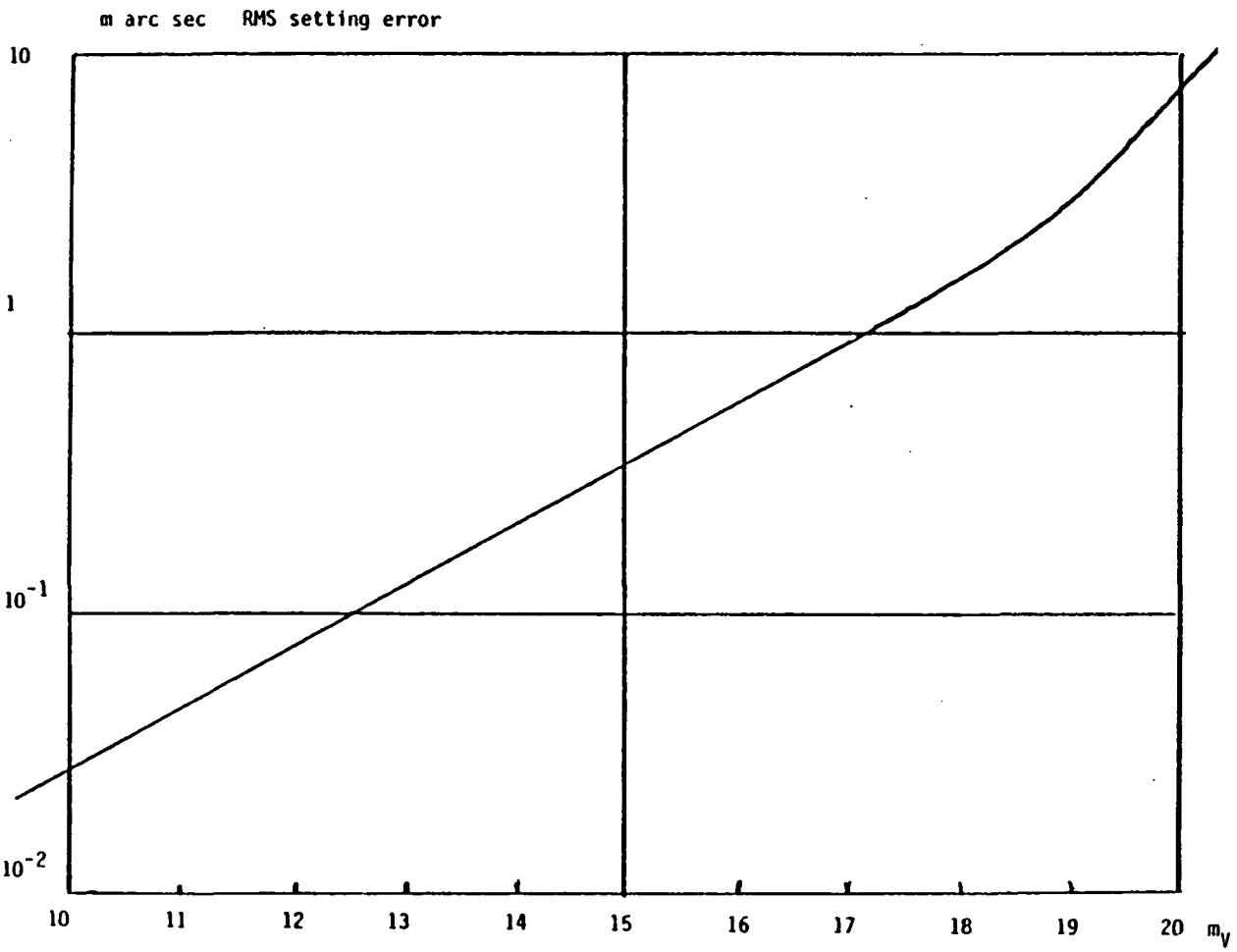

Figure 3.- RMS angular setting error on seeing disk photocenter due to photon statistics. One assumes a 1-m telescope, 30% instrumental transmission, 2 arc sec seeing, a Ga-As photocathode, 4000 to 9000 Å bandpass, 1000 s observing time. Result varies very little with spectral type. Up to $m_V = 17$, one finds a slope 1/2 straight line, changing to slope 1 for fainter stars because of sky background.

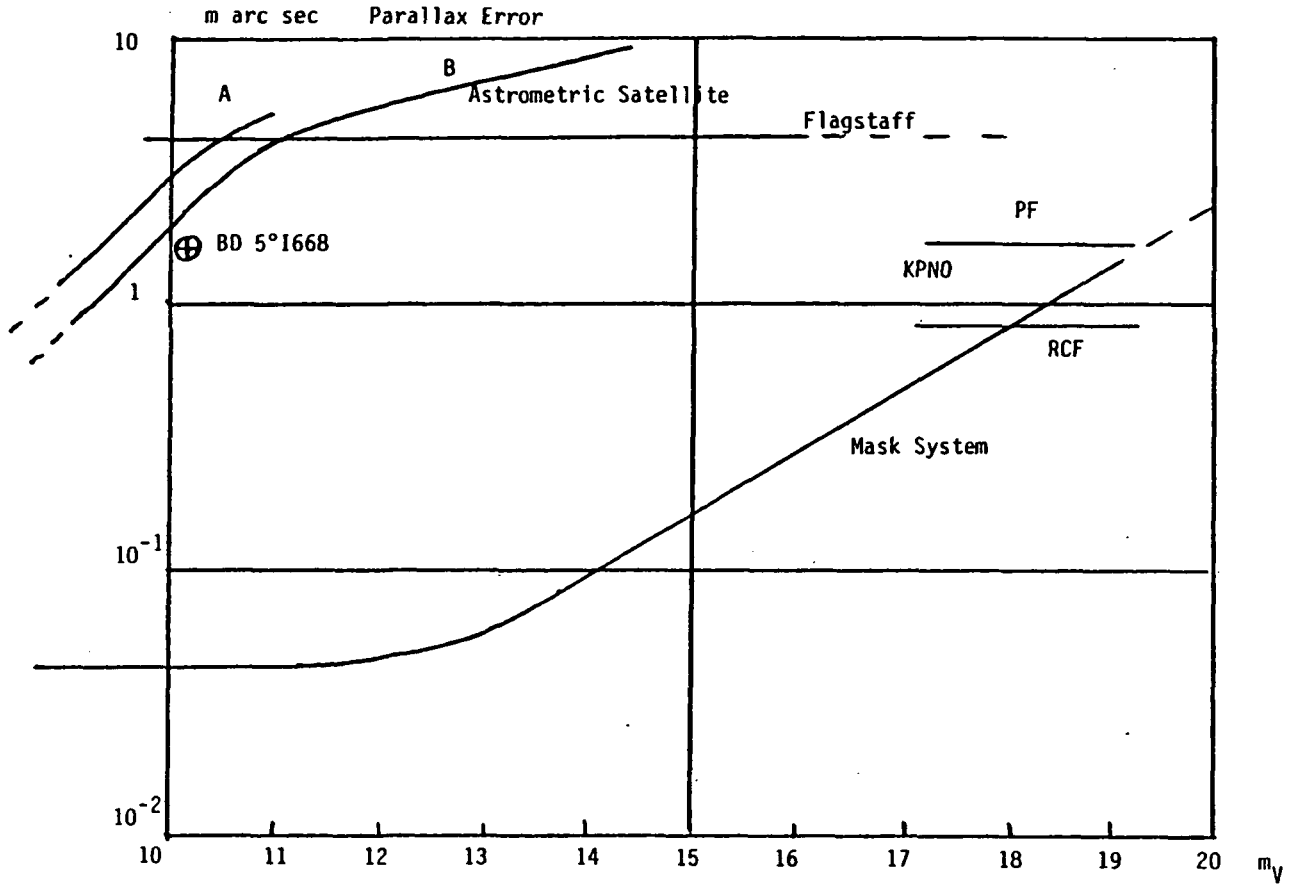

Figure 4.- Sloping curves give computed photon noise accuracy limits to parallax measurements. Astrometric satellite: Two curves are given for Version A and B, from (1). Mask system: One uses the assumptions of figure 1 plus the one of 5 hours total observing time per star (leading to 200 parallaxes per year) at a mean parallax factor of 0.8. Flattening of curve at left is due to limitations from reference star configuration which also contributes some photon noise. BD 5°1668: Most accurate parallax reported in literature according to Van de Kamp (15). Flagstaff: In the USNO 1.5-m reflector parallax program, the external mean error is now essentially equal to the mean internal mean error according to (16) and to Harrington (BAAS, 9, 1977); they are both 4 m arc sec. KPNO: Recent results by Van Altena with 4-m reflector. Upper trace gives actual results at prime focus from pilot program (2.4 m arc sec standard error, BAAS, 9, 599, 1977); lower trace anticipated results at Ritchey Chretien focus (0.8 m arc sec s.e., private communication). Both are for 22 single exposure IIIaJ plates.

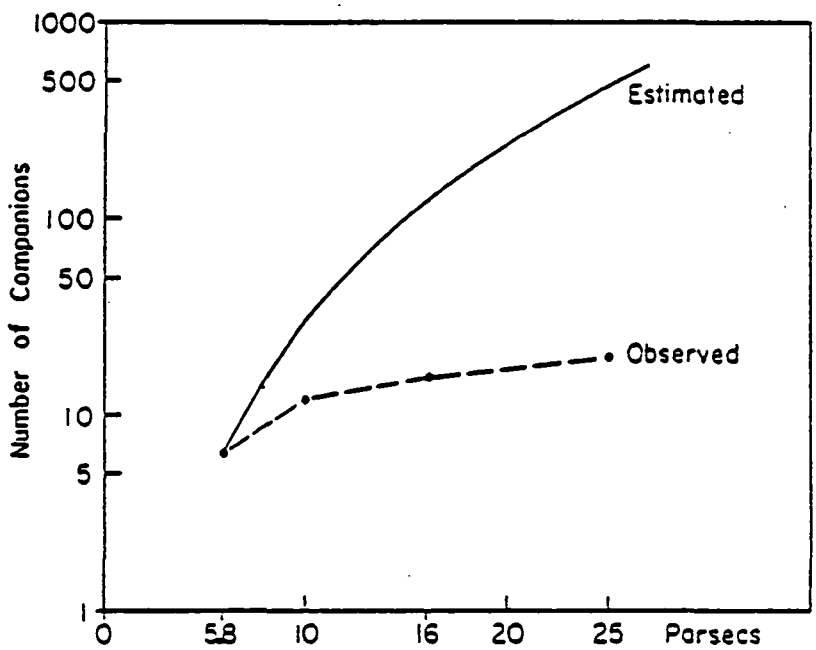

Figure 5.- Number of unseen companions up to different distances. Because the density up to 5.8 pc must be a minimum value, the extrapolated values beyond 5.8 pc likewise are minimum values, assuming the density function to remain constant with increasing distance (from P. Van de Kamp (9)).

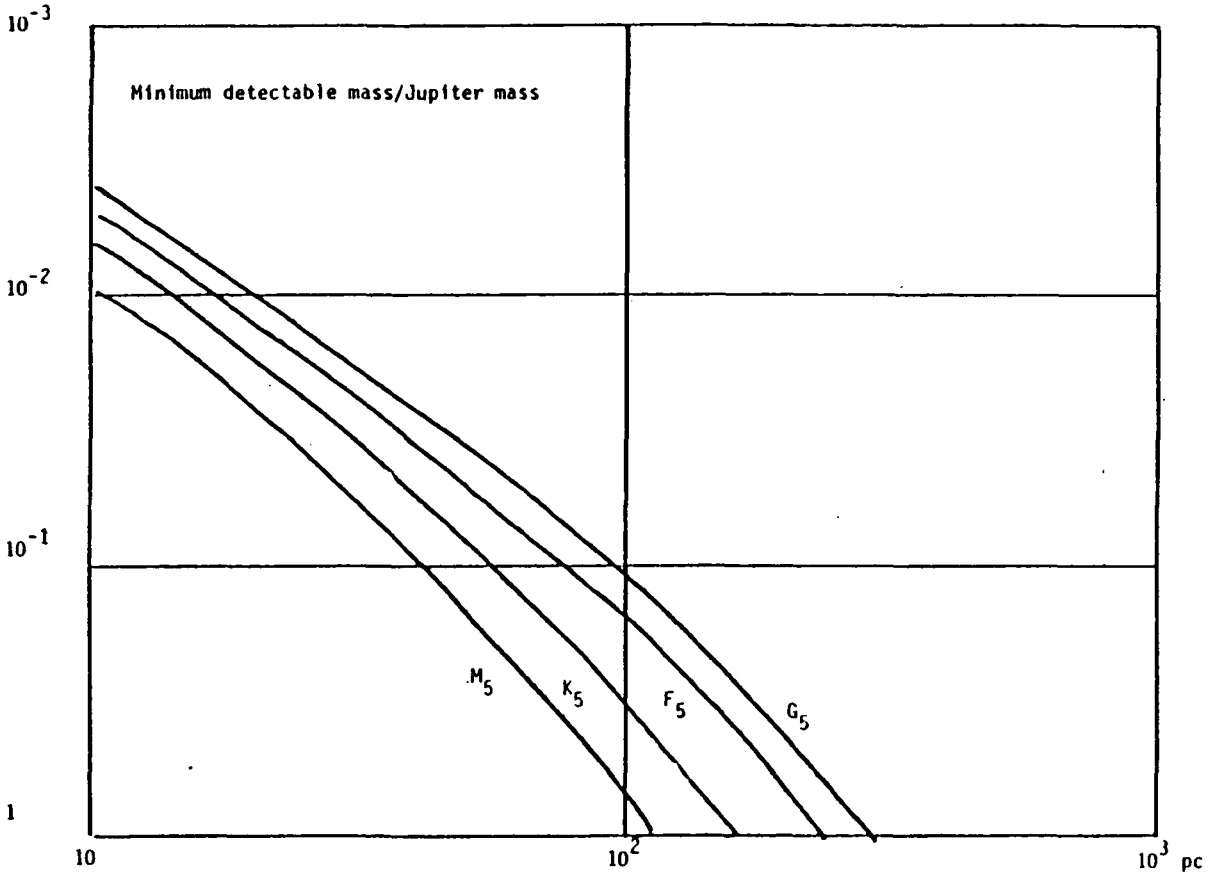

Figure 6.- Minimum detectable planetary mass as a function of distance, for a one solar mass central star and different spectral types - a Jupiter-like orbit (a = 5.2 AU) and the assumptions of figure 1 plus 30 hours total observing time per star stretching over up to 30 years.

PAPER 4

ON THE ASTROMETRIC DETECTION OF NEIGHBORING PLANETARY SYSTEMS, II.

George Gatewood, Lee Breakiron,* Ronald Goebel, Steven Kipp,
Jane Russell, and John Stein

Allegheny Observatory, University of Pittsburgh,
Observatory Station, Pittsburgh, PA 15214

SUMMARY

Extensive testing suggests that astrometric techniques can be used to detect and study virtually any planetary system that may exist within 40 light years (12.5 parsec) of the Sun. Following the conclusion of Paper I, the astrometric group at the Allegheny Observatory began an intensive survey of 20 nearby stars to detect the nonlinear variations in their motion that planetary systems would induce. Several tests conducted to further our understanding of the limitations of this survey indicated that the photographic detector itself is responsible for most of the random error. A new photoelectric detector has been designed and a simplified prototype of it successfully tested. The new detector is expected to be able to utilize virtually all of the astrometric information transmitted through Earth's atmosphere. This is sufficient to determine relative positions to within an accuracy of 1 marcsec/hr. Such precisions exceed the design capabilities of the best existing astrometric telescopes; thus a feasibility study has been conducted for the design of an improved instrument. The study concludes that a new ground-based telescope and a new detector combined should be able to study stars as faint as 17th magnitude with an annual accuracy of a few tenths of a milliarcsecond. However, to obtain the ultimate accuracy possible from current technology, we must place an astrometric system above Earth's atmosphere. A spaceborne instrument utilizing the new detector would in theory have sufficient accuracy to detect any Earth-like planet orbiting any of the several hundred stars nearest the Sun.

INTRODUCTION

Shortly after the publication of Paper I (Gatewood, 1976), the astrometric group at the Allegheny Observatory undertook a concentrated study of 20 neighboring stars in an effort, using current techniques, to detect the perturbations extrasolar planets might introduce into the apparent motions of their primary stars. This review details the initial results of that effort

*Now at the Van Vleck Observatory, Wesleyan University.

and of the several studies that grew quite naturally from our analysis of its sources of error. Besides some preliminary results from the survey, which is still too immature to provide definitive results, we relate the following: some of our thoughts on the positional precisions required for detection; a brief report on the sources of error in the photographic program, including a study of the astrometric errors caused by the atmosphere; a design for a focal plane photoelectric detector having a more rapid response and greater sensitivity than the photographic plate; a brief report on observational tests with a simple prototype of the proposed new detector; a few comments on proposed interferometric techniques for astrometry; a feasible design for what we consider to be the optimum ground-based astrometric telescope; and a design for a spaceborne survey instrument. Finally, we describe what we consider to be the logical course in applying each of these improvements in a systematic program to detect and study all the planetary systems within 12 parsec of the Sun.

Throughout this review we attempt to combine empirical tests and theory to yield error estimates that include all probable effects. Past failures to do this have made astrometrists, as a group, wary of any predictions of extreme accuracy. Oversights are easily made and their effects are dramatic. Thus we propose a step-by-step development which includes a reassessment of the probable gain of each future phase with each step. Nevertheless, despite the uncertainty of some of our most enthusiastic predictions, the trend toward higher precision is quite clear, and sizeable gains in astrometric precision are definitely indicated. With these will come new insights in virtually every branch of astronomy and astrophysies and, as the frequency and nature of planetary systems become known, we will gain a better perspective of the solar system and our relationship to it.

SURVEY

A. Background

The distance from which our planetary system could be detected and studied by an extrasolar observer depends only on the technological sophistication of the instruments employed and their access to electromagnetic radiation emitted by the Sun since the planetary system evolved. At least eight planets cause variations in the otherwise nearly linear motion of the Sun which are greater than the apparent photocentric shifts that may result from normal sunspot activity. The telltale perturbations are almost equally evident from any orientation in space and their detectability can be reduced to parameters in photon statistics, duration of observation, and the field scale of the optical system used. The astrometric visibility of our planetary system is so evident that we must first remove the effects of the Jovian planets from the apparent motion of nearby stars before their position/time relationship may be studied for evidence of their planets.

Astrometrists have possessed instrumentation and techniques capable of detecting substellar masses for several decades (Schlesinger, 1917). These objects are predicted by theory and suggested by observation to be quite numerous (Abt and Levy, 1976). For a while it seemed that they were evident in many astrometric studies; for example, a veritable menagerie of substellar companions discovered over a period of several decades was listed as recently as four years ago (van de Kamp, 1975) and even more recently by Lippincott (1978). These reports stimulated theoretical papers defining the lower mass of a main sequence star (e.g., Kumar, 1963) and the maximum mass of a planet (Kumar, 1972). However, while confirmed astrometric discoveries have shown the existence of stellar objects whose masses fall considerably below the theoretical nuclear burning cutoff (Heintz, 1978; Lippincot and Hershey, 1972; Gatewood, 1976), they have not shown the existence of objects whose masses are less than the 10 millisun (1 millisun = 1 mS $\approx$ the mass of Jupiter) degeneracy predicted by Kumar and suggested by him as the upper limit to planetary masses.

This situation may be attributed to the custom in astrometry of modeling the imaging characteristics of an optical system so that the model has the precision of a single plate and then averaging tens or even hundreds of plates into normal points. This leaves the study based on these normal points open to systematic errors nearly as large as the standard error of a single plate. Notably, virtually all of the studies that have reported the discovery of extrasolar planetary masses rely either wholly or partially on observations acquired with the 61-cm visual refractor at the Sproul Observatory. As observations acquired with that telescope have accumulated, it has become increasingly clear that more sophisticated modeling is required. To minimize exposure times, these plates (yellow sensitive) have been exposed only long enough to acquire well-darkened images of the target star and three or four well-placed reference stars. This barely exceeds the minimum requirements for a simple affine transformation of the measured coordinates

of each plate into a standard reference frame. The transformation produces the constants necessary to place the measured position into the standard frame with an error only slightly larger than that of the measurement itself. However, the standard frame is defined in terms of magnitude, color, or higher order combinations of the coordinates. The first indication of difficulties was noted by Land (1944), who showed that the standard error of normal points formed from observations obtained with that telescope did not decrease with the square root of the number of observations they contained (indicating that they are nonrandom), and that nightly normal points tended to fall in patterns above and below their mean (indicating an unmodeled effect). He also pointed out that the standard error of the positions obtained from a region was dependent on the size of the area over which the reference stars were spread, thus showing that the unmodeled term or terms included parameters in the measured coordinates. Further difficulties were indicated when Lippincott (1957) found that a color term was necessary to model the effects of a realignment of the 61-cm lens. Later a distortion term was noted in the region of AC + 65° 6955 by Hershey (1973). More recently, a cross of coordinate terms into x from y and vice versa was noted in Paper I and in a study combining the observations of the 61-cm refractor with those obtained with the 155-cm astrometric reflector. Strand (1977) showed that the unmodeled color terms of the refractor displace the apparent separation of the red and blue components of Stein 2051 by 37 marcsec (1 marcsec = 0.001 arcsec). In the meantime, unsuccessful attempts to confirm the reported planetary systems were underway at other observatories (Gatewood and Eichhorn, 1973; Gatewood, 1974; Gatewood and Russell, 1979b). Finally, Heintz (1976) found an unexplainably high number of coincidences in the parameters that describe the small mass orbits suggested by the 61-cm data.

All of these reported difficulties with the Sproul instrument and the failure of other observers to confirm the alleged unseen companions cast grave doubts on the existence of the small-magnitude perturbations observed in that instrument. Unfortunately, due to the lack of well-exposed reference stars, the bulk of these data cannot be rereduced. To include higher order terms in the transformation requires several more reference stars that can be measured on most of the Sproul plates. But even as we discount the planetary discoveries reported so far, several comments must be made. First, to credit telescope errors for the "planets" does not mean those central stars have no planetary systems, only that those planets reported so far do not exist. Also, the Sproul telescope, used with an accurate model of its imaging characteristics and sufficient reference stars, probably has the capability to detect extrasolar planets. Finally, these instrumental difficulties in no way indicate a flaw in the astrometric technique in general.

Instead, these experiences indicate that which, with hindsight, seems obvious. If we are to rely on the randomness of residuals, we must first actively remove their systematic errors. No telescope should be blindly trusted to be free of systematic error at the precision of these normal points. This requires gathering observations by time-delineated groups and processing them as a whole into a well-defined standard coordinate system, testing each group for the presence of significant systematic terms (Eichhorn and Williams, 1963) with the latter sensed against a unified least-squares

format (Gatewood and Russell, 1979a). Only in this manner can the accuracy of a normal point be guaranteed to the precision indicated by its statistical weight.

B. Astrometric Precision and Detectable Mass

Paper I concluded that the improved techniques of current astrometry could be used to detect, if present, the Jupiter-like (in mass and orbital period) planets orbiting any of a number of our stellar neighbors. The detectability of extrasolar planets was shown to vary directly with the primary star's parallax and inversely with the two-thirds power of its mass. The arguments presented in Paper I indicate that current techniques are sufficiently precise to detect in a 12-yr study the existence of a Jupiter-like planet orbiting a star with a detection index of 1.0. A survey with three times this sensitivity could detect, with similar confidence, either a planet with one-third the mass or a similar planet orbiting a star with a detection index of one-third.

These approximations are useful in setting up survey observation programs and can be reasonably carried a bit further. We can, for example, form an approximation for the smallest planet which will probably be detected even for the least favorable orientation of the orbit and instrument. Of course, the smallest mass detectable for the average star in the survey will be smaller than this value. We will call the first of these the "detectable mass" and the second, the "average detectable mass." The detectable mass is a useful concept in the individual study where no planet has been found. Here the investigator is not sure of the orientations involved and must assume the worst when stating that planets of a certain mass and orbital period do not accompany a given star. The average detectable mass applies to a sample large enough to assure a meaningful average orientation.

Presently accepted theory and a number of dynamical considerations (Huang, 1973) indicate that planetary orbits generally have small eccentricities. Little error will be encountered then if we assume that the orbits we seek to detect are circular. A 10% difference in the length of the semimajor and semiminor axes does not occur until we encounter the very unlikely eccentricities greater than 0.45, nearly twice that of any in our system.

As seen from a point in the orbital plane of the planetary system, the star's motion, corrected for all other effects, will appear to be oscillatory along a straight line whose length is twice the orbital radius A. It can be shown that the standard deviation about the mean of a large number of error-free positional observations acquired at random times during several orbits of the system is approximately

$$\sigma_o = A/\sqrt{2} \qquad (1)$$

The least detectable position angle for this motion is 45° from either of the axes of the Cartesian coordinate system of the hapless observer. At this angle the perturbation is diminished by sin 45° being spread into the noise of two sets of measures. From equation (1) we see that the standard deviation of this projected motion (σ_p) on either axis is

$$\sigma_p = A/2 \tag{2}$$

If a large number of observations is acquired with a system for which the standard error of a single observation (σ_1) is well known, we can make use of the approximate relationship:

$$\sigma^2 = \sigma_1^2 + \sigma_p^2 \pm \sigma_1^2/2\ (n-4) \tag{3}$$

where σ_p is treated as if it were an independent source of random noise, n is the number of observations, and, as we will see from equation (4), n-4 is the number of degrees of freedom. If the star has been observed for less than several full revolutions of the unseen component, equation (2) will not give a valid approximation of A, but equation (3) may still be used to determine if the effects of an unseen companion have been noted. In this case, σ will increase with the time span of the observations, eventually becoming significantly larger than σ_1.

A series of positions of a star with linear space motion, reduced into the standard coordinates (ξ,η), can be modeled by the expression

$$\xi_t = \xi_o + \mu_\xi t + P_\xi \pi + \frac{\Delta\mu_\xi}{2} t^2 \tag{4}$$

where ξ_t is the position observed at time t, ξ_o is the calculated position at some central epoch t_o, μ_ξ is the best linear (proper) motion, P_ξ is a parallax factor determined by the relative alignments of Earth, Sun, and the star, π is the annual parallax of the star, and $\Delta\mu_\xi$ is the rate of change of its proper motion. (The equations in η are, of course, similar.) The term σ is the standard error of an observation determined from a least-squares solution in which the conditional equation takes the form of equation (4). If the star is single, we will not be able to detect a significant difference between σ and σ_1. Likewise if only a fraction of the orbit is covered by the observations, the standard error of the observations will not be significantly different from the standard error of measurement. The slope of the perturbation will be absorbed into μ, while changes in the slope will be absorbed into $\Delta\mu$; thus at first the perturbations will probably be quite undetectable. However, if new solutions are run from time to time, as the span of the observations approaches an orbital period, an increasing amount of the orbital signal will be noted. In fact the investigator will note that σ increases until approximately one full period has been observed. Then slight variations in σ will be noted until several periods have been observed.

From equations (3) and (4), it can be shown that the number of observations (n) necessary to detect (at a 68% confidence level) the presence of the effects of orbital motion on σ is

$$n = 2\sigma_1^2 A^{-2} + 4 \tag{5}$$

while the detectable mass (m_d) is

$$m_d = 1.4\ \sigma_1\ I^{-1}\ p^{-2/3}\quad (n-4)^{-1/2} \tag{6}$$

where $I = \pi M^{-2/3}$, the detection index derived in Paper I, and π is the star's parallax (in arcsec), P is the period (in yr), and M, its mass (in solar masses). The term σ_1 must be an external estimate (in arcsec), including all sources of random error, and the systematic accuracy of the observations must be actively assured to the precision sought in the reductions. Sensible systematic error will invalidate equations (5) and (6).

In equation (6), n is related to the characteristics of the detector and the apparent magnitude of the target object. In effect the faster or more efficient the detector and the brighter the target and the reference stars, the larger n may be. This can be expressed in an index that will indicate the best choices for a program based on a specific instrument and detector:

$$K = C\ \sqrt{t}/I \tag{7}$$

where t is integration time (in min) and I is the detection index; C may be adjusted so that the relative detectable mass (K) equals 1.0 for some standard object such as Barnard's star — K will then be larger for more difficult target objects, and smaller for easier target objects.

In an individual study of a given region, the residuals in equation (4) are first analyzed for all likely periodicities. Any periods suggested are then used as starting points in an iterative orbital analysis to determine the most significant orbit near each suggested period. Next the viability of each set of parameters is appraised by a test similar to that proposed by Eichhorn and Williams (1963). This test, in effect, asks if the increased parameter variance associated with the terms that describe the proposed orbit (or orbits) is greater than the decrease in residual variance resulting from the added degrees of freedom in the orbital model. The significance of this magnitude comparison may then be translated into a t test form. Thus we derive, over the full range of the observations, a table of all possible orbits and their likelihood of occurrence. Or perhaps even more importantly, when no periodicity is considered indicative of a real orbit, we obtain, with statistical measures of certainty, information on what planets (in terms of orbital period and detectable mass) do not orbit the observed star. The latter information may have as much long-term significance as the discoveries we hope to make.

C. Current Observing Program

To achieve high astrometric precision from a photographic program, we must concentrate our observations on a small number of target objects. A number of considerations suggest that the maximum concentration is obtained

for target regions spaced approximately 2 hr of right ascension. To select the best target objects for our initial effort, we calculated the relative detectable mass for a photographic program for the 300 stars known nearest the Sun. From this, 20 stars in 16 regions were chosen and placed on an intensive program which began in the fall of 1976. These objects (denoted with an asterisk in table 1), are observed during the 2 hr preceding and following midnight, time not used in the trigonometric parallax program.

During its first 3 yr, this survey has achieved an average precision of 5 marcsec, standard error per season per star. This exceeds the combined average weight of the three-telescope study of Barnard's star detailed in Paper I, the most extensive published astrometric study to date, and reaches the average sensitivity originally sought. If the observing time was evenly distributed, and the program continued for 12 yr, the detectable mass for each target star would be 0.16 mS times the value of K listed for it in table 2. Unfortunately, the coverage has varied somewhat more than expected, the brighter stars at smaller zenith distances acquiring more good exposures than expected while others received less than hoped. This situation has been partially corrected by a redistribution of observing time and will be further aided by the addition of an automatic tracker.

Most of the survey stars, 65%, are included on a sizeable number of early plates in the Allegheny Observatory plate file. Although of lower concentration and regularity, these observations allow us to better determine the time-dependent parameters of proper motion and perspective acceleration, thus lowering the parameter variance of each study and increasing its sensitivity to small perturbations. This material is also of value in our attempt to find long-period orbits. From equation (6) we note that m_d is proportional to the -2/3 power of the orbital period. Thus for a given astrometric sensitivity, the detectable mass is diminished by over two if its orbital period is three times longer. By the same arguments, we note from equation (6) that, as a continuing survey follows the motion of a star long enough for a planet to complete longer and longer orbits, the detectable mass decreases more rapidly than the inverse of the span of the observations, or $m_d \propto T^{-7/6}$.

The available plate material has been measured and analyzed for Barnard's star (Gatewood, 1976), Lalande 21185 (Gatewood, 1974), van Maanen's star (Gatewood and Russell, 1974), and Epsilon Eridani and Tau Ceti (Gatewood and Russell, 1979b). The residuals of van Maanen's star and Tau Ceti are both suggestive of unseen (probably stellar) companions, but the data are not sufficient for the calculations of orbits.

Both the sensitivity and program size will be increased significantly if the detector discussed below succeeds. In anticipation of its success the unmarked stars in table 1 are being added to the current program. As will be noted below, the photometric characteristics of the new detector are radically different from those of the photographic plate and the precision per measurement is nearly constant for stars over a wide range of apparent magnitudes. Thus the latter additions to table 1 are selected by their detection index alone and, to prevent confusion, K has been omitted. These

stars bring the total to 35 stars in 27 regions, 55% of which have a sizeable collection of early plates in the Allegheny Observatory plate file.

D. Extension of Survey to a Large Sample

Our understanding of planetary systems generally depends on our ability to determine the frequency of occurrence of orbital characteristics and mass distributions of planetary systems orbiting stars of all spectral types and masses. This task is best accomplished by studying, at least at first, a homogeneous sample. Stars in the vicinity of the Sun are, to a good approximation, a valid cross section of those found throughout the spiral arms of the galaxy. It appeals to reason that, for any given mass and orbital period, the smallest detectable planetary mass will be found by directing our study to the nearest stars. This is quantitatively apparent from equation (6), which may be written as

$$m_d = 1.4\ \sigma_1 \pi^{-1}\ M^{2/3}\ p^{-2/3}\ (n-4)^{-1/2} \qquad (6a)$$

Thus, to give the maximum range to the masses which can be detected for each type of star, parallax should be made a prime factor in the selection of the stars to be included in future observation programs.

To obtain a sample of approximately 500 stars, the survey will have to be extended to parallaxes as small as 80 marcsec or to a distance of 40 light years. Within this distance of the Sun there are approximately 10 A, 16 B, 50 G, 80 K, and 330 M type main sequence or near main sequence (luminosity classes IV, V, and VI) stars. The detection indices of these stars range from 0.06 to 3.21. Thus current photographic techniques could be employed to survey a small sample of even the most massive and most distant stars in this group to a detectable mass as small as 5 or 10 mS.

However, a general understanding of planetary systems will require a detailed knowledge of several dozen planetary systems to masses as small as that of Earth and periods shorter than 1 yr. To survey the large sample necessary to find these planetary systems and to obtain the extreme precisions necessary to detect and study their smaller masses will require specially designed, fully dedicated instrumentation such as discussed below.

PHOTOGRAPHIC TESTING OF SOURCES OF ERROR IN SURVEY

A. Random Errors Caused by Photographic Plate

For over a century (Gould, 1866), the photographic plate has served as the prime detector for long-focus astrometry. Although its quantum efficiency and resolution are not high by today's standards, it allows integration of the light intensity in all parts of the field simultaneously. This latter feature is absolutely necessary for systems operating beneath Earth's atmosphere in the presence of constant variations in atmospheric refraction and instrumental tracking. However, the photographic process has been suspected as a source of both random and systematic error (Land, 1944; van Altena, 1974; Levinson and Ianna, 1977).

In our examination of the relative importance of the photographic plate in the formation of the standard error of a position reduced from the measurement of an average exposure, we adopt the expression

$$\sigma^2 = \sigma_A^2 t^{-1} + \sigma_B^2 \tag{8}$$

where σ^2 is the variance of the exposure, σ_A^2 is the dependence of σ^2 on the inverse of exposure time t, and σ_B^2 is that portion of σ^2 which is independent of the integration time; σ_A is essentially the standard error due to the rapid variations in the refractive properties of the atmosphere in the line of sight, while σ_B is the standard error of the detector. That σ_B does not contain significant contributions from slowly varying unmodeled parameters of the Allegheny telescope's optical system and that the -1 power of t is correct to much smaller variances than we are dealing with here is shown later by an intercomparison of the nightly mean positions of field stars.

Points 1 through 4 in figure 1 are each the mean standard error of an average exposure t determined from several hundred plates with t near the indicated means. The value of σ does not show a convincing dependence on t, changing little for exposures as short as 45 sec (point 1). A least-squares reduction of equation (8) to these points yields $\sigma_A = 64 \pm 47$ marcsec and $\sigma_B = 34 \pm 5$ marcsec, where t is in seconds. This leaves σ_A poorly established but indicates the importance of σ_B in photographic work.

Two methods were employed to better determine σ_A. The camera was not originally designed to take exposures as short as 1 or 2 sec, so we used a test based on star trails. The telescope was turned to a region of bright stars, a 1-min exposure taken, the shutter closed, and the drive turned off. Once all drive motion had ceased, the shutter was reopened and the star's motion across the focal plane recorded. By measuring the relative north-south positions of the trailed stars, starting at some arbitrary distance from the position indicated by their 1-min exposure and advancing 50 μm

along the axis of motion between sets of measurements, we were able to determine the distortions caused by the atmosphere every 0.05 sec of time. These measurements revealed much of interest (KenKnight et al., 1977). In particular, they yielded the standard error of a 1-sec exposure, point 5 on figure 1. Points 6 and 7 result from the reduction of plates taken after alterations to the camera, with 1- and 2-sec exposures of the standard region centered on the Praesepe cluster (Russell, 1976). Utilizing these new data at one-half weight each, a new least-squares reduction for the parameters in equation (8) revealed that $\sigma_A = 61 \pm 6$ marcsec and $\sigma_B = 33 \pm 4$ marcsec.

Thus the positional information transmitted by the atmosphere through the Thaw 76-cm photographic refractor at its Pittsburgh site has a potential precision of approximately 1 marcsec/hr of observation. Under favorable circumstances the current program achieves a normal point with a precision of about 7 marcsec/hr (standard error). Based on thse facts, we are currently detector-limited.

B. Astrometric Errors Caused by Atmosphere

The effects of Earth's atmosphere on astrometric precision have been studied in some detail by a number of authors, for example, Schlesinger (1916), Hudson (1929), KenKnight et al. (1977), and doubtlessly others. Our own studies have added several points of information which will be useful in the present discussion.

The multiple-star trail plates discussed earlier allow a study of correlated image motion across the field of the instrument. Schlesinger and Hudson studied the average offset of images from trail plates for intervals of several seconds, finding oscillatory motion with a period of approximately 1 min. This motion was nearly perfectly correlated across their plates. KenKnight et al. found similar patterns of image motion with periods near 1 sec (fig. 2) and near 5 min, with much longer period motions indicated. Besides the oscillatory motion we also found "periodic" variations in the field scale at both periodicities (figs. 3 and 4), which indicate a refractive wave nature for the responsible phenomena and indicate the need for modeling to remove their effects from astrometric positions.

Figure 5 shows the correlation in image motion, measured each 0.05 second, versus field separation. This correlation is related to seeing quality, consistently increasing in periods of bad seeing. This factor has not been removed from figure 5 and is responsible for much of the apparent scatter. Nevertheless, two major features are apparent. There is a large range of separations (from 0.25° to over 1°) over which the correlation is nearly constant at a coefficient near 0.4, and there is an area of increasing correlation for separations less than 0.25°, approaching 0.9 at separations of several arcseconds.

The standard error of a single trail about its line of motion averages 190 marcsec per second of time. By averaging the star trail measurements for greater or lesser periods than 1 sec and then finding the standard deviations of these averages, we find that this value varies inversely with the fourth root of the integration period. An inverse-square root relationship in the quantity would indicate random variation about the line of motion. Inspection of figure 2 shows that the motion of the five star trails shown there are highly nonrandom.

The standard error of the difference between the positions of two stars depends on the separation between the stars. For two stars separated by 7.3 arcsec we found this value to be 56 marcsec per second of time, with the value growing rapidly at greater separations. However, for the close pair, the standard error of the difference varies inversely with the third root of the integration period, indicating that the differences are more nearly random than the absolute motion of either star about its trail. At greater separations the inverse third root character deteriorates toward an inverse fourth root. The reason for the still present nonrandom effect is what we call "scaling," indicated in figure 3 (KenKnight et al., 1977).

The presence of the scale term was found by constants, not unlike plate constants, determined by reducing the instantaneous deflections of multiple stars trails (like those shown in fig. 2) to their known positions in the Praesepe Astrometric Standard Catalog (Russell, 1976). The average 1-sec mean residual from those modeled positions has a standard deviation of 70 marcsec. This is in good agreement with the average standard error of 1-sec exposures of the standard region which have been measured and reduced by standard techniques (fig. 1). Over the range studied by trail plates, the means of the residuals of these solutions follow an inverse-square-root law in n and appear random. Thus, allowing for both shifts in zero point and scaling greatly increases our ability to predict the position of an image relative to that of its neighbors.

C. Potential Nightly Precision

To test how far the latter effect holds, and thus the ultimate precision obtainable per night from high-speed measurements, modeled as noted, we acquired an average of 42 1-min exposures per night, for several nights, of the same star field. The standard error of each field star position about its mean was then determined. As noted from figure 2, the standard error of a single averge 1-min exposure with the Thaw refractor is 34 marcsec. The average standard deviation of the exposures acquired on each night was found to be 5.4 marcsec, a value very near that predicted by an inverse-square-root law (t^{-1} in expression (8)). This result suggests that the still unmodeled nonrandom effects in the Thaw telescope's optical system are less than a few milliarcseconds, therefore not affecting σ_B^2 in expression (8), and that the estimated precision of the proposed detector (see next section) combined with the Thaw will on the average be considerably better than the best obtained to date.

D. Modeling Instrumental Projection

If very high precision positions are to be obtained from a given astrometric telescope, it must be possible to model the imaged field of that instrument with an affine transformation (plus any necessary higher order terms) so that the measured field position of an image may be transformed into the relative position of a star. The precision with which this can be done is a function of (1) the errors of the detector and measuring device, (2) the number of relevant parameters in the reduction model, (3) the secular constancy of the relevant parameters, and (4) the number of reference stars measured.

To calibrate various presently and previously used astrometric telescopes to one another, we borrowed and measured 120 plates, from 15 telescopes spanning 113 years of observations, of the region of the Praesepe cluster. To ensure a wide separation of effects, we measured 200 noncluster members, picking those that fell well off the cluster's H-R diagram. Thus the 408 stars measured in the region are practically free of a color-magnitude correlation over their 10 apparent magnitude, 2.0 magnitude color index range. An absolute reference frame was established using the positions of 138 stars which appear in a wide variety of meridian and photographic catalogs.

By careful intercomparison of the positions obtained for these stars from the measurements of each telescope, with the reference frame positions and with the positions obtained by averaging the results of all of the other telescopes, we were able to derive the parameters of each instrument and often to estimate the consistency of those parameters. For existent telescopes, the required number of parameters varied from three to eight. This number is directly related to the number of reference stars that must be measured to yield an acceptably low parameter variance (Eichhorn and Williams, 1963). However, assuming an order of consistency in these parameters similar to that found in the Praesepe study, and providing that the proper models are used with a sufficient number of reference stars being measured, we find that high-precision field positions can be obtained with any existing long-focus instrument.

In summary, our photographic tests indicate that: (1) the highly correlated, atmospherically induced wavelike motion of star images may be modeled (by parameters similar to those of a standard plate constant reduction) to precisions of approximately 1 marcsec/hr, (2) the inverse-square-root law holds for properly reduced observations to values as low as 5.4 marcsec, indicating that the remaining systematic errors of the Thaw telescopes are less than a few milliarcseconds, and (3) with a sufficient number of reference stars and proper reduction of systematic errors, existing astrometric telescopes could achieve precisions well in excess of those now obtained.

Two conclusions important for the tests outlined later pertain only to the single star trail. We note that the standard error of 1 sec averaged positions along a trail is approximately 190 marcsec, and, if we take longer

averages of the deflections, the standard error decreases with the inverse fourth root of the integration period.

MULTICHANNEL ASTROMETRIC PHOTOMETER (MAP)

The multichannel astrometric photometer (MAP) is a proposed photoelectric measuring device that meets all the criteria for an astrometric detector, i.e., it has high spatial resolution and quantum efficiency, it is free from sensible systematic and random errors, and it provides concurrent records of a sufficient number of reference stars to allow optimum use of the optical system. The MAP is two orders of magnitude more efficient than the photographic plate and will yield, with increased resolution, the real-time relative positions of stars up to 2.5 magnitudes fainter. In essence the MAP converts the measurement of relative positions to the measurement of phase shifts of electronic signals. Its success is virtually assured because it requires no complicated or untried technologies.

The MAP was inspired by Drake's suggestion that precise positions could be obtained by photoelectric timing of stellar transits (Drake, 1975). Consider the brightness measurements obtained with a photomultiplier tube placed behind a Ronchi ruling located in the focal plane of a telescope. As a ruling line, moving perpendicular to its length, cuts a star image, the objective appears to darken as in a Foucault test. If the ruling line is slightly smaller than the image, the objective will not go completely dark but will pass through a minimum; if the transparent spaces between the lines have a similar width, the observed illumination will approach a similar maximum. This variation in brightness plotted against time is represented by the solid line in figure 6. If the ruling is long enough and a second photomultiplier tube is placed behind a second image, the observed brightness variations plotted against the same time standard may be similar to those represented by the dashed line in figure 6. Assuming that the approximate distance between the two stars is known to the nearest whole number of ruling lines, the exact distance can be estimated in terms of this number of lines and the phase difference of the patterns (figs. 7(a) and 7(b)).

This principle may be extended to a large number of stars. In essence the MAP modulates the apparent brightness of the reference and target stars against a high-precision, rigid spatial metric, the Ronchi ruling. These brightness variations are amenable to a translation and rotation transformation that reveals the ruling's instantaneous location with respect to its mean on that star field. Fortunately, this transformation, which may be expanded to allow for linear and second-order scale variations as well as tilt of the ruling out of the focal plane, is identical in form to the terms required to gnomonically map the apparent instantaneous positions of the field stars against their mean positions. Thus the errors of the measuring device are absorbed into the star field reduction (similar to plate constants) without an increase in the parameter variance.

The MAP's ability to yield a virtually constant flow of positional information about the target star and a moderate number of reference stars sets it apart from the several other photoelectric detectors that have been proposed. Two of these, proposed by van Altena (1974) and Connes (1978), would determine the positions of the target stars with respect to the average positions of a large number of reference stars, thus losing the individual reference star positions and along with them the ability to model the imaging characteristics of the optical system and passing refractive anomalies. The AMAS (Frederick et al., 1974) would provide the individual star positions, but the need to deconvolve these from the complex signal obtained by viewing the entire field with a single photometer through a rotating Ronchi ruling suggests that the astrometrist will have to be content with the positions of the several brightest stars in the field. In contrast, the MAP takes full advantage of high-speed computer and photoelectric technology to yield all of the dimensional information available for each and every star selected by the astrometrist (fig. 8).

Allowing for the effects of photon noise, Drake has developed an expression for the accuracy with which the centroid of the photocell response can be located. The expression for positional error ε may be shown to be

$$\varepsilon = \frac{\lambda\omega}{D^2\sqrt{\pi m E I \tau}} \tag{9}$$

where λ is the central wavelength of observations, ω is the ratio of image size to the diffraction-limited size, D is the objective diameter, m is the time of observation during which half or more of the star's radiation is passed by the ruling, E is the quantum efficiency of the detector, I is the photon flux in the wavelength band observed, and τ is the integration period.

Using expression (9) for a 15th magnitude star measured with the 76-cm Thaw refractor using an 800-Å bandpass, $\omega = 5$, $E = 0.23$, we find $\varepsilon = 1.0$ marcsec on each axis during 10 min of observation. The effects of atmospheric seeing during this period, that required to secure a positional accuracy for this star of 34 marcsec photographically, is 3.5 marcsec on each axis. Thus, even at the 15th magnitude, photon statistics are not an important error source. If we assume that the ruling lines are each known to within 2 μm for a temperature-exposed ruling, the MAP-Thaw combination should develop a precision of approximately 4 marcsec within 10 min of observation. Since the Thaw is exposed to all effects of its environment, it is doubtful that an annual precision exceeding 1 marcsec can be achieved, but this would be a factor of 3 improvement over the best presently attainable.

An added advantage of the MAP is that it will be possible to improve our knowledge of the exact spacings of the lines of the ruling as the MAP is used. Each measurement of the distance between two stars yields the relative positions of the lines with which the measurements were made. Actually, each centroid determination with a 12-channel MAP would yield the relative positions of each line with respect to the 11 other lines used for that measurement. If we make the ruling more than twice the size of the field to be measured, we can determine with great redundancy the location of every line

on it. A measuring session with the MAP, which would consist of a double sweep (forward and reverse) of the field in each of 4 ruling positions (90° apart), would provide nearly 10^5 centroid determinations and 10^6 intercomparisons of line positions. After a few years of usage, the relative position of each ruling line will be known to a precision limited only by the stability of the material on which the ruling has been formed.

The MAP may also be used for the real-time calibration of the focal plane of the telescope. Because it measures the relative positions of all stars simultaneously, it will be possible to let them drift slowly about the field. This will require following the motion with the apparatus carrying the light pickups, but not with high precision; a half-millimeter error should go unnoticed. As the field drifts, the instantaneous nongnomonic characteristics of the optical system would show as deformations of the apparent positions of the reference stars. The effect would be similar to studying the field of an astrograph with a very large number of overlapping plates. Assuming a reasonable number of imaging parameters, the precision with which the field could be mapped greatly exceeds that with which the measurements themselves are made. This adds directly to our ability to model the systematic errors of the optical system and presents the very real probability that existing astrometric telescopes will be able to achieve precisions beyond all expectations of their designers.

IMAGE TRAILER — A SINGLE-CHANNEL MAP

The image trailer (IT) was devised to confirm our approach to the concept of photoelectric centering and its implementation. This single-channel MAP records the modulation of the apparent intensity of a star image as it is trailed (by Earth's rotation) across a focal plane Ronchi ruling. The opaque lines, and the transparent lines between them, have widths approximately equal to the diameter of the star image, so the brightness variations plotted against time mimic a sine wave. Of course, the brightness variations are a function of the image's position on the ruling and thus relate time to focal plane position, or through the focal length of the telescope, time is related to angle. This is the principle of the MAP. Because it carries the most information, we define the center of the brightness wave as that point in time, approximately halfway between two minima, that divides the photon counts into halves. Hence we must observe the brightness as a function of time.

The IT accomplishes this with an equipment train consisting of a small 4-line pair per millimeter Ronchi ruling, an EMI bialkali (blue-sensitive) photomultiplier tube, a Princeton Applied Research 1120 amplifier/discriminator, a PAR-1109 photon counter, an LSI-11 computer, an LA 36 Decwriter, and a paper tape reader/punch (fig. 9). The photomultiplier tube is encased in an uncooled housing with a Fabry lens positioned to focus a 37-mm^2 image of the telescope's objective on the 80-mm^2 cathode of the tube. (The dark current of this tube, uncooled, is only 10 counts/sec.)

Between the Fabry lens and the focal plane of the telescope, within the tube housing, is a mirror and a pair of transfer lenses. These can be inserted into the beam to bring an image of the field to a reticled eyepiece (not shown in fig. 9).

To operate the IT, the telescope is pointed slightly to the west of a star and the electronics are activated. Next the refractor's main drive is turned off and the telescope is allowed to come to a rest position. The image of the star (approximately 0.12 mm in diameter in 1.5 arcsec seeing) now drifts across the focal plane at the rate

$$\frac{dx}{dt} = \frac{15}{14.60} \cos \delta \tag{10}$$

where dx/dt is in millimeters per sidereal seconds, 14.60 is the mean focal plane scale of the 30-inch refractor in arcsec/mm, and δ is the apparent declination of the star. As the star image drifts onto the center of the reticle, the x guiding motor on the tailpiece (whose translator rate has been set for the declination of the star) is turned on. This motion will keep the image of the telescope objective near the cathode's central area.

A star with a declination of approximately 13° drifts across 1 mm of ruling per second of time, producing a 4-Hz signal. With the integration period of the photon counter set at 15 msec, approximately 17 samples of the apparent intensity are obtained for each pulse determination. For a 12.5 magnitude star the count rate varies from 1 or 2 counter/sample to nearly 60 as the star's image passes over the center of a transparent line.

We define the pulse center, the time at which the image is central to the transparent line, as

$$t_c = \frac{\Sigma\ c_i\ t_i}{\Sigma\ c_i} \tag{11}$$

where the summations are between successive minima, c_i is the count of the ith sample, and t_i is the central time of the ith sample. Because there are 4 line pairs per millimeter of ruling, the pulse centers occur every 3.65 arcsec of image motion.

The ruling that modulates the light is a metal deposit on glass with relative line spacings and edges accurate to better than 1 μm. The IT's clock is based on a quartz crystal and the main motion of the image is caused by Earth's rotation. The imaging characteristics of the photographic refractor are well known and may be taken as strictly gnomonic near the center of the field where the IT operates. Photon statistics and the noise caused by dark counts do not become significant at magnitudes brighter than 16.7. Thus pulse errors larger than a few microns or, approximately 30 marcsec, should be primarily due to the atmosphere.

To determine the error of a pulse, the pulse centers (times of central passage of the image over a transparent line) were fitted to a linear model in time. This proved of sufficient precision, at all observed declinations,

for the short trails observed. The standard deviations of the residuals to these least-squares solutions are plotted in figure 10 against pulse duration (effectively, the declination of the region observed).

The success of the IT may be surmised from a comparison of two features in figure 10 with characteristics of single star trails noted earlier. First, the best fit line in figure 10 passes through 1 sec at 170 marcsec, insignificantly more precise than the average 1-sec standard deviation of all the single star trail data. Second, the power law is identical, the fourth root of t, to that of the single star trail plate data. This agreement indicates that, like photographic plates, at these short integration periods the errors caused by the detector are considerably less important than those caused by atmospheric seeing.

One area in which our tests indicate a significant advantage over the trail plate is in the magnitude of the trailed objects. A star fainter than 5th magnitude leaves a photographic trail too faint to measure. The IT, on the other hand, can track objects more than 10 magnitudes fainter. This gain is reasonable but still startling. Its implications are that a MAP-equipped Thaw refractor will be able to study 15th and 16th magnitude objects with virtually the same precision as it can measure objects many magnitudes brighter. This is certainly not the case in the current photographic program, where the number of exposures obtainable per night is highly dependent on the magnitude.

The success of the IT has shown that: (1) the relative focal plane position of a star image can be found photoelectrically, (2) star positions can be determined during an interval short in comparison to the time required for atmospheric seeing features to change, and (3) the high quantum efficiency of the photoelectric photometer will allow a MAP to measure, with a given telescope and at full precision, the positions of stars many times fainter than normally included on their photographic programs. For further discussion of the IT, see Stein (1978).

COMMENTS ON ASTROMETRIC INTERFEROMETERS

With their ability to span many cells of atmospheric turbulence, long baseline interferometers offer some degree of immunity to the effects of astronomical seeing. Unfortunately, they are not readily adapted to high-accuracy astrometry, which requires the establishment of a suitable reference frame. Furthermore, the dimension that defines their advantage over seeing limits their application in the study of the nearest and most interesting stars.

The development of the interferometer from its original applications (Michelson, 1920) to a device of interest to astrometry began with a series of papers by Miller (1966, 1968, 1970, and 1971) with later modifications by Currie et al., (1974) and by Shao (1978). However, to our knowledge, the

only interferometer designed specifically as an astrometric instrument resulted from the NASA-sponsored Stanford-Ames study on Project Orion (Black, 1980). Operating as an expansion of the astrometric imaging interferometer proposed by Gatewood (1976), the Orion device uses focal plane separations instead of the delay lines proposed by Miller. Although relatively massive and complex, this system offers several critical advantages over earlier proposals. Through its ability to determine focal plane positions, the 50-m interferometer is able to track the simultaneous positions of 20 or more stars in a given region. Thus it is able to model, much as is done in current long-focus astrometry, the effects of refraction and its anomalies directly, at the full precision of the observations. The detrimental effects of the optical system can be modeled from the apparent distortion it causes in the relative positions of these stars as they sweep through the field. Furthermore, the 20 or so reference stars define a catalog system in which the motion of the target star and each of the reference stars can be accurately defined.

In comparison, previously proposed systems would observe only one star at a time, either evaluating the direct and differential effects of refraction and its anomalies by the rapid successive observation of a handful of stars, or by observing the target object and a few reference stars in several widely spaced colors. The former technique has lost favor because of the need to observe at least seven stars every few minutes. This is a difficult procedure amidst the complexities of not only finding fringes but estimating their distance from the central fringe or, in one case, where one is on the fringe envelopes. The approach of observing in several wavelengths is more workable than that of shifting rapidly between several stars, but it carries with it a heavy penalty. The refractive indices of the observable colors only differ by approximately 1/50 of their mean value. Thus, to approximate the nonrefracted, above atmosphere position, the computer must extrapolate to a point that lies nearly 50 times outside the range of observation. Hence both the accidental and systematic errors of the observation are magnified by this factor. While some of the resultant increased random error may be overcome by repeated observation, no such reprieve is possible for the loss of systematic precision. Finally, these proposed interferometers are limited by time to a few reference stars in each region. Thus, the individual peculiarities of each star's motion are more difficult to find and model against their mean system. This presents the very real possibility of misinterpretation of the data.

Despite the advantages of the Orion concept, the size of the structure and the complexity of some of its subsystems suggest that lead times of many years would be necessary for successful funding and construction. Furthermore, interferometers suffer from a paradox. Generally, both their precision and the distance of source resolution vary approximately as the length of their baseline. (The situation is actually worse for baselines less than 50 m where the resolution increases much more rapidly with baseline than does astrometric precision.) Resolution is noted by the loss of fringe detection, with the signal being significantly reduced well before resolution (Anderson, 1920). Thus as one increases the baseline to gain precision he also increases the distance to the nearest stars for which the interferometer can

determine astrometric positions. But equation (6a) implies, all other things being equal, that

$$m_d \propto \pi^{-1} \tag{12}$$

Hence, the detectable mass is not generally a function of the baseline of the interferometer. As a consequence, if their practical problems can be overcome, interferometers will probably be employed in surveys to detect massive planets at relatively large distances, but will be of little use in the type of survey we propose below.

Equations (9) and (12) suggest that the smallest detectable masses will be found by diffraction-limited full apertures whose effective baseline is less than 10 m.

81-cm REFRACTOR

The instrument recommended in this section is a state-of-the-art variant of the 76-cm Thaw telescope. It is relatively inexpensive, approximately 10% of the cost of the Orion interferometer mentioned above, with a nightly precision per object approaching that projected for the interferometer and, because it relies on proven technology, it has a high probability of success.

Our approach has been to examine existent astrometric systems to determine their strengths and weaknesses and to find where six decades of technological evolution could improve their general design. The continuity gained in this manner lessens the chance of catastrophic oversights, while our possession of the arts of modern electronic and material engineering virtually assures substantial progress. The long success of existing systems can be attributed to several factors:

(1) Use of a single optical system for the simultaneous formation of the images of the target object and a moderate number of reference stars;

(2) Placement of all optical components at the pupil of the system;

(3) Simultaneous focal plane detection of the apparent relative positions and brightness of the target object and reference stars;

(4) Reduction of the observations using conditional equations with sufficient flexibility to model the significant effects of precision, mutation, stellar aberration, variations of latitude, general refraction, differential refraction, atmospheric scaling and/or displacement, variation of focal length, tilt of the optical axis and/or components, distortion, field curvature, and magnitude and/or color displacement and/or magnification.

Limiting these systems are observational errors arising from random variations in the detector and the astmosphere and the subjugation of the optical components to environmental variations. These errors enter at two levels. The first, and largest, are purely random in nature and can be diminished by repeated observation. The second error can affect groups of observations, slightly biasing their mean. The time extent of this second grouping ranges from those identified as "night errors" (Land, 1944) to the "discontinuities" associated with the occasional realignment of the optical components of a system (Gatewood and Eichhorn, 1973; Hershey, 1973; Gatewood, 1976; Heintz, 1976).

Figure 11 shows the major features of an optical system that shields the active components from the influences of its environment while incorporating the advantageous features of existing systems. To eliminate temperature variations in these components, they have been placed in a thermally controlled cell with an infrared coating on the front window of the system. Since a temperature difference between the glass and adjacent air would cause a deformation of the lens surface and cause local turbulence, the elements have been sealed in a light vacuum. To eliminate variations in the gravity vector, they have been placed so that their optical axis is parallel with Earth's axis of rotation and light from the target and reference stars are brought to the system by a single flat mirror. The necessary diameter of this mirror and its mounting requirements are minimized by placing it below the optical system. Made of a nearly temperature inert substance, the siderostat has a planned limited motion of $\pm 8^{\circ}$ from the meridian and only requires a declination motion of $\pm 18^{\circ}$ to survey 95% of a hemisphere. Like existing instruments, this one would (1) utilize a single optical system to image the simultaneous relative positions of the target and reference stars, (2) place all active optical elements at the system's pupil, (3) use a detector, the MAP, that simultaneously records the relative positions of the target and reference stars, and (4) allow the use of a truncated conditional equation to model all effects that can significantly affect the measured positions.

Combined with the high quantum efficiency of the MAP, the 81-cm objective would gather sufficient photons for high-speed positional determination of stars as faint as visual magnitude 17, thus eliminating the need for a large field and the associated complex objective design. The field scale is 10 arcsec mm^{-1}, giving the system a focal ratio of 25.3. At such ratios all optical surfaces can be spherical and the curvatures slight. Secondary spectra could be kept within the Airy disk of the system over a bandpass of 4700 to 5300 Å by the proper choice of optical glasses, such as Schott SKII and KZF2.

The siderostat is the only component more than a few percent of the focal length of the system from the optical pupil. Hence, variations in its surface do not affect all stars equally, but cause an apparent scale variation. The smoothness of this variation depends on the linear abruptness and magnitude of the surface features. Preliminary calculations indicate that abrupt variations of 0.05 wave can be modeled to better than 0.04 marcsec and, if constant, may be prereduced from the data. A feasibility study of this system conducted by the Boller and Chivens Division of the Perkin-Elmer

Corporation indicated that such tolerances could be met. They noted that the 1.75-m circular flat (only an elliptical portion will be used) was actually easier to mount than a Cassegrain primary. An air flotation system with push-pull gravity-actuated side supports was recommended.

A SPACEBORNE ASTROMETRIC INSTRUMENT

Four sources of observational error are encountered by a spaceborne astrometric instrument, but we believe that, with careful attention to detail, their combined effect can be reduced below the signal produced by an Earth-mass planet orbiting within the ecoshell of a star at 12 parsec. The errors originate in the instrumentation, photon statistics, reference frame, and astrophysical phenomena that shift the photocenter of the primary star.

The latter, star spots for example, would cause small but perceptible shifts in the photocenter of the star. The effects of large spots can be modeled and reduced from the observations. These are distinct in that they have similar, probably short, periods and show for only half a rotation. Analysis of their motion will reveal the stellar rotation rate, the direction of the star's axis of rotation, and the latitude of the surface feature. Large numbers of small spots would cause a quasi-random variation in the apparent position of the photocenter which, in the case of the Sun, might mask the existence of the planet Mercury.

Another limitation is the stability of the reference frame. With the precisions sought, each reference star's motion will reveal a number of parameters. Depending on the complexity of its relative motion, it can be represented by focal plane equations similar to equation (4), to which terms will be added to model the orbital motion of the primary of an unresolved binary system. For extended observation at the potential precision of a spaceborne instrument, most of the reference stars will require all of these terms to describe their past, and thus to predict their future, positions. But the variance to the parameters is a function of the number of observations and will, if a sufficient number of reference stars are observed, gradually decrease so that eventually almost any desired precision can be obtained.

Photon statistics are the ultimate limitation on any observational effort in that the positional data is carried by the electromagnetic radiation. Equation (9) shows that, all other things being equal, the theoretical precision of a spaceborne instrument goes as the second power of its aperture and approximately as the square root of its effective bandpass. Thus aperture and bandpass will be very important aspects of any spaceborne astrometric instrumentation.

Finally, there are limitations that depend on the design and engineering of the instrument itself. At first glance, these would seem to be the bane of the entire effort. However, if we return to the basic principles of

high-precision astrometry outlined earlier and carry them to the extreme, we find the question of not whether such instruments can be built but rather when they will be built. The provisions for simultaneous observation and careful modeling will be similar to those on the ground, and one optical system will image the entire region. However, we must now strictly enforce the condition that all optical components are at the pupil of the system. That portion of the optics that can be seen from all extremes of the instrument's field affects all stars similarly and, if the optical system is better than diffraction-limited, variations in the characteristics of the nonvignetted optics, unless they exceed approximately 1/8 wave, will not introduce new forms of systematic error. Thus there is a range in which a good optical surface may vary, causing only a variation in the magnitude of the terms, but not the form of the equation that models the imaging of the instrument.

This latter requirement determines the design of the instrument. Only a simple reflector has all of its optics directly in the pupil, and to be diffraction-limited over an extended field it must be of long focal ratio. The necessary focal length increases rapidly with aperture while the potential precision is a function of the aperture — hence the greater the required precision, the larger the required instrument.

Specifically, the optical component of the spaceborne astrometric survey instrument (SASI) would be formed from a single parabolized disk of zero expansion material such as CER-VIT with a diameter of approximately 2.1 m. To achieve a reasonable field in which the effects of coma and astigmatism are confined to the diffraction pattern of the aperture will require a focal ratio of approximately 20, or a focal length of 42 m. Fortunately, the required satellite platform is quite light so that the several sections may be telescoped into each other and opened automatically after being placed in orbit by the Space Shuttle. The measuring device, similar in every respect to the MAP described earlier, is placed directly in the primary focal plane facing the aperture. Because the ruling would otherwise define the inner edge of the aperture, the central portion of the primary under the ruling is covered along the axis being measured (fig. 12). The ruling spacing is approximately 140 μm. The bandpass will be 4000 Å, centered near 5000 Å, with a light-collecting area equal to that of a 1.37-m mirror, allowing the study of objects as faint as 20th magnitude. The perpendicularity of the ruling to the optical axis is less critical than it would be if it were not reduced by the equation of condition, but accurate focus is important. This may be achieved with a light frame of low expansion metal and near zero expansion ceramic spacers. Alternately, laser ranging active controls could maintain the focus with precision orders of magnitude greater than necessary.

The MAP seems to be the ideal detector for this spaceborne instrument. Its digitally encoded output is easily transmitted to the ground, and backups for its components are simplified by its redundancy. But, most important, the precision of the MAP can be matched to that of the photon statistics. As we have noted, the MAP is a self-improving measuring device. Every measuring session reveals as much about its metric, the Ronchi ruling, as about the star field studied. Nevertheless, there will be some error associated with our knowledge of the exact position of the ruling's lines. There is also an error associated with the photon statistics. This is approximately the same

as indicated by equation (9), from which we find, for a 15th magnitude star, there will be a measuring error of 0.3 marcsec/sec. If the central position of each ruling line is known to 1μ, the error caused by the ruling will equal that from photon statistics when we measure the position against 3 lines/sec. With the double forward and reverse motions of the ruling mentioned above, approximately 3 hr of measurements can be made with the ruling before the same lines are once again situated over the same field stars. During this period of independent measurements, the data stream will have a precision of 0.002 marcsec (2μ arcsec), approximately the size of the effect an Earth-mass planet in a 1-yr orbit would have on Alpha Centauri.

With its ability to make nearly continuous observations in orbit, the SASI may allow us to make a systematic search for Earth-like planets. From our admittedly biased point of view, to be Earth-like implies to be of similar mass and temperature. (Note that we have defined Jupiter-like as having mass and orbital similar to Jupiter's.) This requires us to include an estimate of the primary star's illumination in our calculations, but it gives us the ability to estimate the difficulty or ease of detecting a planet, if orbiting a given star, on which life might thrive. Of most interest are the main sequence stars. For these, assuming the mass-luminosity relationship of Harris et al. (1963), we find that for stars whose abolute magnitude is less than 7.5, the size of the perturbation induced in the apparent motion of the primary star is

$$A = 3 \times 10^{-6} \pi M \quad \text{(arcsec)} \tag{13a}$$

from which we note that Jupiter is 1650 times easier to detect than Earth. Similarly, we may write a detection index for Earth-like planets as

$$I_o = \pi M \tag{14a}$$

The period P of such a planet's orbit is approximately $P = M^{3.5}$, where M is in solar masses and P is years.

For K and M stars, whose absolute magnitude exceeds 7.5, we have

$$A = (2.3 \times 10^{-6}) \pi M^{0.4} \tag{13b}$$

and

$$I_o = 0.76 \pi M^{0.4} \tag{14b}$$

where Earth-like planets have orbital periods of $P = 0.66 M^{2.6}$ yr. It is interesting to note that these equations show that Earth-like planets are easier to detect orbiting, more massive, main-sequence stars.

The principles employed in the SASI are so straightforward it is hard to see how they might fail. Even if the system does not achieve the projected precision, it should exceed values projected for other proposals by one or two orders of magnitude.

CONCLUSIONS

Since the presence of planetary systems can be detected astrometrically from any orientation of the observer and orbital plane, a meaningful study of their frequency and basic characteristics is possible. A survey of the nearby stars would reveal the case-by-case characteristics of their planetary systems and most of their individual planets. Negative results would yield the range of masses and orbital periods not found as well as statistical confidence levels. As a group, both the positive and negative results will give us the statistics necessary to better understand planetary systems in general and thus our own in particular. But perhaps more importantly, it will give us our first detailed picture of our vicinity of the galaxy.

The current survey, which now employs the active processing of systematic errors to the precision of the normal points, has sufficient accuracy to yield detectable masses a fraction of that of Jupiter orbiting any of 20 nearby stars. Tests show that the basic concepts behind the MAP are sound, and we estimate that its implementation will increase our precision by two or three times and allow the search for Jupiter-like planets orbiting any of 35 different stars. However, to obtain a statistically significant sample, including primary stars of most spectral types, further new instrumentation will be necessary. The current survey relies on a single optical system that is fully exposed to all variations of its environment. Thus the kind and magnitude of the processes that affect image position can vary over relatively short periods of time. This in turn limits the unified processing of these parameters to relatively small groups of data and hence restricts the precision of the final normal point. Both the 81-cm refractor and the 2.1-m simple reflector are shielded from the changes that affect current instruments and promise precisions more than 10 times and more than 10,000 times higher, respectively.

Equation (12) indicates that the best sample is the nearest, while the probable program size of a pair of 81-cm refractors (one in each hemisphere) is several hundred stars. This suggests a survey of the stars within 12 parsec of the Sun. With the exception of Population II stars, which are probably deficient in terrestrial planets and organic compounds, this volume of stars is homogeneous. The 81-cm, 12-parsec survey instruments (12ψ) would prepare the way for the 2.1-m spaceborne instrument. With a seasonal precision near 0.2 marcsec, they could detect virtually any Jupiter-like planet in the sample and, in combination with a radial velocity study, detect almost all of the unresolved binary stars within this volume. This effort would give us our first estimates of the true frequency of planetary systems and of the number of stars not members of multiple-star systems.

With this preparation, the spaceborne instrument would have a somewhat smaller program than the 81-cm systems and could concentrate its efforts toward discovering Earth-like planets. Studies by Harrington and Harrington (1978) indicate that these Earth-like planets can occur in a wide variety of, but not all, stellar systems. Thus the efforts of the 12ψ are very meaningful, reducing both the time span and costs of the space mission. In

somewhat the same fashion, the current survey and the MAP-assisted survey would reduce the effort of the 12ψ phase, troubleshooting both design and data-processing problems.

The current lack of known extrasolar planetary systems is probably more indicative of the care necessary in our quest to find them than of their absence. However, the precisions now being achieved and those indicated for the systems now being designed and tested promise a better knowledge of the frequency of the systems thought necessary to sustain life as we know it.

REFERENCES

Abt, H.A. and Levy, S. G. (1976) Multiplicity among solar type stars. Astrophys. J. Suppl. 30, 273.

Anderson, J.A. (1920) Application of Michelson's interferometer method to the measurement of close double stars. Astrophys. J. 51, 263.

Black, David C., editor (1980) Project Orion, Design Study of a System for Detecting Extrasolar Planets, NASA SP-436.

Connes, P. (1978) A proposed ground-based narrow field astrometric system. Coll. on European Satellite Astrometry (in print).

Currie, D., Knapp, S. and Liewer, K. (1974) Four stellar-diameter measurements by a new technique: amplitude interferometer. Astrophys. J. 187, 131.

Drake, F. (1975) Minutes of first planetary detection workshop (edited by J. G. Greenstein), Unpublished report.

Eichhorn, H. and Williams, C. (1963) On the systematic accuracy of photographic astrometric data. Astron. J. 68, 221.

Frederick, L. W., McAlister, H.A., van Altena, W. F. and Franz, O. G. (1974) Astrometric Experiments for the Large Space Telescope. ESRO Symposium on Space Astrometry, Frascati, Italy.

Gatewood, G. (1974) An astrometric study of Lalande 21185. Astron. J. 79, 52.

Gatewood, G. (1975) Minutes of the first planetary detection workshop (edited by J. L. Greenstein), Unpublished report.

Gatewood, G. (1976) On the astrometric detection of neighboring planetary systems. Icarus 27, 1.

Gatewood, G. and Eichhorn, H. (1973) An unsuccessful search for a planetary companion of Barnard's star (BD + 4° 3561). Astron. J. 78, 777.

Gatewood, G. and Russell, J. (1974) Astrometric determination of the gravitational redshift of van Maanen 2 (EG5). Astron. J. 79, 815.

Gatewood, G. and Russell, J. (1979a) On the formation of normal points (to be published).

Gatewood, G. and Russell J. (1979b) Astrometric studies of ε Eridani τ Ceti (to be published).

Gould, B. A. (1866) On the reduction of photographic observation. Mem. Nat. Acad. Sci. IV, 173.

Harrington, R. S. and Harrington, B. J. (1978) Can we find a place to live near a multiple star? Mercury ___, 34.

Harris, F., Strand, K. Aa. and Worley, C. (1963) Empirical data on stellar masses, luminosities, and radii. Basic Astronomical Data (edited by K. Aa. Strand), University of Chicago Press.

Heintz, W.(1976) Systematic trends in the motions of suspected stellar companions. M.N. 175, 533.

Heintz, W. (1978) Astrometric study of four binary stars. Astron. J. 77, 160.

Hershey, J. (1973) Astrometric analysis of the field of AC +65° 6955 from plates taken with the Sproul 24-inch refractor. Astron. J. 78, 421.

Hudson, C. (1929) Irregularities in refraction. Publications of the Allegheny Observatory 6, 1.

Huang, Su-Shu (1973) Extrasolar planetary systems. Icarus 18, 339.

Kumar, S. (1963) The Helmholtz-Kelvin time scale for stars of very low mass. Astrophys. J. 137, 1126.

Kumar, S. (1972) Hidden mass in the solar neighborhood. Astrophys. Space Sci. 17, 219.

KenKnight, C., Gatewood, G., Kipp, S. and Black, D. (1977) Atmospheric turbulence and the apparent instantaneous diameter of the Sun. Astron and Astrophys. 59, L27.

Land, G. (1944) Systematic errors in astrometric photographs. Astron. J. 51, 25.

Levinson, F. and Ianna, P. (1977) Emulsion shifts and the astrometric accuracy of the photographic plate. Astron. J. 82, 299.

Lippincott, S. (1957) Accuracy of positions and parallaxes determined with the Sproul 24-in. refractor. Astron. J. 62, 55.

Lippincott, S. (1978) Space Science Reviews, 22, 153.

Lippincott, S. and Hershey, J. (1972) Orbit, mass ratio, and parallax of the visual binary Ross 614. Astron. J. 77, 679.

Michelson, A. A. (1920) On the application of interference methods to astronomical measurements. Astrophys. J. 51, 257.

Miller, R. (1966) Measurements of stellar diameters. Science 153, 581.

Miller, R. (1968) A modest Michelson stellar interferometer. Astron. J. 73, 5108.

Miller, R. (1970) A fringe detector for use with Michelson stellar interferometer. AURA Engineering Tech. Rep. 29.

Miller, R. (1971) A 100-meter Michelson stellar interferometer. AURA Engineering Tech. Rep. 40.

Russell, J. L. (1976) The Astrometric Standard Region in Praesepe (M44). Ph.D. Dissertation, University of Pittsburgh.

Schlesinger, F. (1916) Irregularities in atmospheric refraction. Publications of the Allegheny Observatory 3, 1.

Schlesinger, F. (1917) Photographic determinations of the parallaxes of fifty stars with the Thaw refractor. Publications of the Allegheny Observatory 4, 1.

Shao, M. (1978) Optical interferometers in astrometry. I.A.U. Colloquium No. 48, Vienna, Austria.

Stein, J. W. (1978) Development of the image trailer, a prototype of the multichannel astrometric photometer. Ph.D. Dissertation, University of Pittsburgh.

Strand, K. Aa (1977) The triple system, Stein 2051 (G175-34). Astron. J. 82, 745.

van Altena, W. (1974) The Yerkes Observatory photoelectric parallax scanner. I.A.U. Symposium 61, 311.

van de Kamp, P. (1975) Unseen astrometric companions of stars. Ann. Rev. Astron. and Astrophys. 13, 295.

TABLE 1.- ALLEGHENY OBSERVATORY SURVEY FOR EXTRASOLAR PLANETARY SYSTEMS

No.	Name	RA 1950			Dec		Spec	π	V	B-V	Mass	I	K	Comments
1*	Groom 34 A	0^h	15^m	31^s	43°	44'.4	MIV	.296	8.08	1.56	0.30	0.61	5.2	P ∿ 2600 yr, SB
2*	Groom 34 B	0	15	34	43	44.7	M6Ve		11.04	1.80	.15	1.03	3.3	ρ = 44", FS
3	Van Maanen 2	0	46	31	5	9.2	WDg	.229	12.37	.56	.70	.29		
4*	Tau Ceti	1	41	45	-16	12.0	G8Vp	.277	3.49	.72	.80	.32	9.5	
5	L1159-16	1	57	28	12	50.1	M8 e	.226	12.26	.81	.14	.84		FS
6*	Epsilon Eri	3	30	34	-9	37.6	K2V	.302	3.73	.87	.75	.37	9.2	
7	40 Eri A	4	12	58	-7	43.8	K1V	.205	4.43	.45	.77	.24		
8	40 Eri B	4	13	4	-7	44.1	WDa		9.52	.03	.42	.37		ρA = 83"
9	40 Eri C	4	13	4	-7	44.1	M4Ve		11.17	1.64	.18	.64		ρB = 7".0, P = 250
10*	Stein 2051 A	4	26	48	58	53.6	M4	.179	11.09	1.64	.20	.53	4.1	P = 370 yr
11*	Stein 2051 B	4	26	48	58	53.6	WDa		12.44	.32	.70	.23	9.4	ρ = 7".2
12*	Ross 47	5	39	14	12	29.3	M5	.165	11.54	1.65	.15	.58	7.3	SD
13	Sirius A	6	42	57	-16	38.8	A1V	.377	-1.46	.00			3.3	P = 50 yr, ρ = 7".5
14*	BD+5 1668	7	24	43	5	22.7	M5	.266	9.82	1.56	.21	.74	2.1	
15	G51-15	8	26	52	26	57.1	M	.281	14.81	2.06	.09	1.38		
16	BD+53° 1320	9	10	59	52	54.1	M0V	.166	7.61	1.39	.45	.28		P ∿ 700 yr
17	BD+53 1321	9	11	1	52	54.1	M0V		7.71	1.36	.44	.29		ρ = 17
18*	Groom 1618	10	8	19	49	42.5	K7V	.222	6.59	1.38	.53	.34		
19	Wolf 359	10	54	5	7	19.0	M7 e	.423	13.54	2.00	.10	2.00		FS
20*	Lal 21185	11	0	37	36	18.3	M2V	.386	7.49	1.51	.31	.85		
21*	Ross 128	11	45	9	1	6.0	M5	.301	11.09	1.68	.15	1.06	2.9	
22*	Lal 25372	13	43	12	15	9.7	M3V	.199	8.47	1.47	.34	.41	6.4	
23	BD-11° 3759	14	31	35	-12	18.6	M4	.162	11.36	1.63	.19	.48		
24	BD-7° 4003	15	16	50	-7	32.4	M5	.153	10.57	1.61	.24	.40		
25*	Bd-12° 4523	16	27	31	-12	32.3	M5	.249	10.11	1.60	.21	.71	2.1	SB?
26*	Barnard's Star	17	55	23	4	33.3	M5V	.548	9.54	1.74	.15	1.90	1.0	
27*	Struve 2398 A	18	42	13	59	33.3	M4	.284	8.92	1.54	.26	.71	3.7	P ∿ 450 yr
28*	Struve 2398 B	18	42	14	59	33.0	M5		9.69	1.59	.21	.79	3.3	ρ = 16"
29	G208-44	19	52	16	44	17.4	M	.216	13.41	1.90	.12	.88		
30	G208-45	19	52	17	44	17.4	M		13.99	1.96	.11	.93		
31*	61 Cygni A	21	4	40	38	30.0	K5V	.296	5.23	1.18	.60	.42	2.6	P = 650 yr
32*	61 Cygni B	21	4	40	38	30.0	K7V		6.04	1.37	.53	.45	2.4	ρ = 24"
33	L 789 - 6	22	35	45	-15	35.5	M6 e	.290	12.18	1.96	.13	.12		
34*	E V Lac	22	44	40	44	4.6	M5 e	.195	10.02	1.38	.24	.51	5.2	FS
35*	Ross 248	23	39	27	43	55.2	M6 e	.312	12.29	1.92	.13	1.24	3.5	FS

*On current photographic survey.

e = hydrogen emission, P = period of orbit, ρ = separation or semimajor axis, FS = flare star, SD = subdwarf, SB = spectroscopic binary.

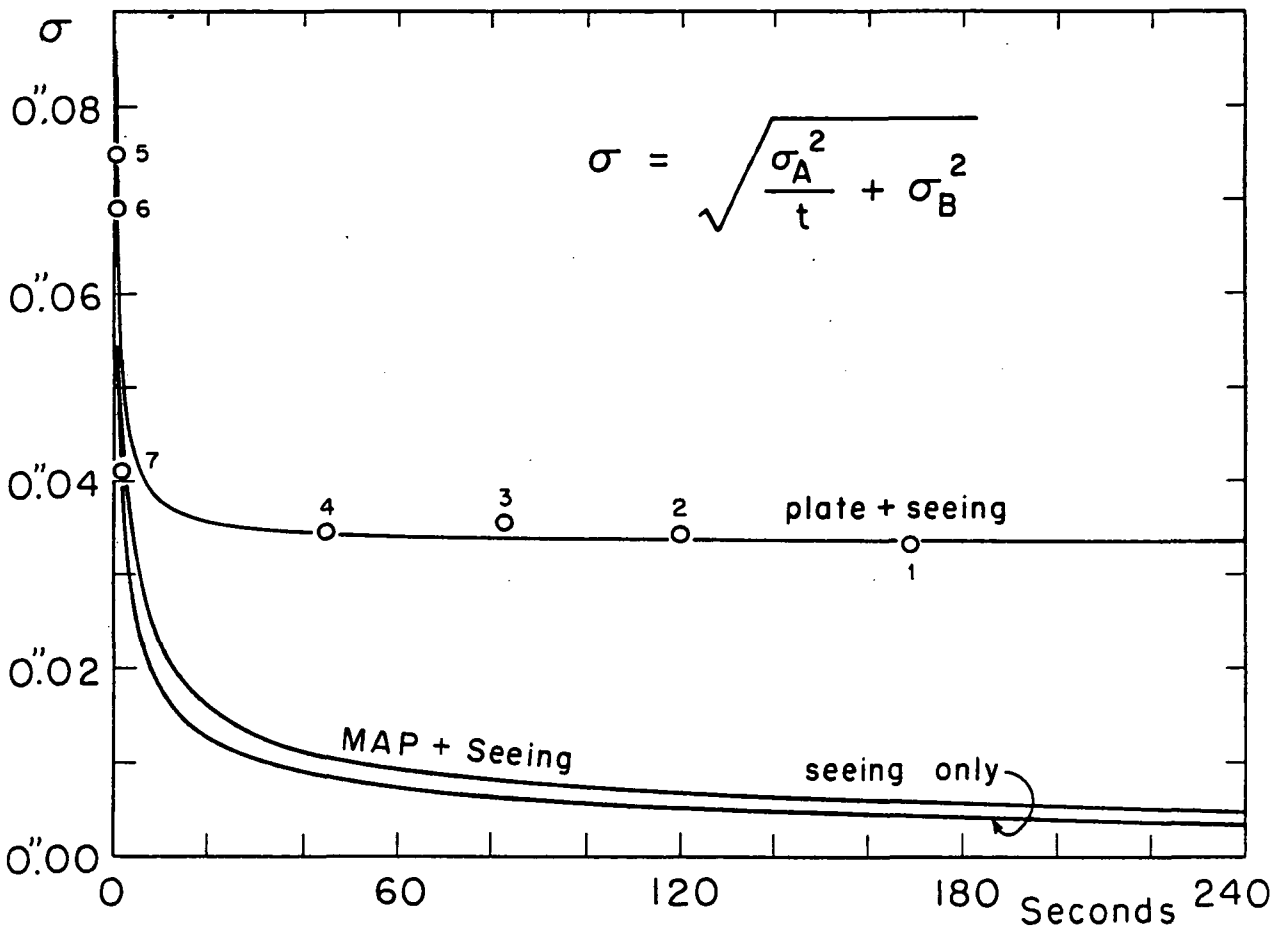

Figure 1.- Points 1 through 4 are the mean standard errors of exposures with integration times t obtained as part of the regular photographic program with the 76-cm refractor. Point 5 was obtained from similar reductions using 1-sec "exposures" obtained from cluster trail plates. Points 6 and 7 are from a short series of 1- and 2-sec exposure plates of the astrometric standard region in Praesepe. The solid line is the best least-squares fit to σ_A and σ_B. The random errors of the photographic process dominate where the exposure time is greater than 4 sec. The random errors of the MAP would enter when those of the seeing are highest. Thus, even if the MAP were no more accurate than the photographic process, 1 hr of observation would yield relative positions with a precision approaching 1 marcsec.

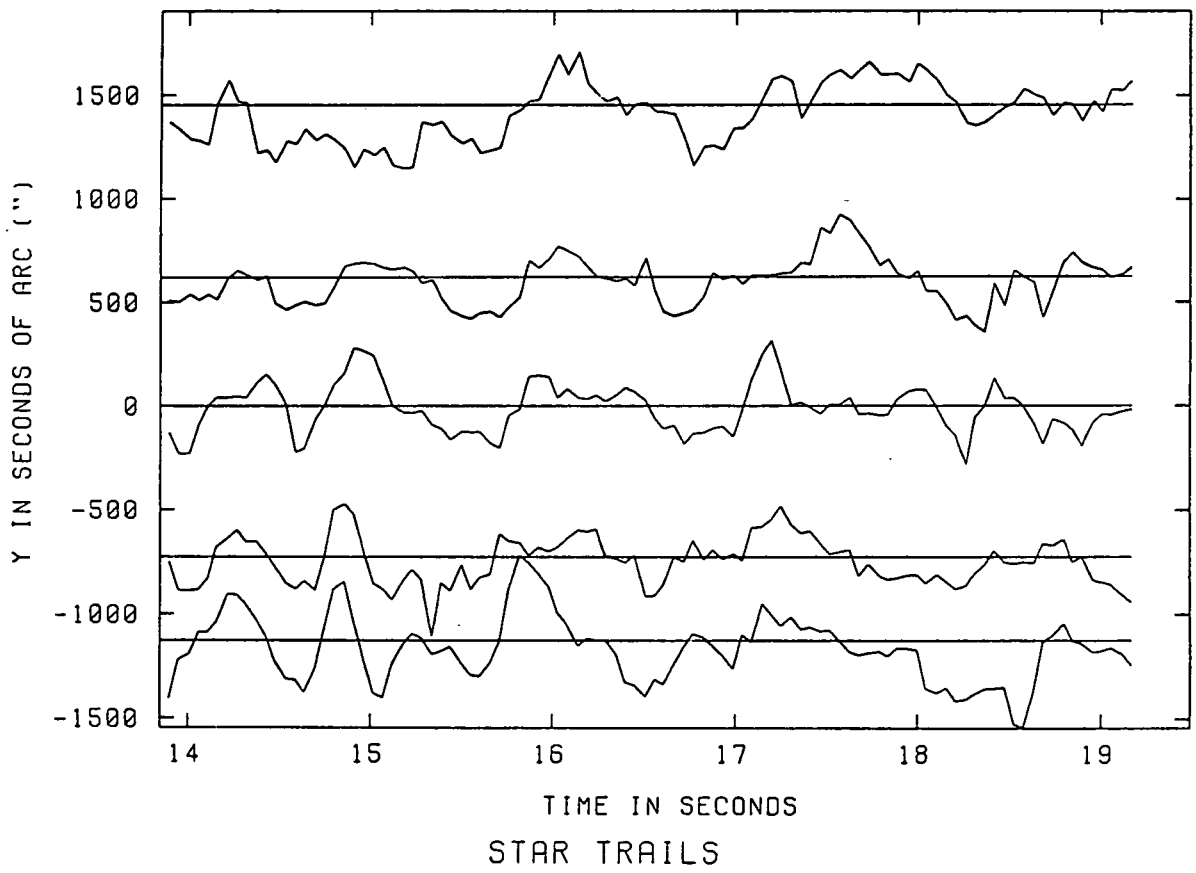

Figure 2.- The above tracings indicate the nature of atmospheric turbulence. Obtained with the telescope drive turned off, the plate records the relative positions of five stars as a function of time. These stars were chosen on the basis of similar apparent magnitude and right ascension. The deviation from their mean positions, determined every 0.05 sec, is magnified 400 times, the plate scale of the telescope being 14.6 arcsec/mm. Preprocessing these data to remove the effects of wavelike patterns could further increase precision of the MAP-seeing curve plotted in figure 1.

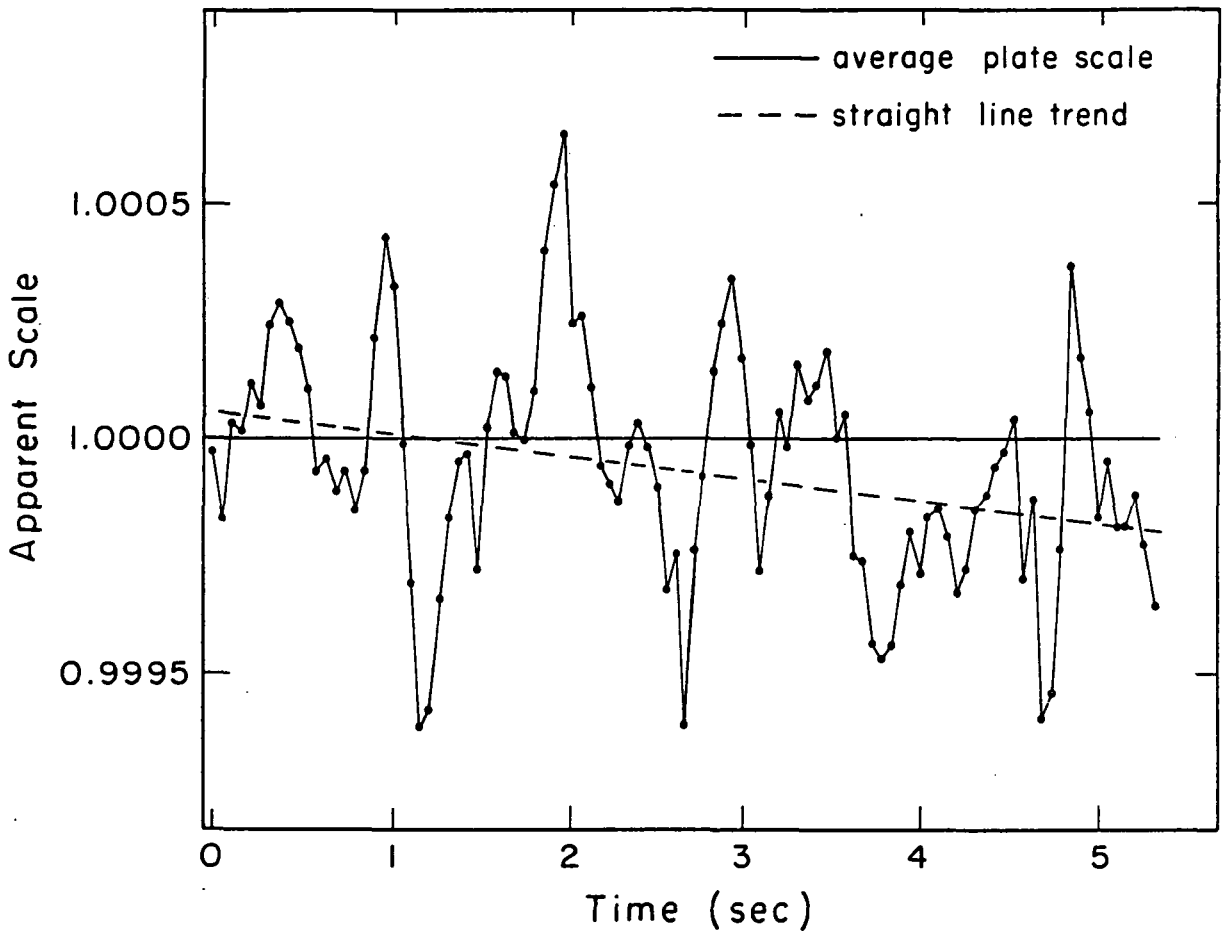

Figure 3.- Variations in the apparent scale of the 76-cm refractor are plotted as a function of time. The scale term was found from a trail plate similar to the one illustrated in figure 2. The average scale of the telescope is shown with a solid line. A trend lasting more than 5 sec is shown by the dashed line. The scale is given as a fraction of the normal scale = 14.60 arcsec/mm. Very similar star trails and atmospheric scaling are found on plates obtained with several other telescopes.

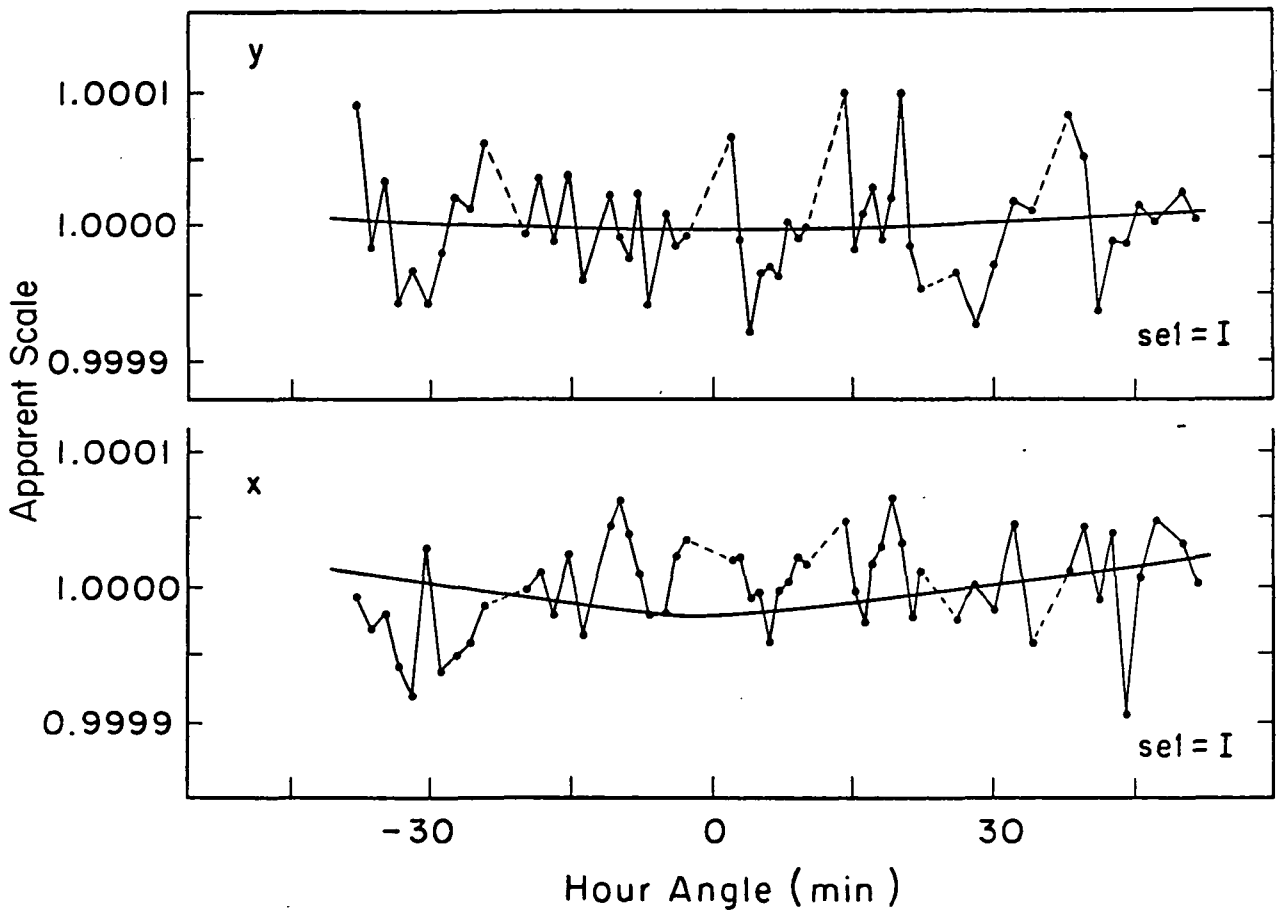

Figure 4.- Atmospheric scaling of a reduced magnitude but increased period is found by examining the scale terms of successive exposures within a survey region. These effects may be modeled and removed, as they were in this region, if sufficient reference star positions are measured. The periodicities and magnitudes observed here are similar to those reported for the Sun (KenKnight et al., 1977). The refractive features responsible for some of the longer term variations noted here are thought to be several kilometers long.

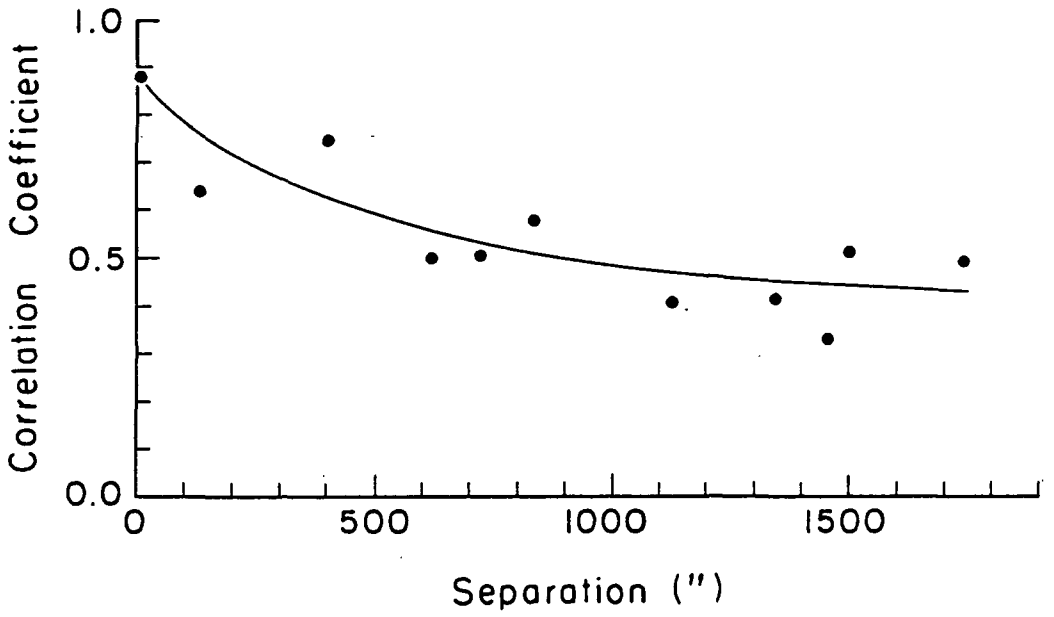

Figure 5.- At separations greater than 1000 arcsec there is little dependence of the correlation coefficient on separation. However, the motion of stars about their mean trails becomes more correlated at smaller separations, reaching 0.89 at a separation of 7.3 arcsec.

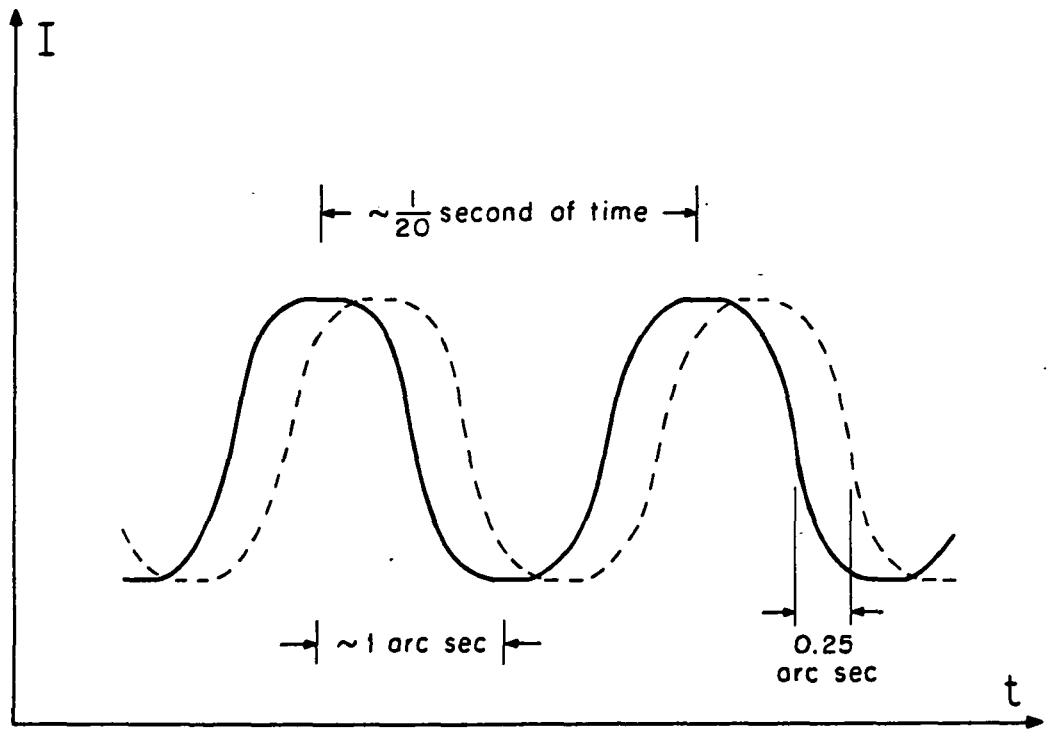

Figure 6.- As a line of the MAP's Ronchi ruling moves across the star image, the image of the objective appears to darken as in a Foucault test. However, since the line width is slightly less than the seeing disk of the image, the image of the objective on the cathode does not go completely dark. Likewise, the space between the ruling lines is not sufficient to let all of the star's light through. Thus a series of maxima and minima are seen (solid line). A second star, viewed by a second photometer, will cause a very similar output (dashed line). If the separation between the two stars is known to the nearest whole number of line spacings, the exact separation in these units may be obtained by adding to this the phase difference of the two signals. Illustrated here is the phase difference for two stars 0.25 arcsec apart. Since only the phase difference is sought, the MAP is insensitive to most of the factors important in absolute photometry.

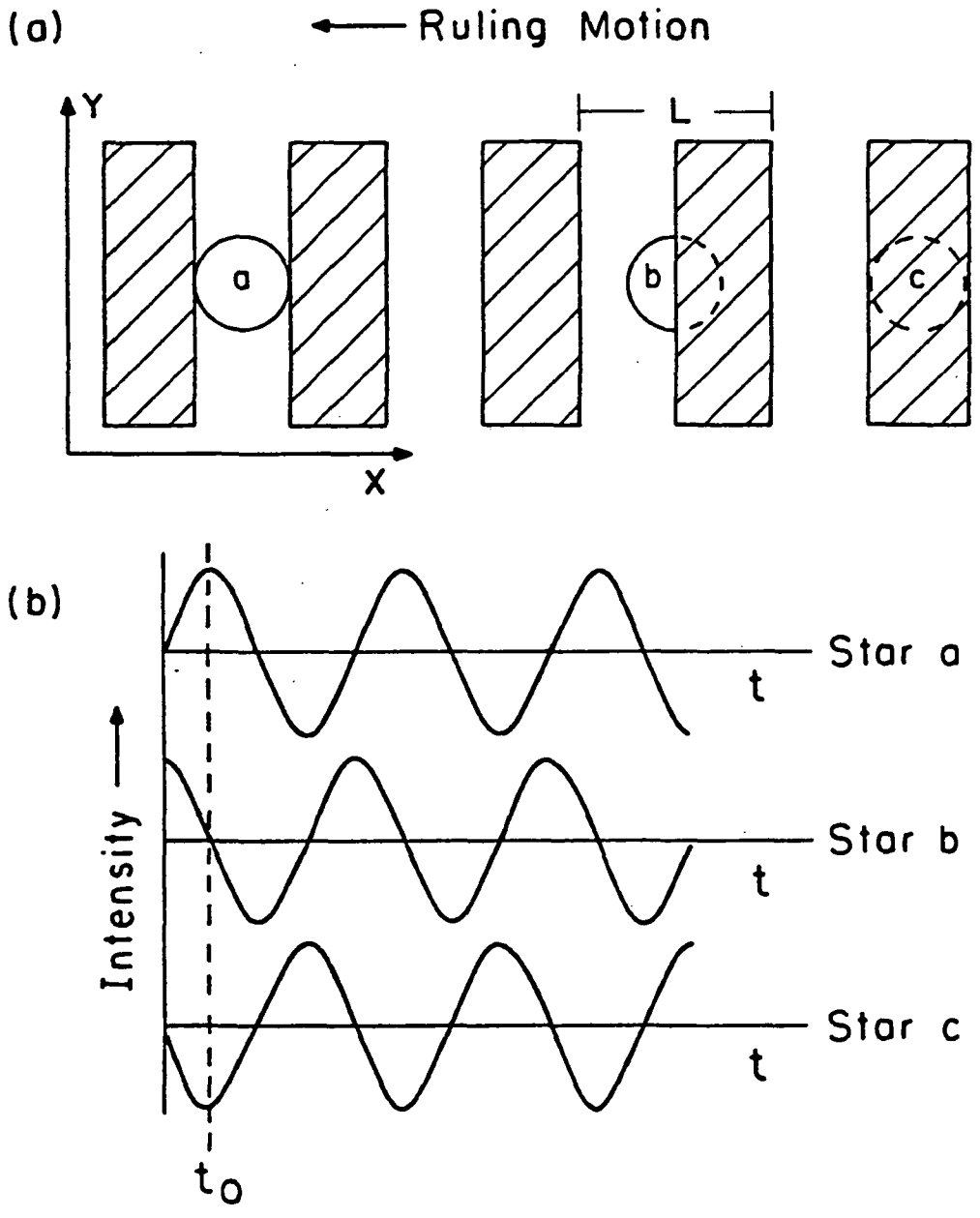

Figure 7.- (a) Ronchi ruling position with respect to star images a, b, and c at time t_o. (b) Signals in the channels monitoring star images a, b, and c showing the relative phases at time t_o.

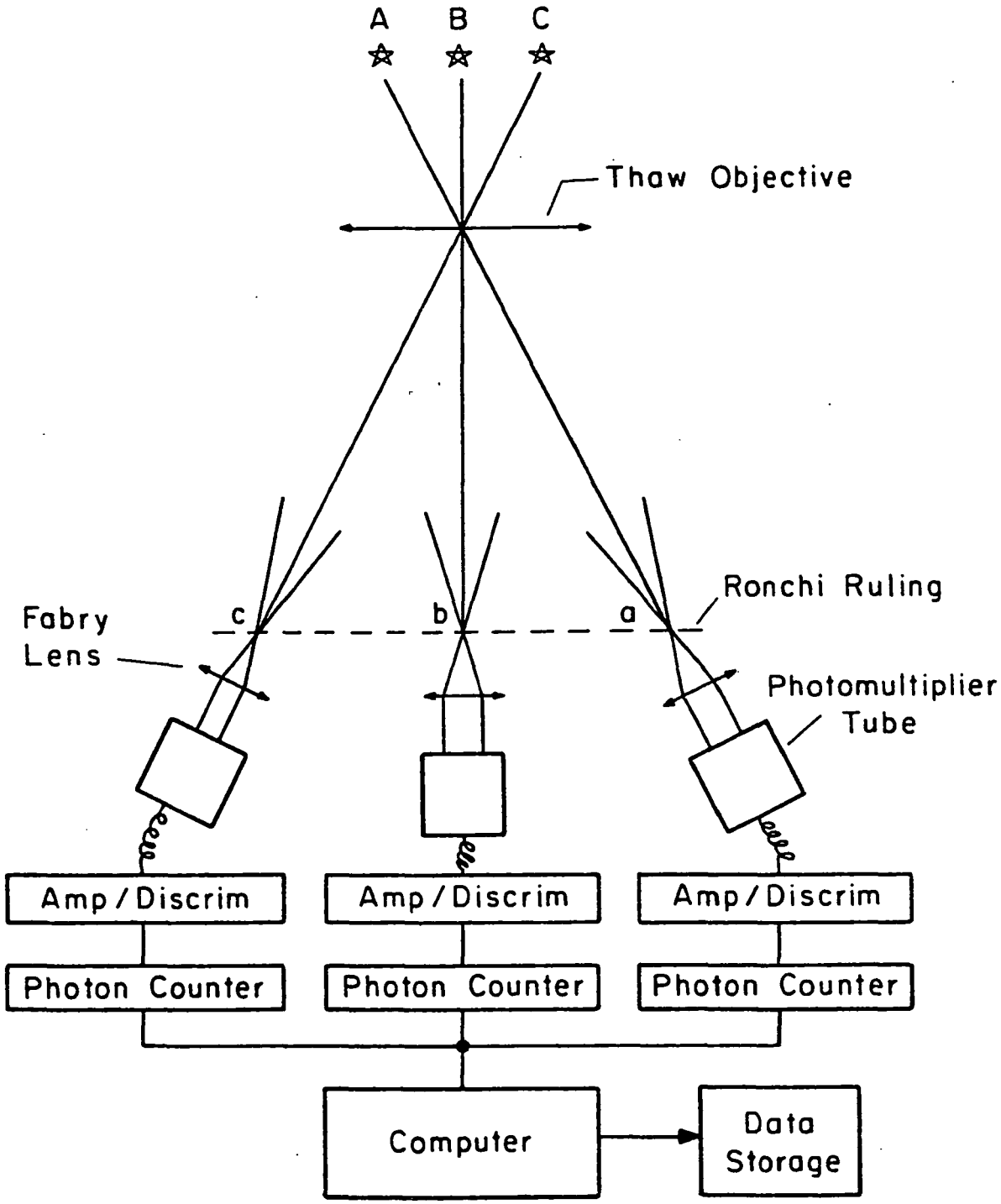

Figure 8.- The MAP will employ approximately a dozen light pickups, each transmitting light to an independent photomultiplier tube. The photon counters of each channel accumulate counts simultaneously, transmitting their counts to the central computer on the command of a single clock. The light pickups are clipped into masks made up for each survey region. Exact alignment is not important since the ruling and not the mask is the linear metric against which the star images are measured.

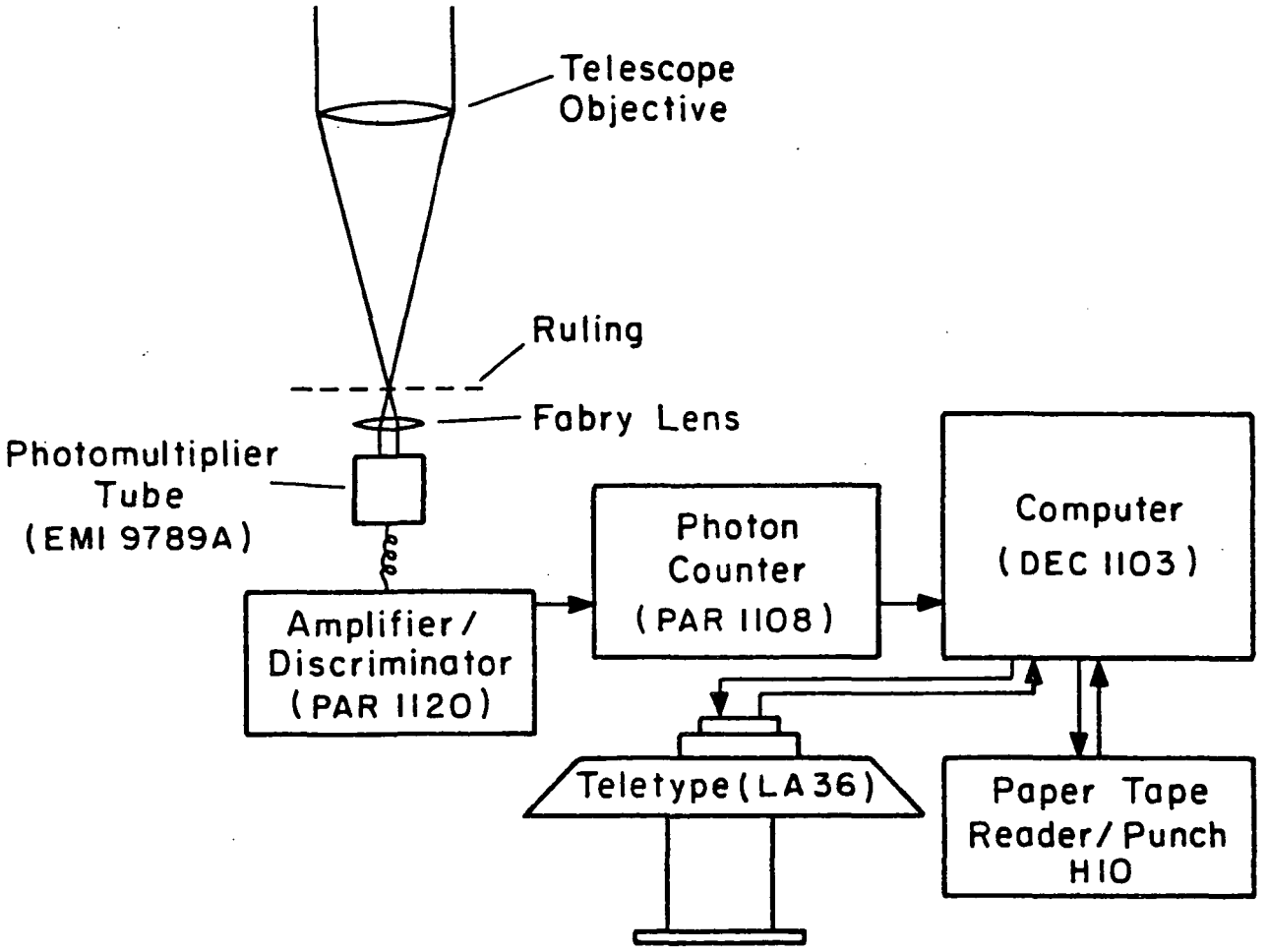

Figure 9.- Schematic of the components of the Image Trailer System

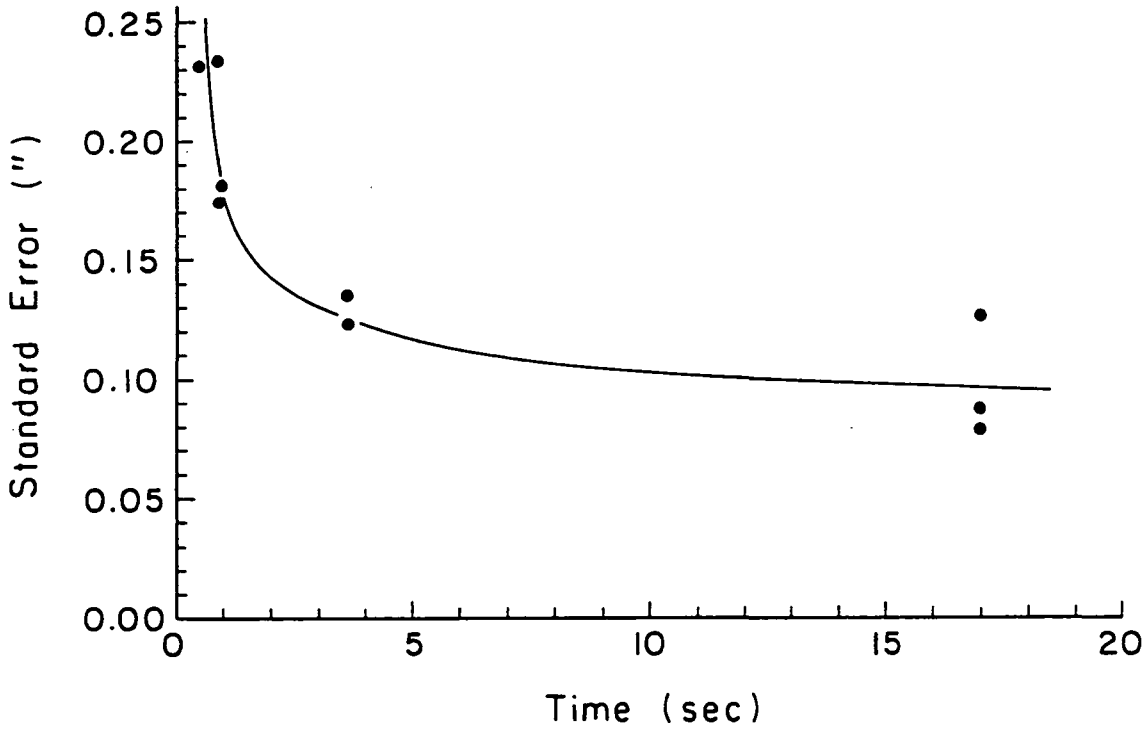

Figure 10.- The standard error of pulse centers about their best straight line fit indicates that data acquired with the image trailer is similar to data obtained from trail plates. The standard error of a 1-sec pulse is found to be 0.17 arcsec and the standard error decreases with the inverse of the fourth root of the integration period.

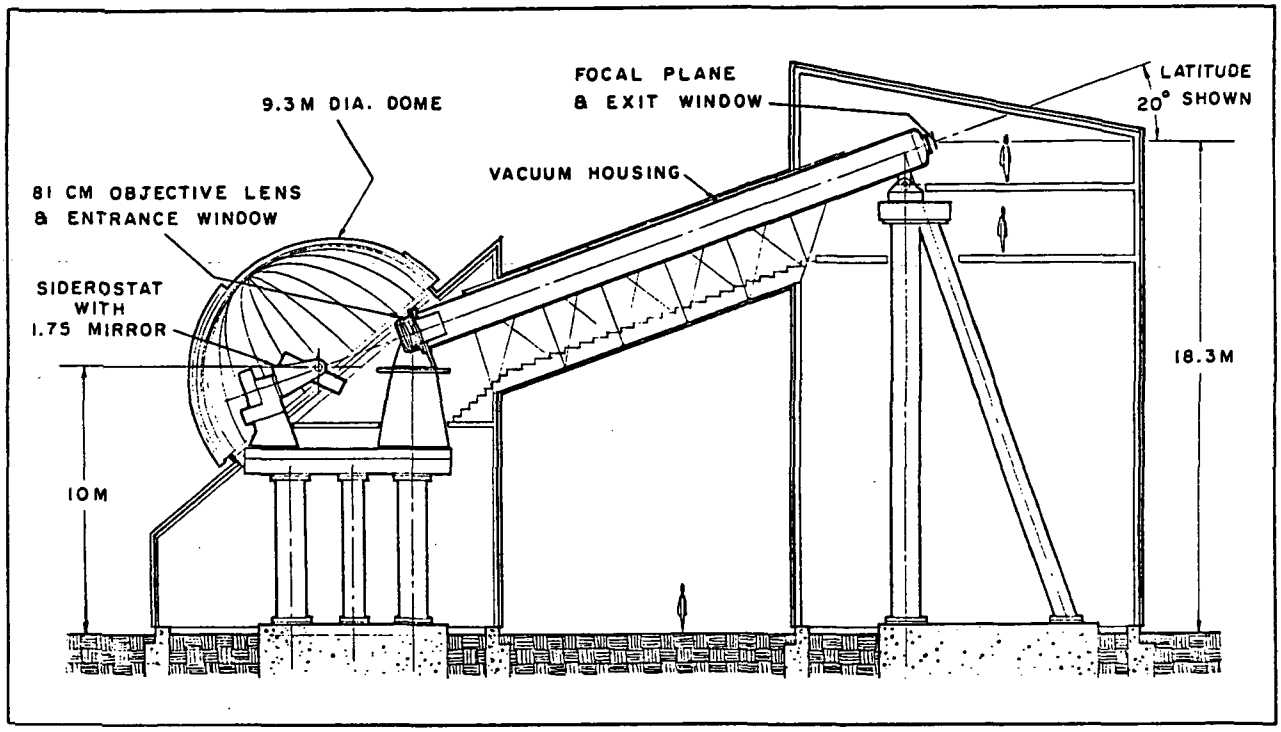

Figure 11.- The optics of the 81-cm refractor lie parallel to Earth's axis of rotation so that light can be brought into the system with only one flat mirror. This mirror is made smaller by placing it at the bottom of the optical axis. A refracting system is chosen so that the optical pupil is near this mirror as well as all other optical components. The secondary spectrum is kept within the Airy disk by a combination of glass choices and a limited bandpass (600 Å centered on 5000 Å). By fixing all nonzero power optical elements and placing them into a temperature-controlled vacuum, we have virtually removed all potential sources of systematic error. The figure of the flat, which has a limited range of motion and is made of temperature inert ceramic, can be held flat, controlled to approximately 1/20 of a wavelength.

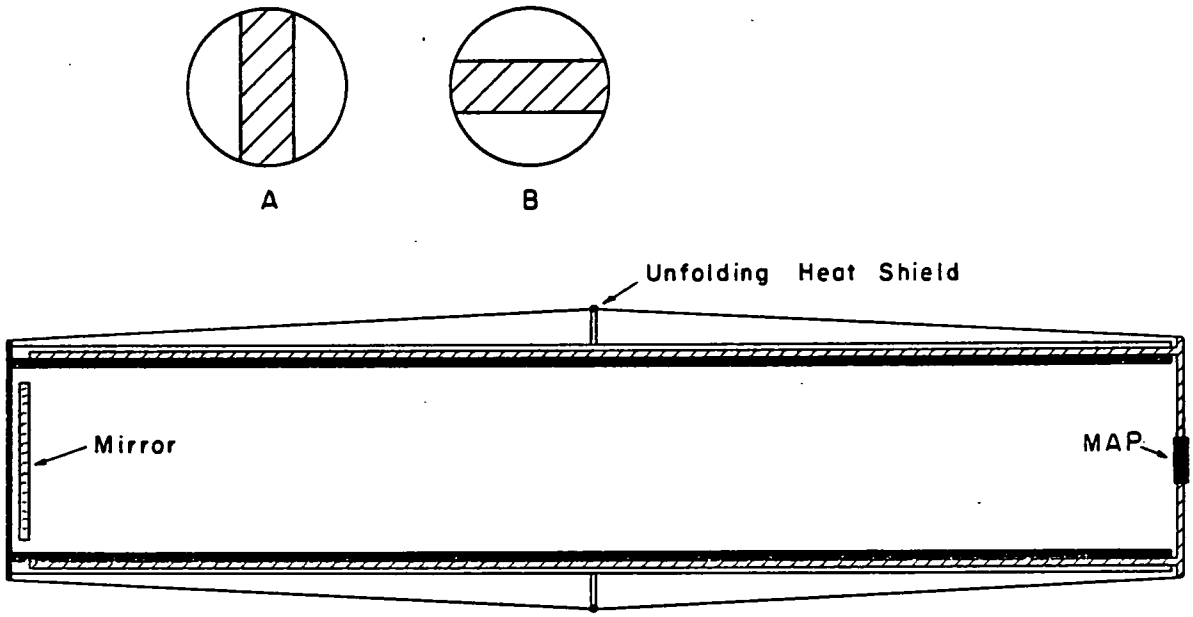

Figure 12.- The 2.1-m space-borne astrometric survey instrument (SASI) requires an f/ratio of approximately 20 to bring its comatic and astigmatic aberrations within the diffraction pattern of its aperture. The MAP ruling will shadow nearly 1/3 of the mirror. To keep the pupil on the mirror, an area slightly larger than that shadowed is covered by a thin film on the mirror surface, A. This cover film could be reconfigured to measure different coordinates without rotating the satellite, B. The heat-shielded frame telescopes open to place the MAP-type detector in the focal plane after the satellite is launched from the Space Shuttle. Support modules could be placed between the heat shield and the instrument tube. The instrument carries the principles of high-precision astrometry to the extreme, placing all optical components exactly in the pupil where variations of less than 1/8 wave do not cause new forms of astrometric error. The MAP-type detector is self-improving in that its errors are easily determined from the measurements themselves and can be removed. If utilized in a survey including the 81-cm refractors, the instrument may have the potential precision necessary to detect every Earth-mass planet within the ecoshell of any solar-type star within 12 parsec of Earth.

PAPER 5

DETECTION OF EXTRA SOLAR PLANETS USING OPTICAL AMPLITUDE INTERFEROMETRY

by

Douglas G. Currie

Technical Report # 77-055

PP # 77-181

Presented at the

Conference on Extra Solar Planetary Detection

University of California at Santa Cruz

April 1976

UNIVERSITY OF MARYLAND

DEPARTMENT OF PHYSICS AND ASTRONOMY

COLLEGE PARK, MARYLAND

DETECTION OF EXTRA SOLAR PLANETS
USING OPTICAL AMPLITUDE INTERFEROMETRY

presented at the

Conference on Extra Solar Planetary Detection

University of California at Santa Cruz

23 April 1976

Amplitude Interferometry is a unique electro-optical technique which should provide a new level of accuracy and resolution in the measurement of angles in optical astrometry. This technique has already proven quite successful in a long term program of measuring stellar diameters. In this application, the instrument has a resolution of 0.015 arc-seconds with a year to year reproducibility of 0.002 arc-seconds. These measurements have been conducted on stars as faint as sixth magnitude, using the 200-inch telescope at Palomar Mountain and the 100-inch telescope at Mt. Wilson. For differential astrometric observations, an Amplitude Interferometer which has two separate telescopes to collect the light should permit effective observation of stars as faint as 14th magnitude, and with a typical positional accuracy of 0.00005 arc-seconds.

The new technique of Amplitude Interferometry was proposed in 1967 (Currie 1967a,b), and was initially demonstrated in 1971 (Currie 1971a). The current mode of operation uses two separately defined apertures on the primary mirror of a large telescope. In this mode, the Amplitude Interferometer has been used in an extended program of measuring stellar diameters which has been reported in the literature (Currie et al., 1976, Knapp et al. 1975, and Currie et al. 1976). Within this program, the diameters of more than twelve stars in up to ten wavelength regions have been measured.

The measurements of these stars range from 13 milli-arc-seconds to 52 milli-arc-seconds (or $^{m}\!\!''$) with a reproducibility of repeated measurements from year to year of typically between $2^{m}\!\!''$ to $4^{m}\!\!''$. Various internal comparisions have been made to verify these estimates of the accuracy.

In order to obtain sufficient resolution to detect a significant number of extra solar planets, an interferometric baseline which is greater than the currently used five meters is required. This will be achieved by using two separate siderostats to collect the light and direct it to a central station. The relative coherence of the two beams is detected and measured by equipment which is essentially identical to the Amplitude Interferometer which is currently in operation. Thus the primary new aspects involved in increasing the resolution is a test of the equipment stability, and the interferometric laser system for monitoring the positions of the siderostats. In order to verify our ability to extend these measurements from the use of a single telescope to two separate telescopes, a demonstration instrument is currently being fabricated. This system will be in operation this summer using a telescope separation of 3.3 meters for the first tests.

This demonstration will be followed by an observational program which will be performed by moving this equipment to a site which permits a 30 meters separation of the telescopes. At the latter site, this instrument will be able to resolve about $1.7^{m}\!\!''$ and will determine the centroid of an unresolved star to about $0.25^{m}\!\!''$. Projecting from the measured performance of the currently operating instrument, this measurement of the separation of a program star and a reference star may be done in about ten minutes on stars which have a brightness of 6.5 magnitudes. At a later time, the demonstra-

tion instrument will be moved to another site which permits a test with a one kilometer separation of the telescope. In this case, the resolution and positional accuracy should be 52 μ'' and 8μ'' respectively.

The performance discussed above presumes the use of a set of four centimeter apertures. To provide increased sensitivity to faint objects, a separate instrument, which is currently nearing completion, will permit the operation of 10,000 channels at the same time (or i.e., 10,000 independent Amplitude Interferometers). While the current version of this Multi-Aperture Amplitude Interferometer (MAAI) will be designed for operation at the Cassegrain focus of a conventional telescope, the basic design is identical when it is used with two telescopes of intermediate aperture. In a typical case for separated telescopes, we may increase the data rate by one thousand and thus increase the accuracy of a single determination of the location of the centroid by a factor of thirty.

The instrument which is currently being built for tests at various baselines will permit the test of a two color system for the removal of error due to atmospheric refraction and its uncertainty (Currie 1971b). While this is essential for fundamental observations (of the type made by a transit circle) this technique is not particularly desirable for the differential astrometric measurements required for planetary detection. This is due to the fact that the absolute accuracy is reduced by a factor of about forty worse with respect to the precision of the individual measurements in each color. Thus for the astrometric work under discussion here, a differential method for simultaneous measurement of the program star and reference star would be used. This procedure eliminate a number of classes of errors in the same manner that the techniques using a classical long-focus telescope in astrometry have higher accuracy in measuring

differential angles than may be achieved in the fundamental measurements using a transit circle.

Let us now consider several possible effects which might affect the accuracy of the Amplitude Interferometry measurement at a level which is relevant in the search for extra solar planets. Some of these consist of:

Effects of the Atmosphere

The primary effect of atmosphere, that of turbulence, has already been addressed and solved as is illustrated by the measurements of the observational program using the Single Aperture Amplitude Interferometer (SAAI). The detector for the long baseline instrument is essentially identical to that of the SAAI and so no new significant questions are expected in this area. We have found that the fringe visibilities for an unresolved source are high (close to full unit visibility) and do not significantly decrease when measured for the large separations of the interferometric apertures.

Atmospheric effects which cover a more extended area might affect us in two ways. The first is to make the measurement procedure more difficult or more "noisy". Calculations, and the tests performed on the shorter baselines, imply that this should not be a significant problem. These extended effects could also induce systematic error. However, to first order, these errors are removed by the differential procedure mentioned in the previous paragraph.

Optical Mechanical Stability

The mirror supports and drives and the basic structure comprising all the system optical components must be highly stable on the micron level. The most sensitive element, the siderostats, were carefully

specified and have already been tested. They show stability at the submicron level for those motions to which the interferometer is sensitive. In normal operation for making astrometric measurements, this motion will be monitored both by a laser interferometric technique and by a technique using the light from the star itself. For the remaining parts of the system, similar stability has been demonstrated on the SAAI at the Cassegrain focus of large telescopes.

Pier Stability

The piers on which the heliostats and the control station rest must not vibrate and must also be stable over a longer period to a few microns, rather than the more stringent submicron stability required for fundamental astrometric measurements (Currie 1971c). This requirement may be properly expressed in terms of the acceptable spectral power of motion at different frequencies. However, if one compares these requirements of the Amplitude Interferometer with measurements which have been made (using a laser interferometer) of the relative motion of piers separated by over a kilometer (Berger 1971) one finds that the horizontal component pier motion is quite acceptable. To address the vertical motion, one must convert vertical acceleration (Block 1972) to relative vertical motion. The result of this analysis also indicates that properly placed piers will be quite stable enough for these measurements.

The expected accuracy for a single measurement of the relative stellar position depends on the program star and its brightness. There are more than a thousand main sequence stars with a spectral type of F or later for which the Amplitude Interferometer could measure a displacement of the photocenter

with an accuracy which is 1% of the amplitude produced by the motion of Jupiter in its orbit around the sun. This measurement would require a single observation period of ten minutes to perform the simultaneous measurement of the program star and two reference stars in declination. Thus the system has sufficient sensitivity to perform an extended survey in search of extra solar planetary systems. For relatively bright program stars, one should be able to detect a displacement of the photocenter which has an amplitude equal to that which would be caused by an earth-type planet. For example, there are more than forty main sequence stars for which one could detect (at one sigma) a displacement of the photocenter equivalent to the earth-type amplitude in a single forty minute observation period. Since the measurements would be photon noise limited, as are such measurements made at the present time, conducting a series of one hundred of these measurements should yield a signal-to-noise ratio of ten for earth detection. However, for many of these cases, there do not exist a proper set of reference stars which will permit one to take advantage of this accuracy in a proper program. The full capability of such an "earth-search" program has not yet been carefully addressed.

Thus in conclusion, we see that an extrapolation of the existing and demonstrated techniques in Amplitude Interferometry, with a rather straight forward observing procedure, will provide a very interesting search and measurement program for the detection and measurement for extra solar planets.

REFERENCES

Berger, J. and Levine J. (1974) JGR, 79, 1210.

Bartholomew, B., Block, B., and Drafter, J. Jr., (1972), Nature Phys. Sci. 236, 123-5.

Currie, D. G., 1967a, Woods Hole Summer Study on Synthetic Aperture Optics Vol. 2 (Washington: National Academy of Sciences, National Research Council).

_____, 1967b, Ibid., Vol. 2.

Currie, D. G., Knapp, S. L., and Liewer, K. M. (1974) Four Stellar Diameter Measurements by a New Technique: Amplitude Interferometry, Ap. J., 187, 131.

Knapp, S. L., Liewer, K. M., and Currie, D. G., (1975) On the Effective Temperature of α Herculis A, Ap. J. 198, No. 3., Part 1.

Currie, D. G., Liewer, K. M., Knapp, S. L., Braunstein, R. H. (1976), Stellar Disk Diameter Measurements by Amplitude Interferometry, 1972 - 1976.

Currie, D. G. (1971b) On the Use of Wideband Optical Very Long Baseline Interferometry for the Determination of the Position of the Pole: Atmospheric Correction by the Use of Dispersion.

Currie, D. G., (1971c) On the Use of Wideband Optical Very Long Baseline Interferometry for the Determination of the Position of the Pole: Local Reference Frame

Currie, D. G. (1971a) A New Interferometric Technique for Very High Spatial Resolution, Bulletin Amer. Astron. Soc. 3, 244

PAPER 6

OPTICAL INTERFEROMETERS IN ASTROMETRY*

Michael Shao

Research Laboratory of Electronics
Massachusetts Institute of Technology
Cambridge, Massachusetts 02139

ABSTRACT

Long baseline stellar interferometers for astrometry are potentially capable of extremely high accuracies, 10^{-4} to 10^{-5} arc sec for a single measurements. There are three categories of errors that apply to an astrometric interferometer, instrumental, atmospheric and photon noise. Of these, only photon noise has a flat power spectrum. All of the other sources of error are systematic in the sense that the accuracy does not increase as the square root of the measurement time. The elimination of atmospheric error is the major difference between interferometers and other photoelectric astrometric instruments. Two types of interferometers, image plane and pupil plane, are described. The advantages and limitations of these two approaches are discussed.

*Work supported by the National Science Foundation.

I. Introduction

Stellar interferometers are capable of very high resolution, 0.001 arc sec for a 50 meter interferometer versus 1 arc sec for a conventional ground-based telescope. If this increase in resolution can be turned into a similar increase in astrometric accuracy, the impact on astronomy would be very significant. This paper reviews the advantages and problems of using an interferometer for astrometry.

With the introduction of any new instrument in astrometry, it is necessary to examine the causes of error thoroughly. We must determine what errors are systematic and correctable and what errors are random.

II. Power Spectrum of Astrometric Errors

Astrometric errors in three categories plague all ground-based astrometric measurements. One category is optical errors. Optical errors are caused by the fact that the instrument is not constructed with perfect components, and that thermal expansion will change the dimensions of the instrument. Optical errors for interferometers will be discussed later. The two remaining sources of errors are photon noise and atmospheric noise. The words noise and error are used here to mean the same thing.

If the accuracy of a measurement is limited by random errors, the accuracy will increase with the square root of the measurement time. This type of measurement noise is usually referred to as white noise and has a flat power

spectrum. For the worst type of systematic error, the accuracy does not increase with longer integration time. This type of noise has a 1/f power spectrum.

The astrometric error due to photon noise is well known (Eq. 1).

$$\sigma_\alpha \text{ (1 sigma error)} \simeq \frac{W}{\sqrt{N}} \qquad (1)$$

where W is the width of the image

N is the number of detected photons

W is 0.001 arc sec for a 50 m interferometer

W is 1 arc sec for an ordinary telescope

The power spectrum of the astrometric error due to photon noise is a white noise spectrum.

The atmospheric noise spectrum is quite complicated. At frequencies above 0.1 Hz, atmospheric turbulence caused by thermal fluctuations is responsible for seeing and image wander. The astrometric error has a $f^{-2/3}$ power spectrum for Kolmogorov turbulence.[1] At very low frequencies, 0.001 Hz, atmospheric errors are caused by pressure waves or weather patterns. There is very little data on the power spectrum of astrometric error caused by weather; however, it is probably safe to assume that the spectrum is not flat.

For ground-based astrometric instruments, atmospheric noise is much greater than photon noise. In addition, atmospheric noise does not have a constant power spectrum, hence it is a systematic error. For an astrometric instrument whose accuracy is limited by turbulence, the accuracy would increase as the 6th root of the measurement time $T^{1/6}$.

III. The Elimination of Atmospheric Error

To some extent, all astrometric measurements correct for atmospheric error. For a telescope pointed at the zenith, a change in barometric pressure would change the effective focal length of the telescope. However, since the focal length is derived from measurements of reference stars, this component of atmospheric noise is eliminated. Similarly, it is possible to model more complicated atmospheric errors caused by weather by using a large number of reference stars.

An astrometric interferometer must go one step further by eliminating the error due to turbulence. Without correcting for turbulence, an interferometer would be no more accurate than a low resolution (1 arc sec) astrometric telescope.

The technique used to eliminate the astrometric error due to atmospheric turbulence is based on the dispersive property of the atmosphere. The index of refraction of the atmosphere is a function of wavelength, hence the apparent position of a star is also a function of wavelength. It is easily shown that the measurement of the apparent position of a star at two wavelengths simultaneously will enable the true position of the star to be derived. If we let x be one coordinate of the star's position, Eq. 2 gives the true position of the star in terms of the apparent position at the two wavelengths, and the index of refraction of air.

$$x_o = x_1 - (x_2 - x_1) \left[\frac{1 - N_1}{N_2 - N_1}\right] \qquad (2)$$

where x_o = true position

x_i = apparent position at λ_i

N_i = index of refraction at λ_i

The importance of the two-color technique is that atmospheric errors may be eliminated. If equal care is applied to optical errors, the accuracy of an interferometer will be limited only by photon noise. From Eq. 1 we see that the accuracy of a photon noise limited interferometer increases linearly with the size of the interferometer.

However, the use of the two-color technique in the visible will increase the effect of photon noise by roughly a factor of 50. In the infrared, the atmosphere is not sufficiently dispersive for the two-color technique to be used.

IV. Limitations of Interferometers Due to Turbulence

The measurement fringe position in the presence of atmospheric turbulence is not a trivial task. The wavefront from the star is distorted by the atmosphere. A stellar interferometer that measures fringe phase works only when the phase distortion of the wavefront over the entrance apertures of the instrument is much less than a wavelength. The effect of turbulence on the size of the maximum usable aperture has been extensively studied.[2] The maximum usable aperture is a function of the "seeing" and wavelength. It is inversely proportional to seeing and proportional to $\lambda^{6/5}$. For $\lambda = 0.55u$ and 1 arc sec seeing, the maximum aperture is approximately 10 cm.

Turbulence will also cause the fringe pattern to move. The time interval during which the atmosphere can be assumed

frozen is a function of seeing, wavelength, and wind speed. At a good site, the atmospheric coherence time will be on the order of 0.01 sec.

A measurement of fringe position must be made every 0.01 sec with two 10 cm apertures. These restrictions make it impossible for any ground-based interferometer to observe dim stars. With modern high quantum efficiency photomultipliers, this limit would be approximately 10 mag.

For a 50 meter interferometer, the astrometric error due to photon noise using the two-color technique would be approximately $0.05/\sqrt{N}$ arc sec, where N is the number of detected photons. 0.001 arc sec accuracy would require 2500 detected photons, 10^{-5} arc sec would require $2.5 \cdot 10^{7}$ detected photons. At the magnitude limit imposed by turbulence this would take a few hours.

This high level of accuracy is achievable only if the major sources of error are photon noise and atmospheric noise. Optical and thermal errors must also be reduced to this level. However, many of the techniques used to minimize optical and thermal effects have already been developed. This will be discussed after the two types of interferometers for astrometry have been introduced.

V. Summary of Photon and Atmospheric Errors

Figure 1 shows the astrometric accuracy as a function of measurement times of several types of astrometic instruments. The most accurate instrument is of course the photon noise

limited orbiting interferometer. Next is the photon noise limited two-color ground-based interferometer. The accuracy of a turbulence noise limited instrument is also shown. The accuracy of a 1 second measurement was derived from data taken at Wallace Observatory (MIT) in 1976.[3] For longer measurement times the accuracy increases as $T^{1/6}$. However, for very long measurements, it should be possible to use a large number of reference stars to model the astrometric errors caused by weather. The two lines in Fig. 1 correspond to accurate modeling of atmospheric errors on a time scale of 100 and 1000 seconds.

Currently there is a considerable amount of uncertainty as to what the atmospheric limit to astrometric accuracy is. The line in Fig. 1 representing the accuracy of an atmospherically limited instrument is only a rough estimate. However, in spite of this uncertainty, the difference between a ground-based two-color interferometer and an atmospherically limited telescope is clear.

VI. Two Types of Interferometers for Astrometry

There are two different types of interferometers for astrometry, image plane and pupil plane interferometers. Astrometry with an image plane interferometer is somewhat similar to photographic astrometry, while the operation of a pupil plane interferometer is similar to the operation of a radio interferometer.

VI.A. Image Plane Interferometer

Figure 2 is a schematic of an image plane interferometer. The fringe pattern at the image plane is also illustrated in Fig. 2.

The fringe pattern may be understood as follows. The large blur is the diffraction pattern of the entrance apertures

with 10 cm diameter. The fringe spacing is determined by D, the baseline length. The width of the fringe pattern is determined by the optical bandwidth of the star and detector. The fringe pattern is offset from the center of the diffraction pattern by an amount that depends on the position of the star in the field of view, this is a geometric effect similar to coma.

The properties of an image plane interferometer are as follows. The sensitivity, ratio of fringe pattern width to diffraction pattern width, is proportional to d/D. The position of the fringe patterns of all the stars in the field of view may be measured simultaneously. The field of view as defined by the off axis angle at which the fringe pattern is no longer on the top half of the diffraction pattern is $8\ F^2\lambda/d$ radians, where λ is the wavelength of light, d is the aperture diameter (10 cm), and F is the focal ratio, focal length divided by the baseline length.

For a ground-based interferometer, sensitivity is a very important parameter. For this reason, it would not be practical to build a long baseline image plane interferometer. For example, an image plane interferometer with d = 10 cm and D = 10 m would be 100 times less sensitive than a similar pupil plane interferometer. Since the magnitude limit for a pupil plane interferometer is approximately 10 mag, a 10 meter image plane would not be usable on stars dimmer than 5 mag.

VI.B. Pupil Plane Interferometer

A schematic of a pupil plane interferometer is shown in Fig. 3. The key difference is that light is directed toward a fringe detector with flat mirrors. Although the fringe detector in Fig. 3 uses a beam splitter, another fringe detector could have been used. Michelson's 20 foot interferometer is an example of a pupil plane interferometer which used an image plane interferometer as a fringe detector. The use of flat mirrors means that the baseline can be extended simply by moving the end mirrors further apart without changing the fringe pattern. Hence the sensitivity does not decrease with longer baselines.

In Fig. 3 the path length difference in the two arms of the interferometer must be less than a few wavelengths of light to maintain temporal coherence. If two stars are separated by an angle much larger than the resolution of the interferometer, temporal coherence cannot be maintained for both stars simultaneously. This means that except for double stars, the interferometer can only measure the fringe position of one star at a time.

In Fig. 3 the difference in the pathlength of the two arms may be adjusted by moving the fringe detector left or right. The star's fringe position is defined as the position of the fringe detector when the optical path difference is zero. The position of the fringe detector in turn is measured by a laser interferometer. The star's fringe position is related to the star's coordinates by Eq. 3

$$x \text{ (fringe position)} = \hat{S} \cdot \vec{B} \qquad (3)$$

where x is the fringe position

$\hat{S}$ is a unit vector to the star

$\vec{B}$ is the baseline vector in Fig. 3

If the baseline vector $\vec{B}$ is known, two measurements of fringe position with two different baseline orientations are sufficient to determine the position of the star. In general, both the stellar positions and baseline vectors are unknown at the desired level of accuracy (10^{-4} to 10^{-5} arc sec). The procedure to calculate both stellar position and baseline orientation from fringe position measurements for optical interferometry is similar to the procedures used in VLBI radio astrometry. The essence of the procedure is as follows. The baseline vector is fixed to the earth. The end mirrors are rotated to track the motion of stars and to point the interferometer at different stars. With the baseline fixed to the earth, it is possible to measure the fringe position of several stars with the same baseline orientation.

For each measurement of fringe position, there are two unknowns in the star's position. The measurement of n fringe positions with the same baseline will result in 2n+3 unknowns. With m different baselines, there will be mn measurements and 2n+3m unknowns. In order to solve for the stellar positions and baseline vectors simultaneously, mn must be greater than 2n+3m.

For stars near the poles, only a single interferometer is needed. The different baseline orientations may be derived from earth rotation. For an astrometric observatory capable of measuring the position of stars near the equator, several interferometers are needed.

VII. Instrumental Errors

Since the photon noise and atmospheric noise for the two-color interferometer is so low, it is necessary to keep instrumental errors to a minimum. The instrument should be designed in such a way that instrumental parameters that affect position measurements can either be independently monitored, or derived from the data.

For example, it should be possible to monitor the baseline length with a laser interferometer, and as shown in the last section derive the baseline orientation by measuring the fringe position of several stars. Another example is the derivation of the dispersion factor F.

The dispersion factor $(1 - n_1)/(n_2 - n_1)$ for the two-color technique must be known to extremely high accuracy. In addition this factor will be different for stars of different spectral type because the effective wavelength of the two pass bands will depend on the color of the star. Rewriting Eq. 2, we get Eq. 3. (Earth rotation has been ignored to simplify the algebra.)

$$x_o = x_1 - (x_1 - x_2)F \qquad (3)$$
$$x_o = x_1' - (x_1' - x_2')F$$

where x_o = true position of star

$x_{1,2}$ = apparent position at time t

$x'_{1,2}$ = apparent position at time t'

Equation 3 represents two equations in two unknowns, x_o and F. Since the composition of the atmosphere and the color of the star are usually constant for a much longer time than 20 msec, the data analysis procedure should be to perform a least squares fit for x_o and F from a whole night of data for each star.

The key to reducing instrumental errors is an accurate mathematical model of the instrument with parameters that can be derived from the data.

VIII. Conclusions

In conclusion, the limitations and advantages of a ground-based interferometer for astrometry are:

1) The only direct advantage of an interferometer is the reduction of photon noise.
2) Atmospheric error is a systematic error in the sense that accuracy increases much more slowly than $\sqrt{T}$.
3) For photoelectric instruments, atmospheric noise is much greater than photon noise.
4) It is possible to eliminate atmospheric noise with a two-color technique.
5) Turbulence will limit the operation of an astrometric interferometer to $\sim$ 10 mag stars.

6) Image plane interferometers are capable of simultaneous measurements of several stars. However, their sensitivity decreases linearly with the baseline length.

7) Pupil plane interferometers do not have lower sensitivity for longer baselines but simultaneous measurements are not possible. Quasi-simultaneous measurements for the fringe position of several stars means that baseline stability will be the major source of optical and thermal errors.

8) An interferometer only measures the dot product of the stellar position and baseline vector. A number of different baseline orientations are needed to derive the coordinates of the stars.

References

1. Lawrence R., and Strobehn, J., Proc. IEEE, vol. 58, p. 1523, 1970.

2. Fried, D., and Mevers, G., Appl. Optics, vol. 13, p. 2620, 1974.

3. Shao, M., "A Long Baseline Optical Interferometer for Astrometry," Ph.D. thesis, Department of Physics, M.I.T., 1978.

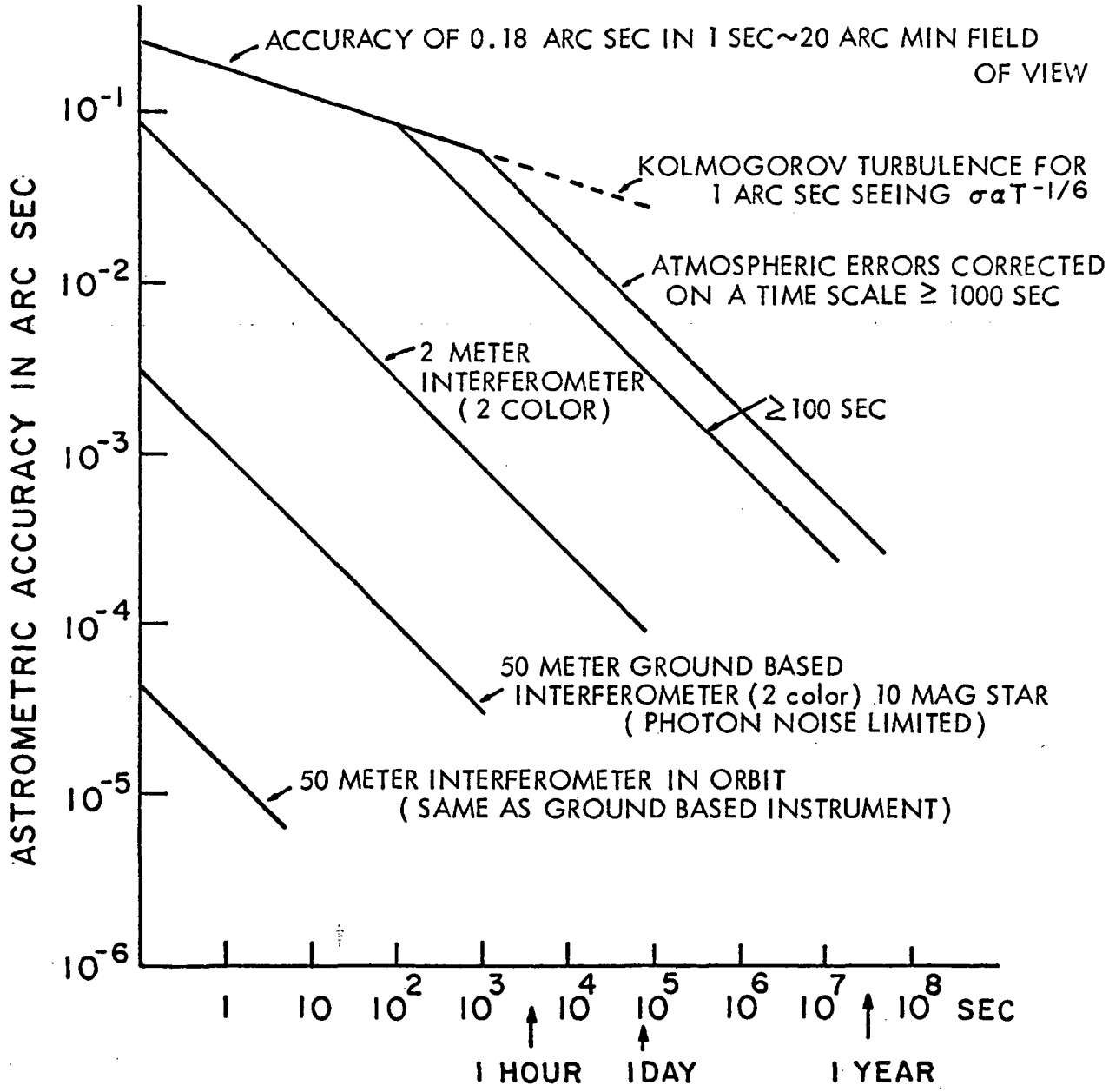

Figure 1.- Astrometric accuracy vs integration time for turbulence limited instruments and photon noise limited interferometers.

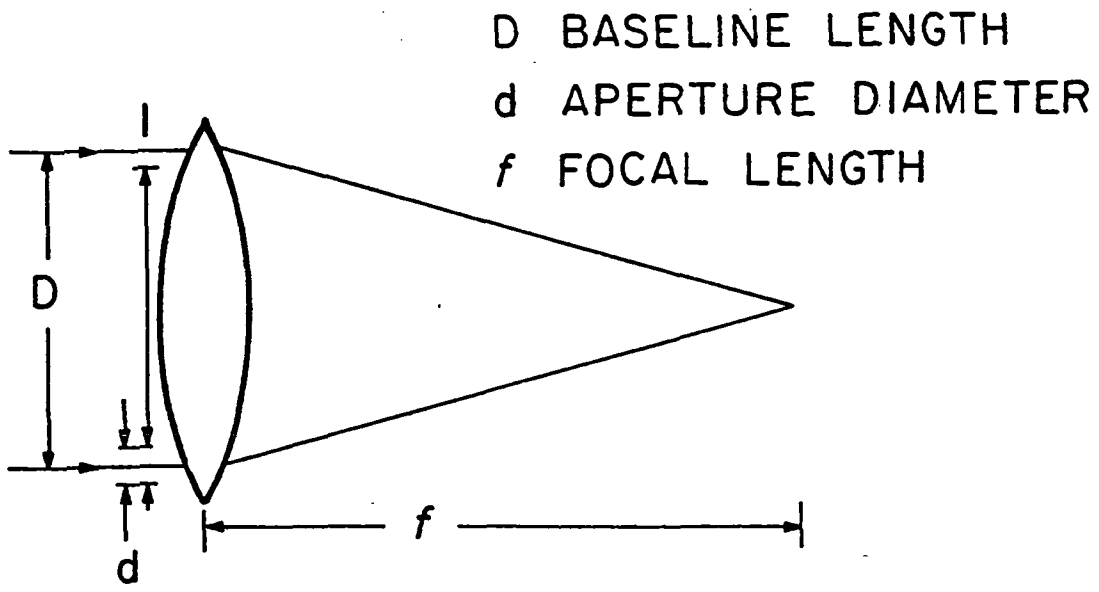

IMAGE PLANE INTERFEROMETER

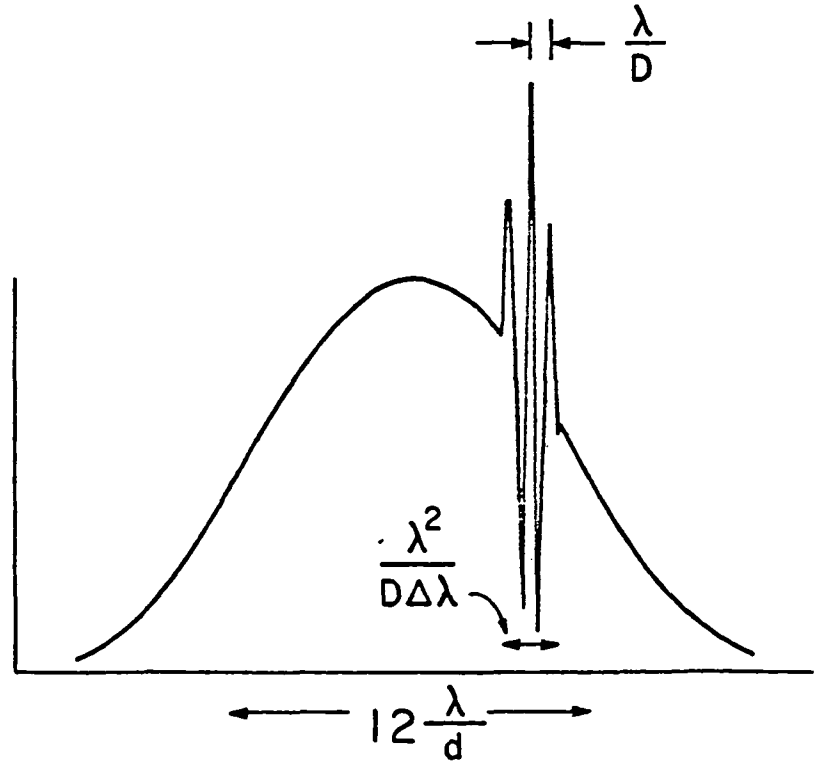

Figure 2.- Fringe pattern of image plane interferometer.

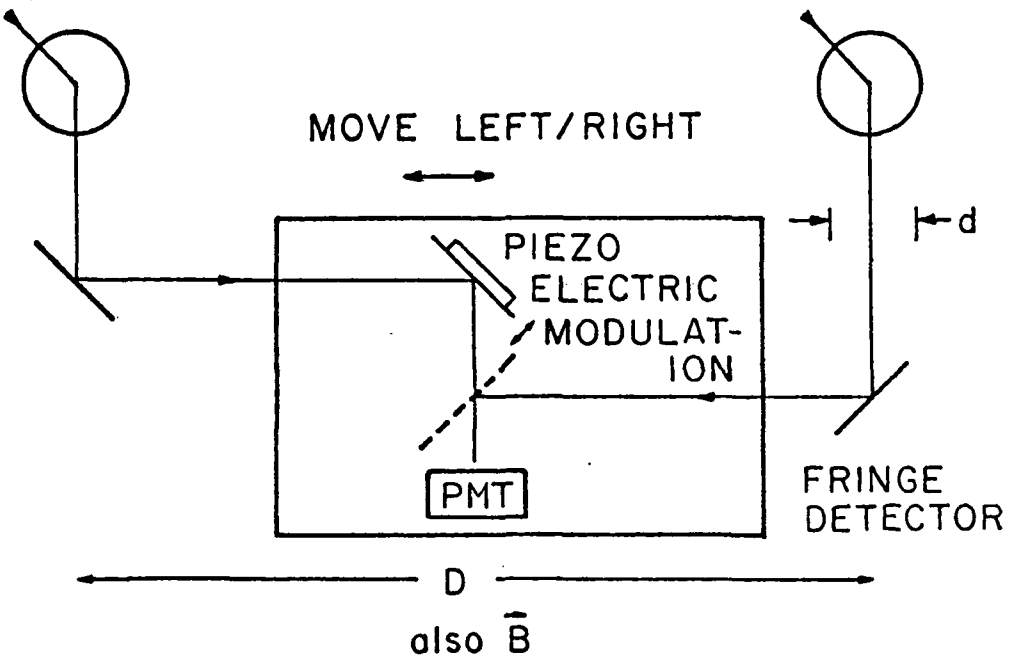

D BASELINE LENGTH

d APERTURE DIA.

$\bar{B}$ BASELINE VECTOR

Figure 3.- Pupil plane interferometer.

PAPER 7

PRECISION STELLAR CATALOGS AND THE ROLE OF ANOMALOUS REFRACTION

Douglas G. Currie

Technical Report # 77-076

PP # 77-230

Submitted as a part of a proposal to the

Office of Naval Research

February 1977

UNIVERSITY OF MARYLAND

DEPARTMENT OF PHYSICS AND ASTRONOMY

COLLEGE PARK, MARYLAND

I. INTRODUCTION

Atmospheric refraction, with its non-predictable variations, is one of the dominant sources of error in the precise determination of the apparent position of a star. It appears that this will be the dominant error source for the new generation of instrumentation now being installed for the determination of stellar catalog and Universal Time (i.e., the USNO 65-cm PZT). The effects of anomalous refraction measurements of stellar position propagate to the various quantities derived from this data. This includes the compilation of stellar catalogs, the determination of Universal Time, and variations in the latitude.

A unique instrument, the Two-Color Refractometer, can, for the first time, directly measure the total deviation which the light of a star suffers due to refraction and thus can be used in a measurement program to evaluate the various aspects of anomalous refraction. In addition, this system may be used to make fundamental astrometric observations which are free from the deleterious effects of refraction.

A. Atmospheric Refraction

There are two aspects of refraction errors which are useful to discuss separately. The first of these effects are the short-term errors or the "random error" in an individual measurement. These errors affect an individual measurement so that it may be significantly different from measures made before and after it on the same night. This type of error may be of the order of 0.15 arc-seconds or larger. When we later discuss all of the errors more generally in terms of the power spectra of the anomolous zenith refraction, the random error is characterized by the magnitude of the power spectra in the domain having periods of a few minutes.

The many individual measurements may be analyzed and the results averaged together for an entire night. This procedure should result in

an improved determination of the quantities derived from the stellar position measurements. The improvement should be parameterized by a factor proportional to $1/\sqrt{n}$. This will occur if the errors of each separate measurement are independent. However, if there are phenomena which affect the anomolous refraction which have long periods, then the determination of the averaged quantities may now show this improvement. Again, discussing the question in terms of the power spectra, one will obtain the improvement in performance only if the power spectra vanishes for periods longer than a few minutes. We now address the effects of the power spectra for periods greater than the time which is required for a single observation. The systematic error to be expected may be derived from the power spectra and it will be dominated by the magnitude of the power spectra with the period in question.

B. Derivation of Star Catalogs

We wish now to consider the question of the improvement of the star catalogs. This will require one to both improve the measurement of the single observation and reduce the systematic errors obtained when averaging data over long periods. The former will improve the basic random error and the latter will insure that the result of many measurements will reduce this diminished random error in proportion to $1/\sqrt{n}$. In general, the stellar catalog measurement using the Transit Circle is most affected by three types of error. These are: the anomolous refraction, the encoder errors, and the lack of stability of the personal equations. It is difficult to separate the effects of these errors prior to the measurements of anomolous refraction. Therefore, we shall address the remaining remarks to measurements made with the Photographic Zenith Tube (PZT). For the PZT, the errors of encoders and lack of reproducibility of personal equation are far less significant than in the Transit Circle. In addition, to first

order one is independent of normal refraction and only sensitive to the anomolous refraction. In this discussion, we refer to the "normal refraction" as that theoretical quantity derived from the zenith distance of the star, and the local pressure, temperature, and humidity. The anomolous refraction is the difference between this normal or calculated refraction and the actual measured refraction.

In the case of the PZT, the normal random error is of the order of 0.18 arc-seconds. This is the internal precision for one night and does not include the effects of longer period phenomena which is probably significantly smaller. It is more difficult to estimate the errors with a longer period. These effects, due to phenomena like the heat island effect of Washington, D.C., the seasonal variation of the heat island effect, and long term weather effects may lead to violation of the horizontal uniformity which is assumed in the normal data reduction procedure. The derivation of the averaged measures for one night at the USNO may be of the order of 0.06 arc-seconds for periods between one and one hundred days.

C. Two-Color Refractometer

In order to address the role of anomolous refraction in these determinations of star position, we suggest the development and use of the Two-Color Refractometer (TCR). The TCR is a system which measures the magnitude of the refraction due to the atmosphere when observing a star. This measurement is not affected by problems of an encoder, a star catalog, or variations in personal equation. It is a measurement which isolates the refraction alone.

The primary subsystem of the Two-Color Refractometer is the Quadrant Sensor System (QSS). The QSS is an operating system which has been developed at the University of Maryland. The QSS is an "eyepiece" which permits one to determine the apparent star position with great accuracy. This determination of the apparent direction to the star is performed by observing in two different colors. Using a knowledge of the index of the refraction and the dispersion of the air, one may compute from this data the instantaneous magnitude of the angle of refraction. Using the local temperature, pressure, and humidity, one may then compute the normal refraction. The difference between the normal angle of refraction and the measured angle of refraction is the anomolous refraction. The latter will be done by exactly the same calculation which is normally used by USNO for the reduction of transit circle observations.

In general, the anomolous refraction will depend upon both zenith distance and time. Let us for the moment neglect the time variation. Then a number of stars may be observed "at one instant" (actually a period of about thirty minutes). The measured value of the anomolous refraction may then be expressed in a power series function about the zenith in terms of "east" and "north" direction. The first term, which will be a constant term, which might be due to the use of erroneous values of local pressure, temperature and humidity, for the computation of the normal refractions. Any linear terms which appear would be due to gradients in the atmosphere. Quadratic terms should be small if the theory is proper and the constant term is not large.

II. OPERATION AND PERFORMANCE OF A QUADRANT SENSOR SYSTEM

In this section we consider an ideal Quadrant Sensor System (QSS) and discuss the expected performance of such a system. The objective of the first part of this section is to define the type of sensor system which would be most desirable and to provide a model for the performance analysis which will appear later in this section. The realization of the QSS system will be discussed in Section IV.

The QSS is based upon a special photosensor, the "Quadrant Photo Sensor" produced by the Electronic Vision Company, a division of Science Applications, Inc. The Quadrant Photo Sensor (QPS) consists of a quadrant silicon diode which is mounted in an evacuated envelope. Photons are converted to photoelectrons at the photocathode and accelerated electrostatically to an energy of 15 KeV. They are then electrostatically imaged onto the quadrant diode. The overall mechanical configuration of the Quadrant Photo Sensor (QPS) is illustrated in Figure 1.

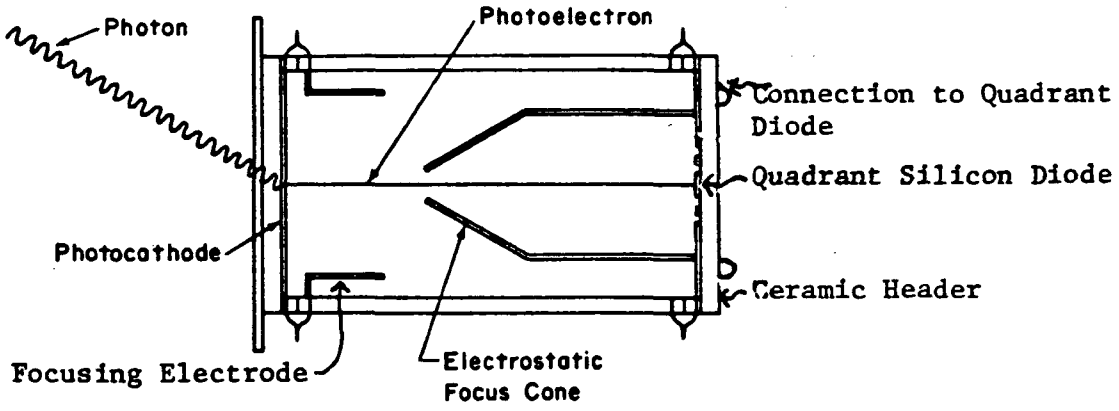

Schematic Diagram of Quadrant Photo Sensor
Figure 1

The photoelectron, which is accelerated to 15 KV, produces extensive ionization within the silicon in the photodiode. The output of a photodiode which is bombarded by a single photoelectron is a charge packet which consists, at the normal operating voltage, of about 2,000 electrons. This pulse signal generated by this charge packet is amplified, shaped, and finally detected with a level discriminator. In order to operate such a

system, we wish to provide functions indicated in Figure 2.

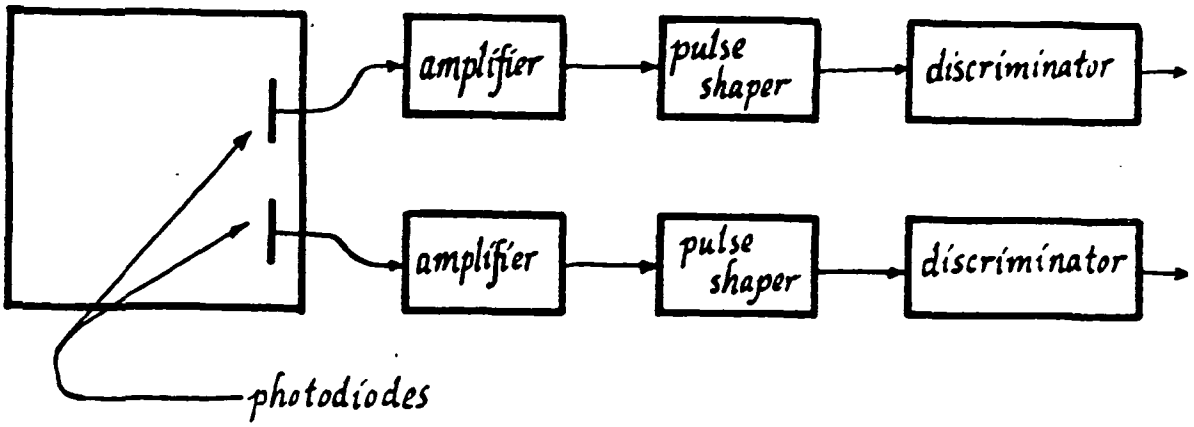

QSS Detection Subsystem for Single Photoelectrons
Two of the Four Channels are Shown
Figure 2

Thus Figure 2 illustrates the photon detection system, which provides a high-level pulse for the arrival of each photoelectron. By accumulating these counts, one would have available the intergal number of counts for any interval. However, we wish to use such a system in several applications where a greater variety of outputs are required. The above system will be used as the basis for the calculations presented in Section II. At present, however, we shall now continue this discussion to describe the full Quadrant Sensor System requirements. The subsystem described in Figure 2 is connected to a data processing subsystem.

The QSS has been designed both to provide the input for a telescope used for the tracking of stars, but also to detect laser returns from satellites and track on these returns. However, the latter function is not used in this application and will not further be considered.

When operating in the photon sensing mode, the system is expected to produce an output signal which is proportional either to the intergal number of counts or the count rate smoothed in some fashion. Two outputs of this type, which are the difference between the counts from each axis, are

available (X high pass, Y high pass). In addition, the output is then filtered with a low pass filter having a time constant of about 1 second. This is available as $X_{\text{low pass}}$ and $Y_{\text{low pass}}$. The high speed outputs will be used as the input for an external subsystem to stabilize the image with a high frequency response. The low frequency output will provide the signals required to move the telescope. The signals described above are available in analog form in order to operate the analog servo-loops. They are also multiplexed onto an A-to-D Converter to provide outputs which may be used for computer control and recording. Thus this unit is capable of both stabilizing the image, and through the photon counts, provide interval number of counts in the various channels.

In this discussion we shall evaluate some of the numerical performance parameters for the quadrant sensor. In this section we shall presume the use of a quadrant photon counting sensor. We will assume that the photocathode has a uniform quantum efficiency and that the electronics system imposes no rate limits. The description of the actual sensor and its limitations appears in a later section.

Photon Noise in Direct Mode

In this section we shall compute the photon noise which affects the determination of the centroid of an image by a Quadrant Sensing System. For pedigogical ease, we shall first consider a stellar image which is square, so the brightness has the form indicated in Figure 3.

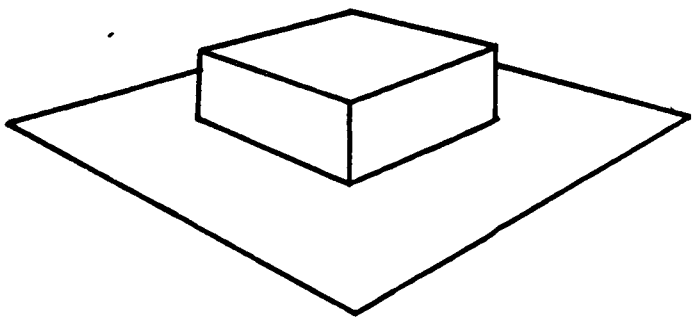

Brightness of Stellar Image
Figure 3

The difference between the performance criteria for this approximation to the stellar image (by a square pillbox) and a more realistic approximation, i.e., a Gaussian or a Lorentzian form, will be discussed later. The more realistic forms will result in about a 2% modification of the numerical results obtained for the square pillbox image.

The results shall be expressed in terms of the total number of photoelectrons which arrive on all four quadrants (denoted by the symbol N) during a time interval denoted by the symbol T. The full width of the image described in Figure 3 is denoted d, which might typically have a value of two arc-seconds for a reasonable telescope used at a good astronomical site. The one dimensional projection of such an image has the form indicated in Figure 4.

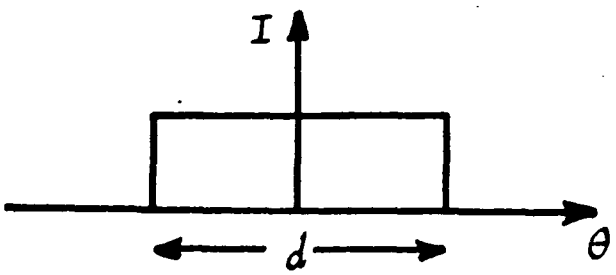

One Dimensional Projection of Square Pillbox Image
Figure 4

The number of photoelectrons per linear arc-second at the center of the square image, denoted by $\tilde{N}$, is given by

$$\tilde{N} = N/d = N/(d_o\sqrt{3})$$

where d_o is the "rms diameter". This quantity is obtained by doubling the rms radius, which is the deviation of the light intensity distribution over the image plane. We may reexpress $\tilde{N}$ in the form

$$\tilde{N} = (\eta N)/(2d_o)$$

where we have defined the symbol η to represent a numerical coefficient which is related to the shape of the image. Thus from the above expressions, we see that for a square image

$$\eta_s = 2/\sqrt{3} = 1.547$$

Now we consider an image with a more realistic profile, i.e., a Guassian. The one dimension projection of such an image is indicated in Figure 5.

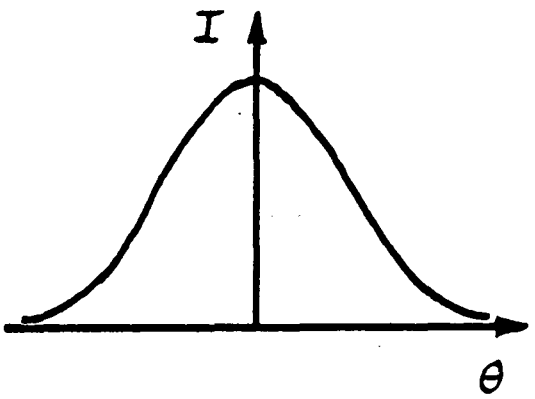

One Dimensional Projection of Gaussian Image

Figure 5

The intensity $\tilde{N}$, expressed as the number of photoelectrons/arc-seconds, has the form

$$\tilde{N}(x) = \frac{\sqrt{2}\ N}{\sqrt{\pi}\ d_o}\ e^{-2x^2/d_o^2}$$

Thus at origin

$$\tilde{N} = \tilde{N}(o) = \frac{\sqrt{2}\ N}{\sqrt{\pi}\ d_o} = \eta_g\ N/2d_o$$

Where we have again used the coefficient as η. Thus for the Guassian we have

$$\eta_g = (2\sqrt{2})/\sqrt{\pi} = 1.5958$$

Thus in general, the value of η will be dictated by the model for the seeing disk, or from a more pragmatic veiwpoint, from an actual measurement of the size and profile of the seeing disk.

We may later take into account a large deflection or error in image position by expressing η as a function of the offset of the image. Thus if there is an average offset of Δ , then $\eta\ (\Delta)$ will have a smaller value. In this way we will be able to address some problems which will arise in the two color application. Thus for a Guassian image

$$\eta\ (\Delta) = \frac{2\sqrt{2}}{\sqrt{\pi}}\ e^{-2\Delta^2/d_o^2}$$

The quantity $\tilde{N}$ is physically related to the change in signal or differential count rate for motion of the image. Thus if we apply a sinusoidal offset or a "dither" to the position by an optical device, we will see a similar variation in $\tilde{N}$. This will obviously be related to the profile, as expressed by η. On the other hand, if we assume a profile, we may invert this relation and use the measured value of $\tilde{N}$ which is obtained by applying a dither to the servo-system to evaluate the seeing disk diameter, using the expression

$$d_o = \eta\ N/2\tilde{N}$$

If the image is nominally centered, then a small image offset which is parameterized by the value of θ will result in a difference in count rates which is given by:

$$\Delta N = N_L - N_R = (N_{Lo} + \tilde{N}\cdot\theta) - (N_{Ro} - \tilde{N}\cdot\theta)$$

We will describe the one-dimensional case. If the image was initially centered and the quantum efficiencies of the effective areas of the photocathode are equal then $N_{Lo} = N_{Ro}$ and the above equation becomes

$$\Delta N = 2\tilde{N}\theta = \eta\, N\theta/d_o$$

which may be reexpressed as

$$\Delta N/N = \eta\, \theta/d_o$$

or using ΔN to compute the offset angle

$$\theta = (\Delta N/N)\, d_o/\eta$$

We may now define a relative angle which is expressed in terms of the image diameter, so we have

$$\alpha \equiv \theta/d_o = \Delta N/N\eta$$

This expresses the angular offset due to an inequality in counts as a dimensionless angle.

Now let us determine the standard deviation of the angular position due to shot noise, i.e., the statistical error in the determination of the centroid due to the photon statistics. In each pair of quadrants (presuming we sum the photocounts from both quadrants of each side to determine the error) the mean value is

$$\bar{N}_L = \bar{N}_R = N/2$$

Thus for large values of N, the statistical noise in the value of each of these is

$$\delta N_L = \delta N_R = \sqrt{N/2}$$

Since the statistical noise in each of these quantities are independent, we have

$$\delta N = \sqrt{(\delta N_L)^2 + (\delta N_R)^2} = \sqrt{N}$$

inserting this value of δN into the above expression for α yields an equivalent angular offset due to the noise. Thus we have

$$\alpha = 1/\eta \sqrt{N}$$

At this point, these considerations will be extended to include the effect of a uniform sky background on the performance. Thus the presumed brightness now takes the form

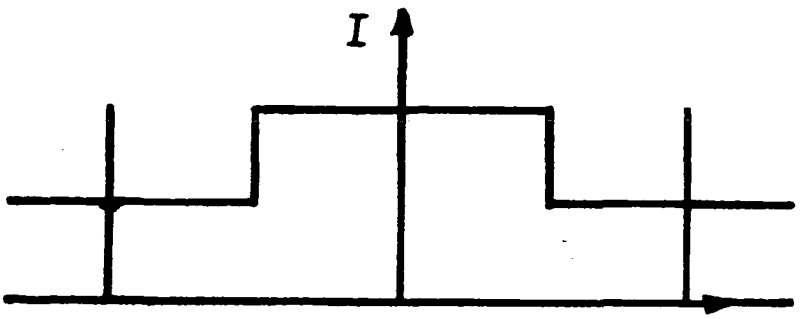

Brightness Distribution for Sky Background With Boundary of Photosensitive Region Marked

Figure 6

where N_b is the total number of counts which appear in the four quadrants due to the brightness of the background sky. This is equal to the product of the field of view (in arc-seconds), the background illumination (in photoelectrons/arc-second/sec), and the integration time (in seconds). The product is expressed in photoelectrons. The image of the star is characterized as in the previous discussion. In this treatment, one simply adds the background to the image, so the mean number of counts on each side is given by

$$N_L = N_R = (N + N_b)/2$$

Thus the photon shot noise in one of the pairs of quadrants (again for relatively large signals) is given by:

$$\delta N_L = \sqrt{N_L} = \sqrt{(N + N_b)/2}$$

and the values for N_R and δN_R have similar expressions. Now if we take the difference of these two independent qualities and use this quantity to determine the apparent error in pointing angles, with the presumption that the photon statistics on the two sides are independent and the sky illumination is spacially uniform, we have

$$\Delta N = \sqrt{N + N_b}$$

Thus for α we have

$$\alpha = \sqrt{N + N_b}/\eta N = \sqrt{1 + (N_b/N)}\Big/ \eta\sqrt{N}$$

where we have used the total counts for the noise in the numeration, and the counts in the image for the signal which appears in the denominator. We have two types of behavior of interest, the first of which consists of the case when the background is negligible. For this case the error becomes

$$\alpha = 1/\eta\ \sqrt{N}$$

as discussed earlier. This is illustrated for the case of a Gaussian image in Figure 5 by the solid line.

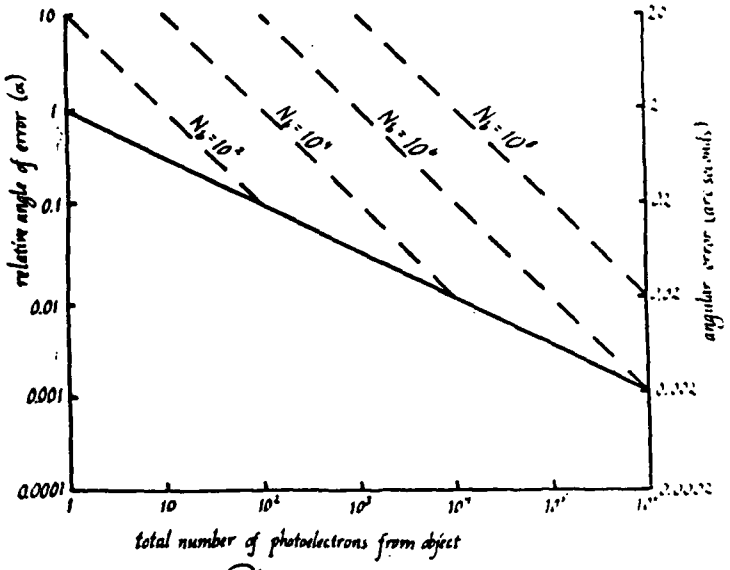

Figure 7.

The other extreme case is when there is a high level of background illumination. This might represent observations conducted in the daytime with a blue sky. In this case we have:

$$\alpha = \sqrt{N_b/N} \Big/ \eta\sqrt{N} = \sqrt{N_b} \Big/ \eta N$$

This may be summarized in graphical form by the dashed line in Figure 7.

Thus Figure 7 indicates the performance that one may expect to obtain with the quadrant sensor. The expected error in the relative angle and the expected error in arc-seconds, presuming a seeing disc diameter of two arc-seconds are related to the total number of photoelectrons received during the observation period.

We may now transform this relationship to describe the behavior with respect to stellar brightness and telescope aperture. Let us, for example, consider a 48-inch telescope and photoelectron count rates which are caused by a particular stellar brightness for a G-2 star (or solar reflection from a satellite). We assume a quasi- S-20 photocathode as measured for a tube of this type and six mirrors with reflectivities of 0.7, 0.7, 0.86, 0.86, 0.86, and 0.86. Thus for the case of a Guassian image with negligible sky background we have the relation indicated in Figure 8.

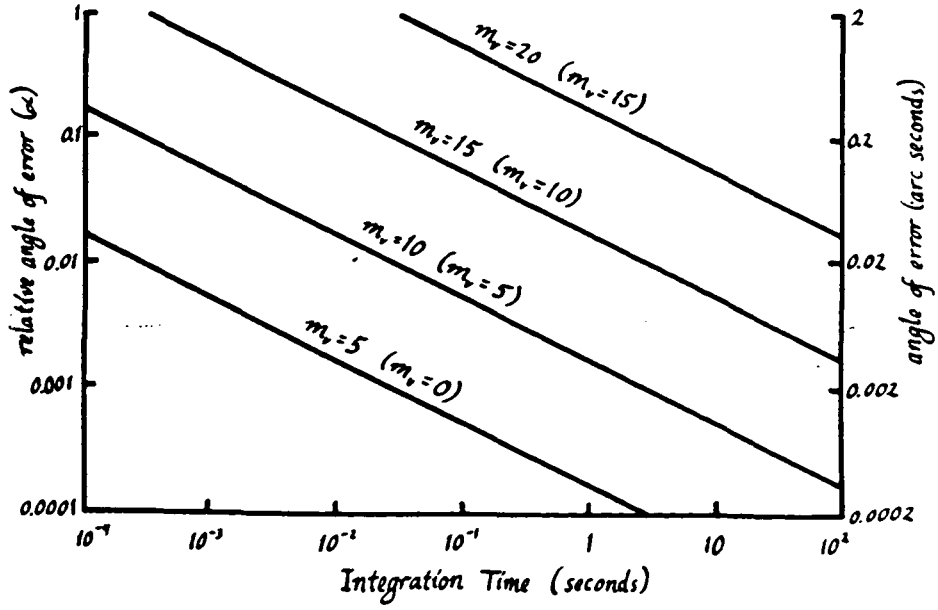

Figure 8.

This indicates the ability to go to rather faint objects and still have very small angular errors due to the photon counting. The numbers in parentheses indicate the results for a 4.8-inch aperture.

III. TWO COLOR APPLICATIONS

The Quadrant Sensor System, as a component of the Two-Color Refractometer system may be used to obtain high accuracy measurements in absolute astrometry. In particular, it will determine the deviation in the apparent star position caused by the earth's atmosphere. As star light enters the earth's atmosphere, the deviation of index of refraction of the atmosphere from that of the vacuum results in a change in the direction of propogation. For a flat, horizontally-stratified atmosphere, this change in direction is a known function of the index of refraction of the air in the immediate vicinity of the telescope (the local index of refraction). This may be determined from the local temperature, pressure and humidity. However, if there are horizontal inhomogeneities, this change of propogation direction can not be predicted from a measurement of local surface conditions. In this section, we address a procedure to determine the magnitude of this change in direction (the "angle of refraction") from measurements made on the light of the star using the Quadrant Sensor System.

We take advantage of the fact that the magnitude of the angle of refraction depends upon wavelength, due to the dispersion of the index of refraction of air. Thus by measuring the apparent position of the star as viewed in red and in blue light, the difference in apparent position may be evaluated. This dispersion angle may be used with a knowledge of the dispersion in the index of refraction to determine the angle of refraction. Thus using the dispersion angle between the red and blue images, and the known dispersion of the air, we may determine the deviation of the direction of propogation of the starlight due to the atmosphere.

In order to illustrate the operation of the Two-Color Refractometer (TCR) let us consider the basic relations governing the refraction. The symbol Θ_λ describes the deviation of a ray of wavelength λ from its initial direction and ϕ is the true zenith distance of the star. The index of refraction of the air at the wavelength λ is denoted by η_λ. Thus from Snell's law, we have

$$\Theta_\lambda = (\eta_\lambda - 1)\phi/\eta_\lambda \quad .$$

Since η_λ is very close to unity, we shall approximate this expression by:

$$\Theta_\lambda = (\eta_\lambda - 1)\ \phi$$

where the definition of these quantities may be seen in the following figure

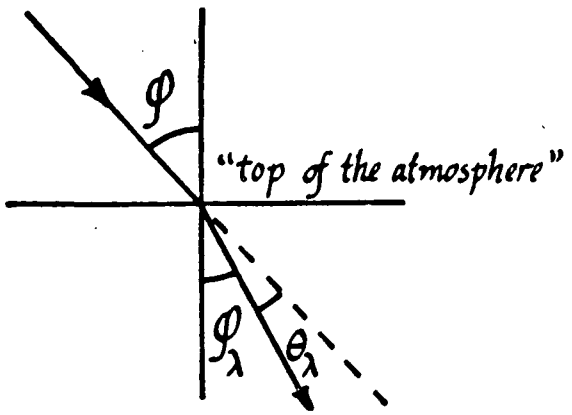

Effect of Refraction on Starlight

Figure 9.

While the figure illustrates a simple idealized case, a little reflection indicates that equations apply to the more general case of a continuously variable, non stratified, spherical atmosphere. For the calculation made in the later part of this section, we use the following expression for the index of refraction for dry air

$$(\eta_\lambda - 1) \times 10^{-6} = 64.328 + 29498.1\ (146 - \lambda_0^{-2})^{-1} + 255.4\ (41 - \lambda_0^{-2})^{-1}$$

This applies for a temperature of 15°C, a pressure of 760 mm and no water vapor. This expression is not the optimal form for expressing the index of refraction when reducing the data for the operational system, but it is entirely satisfactory for the system analysis and error analysis presented in this section.

In order to permit the independent variation of the wavelength selected for observation within a reasonable error analysis, we shall use the blue and red measurements and a parameter which depends on the wavelengths used to determine the magnitude for the angle of refraction at a reference wavelength chosen to be the center of the visual band (5600Å). Thus for the wavelengths at which we will measure the relative angular position, we use:

$$\theta_R = (\eta_R - 1)\phi$$

$$\theta_B = (\eta_B - 1)\phi$$

We will then use these expressions to determine the zenith distance ϕ, which we will relate to the angle of refraction in the green by the relation

$$\theta_V = (\eta_V - 1)\phi$$

Thus we will determine the angle of refraction in the visual band. This particular equation does not appear to represent the optimal procedure for minimizing the propogation of experimental errors but we shall use it as a useful tool for system analysis. Thus we obtain an expression of the form:

$$\theta_V = \Omega\ (\theta_B - \theta_R)$$

where

$$\Omega = (\eta_V - 1)/[(\eta_B - 1) - (\eta_R - 1)]$$

If we measure the difference in apparent angular position of the blue and the red image, this angular difference, multiplied by the quantity Ω, will yield the angle of refraction suffered by the visible light. This is the value for local conditions which are 15°C and a pressure of 760 mm Hg.

In order to provide a general frame of reference, let us consider the numerical values for the refraction and the dispersion angles. Let us consider the value of Ω for various choices of the limiting wavelengths. We have

Effective Blue Wavelength	Effective Red Wavelength	Ω
3500Å	6000Å	30.36
3300Å	6000Å	25.27
3500Å	7000Å	26.89

Relation Between Selected Wavelengths and Ω Multiplier

Table 1

Since the eventual error is proportional to the value of Ω, we would prefer the smallest possible value. From Table 1 we see that the value of Ω decreases and thus the error multiplier decreases as the spread between the wavelengths increase. This dependence is particularly sensitive to the wavelength of the blue observation where a change of 200Å provides as much improvement in Ω as a change of 1000Å in the wavelength of the red observation. However, for various technical reasons we will accept the first case as a reasonable, practical limit.

Let us now evaluate the sources of error in this determination. Differentiating the expression for Θ_V, we have:

$$\delta\Theta_V = \frac{\delta\Omega}{\Omega}\Theta_V + \Omega\,(\delta\Theta_B - \delta\Theta_R)$$

We now presume the uncertainty in the measurement of the angular position of the image in the red and in the blue have the same magnitude, and are independent. Concerning the former, it assumes similar filter widths which will probably not be the case, but it is a useful point for discussion. Thus for the part of the variation due to uncertainty in angular measurement we have

$$\delta\theta_V \quad \sqrt{2}\ \Omega\ \delta\theta$$

where

$$\delta\theta = \delta\theta_B = \delta\theta_R$$

We may now use the relations between the total number of counts and angular errors to express the accuracy of the determination of $\delta\theta_V$ as a function of the total number of photoelectrons. In Figure 10 we have also indicated the various system operating points obtained when the QSS is running at the maximum count rate (the normal procedure) for various intervals of time. These results include the effect of the UV filter and the red filter.

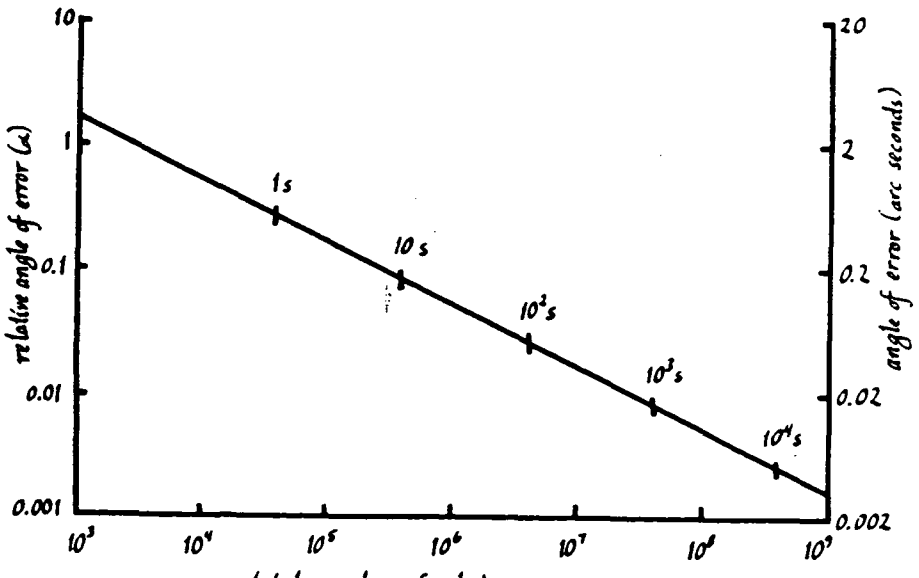

Relation between total number of counts and error in anomalous refraction for TCR.

Figure 10

We now consider the other source of error which appeared in the Equation for $\delta\theta_V$. This is the possible variation in the quantity Ω. It is presumed that Ω is calculated for the local value of refraction (i.e. using pressure and temperature). The predominant remaining reason for an uncontrolled uncertainty in $\delta\theta_V$ is due to the variable water vapor content in the atmosphere. In order to evaluate this phenomenon, the following table is presented. This presents the value of Ω and the change produced in Ω due to precipitable water for various pairs of effective wavelengths. We use the mean water vapor which is expressed in the terms of precipitable water vapor (for a flat atmosphere).

Effective Wavelength for Blue Filter	Effective Wavelength for Red Filter	Ω for no Water	Precipitable H_2O	Ω with Water Vapor	$\delta\Omega/\Omega$
3500	6000	30.3657	10 mm	30.1885	0.0058
3300	6000	25.2696	10 mm	25.1232	0.0058
3500	7000	26.8927	10 mm	26.7351	0.0059
3500	6000	30.3479	1 mm	--	0.00065

The Effect of Water Vapor on Systematic Errors

Table 2

Thus we see that the water vapor correction is approximately proportional to the amount of water and generally independent of the selection of the effective wavelength of the filters.

Let us now consider a numerical example. If we observe a star at zenith distance of 30° as one might with an astrolabe, then using the expression for the refraction under standard temperature and pressure

$$\theta_V = 58''.2 \tan Z$$

which applies to a flat atmosphere we have, at 30°, a deflection of about 34". If we wish to be able to determine this correction with an accuracy of 0".05, then we need

$$\frac{\delta\Theta_v}{\Theta_v} = \frac{\delta\Omega}{\Omega} = \frac{0''.05}{33''.6} = 0.0015$$

This means one to know the water content to 2.3 mm of precipitable water.

However, this requirement is not particularly difficult since commercially available microwave radiometers are accurate to about 1 or 2 mm of precipitable water. In addition, a system ttached to the TCR using near IR measurements in and out of a water absorbtion band should be significantly more accurate and less complicated.

Some Practical Considerations

We now consider a few practical aspects of the design of the TCR. The full discussion of the system will be considered at a later time.

We first consider the procedure for sampling the light at two different colors. One might attempt to measure the position of the red and blue images at the same time with two different quadrant sensors. The parameters which enter Figure 6 are based upon this assumption. However, a more practical approach to this problem is to use a single quadrant sensor. The detailed reasons will be considered in a separate discussion. We shall, briefly, discuss this approach and how we should use it to maximize the accuracy of the evaluation. Thus we note that due to the fact that the refraction in the atmosphere has significant power at various frequencies, one might wish to sample the two different colors continuously and at the same time. If this is done, then both the power at high frequency and the power at low frequency (the image motion) are properly tracked and do not affect the accuracy of the measurement.

However, the mechanical stability requirements strongly suggest the use of a single detector. If one switched the two colors onto the one sensor at a rate of several hundred times a second, one may show that the residual error is expected to be random and has a value of less than 0.01 arc-seconds for a measurement lasting several minutes.

The remaining uncertainty is in the determination of the water vapor. From the previous discussion, and typical values of water vapor to be expected, this effect may be totally ignored for the initial measurements out to a distance of 15° from the zenith.

Expected Accuracy for Measurements of Zenith Refraction

We now discuss the accuracy which we would expect to obtain with measurements using this instrument. These will be expressed in terms of the measurement errors to be expected on the power spectral density, and will be based upon use of the 48-inch telescope at the Goddard Optical Research Facility (GORF). However, approximately the same numbers apply to the set of measurements which would be performed on the 36-inch telescope. For these evaluations, we will presume the use of the present circuit for the quadrant sensor which has a maximum counting rate of 10 kilohertz/quadrant. This will permit the observation of 8th magnitude stars with the proper count rate. Since we will limit our measurements to a region that is between 5 and 10 degrees, it is worth noting that we would statistically expect to have about 80 stars within a five degree circle of the zenith.

In general, the relationship between the stellar magnitude, the telescope aperture and the expected photon statistical error for a ten minute observation is expressed in Figure 11.

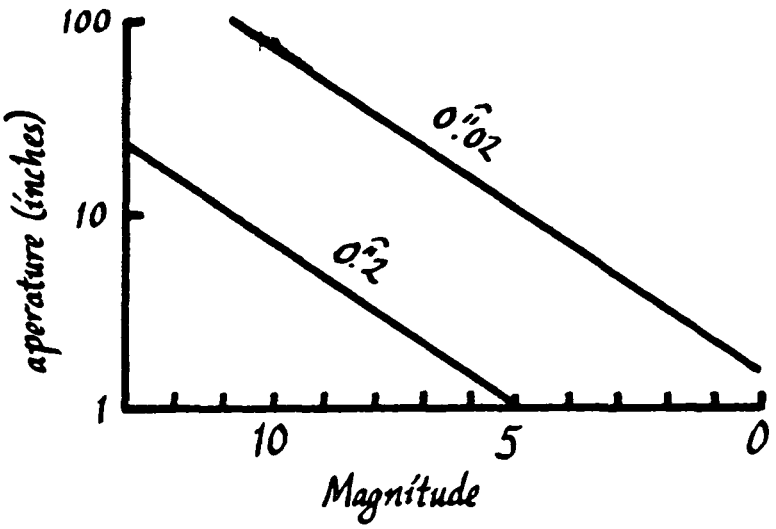

Figure 11

Combining the results of Figure 10 and Figure 11, we see that we may trade off between the aperture size of the telescope with the observing time to use a small telescope and still have a reasonable number of stars to observe.

Now presuming this count rate, we can evaluate the power spectrum of the system errors which we expect. To facilitate this present discussion, we will not consider the true power spectrum but indicate the standard deviation of the system error for a measurement of a given length. The overall results are thus summarized in Figure 12. The system error caused by the photon statistical noise is illustrated by the broad solid line. For periods shorter than one second, one may increase the centroid of the white light image and rely on the smoothness of the telescope tracking to determine the refraction (called image in this domain) rather than the two-color extraction. This is expected, with some study of the records and knowledge of the telescope, to give about 0".2. If these measurements were conducted on the 100-inch telescope at Mt. Wilson, which has a very smooth and regular drive, and were conducted on a night of low wind, this system error could probably be reduced to 0.1 arc-seconds. For periods of more than 10 seconds, however, one would expect that errors in the telescope

drive will become too large. In order to study the behavior for longer characteristic times, we consider a limit for a single observation of twenty minutes which results in an error of 0.01 arc-second. Thus one might expect to obtain an increase in accuracy by about a factor of three, but this will mean the observation of new stars. The feasible accuracy in this region must be more carefully explored. For the longer period term, one averages the data obtained on successive nights to obtain these results. However, since we do not expect to observe for 24 hours a day, there is a break in this curve as one goes to the dashed portion. Presuming an observation period of two hours for a night, we obtain the dashed curve. At about 0.03 arc-seconds one expects to run into systematic errors. It seems possible that these may be calibrated to the 0.001 or 0.002 arc-second level. Accuracies beyond this cannot currently be projected for the first generation instrument.

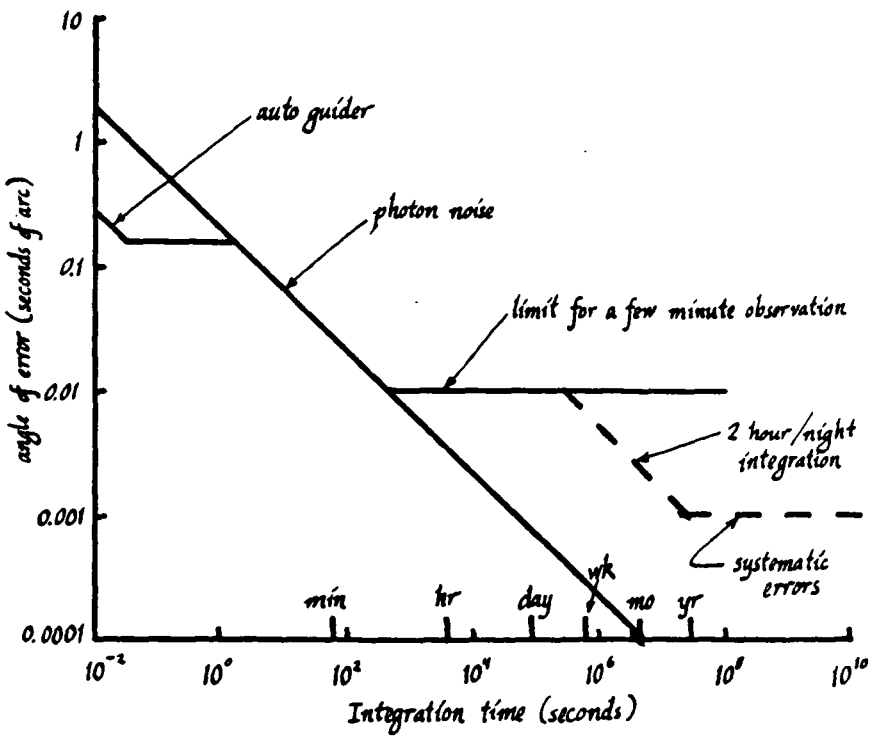

Figure 12

IV. IMPLEMENTATION OF THE QUADRANT SENSOR SYSTEM

In this section we describe the Quadrant Sensor System which has been developed within the Amplitude Interferometry Program at the University of Maryland. This system is the practical realization of the hypothetical QSS which was described in Section II. The basic element of the system consists of two standardized units, the photo-sensor head and the control unit which have been used in three different astronomical systems. The quadrant sensor system is basically a special system which detects light in four channels. These are closely placed and are mechanically and geometrically rigid. In order to satisfy the system requirements, a special device has been obtained from the Electronic Vision Company and an electronic system has been developed at the University of Maryland to make these observations. The requirements on this optical/electronic system demand a very high precision, electronically, optically, and mechanically, as well as a considerable amount of generality. The electronic system will permit the quadrant sensor to interface to a variety of data processing systems, i..e, computers or hardwired processors.

The Photosensor head contains the Quadrant Photisil. The structure has already been indicated in Figure 4 and is shown here

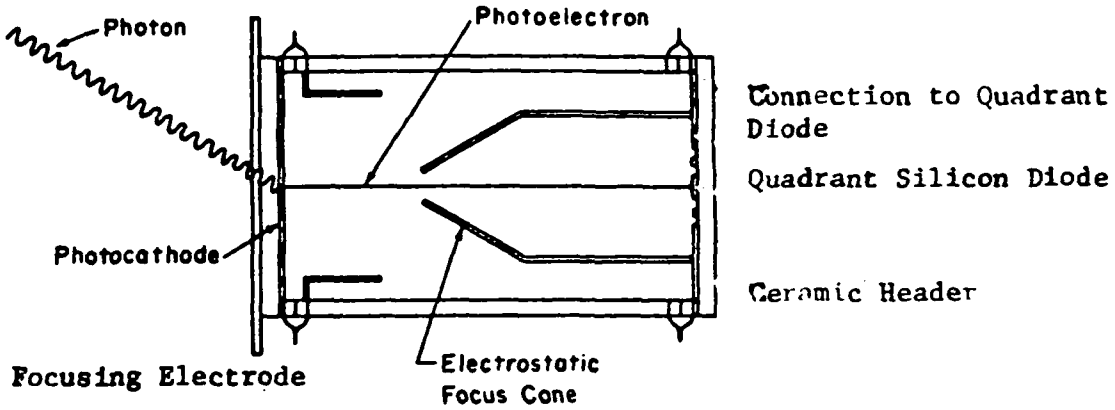

Schematic Diagram of Quadrant Photo Sensor

Figure 13

As discussed in the first section, the circuitry following the Quadrant Photosil is indicated in Figure 14.

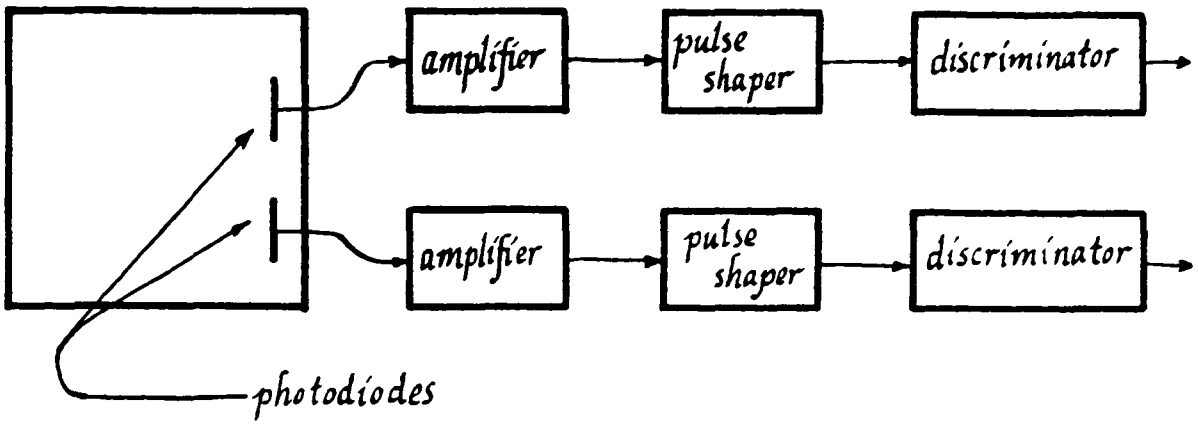

QSS Detection System for Single Photoelectrons
Two of the Four Channels are Shown
Figure 14

This results in a pulse height distribution which permits a straightforward discriminator. The preamplifier is similar to that photon counting Digicon system developed by E. Beaver at UCSD. The pulse height distribution at 16 KV is shown in the following figure.

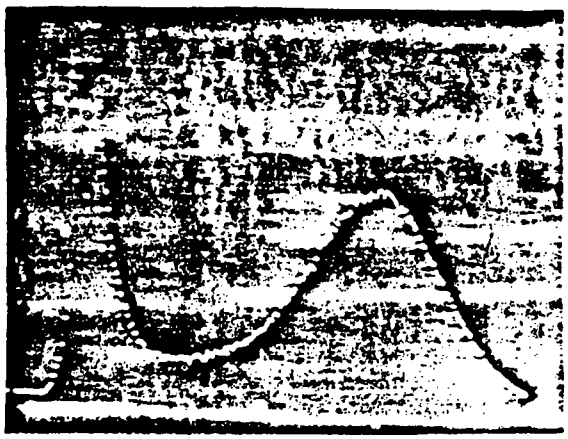

Figure 15

This system is expected to operate in environments with high levels of external EMI. This is a serious problem since the signals are smaller than conventional PMT's by a factor of about 1000 to 10,000.

Special shielding and grounding procedures are required in order to prevent external TVI from interfering with the discrimination process. This has been provided for the input high voltage leads by the use of solid aluminum shields. The amplifiers are specially isolated and grounded. Even so, the pickup is noticable under certain circumstances.

The preamplifier in the QSS head provides a signal which is relatively immume to external problems. This is then sent by four short cables to the QSS Control Unit. Here the signal is reamplified and sent to discriminators. These discriminators may be adjusted independently for each of the four channels. These are normally set at about the point indicated by the arrow in Figure 15. The shape of this pulse height distribution leads to a relative immunity from effects due to the variation one expects in operating voltages and circuits in the field.

In order to interface to a computer and provide data for the closure of a servo-loop, the four signals are multiplexed and then applied to an A-to-D converter. The output is an eight-bit word. The operation acts as an asynchronous peripheral which supplies data when asked. Thus the output of the ADC is available as a digital signal. This generalized system has been used in several applications. We shall now describe how it has already been used.

Application in Single Aperture Amplitude Interferometer

The first application of the quadrant sensor system was to provide image stabilization in Single Aperture Amplitude Interferometry (SAAI). In this system it operates in only one axis. It incorporates a device which provides high frequency stabilization with a frequency response up to about 60 hertz. The gain is set to permit the utilization of the stabilization to this level. The expected noise performancewas discussed in the previous section.

As an indication of the proper performance of this system in Amplitude Interferometry, the measurements of the fringe visibility which are performed when this system is operating are significantly improved. Special procedures have been developed, both for the proper alignment of this system and to permit the simultaneous use of the manual guiding of the telescope. This is required at present since the QSS has not yet been interfaced to the large telescopes due to the necessity of performing the coordinate transformation without a computer.

48-inch Telescope at the Goddard Space Flight Center

The Quadrant Sensor System (QSS) has been used to make an Automatic Guider System (AGS) to control the 48-inch telescope at the GORF. In this case, the output from the high frequency error signal is multiplexed and digitized and fed directly to the computer. There this data on the error in pointing is processed and filtered in a digital form. This system has succeeded in providing precise pointing information and also has been useful in detecting difficulties in the encoder system. Instabilities in the computer processing of the data and the telescope setup drive can cause oscillation under some circumstances. However, the computer procedure for handling the data is now being reprogrammed to handle this properly.

In addition, the GSFC system also provides for the capability to sense the offset of lasers from a satellite reflection. To this end, the capability is provided to gate the photocathode off while the outgoing laser pulse is near the telescope with a high voltage pulse applied to a grid of a modified Quadrant Photosensor. The sensor system can detect the arrival of a laser return. The signal on each diode is amplified, and then compressed for greater dynamic range, and stores before it is presented to the multiplexer. This sequence is activated by the receipt of a photo

pulse which has a value which is greater than three photoelectrons. Thus this gives the error in pointing with respect to the laser return. This system has been implemented and tested in a laboratory but the required computer programs for the 48-inch telescope and the required telescope time are not yet available in order to test the laser tracking system on the telescope.

PAPER 8

THE UNIVERSITY OF ARIZONA RADIAL VELOCITY SPECTROMETER

K. Serkowski, J. E. Frecker, W. D. Heacox, and E. H. Roland

Lunar and Planetary Laboratory
University of Arizona

1. INTRODUCTION

The University of Arizona Radial Velocity Spectrometer is designed to achieve an accuracy of 15 m/s in a single half-hour observation of a solar-type star of fifth magnitude or brighter with a 1.5m telescope. Such an instrument would be capable of detecting the reflex motion due to planets of jovian mass orbiting about several tens of solar-type stars in the solar neighborhood. The precision required corresponds to a wavelength accuracy of about 5 parts in 10^8 for a single observation; consequently, our instrument incorporates:

1) High spectral resolution ($\simeq$ 0.06 Å);
2) Utilization of several hundred angstroms in that portion of the spectrum richest in radial velocity information in solar-type stars (i.e., 4000 - 4500 Å);
3) Wavelength calibration of each resolution element used;
4) Coincidence of optical paths through the spectrometer for both stellar and calibrating sources.

The instrument is briefly described in the following sections. Earlier descriptions were published by Serkowski (1978) and by Serkowski et al. (1979a,b).

The spectrometer consists basically of an echelle spectrograph preceeded by a Fabry-Perot interferometer. The detector is an intensified CID (Charge Injection Device). In operation the spectrograph, interferometer and detector are assembled into a single unit

which is optically connected to the Cassegrain focus of the telescope via an optical fiber several meters long. The calibration lamps and guiding eyepiece are located at the input end of the fiber, i.e., at the Cassegrain focus.

2. DETECTOR

The detector is an Intensified Charge Injection Device (ICID) consisting of a General Electric TN2201 CID of narrow aspect ratio (342 x 42 pixels) optically coupled to an ITT F-4111 microchannel plate intensifier via an f/1.0 Repro-Nikkor (#95161) producing 1:1 imaging scale. Such an arrangement allows the CID to be operated at cryogenic temperatures with attendant significant reduction in noise and dark current and resulting increases in sensitivity, dynamic range and linearity. Operation at cryogenic (in our case, dry ice) temperatures will permit utilization of the unique non-destructive readout capability of CID's; this, together with the parallel injection technique and transparent electrodes incorporated in modern CID's, will allow high quantum efficiency detection with photon statistics as the dominant source of noise (Aikens et al. 1976, Michon et al. 1978). The performance of the chosen CID has been tested by us, while that of our intensifier-transfer lens combination has been thoroughly examined by R. Cromwell (Steward Observatory, University of Arizona). The results of these tests indicate that the objectives stated in Part 1 will probably be achieved or slightly exceeded.

3. SPECTROGRAPH

The dispersion is obtained with an echelle spectrograph operated in an off-plane quasi-Littrow configuration with a transmission grating prism (grism) as a cross-disperser. A Bausch and Lomb echelle with 31.6 grooves/mm and a 64°.7 blaze angle is used in a collimated beam 90 mm in diameter. The reciprocal dispersion is about 3.1 Å/mm and echelle orders are separated by about 0.21 mm in the camera focal plane. The echelle/grism combination functions as a post-disperser to the Fabry-Perot interferometer, enabling all spectral features in spectrometer's passband, about 250 Å wide, to be used for radial velocity determination.

4. INTERFEROMETER

The echelle spectrograph is preceeded by a Fabry-Perot interferometer of finesse 10 placed in a collimated beam 40 mm in diameter. The purpose of the interferometer is to increase the resolving power of the instrument by a factor of about five relative to that obtained with the echelle alone, and to provide the means of calibrating each resolution element (transmission maximum). The Fabry-Perot transmission maxima are about 0.06 Å wide at half maximum and are separated by the interferometer free spectral range $\Delta_{FP}\lambda$(0.63 Å at 4250 Å). The appearance of the spectrum produced by the combination of the Fabry-Perot interferometer and echelle spectrograph is illustrated in Figure 1. The wavelengths of the Fabry-Perot transmission maxima are set by the spacing of the interferometer plates; a precision of 10 m/s requires that this spacing be maintained to $\lambda/16{,}000$. To achieve this our inter-

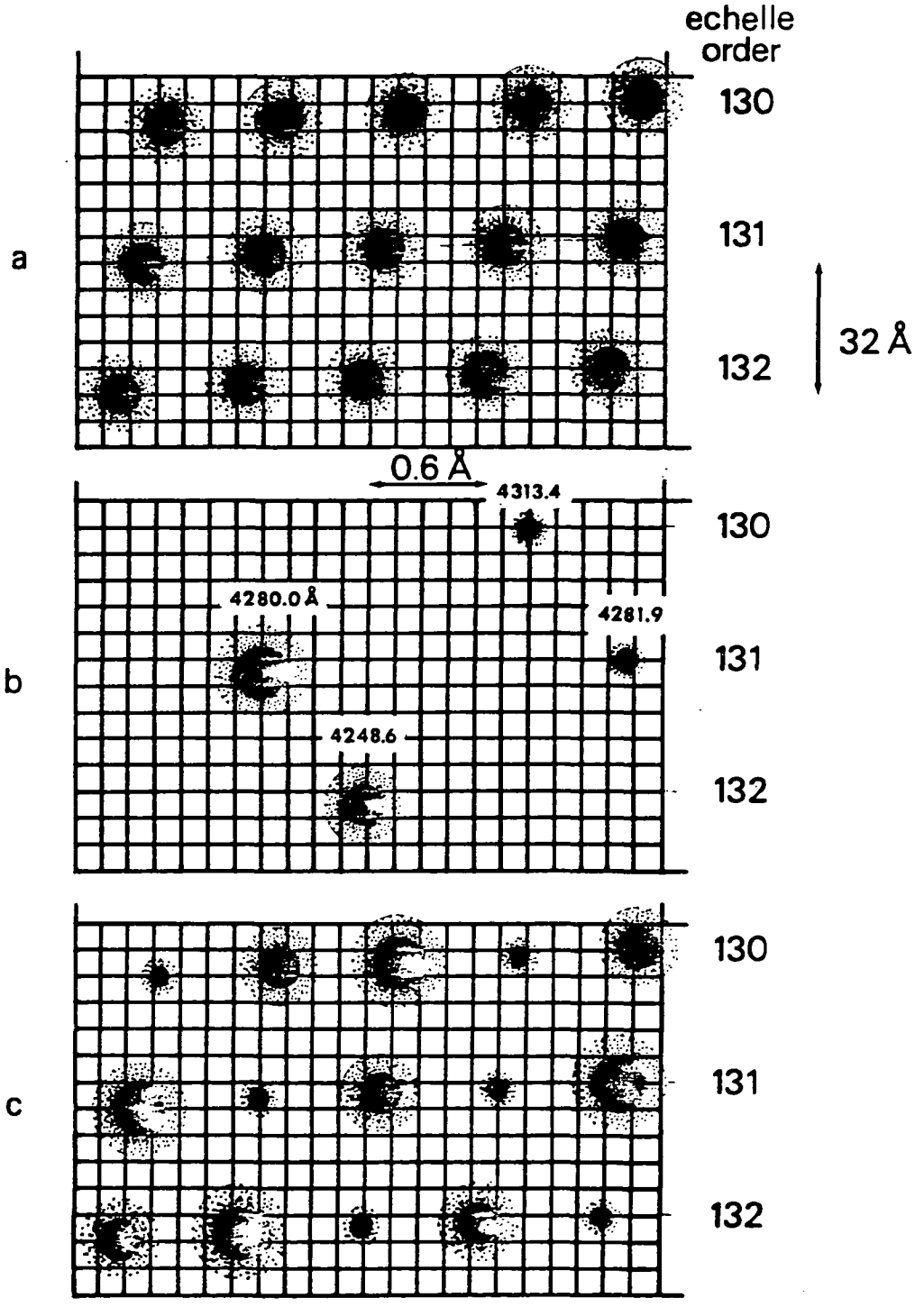

Fig. 1. Fabry-Perot transmission maxima on CID diode array for a) an incandescent bulb, b) a hollow-cathode discharge tube, and c) a star.

ferometer is a monolithic unit made of Corning 7971 Ultra-Low Expansion Titanium Silicate with optically contacted spacers. The unit is mounted in a vacuum chamber and maintained at 52°C, at which temperature its coefficient of thermal expansion is zero.

The spectrum is scanned by tilting the Fabry-Perot over a range of $\pm 1°$ about normal incidence, thereby shifting the transmission maxima by up to a free spectral range. Since the spectral resolution elements are just the Fabry-Perot transmission maxima, the wavelength calibration problem is reduced to one of determining the interferometer plate spacing and tilt. The resulting calibration is independent of small changes in the spectrograph. To illustrate the importance of this last point, a change of echelle tilt by 0.1 arcsec relative to the beam would, in the absence of the Fabry-Perot, produce a velocity error of about 75 m/s. The Fabry-Perot, together with its collimator and the spectrograph grism, is shown in Figure 2.

5. IMAGE SCRAMBLER

Uniform illumination of the spectrograph entrance aperture is of the utmost importance in obtaining radial velocity measurements accurate to within a few meters per second. By providing effective image scrambling we eliminate the effects of guiding errors, variations in seeing, and imperfections in the shape of the Fabry-Perot interferometer plates which could, in the absence of scrambling, induce radial velocity errors of several hundreds of meters per second. Image scrambling is also necessary to ensure that wavelength calibration standards illuminate the spectrograph in a manner nearly identical to

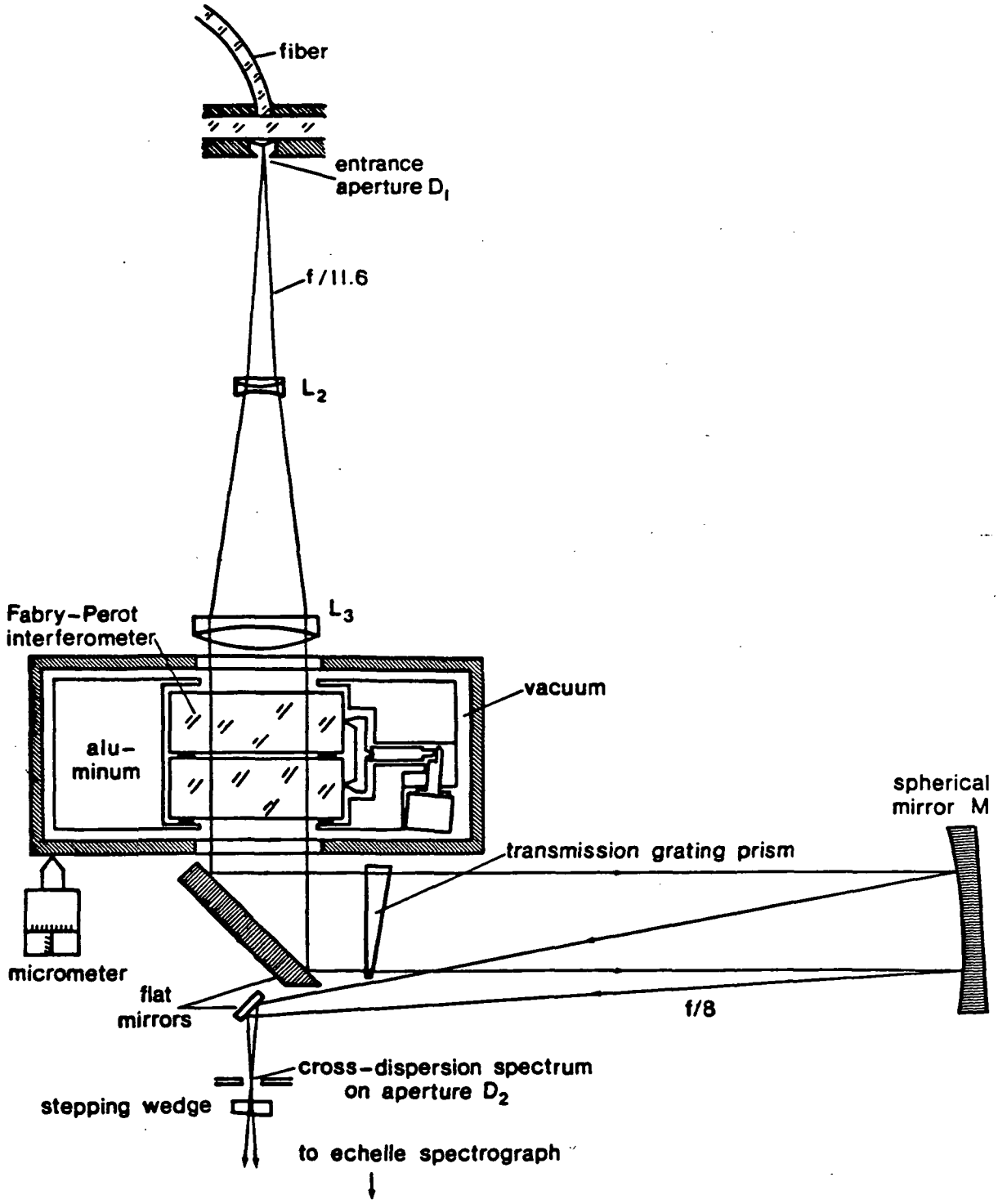

Fig. 2. Upper part of the radial velocity spectrometer, showing the relation of the fiber optics output and associated optical components to the Fabry-Perot interferometer.

that of starlight.

Following suggestions by J. R. P. Angel and P. Connes, we intend to use as an image scrambler a single, step-index, cladded fused silica optical fiber of core diameter 125 μm and length approximately 15 meters. A star image is formed on an input end of the fiber. Alternately, one of three calibrating lamps can be imaged on the fiber. Their light is reflected towards the fiber by a corresponding mirror (see Figure 3), inserted into the stellar light beam by a computer controlled stepper motor. Illumination of the output end of the fiber is highly uniform and almost independent of the illumination of the input end; therefore the fiber provides scrambling of an image formed on its input end.

Besides acting as an image scrambler, the optical fiber allows a spectrometer to be removed from the Cassegrain focus and to sit on the floor of the telescope dome in an enclosure protecting it from thermal variations, vibrations, and mechanical shock. This provides better instrumental stability and may significantly improve the accuracy of the spectrometer.

The fiber and associated optical components are represented in Figure 3. The achromatic lens pair L_a and L_b reduces the f/13.5 beam of the University's 155 cm telescope to f/6.75, so that the 125 μm fiber end subtends about 2.5 arcsec on the sky. Compared with an f/13.5 beam illuminating a 250 μm fiber, this arrangement increases the scrambling by a large factor and reduces light losses due to beam spreading by the fiber. The focus of lens L_b is at the center of an image of the telescope mirror formed by lens L_a. This arrangement ensures that the distribution of directions of light rays entering the fiber end is nearly

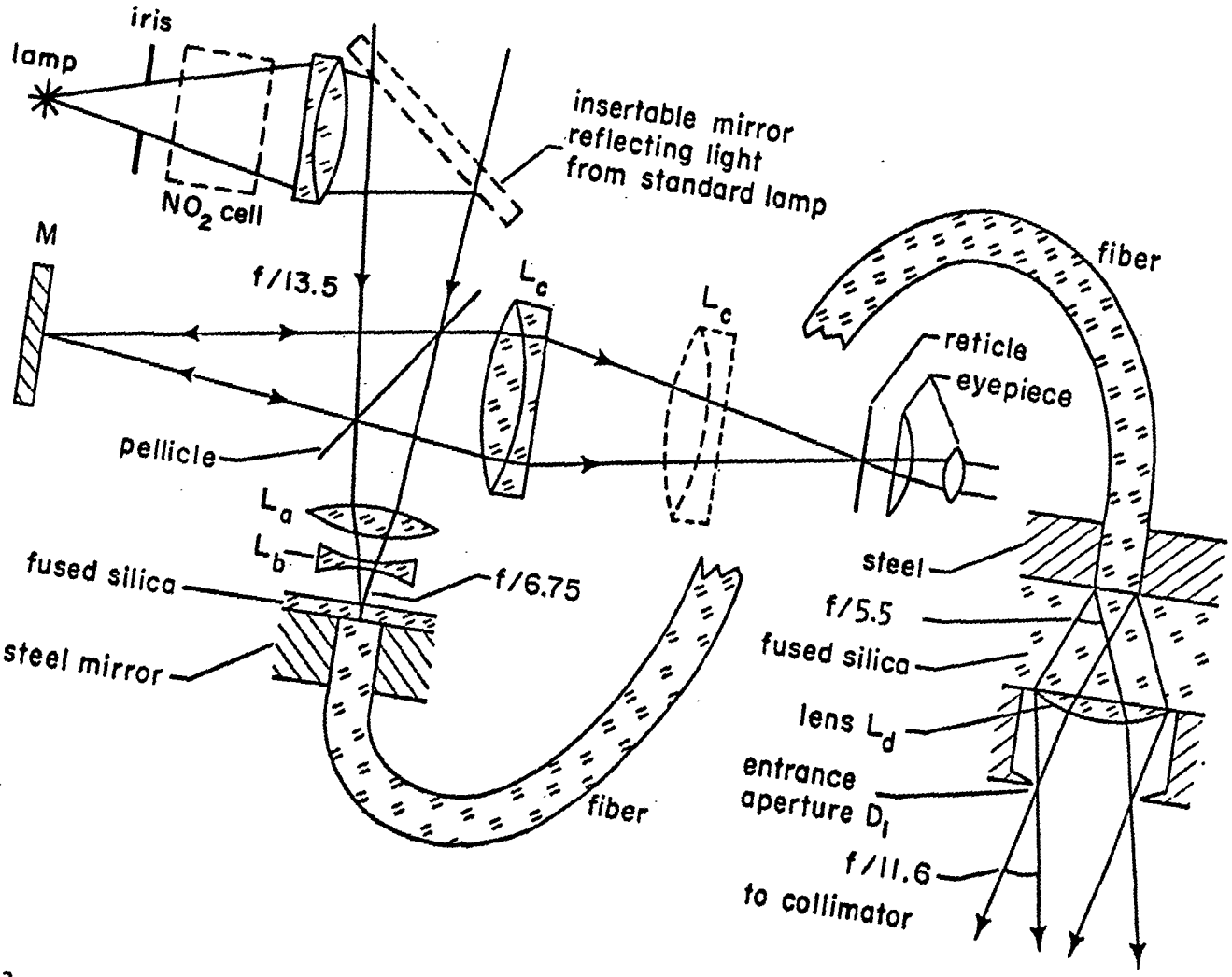

Fig. 3. Optical fiber image scrambler (fiber thickness greatly exaggerated).

independent of the position of the image on the fiber end, thus further reducing the effects of guiding errors and of non-identical illumination of the telescope image plane by starlight and by standard lamps. At the output end of the fiber, the 1.5 mm focal length lens L_d (a Melles Griot stock item) converts the beam to f/11.6 and removes the correlation between the directions of light rays in the input and output beams from the fiber.

Our fiber was provided by Galileo Electro-Optics Corporation. By combining the techniques described by Gloge et al. (1973), Chesler and Dabby (1976), and Gordon, Rawson and Nafarrate (1977), we have been able to cleave the fiber so as to obtain cut faces that are flat across the entire surface to within ½ μm. The resulting 15 m fiber shows very little beam spreading. A collimated input beam yields an f/15 output beam, while an f/6.75 input beam (as will actually be used) yields an output beam of about f/6. As a result, the spectrometer entrance aperture D_1 can be made sufficiently small to avoid loss of spectral resolution without incurring large light losses. We intend to use an aperture of diameter 0.30 mm corresponding to an instrumental profile full width of about 0.29 Å for monochromatic light, which is small enough to prevent mixing of light from neighboring Fabry-Perot maxima imaged on the detector. The relation of this aperture to the Fabry-Perot is shown in Figure 2.

We expect that this arrangement will provide highly efficient, effective, and stable image scrambling. Total light loss in the scrambler, including light lost at D_1 due to beam degradation by the fiber, is not expected to exceed 25%.

6. CALIBRATION

To the best of our knowledge, there is no wavelength calibration source suitable for our instrument whose long-term stability to one part in 10^8 (corresponding to $\sim$ 3 m/s) has been demonstrated. Our approach to this problem is to use a variety of independent calibrators, none of which are known a priori to be incapable of providing the requisite stability, so that systematic errors in any one calibrator are unlikely to go undetected. The best candidates discovered to date are discussed below; we are continuing our search for good calibrators, and have designed our spectrometer with sufficient flexibility to enable us to incorporate internal calibrators superior to those presently being used if they should become available.

The wavelength standard in the prototype instrument, used in 1977-78, was a hollow cathode discharge tube with an iron cathode and argon spalling gas. Iron was chosen over such alternative cathode materials as thorium and uranium because the relatively bright iron lines enable us to considerably reduce telescope overhead time. We are somewhat concerned that changing relations between optical axis and local gravity in this tube, which is mounted at the Cassegrain focus, may induce changes in the emitting plasma that will cause wavelength shifts. Consequently, we are presently treating this tube as a secondary internal calibration source.

The principal internal calibrator is a gas-filled absorption cell illuminated by a tungsten-halide incandescent lamp filtered to obtain a nearly flat continuum. The only good candidate for an absorb-

ing gas we have discovered is NO_2, which has a very rich line spectrum in our passband (4000-4500 Å). Figure 4 shows a representative portion of the spectrum of a 5 cm long $^{14}NO_2$ cell at a pressure of 30 torr as obtained by Dr. J. Brault with the Kitt Peak Fourier transform spectrometer. The spectrum has a resolution of 0.013 Å and S/N > 1000; it is clear that such a cell can provide a large amount of wavelength information. To prevent opacity changes due to dimerization the temperature of our cell will be maintained to within 0.1° C. Since laboratory measurements of our 30 torr cell showed no detectable broadband absorption variation over a 25° C temperature range, such a regulation is probably sufficient. While no NO_2 cell has, to our knowledge, been investigated for wavelength stability of absorption features to the required accuracy of one part in 10^8, we are encouraged by the demonstrated capability of other gas cells - notably iodine - to stabilize lasers to one part in 10^{12}.

The optical arrangement for the NO_2 cell is illustrated in Figure 3; the arrangement for the hollow cathode tube is similar. The achromatic lens in the calibrating beam is used to produce an f/13.5 beam and to project the iris diaphragm to infinity, resulting in illumination of the telescope image plane very similar to that of starlight. Lens L_c is positioned either to view the stellar image on the fiber end or to examine the images of the telescope mirror and iris diaphragm. Coincidence of these two images is necessary to ensure identical illumination of the focal plane by stellar and standard sources.

Both the hollow cathode tube and gas absorption cell will be observed at each tilt of the Fabry-Perot at which the star is observed. The

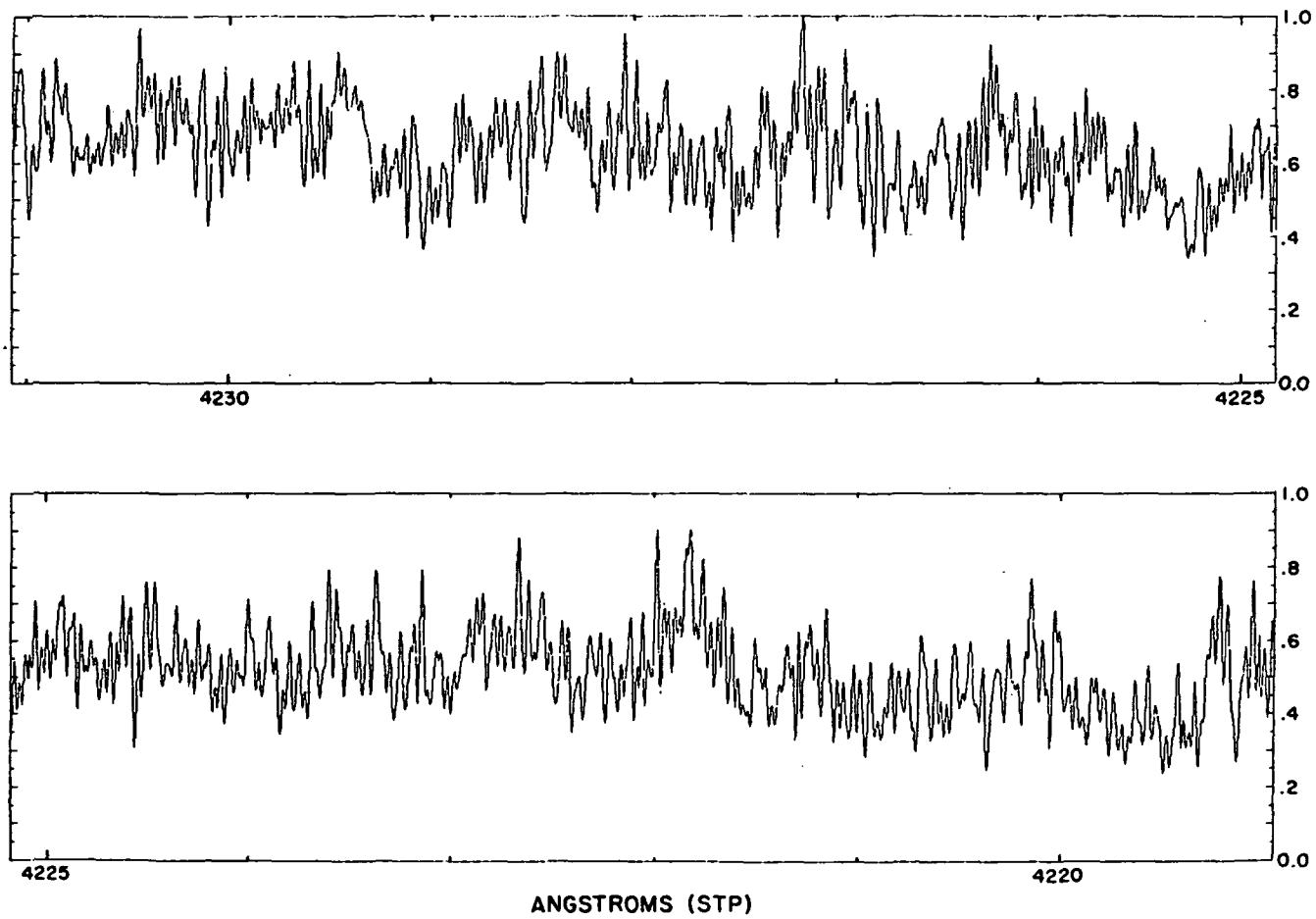

Fig. 4. Portion of spectrum of a $^{14}NO_2$ absorption cell at a pressure of 30 torr. Resolution ≈ 0.013 Å, S/N > 1000.

hollow cathode tube is also observed at a number of intermediate tilts in order to adequately observe profiles of its emission lines. These profiles are used to calibrate the micrometers tilting the interferometer.

An additional internal calibrator is the Fabry-Perot interferometer itself. While the exceptional thermal stability of this monolithic unit is probably sufficient to produce the accuracies required for our program, the mechanical stability of the interferometer has been suspect as long as the spectrometer remained attached to the Cassegrain focus with the attendant problems of flexure, varying local gravity, etc. The incorporation of a fused silica fiber image scrambler allows the spectrometer to remain stationary and raises the prospect of the interferometer tilts being repeatable to within the required accuracy. The situation is further improved by driving the interferometer chamber tilt micrometer (Fig. 2) with a carefully regulated, computer controlled stepper motor.

An external calibration will be achieved by periodically observing integrated sunlight. The Sun is known to exhibit radial pulsation modes of period 5 minutes ($\sim$ 1.5 m/s amplitude) and, possibly, 160 minutes ($\sim$ 0.5 m/s amplitude). Its stability to long period radial velocity changes is not well known and is itself a matter of astrophysical interest. Observations of the solar KI 7698.979 Å line over a period of five years by J. R. Brookes and co-workers at Birmingham have detected the above mentioned radial velocity variations at excellent signal to noise ratios (Brookes et al. 1978, and other articles

referenced therein). As reported by G. Isaak to the Stellar Pulsation Workshop at the University of Arizona, March, 1979, these data reveal no long-term ($5^h < P < 5^y$) solar radial velocity variations of amplitude 0.5 m/s or greater. It thus appears likely that the Sun will provide a reliable external source for calibration purposes.

We expect to measure the solar radial velocity by observing sunlight reflected from a panel coated with a non-fluorescent white paint. Observations of the daylight sky are probably unsatisfactory due to varying wind velocities and Raman scattering, while observations of sunlight scattered from the lunar surface are contaminated by phosphorescence of lunar surface materials. As with all stars observed, portions of the solar spectrum suspected to be of high photospheric or chromospheric origin (e.g., the core of H_γ) will be excluded from the radial velocity analysis in order to avoid confusion due to phonemena associated with the 22-year cycle of solar activity. While some photospheric lines may reflect solar activity (Livingston et al., 1977), the majority probably does not (Beckers and De Vegvar, 1978).

7. DATA ACQUISITION

Since the resolution elements of the spectrometer are Fabry-Perot transmission maxima and not CID pixels, we do not need to measure positions of transmission maxima on the CID; we have only to assign interference order numbers to them. This is easily accomplished by initially illuminating the spectrometer with a hollow-cathode lamp and with an incandescent lamp. The intensity in a given transmission maximum is measured by adding the signals from all pixels clearly illuminated by

the transmission maximum; typically, six to nine pixels are involved. Reference to Fig. 1 may be useful in understanding this discussion and the one to follow.

The substepping wedge visible in Fig. 2 is designed to reduce photometric error by enabling each resolution element to be measured by two groups of pixels. At a given tilt of the interferometer let $I(m,a)$ be the signal in interference order m as measured by the group of pixels denoted a, $I(m+1,b)$ the signal in order m+1 in the next group of pixels, etc. The ratio

$$I(m,a)/I(m+1,b)$$

is independent of such time-dependent effects as seeing since the signals were measured simultaneously. The tilt of the substepping wedge is now changed so as to shift all transmission maxima on the CID by one free spectral range ($\Delta_{FP}\lambda$) of the Fabry-Perot, so that order m-1 is imaged on pixel group a, order m on group b, etc. Then the ratio

$$\frac{I(m,a)}{I(m+1,b)} \Big/ \frac{I(m-1,a)}{I(m,b)} = \frac{I(m,a)}{I(m-1,a)} \cdot \frac{I(m,b)}{I(m+1,b)}$$

is free not only of seeing effects but also of the individual pixel sensitivities, since the linear response of the CID causes such sensitivities to cancel in this expression.

For convenience, we store the quantity

$$S(m) = \ln\left[\frac{I(m,a)}{I(m-1,a)} \cdot \frac{I(m,b)}{I(m+1,b)}\right]^{\frac{1}{2}}$$

as the signal in interference order m. This quantity is independent of spatial or temporal changes in the detector sensitivity and independent of changes in the signal from a star caused, e.g., by seeing

or clouds.

The quantities S, considered as a function of central wavelength of the corresponding Fabry-Perot transmission maximum, represent a stellar spectrum convolved with the interferometer instrumental profile and normalized so that the flux at each wavelength λ is measured relative to an average of fluxes at wavelengths $\lambda - \Delta_{FP}\lambda$ and $\lambda + \Delta_{FP}\lambda$. We combine all available observations of a star with our spectrometer to form an average spectrum $\bar{S}(\lambda)$ by least squares spline smoothing. Each value of $S(\lambda)$ observed on a particular night gives us a difference in radial velocity relative to the mean spectrum,

$$\delta V = \frac{c}{\lambda} \cdot \frac{S(\lambda) - \bar{S}(\lambda)}{d\bar{S}(\lambda)/d\lambda} \quad ,$$

where c is velocity of light and wavelengths λ are corrected for the motion of the telescope relative to the center of mass of the solar system. A weighted average of these differences is calculated, with weights

$$W = \left[\frac{d\bar{S}(\lambda)/d\lambda}{\epsilon(S)} \right]^2 \quad ,$$

where $\epsilon(S)$ is the mean error of an individual value of $S(\lambda)$. All together, about n = 8,000 values of S are obtained at 20 tilts of the interferometer during 30 minutes of observing. They will give radial velocity with mean error (resulting from photon statistics)

$$\epsilon(\delta V) = \frac{c}{\lambda n^{\frac{1}{2}}} \frac{\langle \epsilon(S) \rangle}{\langle d\bar{S}/d\lambda \rangle} = \pm 14 \text{ m/sec}$$

if the r.m.s. average values of $\epsilon(S)$ and $d\bar{S}/d\lambda$ are $\pm$ 0.05 (i.e. 5% photometric accuracy for each I) and 3/Å (a typical value for solar-

type stars around 4250 Å wavelength), respectively. The 5% photometric accuracy should be easily obtained with a 154 cm telescope for 5th magnitude stars.

Calculating the sums of the weights W for various regions in solar spectrum we find that the error of radial velocity is minimized for the spectral region centered on 4250 Å.

The near infrared has sometimes been mentioned as a more suitable region of the spectrum for radial velocity measurements, since existing Fourier transform spectrometers can profitably exploit their multiplex advantage there. This is achieved, however, at the expense of increasing photon noise (Serkowski 1978). The relative paucity of spectral lines in the infrared for solar-type stars forces most of the resolution elements to lie in the continuum, contributing to the noise but not to the signal. In addition, telluric line absorption can be a serious problem beyond 7000 Å. These arguments, buttressed by the long observing times required to achieve good photometric accuracies on very bright, red stars with the Kitt Peak FTS at the 4 m telescope, have convinced us that infrared radial velocity measurements cannot approach the efficiency of our instrument.

It should be mentioned that line blending is of no concern in the choice of passband, providing only that the blending does not vary with time, i.e. that a star is not a double-lined spectroscopic binary. To avoid such binaries we select as our program stars those stars in the Abt and Levy (1976) catalogue which the authors found to be either apparently single stars or wide visual binaries.

8. CORROBORATIVE OBSERVATIONS

Potentially, one of the most serious ambiguities in the interpretation of observed radial velocity variations of a few meters per second is the possibility of such variations arising from activity cycles similar to the Sun's 22-year cycle. We hope to deal with this problem in several ways. We plan to include in our observing program as many stars as possible from the chromospheric variations program of Wilson (1978), which will be continued and expanded by G. Preston and A. Vaughn. Such an arrangement will help in determining the correlation (if any) between long period radial velocity cycles and chromospheric activity cycles. We note also that Sacramento Peak Observatory has recently initiated a synoptic program of Strömgren photometry of the stars in Wilson's program with the 102 cm Air Force Newtonian telescope (J. Zirker, private communication).

There are plans for at least one systematic investigation of photospheric line variations during the solar cycle. O. R. White (High Altitude Observatory) and W. Livingston (Kitt Peak) have indicated that they expect to expand their calcium K line observations to include observations of integrated sunlight in the K line wings and photospheric lines nearby. Such a program will be of great value to us in determining the effects of solar-type activity on inferred radial velocities.

Eventually, we plan to include in our program main sequence stars from either or both of the Hyades and Ursa Major open clusters, in order to obtain radial velocity variations (or limits thereon) along the main

sequence of stars of nearly equal age. Such observations will be useful in determining the extent to which solar-type activity mimics radial velocity variations, since chromospheric activity is known to be correlated with age and spectral type. We feel that improvements in semiconductor and intensifier technologies are proceeding at such a pace as to make dwarfs in these clusters earlier than, say, G5 accessible to our instrument within one or two years.

9. PROSPECTS

In a prototype stage as a Cassegrain instrument with a rotating reversion prism image scrambler and a Digicon as a detector the instrument observed Arcturus with a repeatability of about 25 m/s and Venus with an internal accuracy of 10-20 m/s (Serkowski et al., 1979a). We now feel that a large portion of this scatter was due to small changes in the axis of rotation of the reversion prism, a source of error that is eliminated in the current design along with other possible error sources associated with the Cassegrain mounting. In combination with other improvements, particularly in wavelength calibrators, image scrambling and reduction software, we anticipate that these changes will reduce the error of a single observation to $\sim$ 15 m/s and that the accuracy of measured radial velocity for a given star will be limited mainly by photon statistics. With our present ICID detector we expect to achieve this accuracy on stars of 5th magnitude in a single observation. Detectors and intensifiers are improving so rapidly that we expect to be able to go much fainter than this in the near future.

The improved instrument should be ready for testing at the telescope in September, 1979. By the end of the year it should be sufficiently reliable to enable us to begin systematic observation of solar-type stars in order to determine the accuracy of the data obtained by the instrument.

The development of the University of Arizona Radial Velocity Spectrometer has been supported by the National Geographic Society and by the National Aeronautics and Space Administration.

REFERENCES

Abt, H. A. and Levy, S. G. 1976, Astrophys. J. Suppl., 30, 273.

Aikens, R. S., Lynds, C. R. and Nelson, R. W. 1976, Proc. SPIE, 78, 65.

Beckers, J. M. and De Vegvar, P. 1978, Solar Phys., 43, 289.

Brookes, J. R., Isaak, G. R., McLeod, C. P., van der Raay, H. B. and Roca Cortes, T. 1978, Mon. Not. R. Astr. Soc., 184, 759.

Chesler, R. B. and Dabby, F. W. 1976, Electronics, 90 (5 Aug. 1976).

Gloge, D., Smith, P. W., Bisbee, D. L. and Chinnock, E. L. 1973, Bell Syst. Tech. J., 52, 1579.

Gordon, K. S., Rawson, E. G. and Nafarrate, A. B. 1977, Applied Optics, 16, 818.

Livingston, W., Milkey, R. and Slaughter, C. 1977, Astrophys. J., 211, 281.

Michon, G. J., Burke, H. K. and Brown, D. M. 1978, General Electric Company Technical Report ("Recent Developments in CID Imaging").

Serkowski, K. 1978, in High Resolution Spectrometry, M. Hack, ed., p. 245, Trieste.

Serkowski, K., Frecker, J. E., Heacox, W. D., KenKnight, C. E. and Roland, E. H. 1979a, Astrophys. J., 228, 630.

Serkowski, K., Frecker, J. E., Heacox, W. D. and Roland, E. H. 1979b, Instrumentation in Astronomy III (D. L. Crawford, ed.), Proc. SPIE, 172, 130.

Wilson, O. C. 1978, Astrophys. J., 226, 379.

PAPER 9

A PROPOSED SYSTEM FOR SPECTROSCOPIC DETECTION OF DARK COMPANIONS

Pierre CONNES
Service d'Aéronomie du CNRS
Verrières le Buisson - 91370 - France

SUMMARY

We first review the most accurate radial velocity results available (and also mention some relevant laboratory work) from Fabry-Perot Fourier or grating spectrometers. We next speculate on ultimate performance of each and conclude the correlation radial velocity meter of Fellgett and Griffin is presently our best bet. Some ideas for improvement, none of them radically novel are then discussed. The most important is the use of an optical fiber as scrambler ; we hope to remove totally in this way the effects of seeing and of guiding errors, hence to enable grating spectrometers to achieve on stars the same kind of line position accuracy already demonstrated in the laboratory (equivalent to a few m/s in velocity). The use of image slicers is discussed next and a novel type proposed. We consider three different methods for implementing the velocity scan : pressure scanning, Doppler-normal dispersers and a compensator system. Use of absorption or emission lines is also discussed. A general description of the proposed spectrometer is finally given.

To be presented at the Workshop on Ground Based Techniques of Searching for Extrasolar Planets, Asilomar, October 1978.

I - INTRODUCTION -

In a set of recent papers (I), we have proposed a ground-based system primarily designed for an astrometric search of dark companions. The two parts are

1) a special purpose astrometric telescope
2) a photoelectric detection device.

This proposal may be considered specific in the sense that stellar positions are not measured, only apparent motions.

Here we describe a system specifically designed for detection and measurement of radial velocity fluctuations. The two proposals are technically similar : they both make use of photographic masks and photoelectric detection, also they both attempt to reach fundamental photon noise limits. However the second is less novel, less expensive and less ambitious. First it derives in a rather straightforward manner from the Fellgett-Griffin radial velocity meter; second it should work with any existing moderate size telescope ; third the limitations of spectroscopic detection are well-known : only one orbit parameter is being measured (versus two with astrometry), and spectroscopic detection fails altogether for an orbit perpendicular to the Earth's direction. Furthermore an important by-product of the astrometric device is improved parallaxes and the present interest in the question is such that appreciable support may be expected from this side.

Quite obviously astrometric and spectroscopic detection each have a preferred range of application, the first for long periods and the second for short ones. So far the cases of astrometric binaries also observed as single line spectroscopic binaries are extremely few. But if the sensitivity of both tools is improved, a considerable overlap may be expected. We hope that some day both our systems will be implemented. Then the scientific output would be much increased : we might obtain for a relatively large number of stars with dark companions all three orbit parameters plus accurate distances.

This paper will not discuss the applications, and stick to purely instrumental matters. Neither shall we consider the astrophysical limitations i.e. possible radial velocity fluctuations in integrated stellar light arising from stellar atmosphere motions ; this subject should hopefully be covered by greater experts at the Workshop. We merely hope any more or less coherent oscillations of stellar atmospheres, (or perturbations of any type) to be detected in the future will sensibly stick to the high frequency range and leave the longer periods free for extrasolar planetary research.

The instrumental problem is easily stated : can we define an optimum system for measuring radial velocity variations over extended periods of time (eventually tens of years) ? While not novel it has nevertheless been much less studied than the one of absolute radial velocities for which a distinctly lower accuracy is both feasible and desirable. In any case a short review of presently achieved accuracies is needed. We will consider both actual radial velocity estimates, and also some simple measures of line positions, both laboratory and astronomical, which can be reassessed in terms of radial velocities and give useful figures for instrumental errors.

II - RADIAL VELOCITY PERFORMANCE OF EXISTING DEVICES -

We consider here only some of the most accurate recent results, and not he classical grating and photography ones.

1) Fabry-Perot interferometers -

Duchesne and Guinot (2) have deduced the aberration constant from the radial velocities of Venus and Mercury. The spectrometer was a 4 mm thick, grating crossed, Fabry-Perot etalon and the fringes were recorded with a photographic Lallemand type image tube. The solar lines were measured (and Mercury proved a better object than Venus, by reason of no atmosphere and neglible rotation). Thus the observations are directly relevant to our problem. About 25 lines were used and 40 plates taken close to maximum E and W elongations. The final results are expressed in terms of a figure for the aberration constant with a probable error which corresponds to a ± 7.5 m/s probable velocity error. The authors consider a reduction of about 5 times might have proved feasible by various improvements, and by repeating the observations over several years ; however the aim had been a better figure for the astronomical unit and the technique was obsoleted by planetary radar.

2) Fourier interferometers -

We have developed a brand of Fourier interferometers specifically for high resolution and high accuracy of line positions. They have been abundantly tested on many laboratory sources and on some astronomical ones.

An early version with moderate resolution (10 cm path difference) produced Venus spectra with Pb S detectors (4000 to 10000 cm^{-1}). The aim was a chemical study of the atmosphere, not radial velocity. Light from the whole illuminated part of the disk was used, at different phases. In the spectra CO was detected (3) and a set of 39 lines (around 4300 cm^{-1}) measured. The standard was the green line of Hg^{198}. A list of wave numbers was given, after deducing computed Doppler corrections for Earth - Venus velocity and Earth rotation. The RMS scatter on

individual line positions, when the measured values were compared with the computed ones (from band constants) was 4.10^{-7}.

Let us re-analyse these data in terms of radial velocity. The corresponding RMS error is 120 m/s ; if all 39 lines results are averaged and used to get the Venus radial velocity the probable error is ± 19 m/s. The actual difference found (measured minus tabulated Earth-Venus velocity) is only 7 m/s, thus not significant. There is no evidence either for a systematic error or for a Venus atmosphere rotation (remember all the light is used).

A large fraction of the above mentionned scatter clearly arises from blends - as demonstrated by the much higher accuracy laboratory results on the same band to be discussed later. The effect of course disappears if we are interested in radial velocity variations, each planetary line being compared merely with itself. Lastly some of the errors also arose in uncertainty from the Earth rotation correction, simply because the interferograms had not been timed accurately enough.

More spectra of Venus and Mars were taken later in the same range with a new instrument, and about 5 times greater resolution ; sample results have been published (4). Again the aim was the detection of trace constituents, not radial velocity studies, and results from line position estimates have not been published. Some Venus spectra were taken through a sealed low pressure CO filled cell and show both the laboratory lines and the Doppler shifted Venusian ones (fig. 1). This procedure does eliminate the two major sources of error :

1) long term instability in the monochromatic line used as a reference for the interferometer

2) small beam displacements due to seeing, or to guiding errors.

The RMS individual line scatter for Venus-Laboratory was reduced, compared to the older results - in roughly the same ratio as the resolution, i.e. went down to 25 m/s. This is due both to reduced line width and to fewer blends. From the same set of lines we obtain a probable Venus velocity error of ± 4 m/s.

The number of available sharp, symetrical CO_2 lines is much greater (several thousands). A completely demonstrated feature of Fourier spectroscopy is the ability to provide uniform accuracy through large spectral ranges. For radial velocity variations it is not necessary to have the position of each line in the laboratory. Thus we have no doubt a sensitivity and long term stability of a few times 0.1 m/s might be realized by

1) taking many similar spectra with the same instrument (and of course timing accurately the interferograms)

2) systematically using a cell containing CO and/or other gases as a reference

3) making use of all suitable lines.

Of course, the portion of the disk used should then be well defined and the results would be affected by Venusian winds.

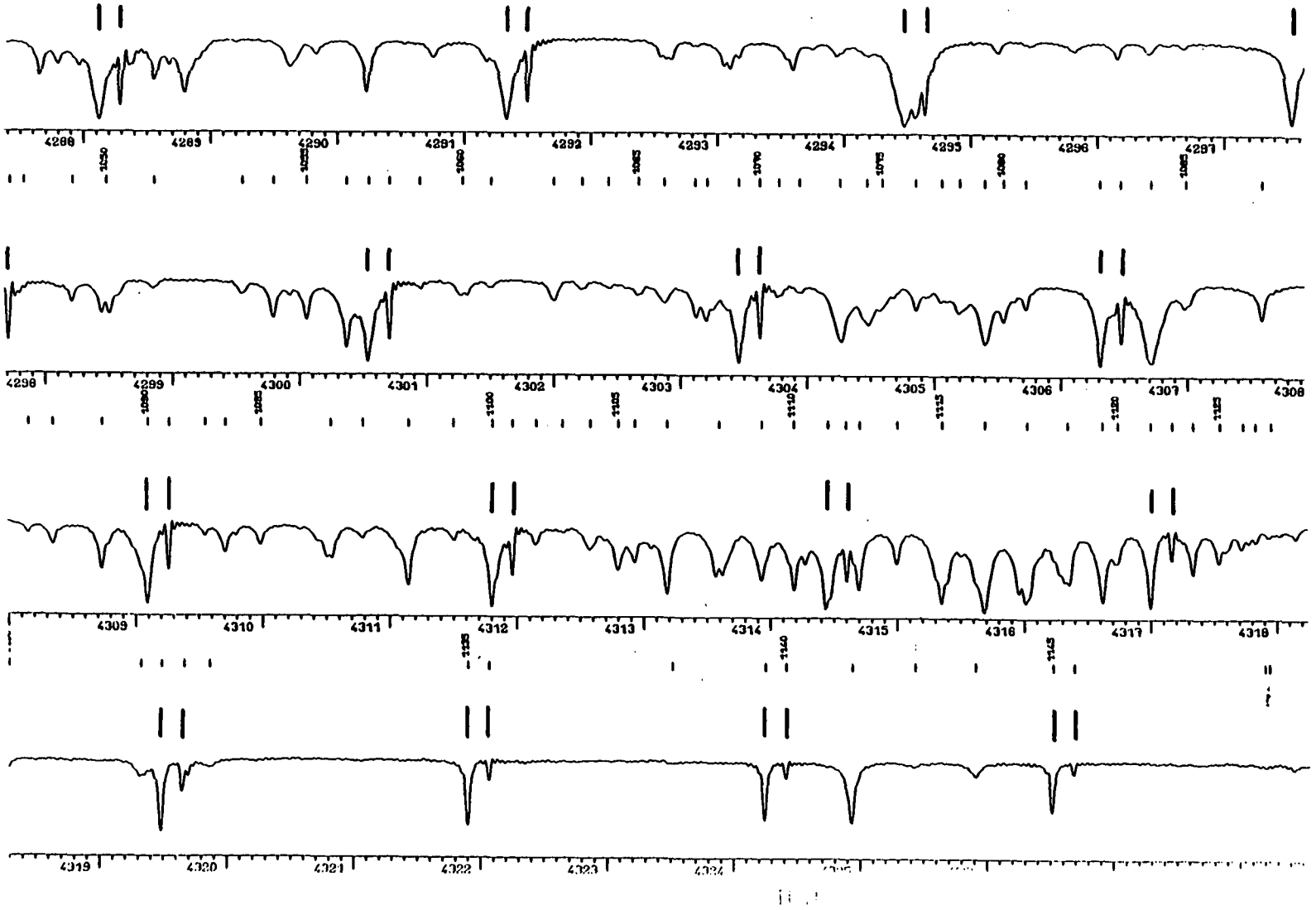

Figure 1.- Small portion of a FTS Venus spectrum showing both the Venusian CO lines around 4300 cm^{-1} and the same band in an absorption cell.

This program has not been attempted because only solar lines are fully relevant here. These should be measured on Mercury (or simply in integrated sunlight). Some loss in accuracy must be expected because solar lines are broader and fewer. A rough calculation shows that by using the same overall spectral domain the radial velocity error might be in the 1 to 3 m/s range. However the near infrared is clearly not optimum for the problem ; how much better a similar system might perform in the visible shall not be extrapolated from our old results, but rather discussed in the next chapter. Nevertheless a test program is desirable. We have built 4 interferometers generally similar to the last one discussed here (4, 5), and designed 4 others presently operating or undergoing tests. All are suitable - with simple changes of beamsplitters and detectors - while one of them is routinely operating in the visible and near UV (6). We regret that none is available for such a program.

Some of our early stellar spectra (α Boo) taken with the low resolution interferometer have been analysed from the radial velocity point of view by Edmonds and Bopp (7) ; however the work was preliminary in the sense the line positions were hand measured on insufficient scale tracings. The results cannot be compared with the planetary ones in which computer programs operating from the digital data were used. None of our recent high resolution stellar spectra, such as the one shown in (4) has been used for radial velocities.

The same band of CO has since been measured with one of these interferometers by Guelachvili (8) in the laboratory. Absolute wavenumbers are given and the individual line error is estimated to be $2.8\ 10^{-8}$ (which would correspond to 8 m/s) and appears random. Since 51 lines were measured the probable error on the mean (or, say, a velocity derived from all lines) would be about 7 times smaller. Then, part of this error arises in the comparison with the Kr^{86} standard, and in minor intrinsic line profile distortions; this would disappear in a study of mere line shifts. Of course, the lines (from a 40 m path, 0.1 mm Hg pressure cell) are very sharp. While the result is not an astronomical one it nevertheless gives a check of interferometer performance.

3) Grating spectrometers -

We shall mention here merely one laboratory result, by Valentin (9) on this same CO band (also on the fundamental at 2000 cm^{-1} and some others in the near I.R.). A large grating spectrometer of particularly careful design was used ; the measurements were done in a classical manner by scanning the spectrum between secondary standards. The key element was an in interferometric goniometer which records grating rotation and permits accurate interpolation. The results are relative

but perfectly relevant to the problem of line shifts. The individual line position RMS error is about the same as in the above case, i.e. $\sim 3.10^{-8}$. The measurements are much slower, a small portion of the band being studied in the same time the Fourier spectrometer gives the entire near I.R.; but they do show an error corresponding to a few m/s is by no means unattainable with a grating.

Lastly a very important device for our problem is the "radial velocity meter" proposed by Fellgett (10) and first constructed by Griffin (11). The general features shall be discussed in the next chapter ; here we are merely concerned with latest and best performance of this highly successful system, many versions of which have been or are being built.

The so-called CORAVEL is the fruit of a collaboration between Geneva and Marseille observatories, and has been operating for more than a year at the 1 m Swiss telescope of Observatoire de Saint Michel. Only preliminary results have been published (12) and we are indebted to Mayor (Geneva Observatory) for detailed information about construction and performance. This is a small Cassegrain instrument using crossed echelle and prism dispersion. It was designed as a radial velocity meter, unlike earlier systems (11) merely adapted to existing spectrographs. The mask contains 3000 slits and covers the 3600 to 5200 Å range. The results are remarkable from the point of view of efficiency. Let us consider relatively faint stars for which all systematic errors tend to become negligible compared to the photon statistics one. The RMS repeatability of the system has been found equal to 700 m/s at $m_{pg} = 11$ for a K star with 30 s integration time. One deduces the photon noise error is approximately the same as with the Griffin spectrometer (11) at the 5 m telescope. Within a year 700 stars have been measured (with about 10 observations/star).

On the other hand, the minimum velocity error is not particularly low ; when the instrument points at the sun - in which case the photon noise error becomes negligible compared to the various systematic ones - a repeatability of merely 100 m/s being achieved. This is because the system has been designed

a) primarily for faint stars

b) for absolute radial velocities and not fluctuations in radial velocities

c) for compactness.

But there is nothing fundamental about any of these choices, while the demosntrated efficiency <u>is</u> a fundamental result.

III - A SEARCH FOR THE OPTIMUM SYSTEM -

The above review suggests three main lines of approach. We may try to start from the F.P. etalon, from the Fourier interferometer or from the grating spectrometer. In each case the difficulties are different.

1) Fabry-Perot interferometers -

The detailed description of a system has been presented by Serkowsky (13) ; it has the distinction of being the only one in which the intent is clearly detection of low mass companions, and incorporates several new features. No actual results were reported yet. Main elements are a F.P., an echelle post disperser, an interference filter and a 100 channel Digicon detector. The essential wavenumber reference is given by a polarization modulator.

The presence of a F.P. means no input slit loss (compared to a grating instrument) ; the whole telescope beam is used irrespective of turbulence. However, if we compare to the Duchesne-Guinot spectrometer (2) we find the spectral range is much reduced (to 25 Å) ; on the other hand one gest real time results, at the cost of some rather complex data handling (a small computer is needed to treat the output). Then the transmission should be rather low due to many cascaded elements.

The polarisation modulator indeed seems potentially able to give the required long term stability ; but it is not clearly better in this respect than the F.P. etalon itself.

The computed photon noise limited RMS velocity error of the device is about 3 times higher than the demonstrated CORAVEL one (fig. 2) (which corresponds to a factor 9 in observing time). A fair comparison should of course rest on demonstrated repeatability for faint stars. Altogether while appearing indeed capable of high stability the system is not a high efficiency one, chiefly because of the small spectral range.

2) Fourier spectrometers -

The above examples show FS are already providing the kind of frequency stability required here. However it is also clear that for solar type stars the optimal spectral region is the visible and near U.V. While, as we have shown (6) there is no difficulty in getting Fourier spectrometry to operate properly in that range, reaching the basic photon noise velocity limit (see next paragraph) is an altogether different matter. Clearly it cannot be done unless we have as many photon counters as resolution elements. Since their width should be comparable to the line width, or smaller, this means at least 10.000 detectors just to cover the same range as the CORAVEL. Thus we have to cascade a F.S., a rather high resolution post disperser, and a photon counting image

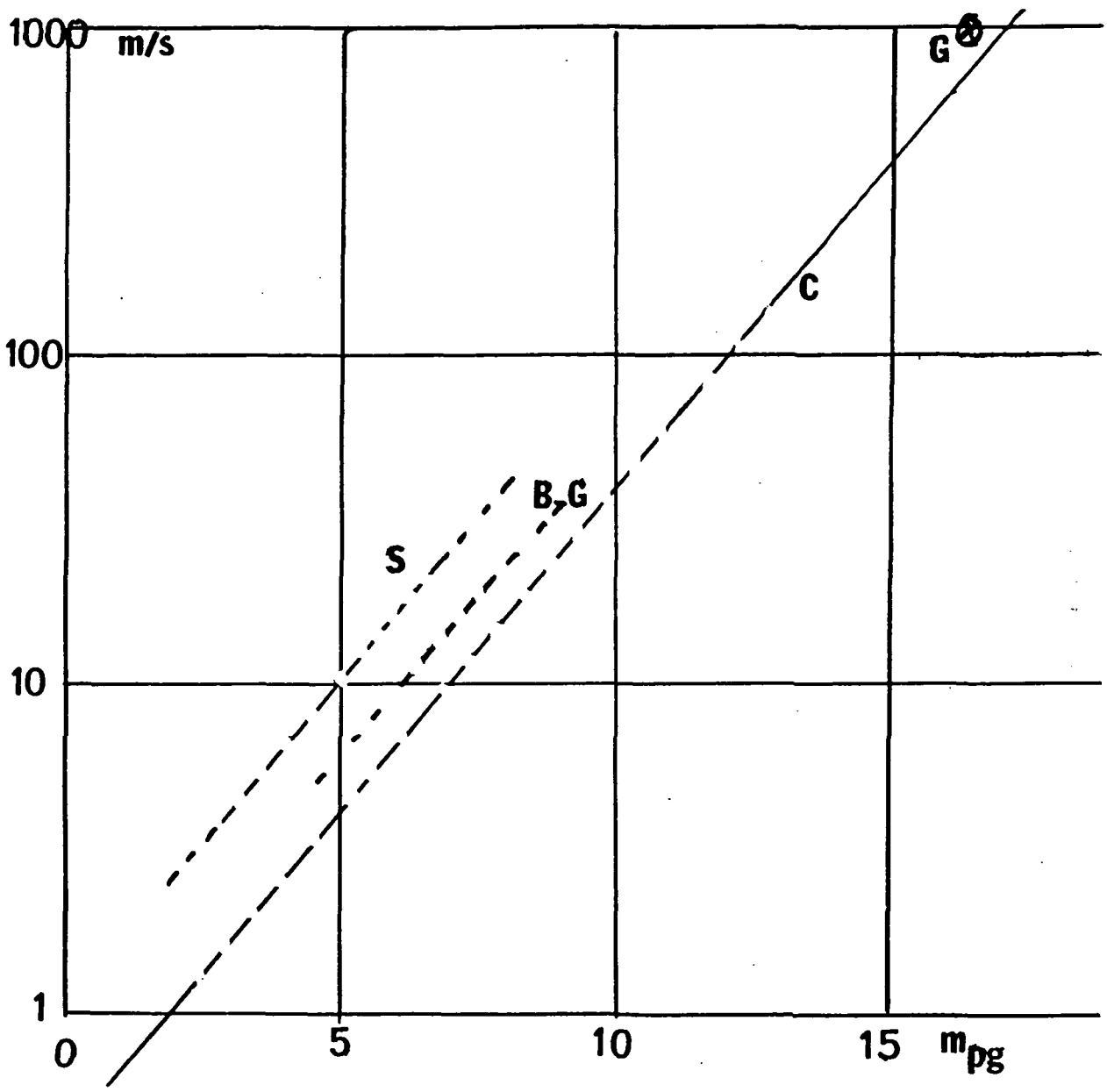

Figure 2.- RMS velocity error for K-type stars, and 1 hr observation time. G: actual results by Griffin (ref. 11) with 5-m telescope; C: CORAVEL (ref. 12) performance with 1-m telescope - at faint magnitudes (m_{pg} > 11) the straight line represents actual results; the dashed part shows the expectations for bright stars if systematic errors were eliminated. B-G: figure quoted as feasible for a correlation spectrometer in the Black-Greenstein January 1977 report on first workshop (reduced to 1-m telescope); S: computed figure for the Serkowski meter (ref. 13) (also reduced to 1-m telescope).

detector with at least 10^4 pixels. Each pixel will produce an interferogram, and all have to be Fourier transformed (of course each interferogram is quite simple because it covers only a small spectral range). Then lines have to be picked out (thousands of them), their positions detected, stored, compared with previous ones, and averages computed. Only then do we get the radial velocity. In principle, the measurement might be done from the interferograms themselves, economizing the Fourier transforms but we doubt the method would be much simpler in practice.

Altogether the procedure appears relatively safe : all the elements have been tested. We know how Fourier spectrometers perform ; similar post dispersers (either with a grating or a crossed echelle - prism system) have been built, and their performance here would be uncritical ; several existing image photon counters may be suitable (we have not studied this point). Nevertheless the whole appears needlessly complex and expensive. An important feature of F.S. is the ability to reach extreme resolutions (i.e. higher than gratings). It is not required here ; accurate line profiles will not improve the radial velocity estimate. One cannot help wondering whether such overall complexity is needed. Probably the system we have just described is not viable. No doubt intermediate forms (with low dispersion at the output and Digicon-type detectors) are already being built or tested for other purposes Still they will not reach the basic noise limitations in this case.

3) Correlation spectrometers -

From a fundamental viewpoint the question of measuring radial velocities has been best treated by Fellgett (10) who proposed the correlation method, and showed it was close to optimum. However no numerical values were given. It would not seem particularly difficult to compute the theoretical photon noise limit to radial velocity accuracy for a given star, a given time of observation and telescope of known aperture, with a perfect device implementing the correlation technique. One merely needs a high resolution spectrum of the star in digital form, such as is available for instance for Arcturus in the visible (14) and in the near I.R. (15). The prediction might then be made more realistic by incorporating figures for quantum efficiency, instrumental transmission etc... So far this does not seem to have been done. But we can get a more practical figure by simply taking the CORAVEL performance and extrapolating to brighter stars and longer observing times (fig. 2). Possibly this might still be improved upon, by increasing the spectral range or instrumental transmission, but we will not speculate here on how large the increase might be in practice. It is perfectly clear that a correlation spectrometer having the efficiency of CORAVEL would be ideal for an extrasolar planetary search if systematic errors could be reduced to a few m/s. No fundamental difficulty is involved ; this is merely a question of understanding these errors and finding remedies. No paper study - such as the present one - shall provide a fully credible answer ; the sooner one gets to the testing stage the better. In the meanwhile we shall formulate at least a coherent proposal.

IV - SPECIFIC PROBLEMS POSED BY A CORRELATION SPECTROMETER -

They are of three main types : a) Input problems : no grating spectrometer working on a star has ever given performance approaching the laboratory one quoted above (9). The central reason is the highly peculiar structure of astronomical beams, or in other words turbulence and guiding errors. These produce relatively high frequency noise ; so far for bright stars wavenumber repeatability is considerably worse than the one expected from simple extrapolations like the one of fig.2, even for observations seconds or minutes apart b) Linearity problems : not only must one reliably detect shifts of a few m/s but these will be superimposed over the telluric one (30 Km/s on the ecliptic). It must be granted Fourier or F.P. systems are near ideal from this viewpoint, while the problem is acute for the correlation spectrometer particularly if the spectral range is wide. c) Long term stability problems are easily stated : to obtain 3 m/s accuracy the wavenumbers have to be repeatable to 10^{-8} and the wavenumber shift itself to 10^{-4}.

1) Input problems -

Normal practice is to focus the star on the input slit. Let S be the seeing disk diameter, s the slit width. If $S > s$ the energy loss is considerable (efficiency $\lesssim s/S$) but the illumination tends to be uniform, hence geometrically stable. If $S < s$ there is no loss but total instability in the measured line positions. One invariably adopts the unsatisfactory solution of taking $s \lesssim S$; one gets some loss and some shift, both fluctuating. The three fundamental quantities which should be characteristia of the spectrometer, i.e. transmission, instrumental line shape and wavenumber calibration are all unstable. The telescope-spectrometer adaptation problem has perhaps been computed a hundred times and need not be repeated here. We shall merely give the actual parameters for the two most interesting correlation spectrometers so far.

The Griffin system (11) used the existing 5m telescope coude spectrograph. The grating is unusually large (40 x 30 cm mosaïc) but so is the telescope. Consequentby adequate resolution is achieved with an input slit angular width (projected onto sky) only 0.3 arc sec ; energy loss is of the order of 3 to 15 depending on seeing. Even so the velocity width (i.e. the change in final reading if a point image crosses the slit) is 15K m/s. For a S s gaussian image the (easily computable) effect is reduced to a fraction of this figure - but nevertheless is still large by our standards. Griffin gives an analysis of 'scintillation' noise for his system ; he predicts that for 'average' seeing repeatability cannot be better than 250 m/s for a 30 s integration time (irrespective of star brightness), which seems roughly verified in practice. For usual, longer runs (a few minutes) repeatabilities of 100 to 150 m/s are realized.

The CORAVEL uses a much smaller grating (l = 9 cm) but this an echelle i.e. provides much higher dispersion ; also, the telescope is 5 times smaller. Consequently normal slit width is 3 times larger (1 arc sec) which partly accounts for better efficiency. At the same time the velocity width is only half (8 K m/s). The repeatability on bright objects nevertheless seems slightly inferior to the Griffin one, while on the sun we have mentioned it is merely 100 m/s ; so, it must be accounted for only in part by seeing-guiding effects.

What we need is total decoupling of the atmosphere, telescope system from the spectrometer. We believe-to some extent we have already shown - this may be done by the association of two devices, a 'scrambler' and an image slicer.

a) Scrambler

We have given this name to a device which destroys the statistically Gaussian (but instantaneously irregular) structure of the star-atmosphere-telescope beam while spreading it very little. We have used two such devices with an early Fourier spectrometer (16) . The first was simply a rotating Dove prism. The solution is only partial ; the new image structure (averaged over a few rotations) has circular symetry, so the photocenter is now stable. But image diameter (hence resolution) is a function of guiding and seeing and with even slightly asymetrical lines (or images), one still gets objectionable effects. The second solution involved short light pipes (internally gold-coated fused silica tubes) (fig. 3). The stellar image is projected at the input, while the pipe sees the pupil (i.e. primary mirrorimage) at infinity through field lens F_1. If the number of reflexions is very large one gets uniform illumination in the output plane , irrespective of image shape or position and very little beam spread i.e. angle α is almost conserved. Actually, the number of reflexions was rather too small (for fear of excessive losses, and difficulties of fabrication). Then Fourier spectrometers are inherently much less sensitive than gratings to small image motions : the effect is second instead of first order. After we perfected an interferometric modulation technique the use of scramblers became unnecessary.

Integrating spheres do not solve the problem : the scrambling is perfect but the spreading (more exactly the increase in $A \times \Omega$) is unacceptable at any spectrometer input. However pure fused silica fibers now offer a near perfect solution within the spectral range of interest here. Transmission has been well measured (fig. 4) and is adequate down to 3500 A° for lengths of the order of 10 to 20 m. Since the considerable literature on propagation of light in fibers is of no great help to predict properties as a scrambler we have made some preliminary tests.

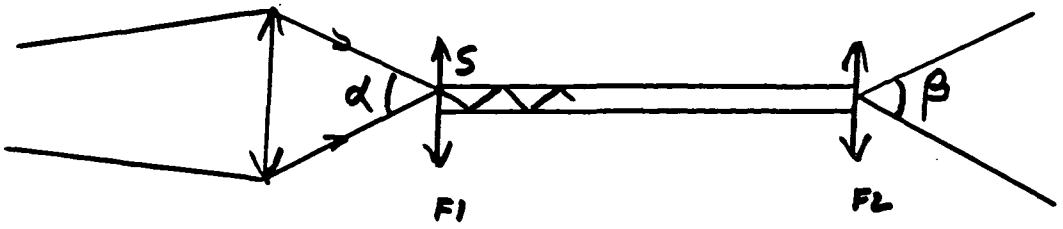

Figure 3.- First version of beam scrambler used with a Fourier spectrometer (ref. 16). The light pipe was 3 mm in diameter and 100 mm long.

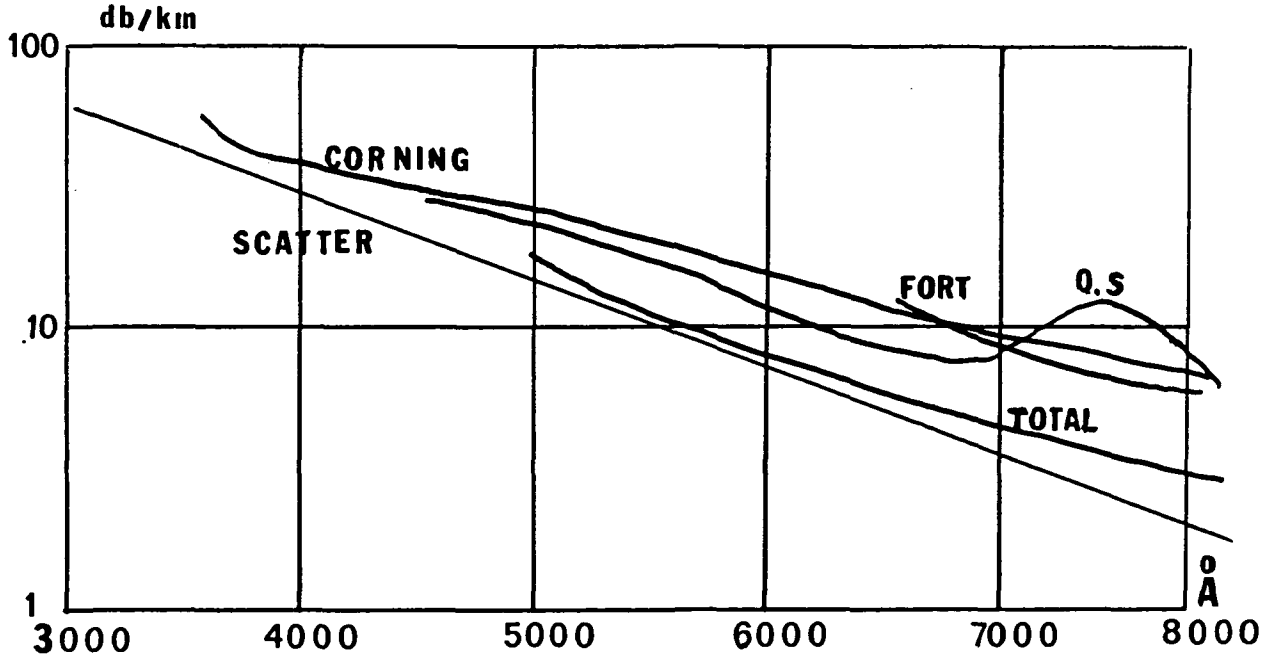

Figure 4.- Losses of pure fused silica fibers. SCATTER and TOTAL: computed figures for Rayleigh scatter alone and for scatter plus absorption according to Pinnow (ref. 23); FORT and Q.S: manufacturer's data, except for the extension of the CORNING curve in the important 3500 to 5000 Å region for which we thank JOCTEUR of CLTO. The figure of 70 db/km at 3600 Å means 0.85 transmission for 10 m length, comparable to results by Angel (ref. 17).

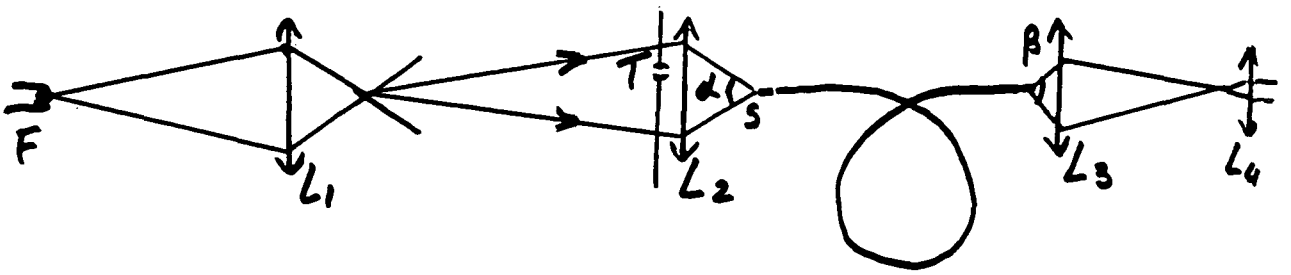

Figure 5.- Optical system for testing fibers as scramblers. F is a lamp filament, L_1 and L_2 microscope objectives giving a total demagnification of the order of 200; T may be scanned in the front focal plane of L_2 to provide a beam of known aperture and incidence on fiber input. The small image S may also be scanned on the input. L_3 and L_4 form a complete microscope for taking pictures of fiber output end; it is taken off for pictures of the angular pattern.

Fibers from 100 to 600 μ and of about 10 m length from several manufactures were tested with the fig. 5 set up. A small image ($\phi < 10\,\mu$) was projected on the input end and could be accurately scanned across with an X Y Z micrometer stage. The entrance beam total angle α was 0.6 rad ($\pm$ 17° inclination) and could be reduced by diaphragm T ; mean incidence was adjustable by X Y motions of T. Photographs were taken, on photometrically calibrated film, of either the fiber output through a microscope), or of the angular light distribution by simply putting the film 50 mm away from the output. Fiber ends were immersed in glycerin against glass plate, to eliminate flatness problems. White light was mostly used ; laser light merely adds the characteristic speckled mode pattern of no interest here. Results were independant of fiber curvature as long as the radius was more than 15 cm (except for the very largest diameter fibers which were not much good anyway).

Graded index fibers behave roughly like the rotating prism : a circulary symetric, but non uniform output is produced. Beam spread is very low but nevertheless these fibers are not a good choice as scramblers.

Constant index fibers invariably gave approximately uniform and perfectly stable illumination in the output plane. This was checked both by scanning the film on a microdensitometer and on ultra high contrast prints. On these prints many small artifacts (due to specks of dust) are visible-our arrangements for handling fibers being primitive-; these limit the accuracy with which the uniformity can be checked but not the stability. When the point source scans the input, or the beam incidence or aperture vary, (within acceptance limits of the fiber) no change is detectable by photography. Of course perfect stability (not uniformity) is precisely what we want here.

All constant index fibers also gave circularly symetric angular patterns at the output, irrespective of input conditions. But the degree of beam spread varies considerably between fibers ; most of it is clearly due to irregularities and not to any basic, predictable phenomena. Let us first recall

that in a light beam propagating through an aberrationless system the quantity $L\alpha$ ("linear etendue", measured in cm x rad) is invariant ; and that actual resolving power of a given grating spectrometer is inversely proportional to $L\alpha$ (as long as it is less than the theoretical diffraction limited value Ro). All aberrations increase $L\alpha$ - and degrade R. The question is then how much loss in R will be induced by passage through a fiber.

We need only report the best results, so far from a $\emptyset$ = 150 μ pure fused silica plasticlad fiber. Numerical aperture is sin u=0.2 i.e. the maximum transmitted beam aperture is $\alpha_m = 2u = 23° = 0.40$ rad corresponding to f/2.5, while the maximum transmitted beam linear etendue (or fiber linear throughput) is $\emptyset\alpha_m = 60\mu$ x rad. If we consider a 1m telescope and take S = 5arc sec = 25 10^{-6} rad (which would include perhaps 90 % of the light under all but very poor seeing conditions) the beam linear etendue at telescope output is 25μ x rad, thus easily accepted.

Larger fibers exist and should prove suitable for larger telescopes- but we have so far not tested one of similar quality.

Uniformly illuminated diaphragms T of increasing angular size α were placed on the fiber input axis. Fig. 6 presents the results of radial densitometer scans on film placed perpundicular to the output axis 50 mm from the fiber end (after correction for film non linearity). These curves are almost totally independent of image S position, size or shape. They would be rectangles of width equal to α if there was no fiber and no spreading. For small input beam widths they tend towards a bell shape function characteristic of fiber spread ; for larger ones they tend towards trapezes.

We can in principale define a total (base) width and plot it as a function of input width : such a curve stays everywhere above the first bissector i.e. there is some spreading under all conditions. However such a width is poorly defined and hard to measure by photography. We have plotted instead, the widths at 0.5, 0.1 and 0.05 intensity levels (fig. 7).

From these results we can also plot the fraction $\emptyset/\emptyset o$ of the input flux from a cone of given diameter α within a cone of diameter β at the output (fig. 8). The spreading is important mostly for low values of α. If one imposes $\beta = \alpha$, one collects only 60 % of the light at α = 0.09 but 95 % at α = 0.3. If one tolerates β somewhat larger than α there is no difficulty in collecting practically all the flux.

Hence we can see two ways of matching a given fiber to a given telescope-spectroscope set. If one insists on maximum resolution one must change the beam f number according to actual seeing both at the input and output ; it may be done by moving (or interchanging) just one lens at each fiber end, and correcting the focus. However for our particular problem it is considerably better to have strictly constant resolution corresponding to the worst turbulence case. With the above mentioned figures (1 m telescope,

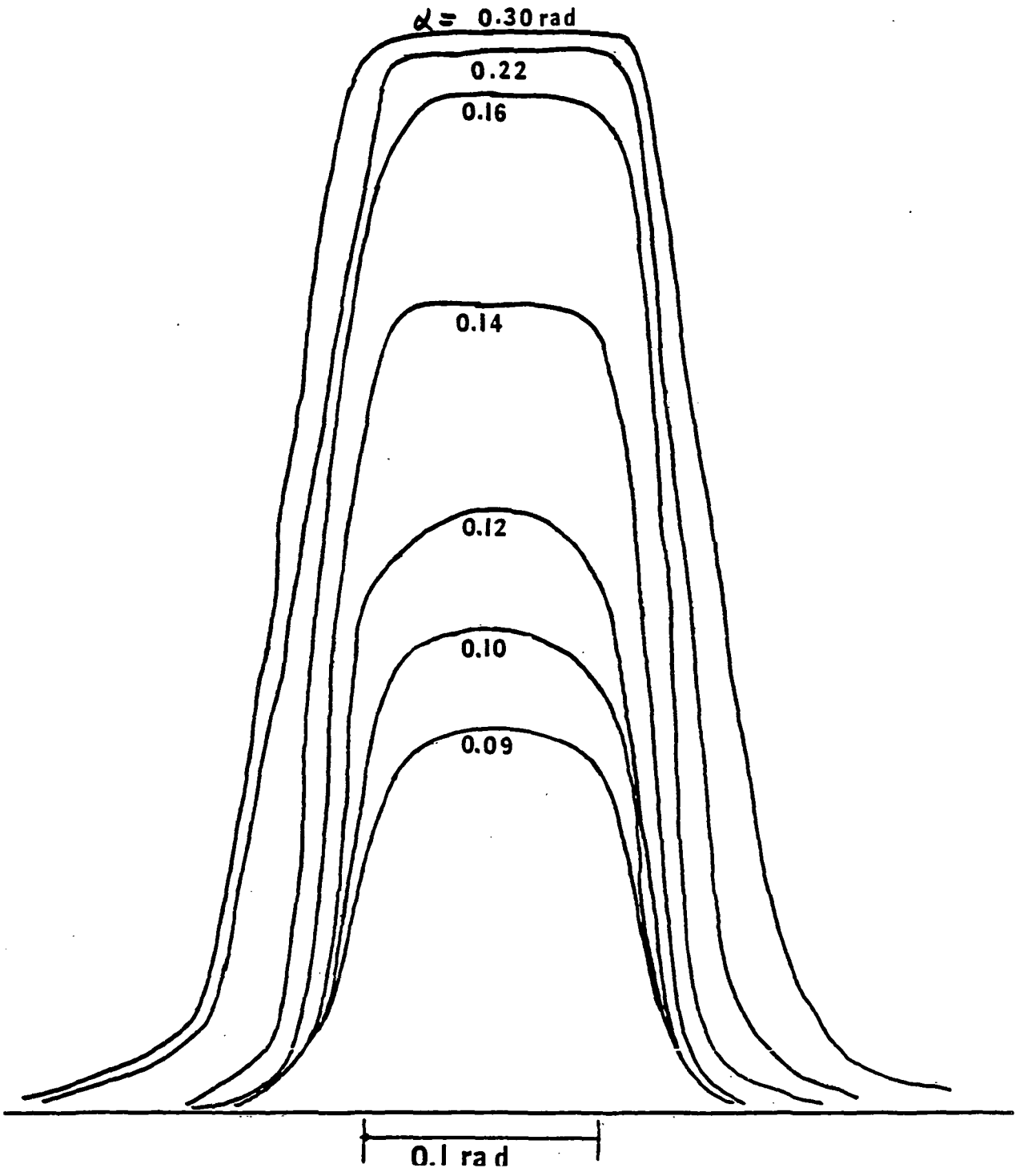

Figure 6.- Radial scans on film exposed 50 mm away from fiber output (after densitometric correction) for different values of the input beam aperture α.

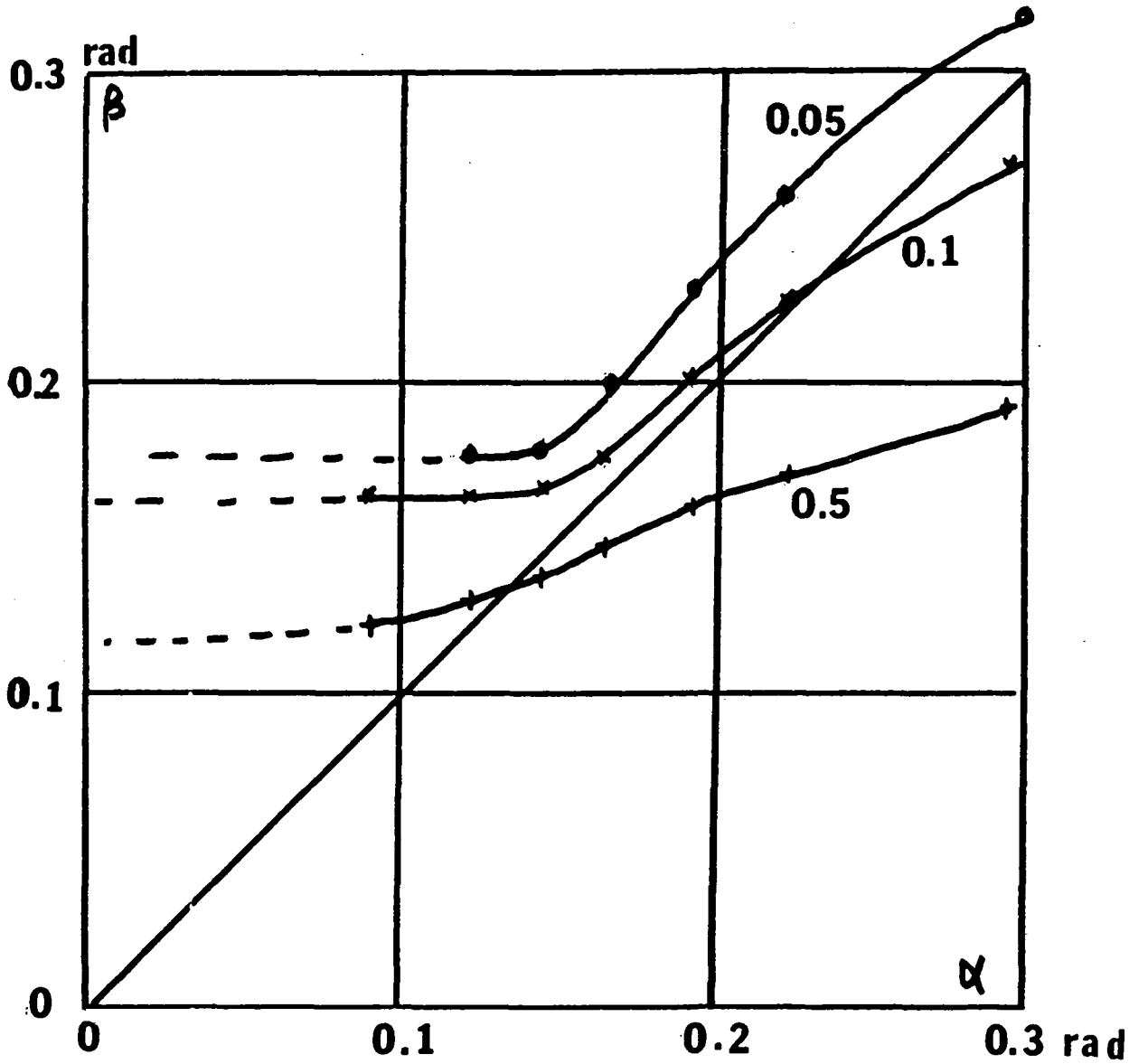

Figure 7.- Width of the patterns on figure 6 at the 50%, 10%, and 5% levels as functions of the input width α.

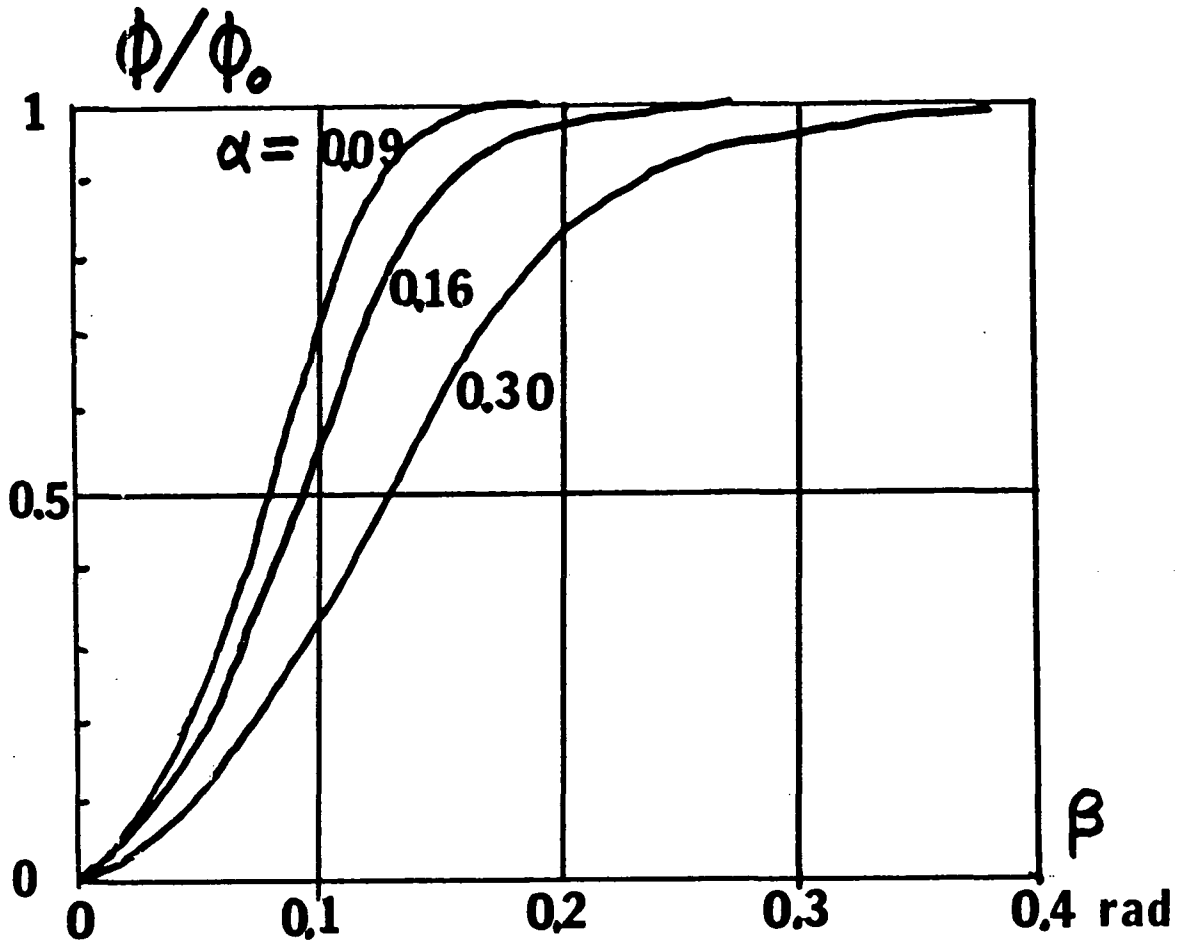

Figure 8.- Fraction of the energy available at the output within a cone of total aperture β for cones of different apertures α at the input.

150 μ fiber, 5 arc sec acceptance in sky) the telescope focal length is 6 m, the focal ratio f/6 or α = 0.16, in the range of our tests. One small fixed lens at input is adequate to adopt the focal ratio (if needed). Should we insist on $\beta = \alpha = 0.16$ efficiency is about 0.8 ; if one tolerates $\beta = 0.24 = 1.5\,\alpha$ (i.e. reduce the resolution by a factor 1.5) it goes up to 0.95.

Altogether the use of the fiber means for our problem :

1) perfect decoupling from seeing-guiding effects (global intensity effects i.e. pure scintillation being easy to take care of).

2) a slight loss of resolution compared to the worst seeing case.

3) a large one compared to optimum seeing.

On an exceptional night with S=1 arc sec we might have increased resolution by a factor of 5. How serious this loss is will be dealt with in the next paragraph.

A non essential -but nevertheless important- point in favor of using a fiber will be the ability to work with any telescope directly from the prime focus even with a large cumbersome spectrometer such as the one proposed here. Light transmission by the fiber is likely to be better than the one of the 3 or 4 additional reflexions for a regular coudé. Then many small telescopes without a coudé are made available. Lastly should a dedicated telescope be built for the project it might be of a very simple type : a low accuracy ($\simeq$2 arc sec images) primary parabolic mirror plus a very light frame supporting the fiber at the focus. Actually fibers have already been proposed by Angel (17) for a large multimirror telescope ; use of the fiber as a scrambler was not considered but the figures quoted for transmission and beam spread are in general agreement with ours.

b) Image slicer

Image slicers improve matching of the telescope to a slit spectrocope, hence improve resolution particularly under poor seeing conditions. Two main types have been described ; the one by Bowen (18) uses two plane mirrors (with only two additional reflexions), but implies some defocussing which increases with the image order number. The Richardson slicer (19) is free from this problem and produces an infinite number of images but their illumination decreases due to multiple reflexions. A slicer derived from the Bowen type has been incorporated by Walraven into a correlation spectrometer (20).

From a fundamental viewpoint very high resolution is not needed in our case ; the SNR increases merely in proportion to the absorption depth in the recorded spectrum. This varies very little if the instrumental line width is less than, say, half of the stellar line width. Actual resolving power in the Griffin (11) and CORAVEL (12) instruments is of the order of 20.000. The photon noise limitation will be very little reduced by increasing this figure. However we have noted that with a 9 cm echelle and a 1 m telescope CORAVEL has only a 1 arc sec entrance slit. If we take 5 arc sec as desirable a 45 cm echelle would be needed without an image slicer. Then our fiber does produce an additional loss in resolution. Lastly it seems likely some of the internal causes of systematic wavenumber errors in the spectrometer will be reduced by increasing resolution.

Altogether the use of an image slicer, while not as fundamental here has the one of the scrambler, is nevertheless desirable. It would be placed at the output of the fiber, hence benefit from spatially stable illumination. There is no reason to believe existing types would be unsuitable. Nevertheless one may speculate on other ones.

First we should note that so far fibers are not suitable. Consider the 150μ fiber discussed above. In principle one might increase the telescope focal length to blow up the linear size of seeing disk to several times 150μ and let it fall on a tightly packed circular array of similar fibers, the outputs of which would be aligned in a single row. Hence the spectrometer slit width would be 150μ irrespective of telescope output. However the divergence of the beam entering the spectrometer could not fall below 0.12 rad for collecting 90 % of energy ; hence the linear etendue in the plane of dispersion could not be less than 18 μ x rad, barely less than the telescope output. Appreciable gain would be realized only for either a) a much larger telescope or b) a requirement that a larger sky patch than 5 arc sec should be transmitted. In our case we would need fibers giving a beam distinctly less than 18μ x rad at the output i.e. either a) smaller diameter ones with the same spread or b) equal diameter but more perfect ones. In both cases the requirement on minimum radius of curvature might become stiffer ; also cladding thickness should be small compared with fiber diameter to make the input array feasible.

We next propose a new type of image slicer which might prove superior to old ones ; no attempt at construction has been made so far. On fig. 9, E represents the stellar seeing disk (or the image of a planet, or the output end of a fiber), B1 the center of a primary telescope mirror image M1 (which might be produced by a field lens close to A). Let us first suppose we put in plane Y, B, Z, a concave spherical mirror of radius R=AB1, slightly off axis. An equal diameter image of E is formed centered at A. We put a similar mirror in plane Y2 A,Zz ; again an equal diameter image M' of M1, is formed centered at B'1. Altogether the set of two mirrors constitute a Z shaped afocal system with magnification -1. Spherical aberration and coma are zero ; there is a slight astigmation that can easily be neglected. Let be the diameter of E and D the one of M1. The linear etendue of the beam is the same in the horizontal and vertical directions ; we have $Uh = Uv = Dd/R$ while the etendue is $U = (\pi\, Dd/4R)^2$

Let us now cut the first mirror in N horizontal slices, each of height D/N (3 are represented on fig. 9) and twist them around B1 Z1. If N is (this is not a requirement) the middle one with center at B1 does not move ; the upper and lower ones turn in opposite directions. The angles of rotation are just large enough to produce a row of identical circular images centered at A1, A2, A3 .... ; the tilt of each mirror relative to the two adjacent ones is d/2R.

Next we cut the second mirror into N vertical slices corresponding to the N images and similarly twist them around A1 Y2 ... in order to bring points B'2 B'3 ... (images of B1 B2 ... on M1) into coïncidence with B'1. We note each slice of the second mirror sees only one from the first mirror ; the total number of superimposed strips at B'1 is N. The output beam now fits within a rectangle (height d, width Nd) in plane Z2 A2 Y2 and a second one (height D/N, width D) in the output plane. Horizontal and vertical etendues

are $U'h = Nd \times D/R = NU$ and $U'v = \dfrac{d \times D/N}{R} = Uh/N.$

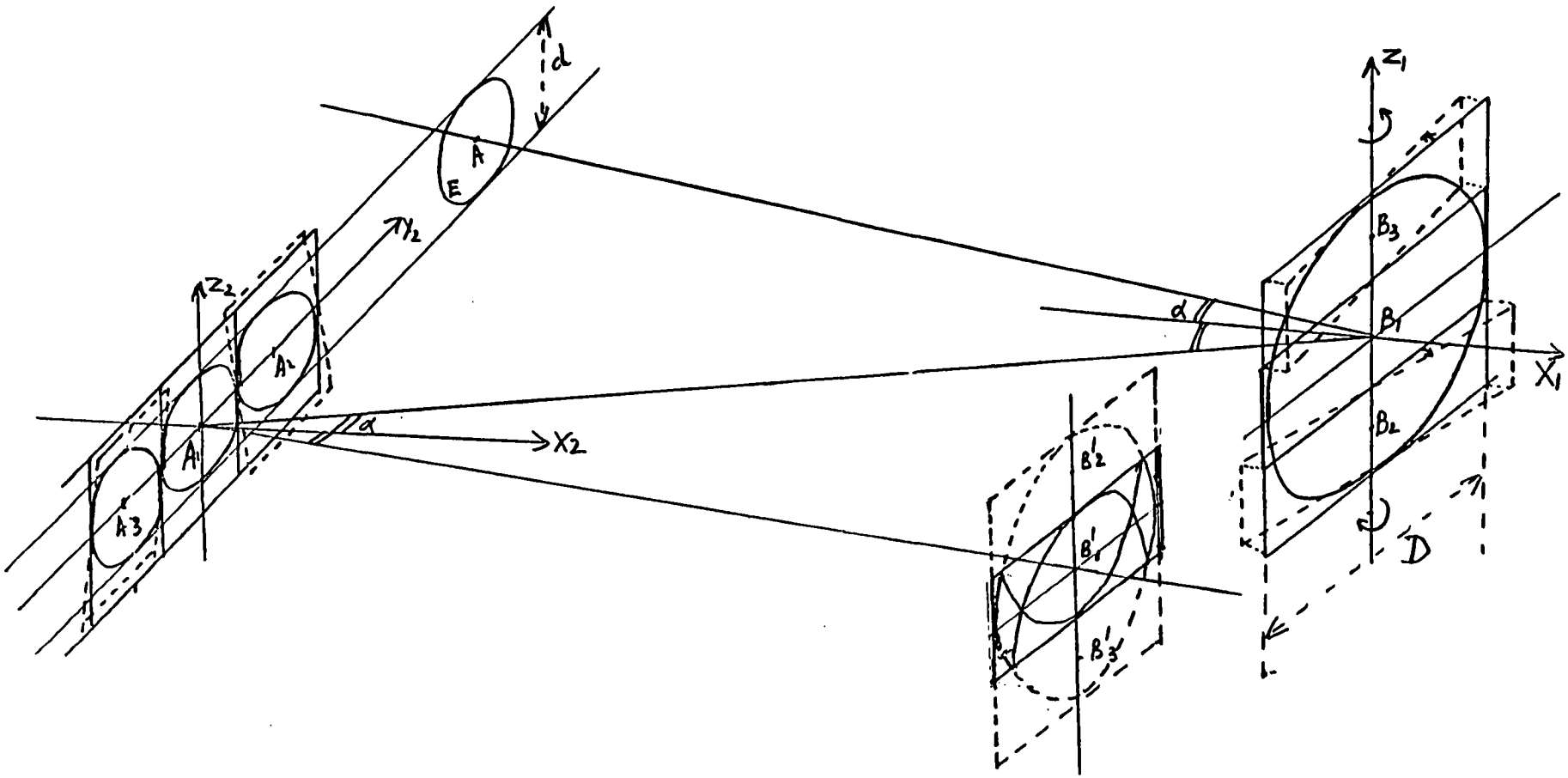

Figure 9.- Image slicer (with only 3 slices, i.e., N = 3).

While at the input Uh/Uv=1, at the output U'h/U'v = N^2. The overall etendue, defined by the two rectangles, is U' = U'h U'v = (16/ ^{2})U ; thus it is slightly increased (as it should be of course) but this is irrelevant. What counts is the change in shape of the beam which makes it suitable for a slit spectrometer.

The beam in a spectrometer is limited by one long rectangle (the slit) and one pupil which does not differ greatly from a circle or a square (the grating, or prism, or lens). Here we have two rectangles ; some further adaptation is needed. But the operation is now a classical anamorphosis which may be done with a pair of cylindrical mirrors or lenses (actually acceptable approximation could be done here with just one small lens). The anarmophosis ratio is again N ; at the output we shall have further stretched the first rectangle (the row of stellar images) into the horizontal direction by a factor of N i.e. width/height is now N^2 ; it will fit on the slit. Simultaneously -and unavoidably- the second rectangle is compressed horizontally also by N and becomes a square so fits on the grating.

A more detailed study is unnecessary here ; one possible solution is presented in Chapter V. The system does not appear particularly difficult to make with a factor N of the order of 10 or 20 and involves only two reflexions, plus one or two thin lenses. It might prove cumbersome to insert within existing systems because of size but this is not a factor here.

Altogether we think the scrambler plus slicer practically cancel the advantages of F.P. or Fourier spectrometers for this particular problem. They might even be considered specific ; they will provide neither the very high resolution, nor the extra large acceptance angle of interferometers which would be required for extended sources. But for moderate resolution stellar spectrography with extreme wavenumber stability as main requirement they should enable grating to do just as well.

2) Linearity problems -

In his first paper Fellgett (10) noted the difficulty : the multislit mask matches the spectrum perfectly at zero Doppler shift only : a mismatch proportional to the shift and roughly to the spectral range width does appear. He indicated this might be corrected by moving two elements e.g. rotating the grating and moving the mask. (In the same paper he also mentions the possibility of "scrambling" the light). This has been done so far only by Walraven (20) who uses mechanically linked translations of entrance slit and mask. However actual performance is not described, and the system is not needed for the rather small spectral range so far used (300 A°or one echelle order). Other experimenters move one element only : Griffin (11) moves the mask, restricts the range to 560 A° , and tolerates a maximum mismatch (at the extremities of the range) which is 1/8 of the shift itself ; for a star on the ecliptic it reaches 4 K m/s even for zero heliocentric velocity.

In the CORAVEL (12) the entrance slit is moved, which is somewhat better. Also with an echelle and cross dispersion one easily shows for a given Doppler shift the line images displacement is the same in the center of each order ; one merely has to contend with a residual effect within orders. Thus while the spectral range is 3 times larger, the mismatch is nevertheless reduced by a factor of 10 to 0.012, i.e. about 400 m/s again from just the Earth's velocity.

Even in this last case the mismatch is still enormous by our standards. However the situation is not hopeless, since it is nevertheless small compared to the actual stellar line widths (at least 10 km/s). Under these conditions one shows there is no loss of SNR since all portions of the mask perform correctly. If a) mask illumination and transmission were stable (they do not have to be uniform) b) spectral composition of the light at the input and instrumental response, particularly of the P.M., was also stable, then a stable radial velocity would be produced ; it would be an average weighted in some way from all masks portions but this would not reduce the accuracy with which small variations in velocity could be followed. Thus there is no first order effect from the mismatch but there might be second or higher order effects proportional to both the mismatch and to variations in factors a) and b). Again the use of a fiber decouples mask illumination from seeing-guiding effects ; but there might still be internal ones in the spectrometer or image slicer. Then light composition changes with atmospheric transmission. Atmospheric dispersion plus guiding errors at the fiber input might also introduce a similar effect ; it should be compensated for instance with a small variable angle prism (i.e. chromatic lens off axis). Slow drifts in overall spectral transmission of the whole system should be checked periodically by illuminating the input with a standard white light source (whithout absorption lines) and measuring the PM response from different portions of the mask. From such data and a known mismatch, the velocity correction may be computed.

Nevertheless it is best to reduce the mismatch to start with. We have considered three techniques : pressure scanning . Doppler normal dispersers and the Fellgett-Walraven synchronized motions system.

a) Pressure scanning

At first glance the solution appears perfect and eliminates all moving parts. A 1 atmosphere pressure variation produces an apparent wavenumber shift of 3.10^{-4}, equivalent to 90 km/s, adequate to cover the majority of stars even with the $\pm$ 30 km/s telluric shift. Air index (rather than pressure) should be measured with adequate accuracy with a long path interferometric refractrometer within the spectrometer itself ; for instance, with a 20 m path (easily folded) and λ = 6438 A° light one would get 1 fringe for 9 m/s of radial velocity. An additional attractive feature is the possibility of using a F.P. etalon in the stellar beam itself to produce a reference ; portions of the mask would carry slits matched to the F.P. channeled spectrum.

If the F.P. is also within the spectrometer enclosure the fringes in the spectrum will stay matched to the mask at all pressures irrespective of geometrical effects i.e. actual optical system, grating dispersion etc... This means grating spectrometer stability would be permanently checked. For all other systems one has to check the zero first, in a separate operation then move something to compensate radial velocity and make the stellar measurement ; hence one relies on mechanical stability in between.

There are two problems. The first comes from air dispersion -and is not improved by considering other gases. Again a perfect match is realized only at one wevelength which may be arbitrarily selected. For the 3600 - 5200 A^{o} range we find the maximum mismatch will be 1 % of the shift, roughly the same as with CORAVEL ; and since this result is independent of geometry it cannot be improved by any tricks.

The second one is temperature changes. For rapid (near adiabatic) preassure changes air temperature will change simultaneously ; for a 10 km/s shift in spectrometer adjustment we find a 13^{o} effect. This is enormous ; equilibrium will only be slowly restored byconvection and even then some temperature perturbation of optical or mechanical components is to be expected. The process may be accelerated with a fan ; nevertheless it is highly disquieting. We might re-introduce in this way some seeing noise, on a scale of seconds or minutes, within the spectrometer. Observations could be planned to avoid important velocity changes i.e. one would on a given night observe only stars with geocentric radial velocities within a few km/s of each other. But the problem is not solved : some kind of velocity modulation has to be introduced in the spectrometer with an amplitude of the order of the line width i.e. 10 km/s to pinpoint the maximum of the correlation function, and this cannot be made very slow ; it probably would have to be made by mechanical-geometrical means and air pressure scanning loses much of its attractive simplicity.

Nevertheless there might be one way out. So farmasks are opaque except for transparent slits with widths comparable to the line half width. If we had two masks, one directing the light from the right hand half of the lines to one PM and the second from the left half to another one no modulation would be needed at least within the spectrometer and efficiency would be doubled. Such double masks might be fabricated with photoresists, or perhaps by pressing the edge of a heated prism against a plexiglass surface (fig. 10).

We conclude that if a radial velocity spectrometer is built within an atmospheric pressure resistant tank -which may be desirable anyway- then pressure scanning might easily be tried, but it seems unrealistic to rely on it at this stage.

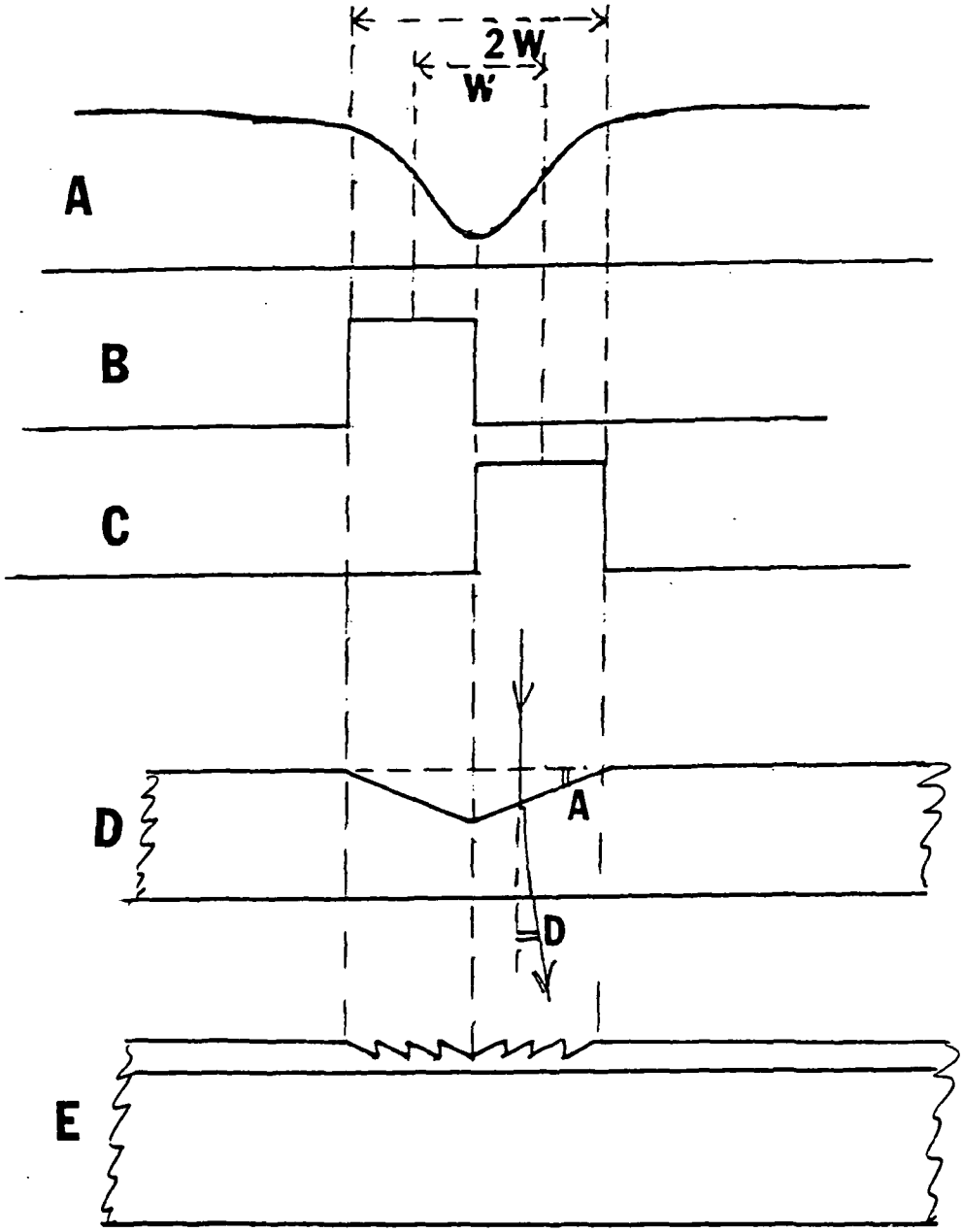

Figure 10.- Proposal for a transparent mask. A: stellar line profile of half-width w. B and C: one wants to send half of the line to two different outputs. D: transparent refracting mask in which double-prism shaped depressions have been impressed; the rays are deviated by D = (n-1)A. E: Fresnel lens type equivalent of the mask above; the microprisms, of perhaps a few microns thickness, are impressed in a photoresist. Construction is simpler and involves only proven techniques, but efficiency would probably be somewhat lower.

b) Doppler normal dispersers

Two types of dispersion laws commonly considered are the wavelength - normal one, well approximated by gratings under near perpendicular emergence conditions and the wavenumber - normal : prisms used far from absorption bands i.e. in low dispersion region.

We introduce the concept of Doppler-normal dispersion : the shape of the spectrum is such that it translates as a whole whithout distortion for small radial velocity variations of the source. Then there will be no mismatch between the spectrum and a rigid mask. One easily shows this is achieved for a logarithmic dispersion law (fig. 11).

While no perfect solution exists it nevertheless seems possible to realize a good approximation by combining gratings and prisms. Let us first consider an ideal case with constant index (zero material dispersion) prisms. The grating provides all the dispersion and the prism acts merely as an anamorphoser.

Fig. 12 shows the general appearance of residual mismatch (expressed as a fraction of the Doppler shift itself). With no refraction (grating alone) the mismatch is represented by a sloping curve. With one refraction one has one degree of freedom and eliminates the first order term. (This would mean using the grating in immersion, which has actually been done and has the advantage of increasing theoretical resolving power (21) . With two refractions (i.e. non immersed prism) one cancels the second order. For instance take a 63°, 73 grooves/m echelle in Littrow mount. The free spectral range is 411 cm^{-1} and high orders are used (k = 30 at 8109 A° , k = 45 at 5406 A° , k = 60 at 4054 A°). With a n = 1.5 and a 60° prism we have a residual mismatch -in any order- of a few times 10^{-4}. Unfortunately actual materials have dispersion, which degrades the results. There are two cases ; in non Littrow spectrometers the anamorphosing prism is placed after the grating, hence is not traversed by incident light ; angle of incidence on grating is constant (independant of wavenumber). In Littrow types it is traversed twice and we have both variable incidence on the grating and variation in anamorphosis with wavenumber. The difficulties are more severe and absorption losses are doubled. However Littrow-spectrometers appear better on two counts. First high incidence echelles show rapidly degrading efficiency with increasing angles of deviation between incident and diffracted rays. Second the parameters of a Littrow are easier to check with the extreme accuracy that will be needed in our case to keep the dispersion law stable.

We have made a detailed search for solutions in both cases, which cannot be given here. Even with the lowest dispersion materials available for large prisms (SiO_2,CaF_2 ,H_2O) the mismatch is too large (fig. 13). Compound prisms were considered next ; we associate a high dispersion small angle prism with a low dispersion large angle one ; they can be either in optical contact or separate. The solution for minimal mismatch within a given spectralrange is not the same as the minimum deviation one for the same range.

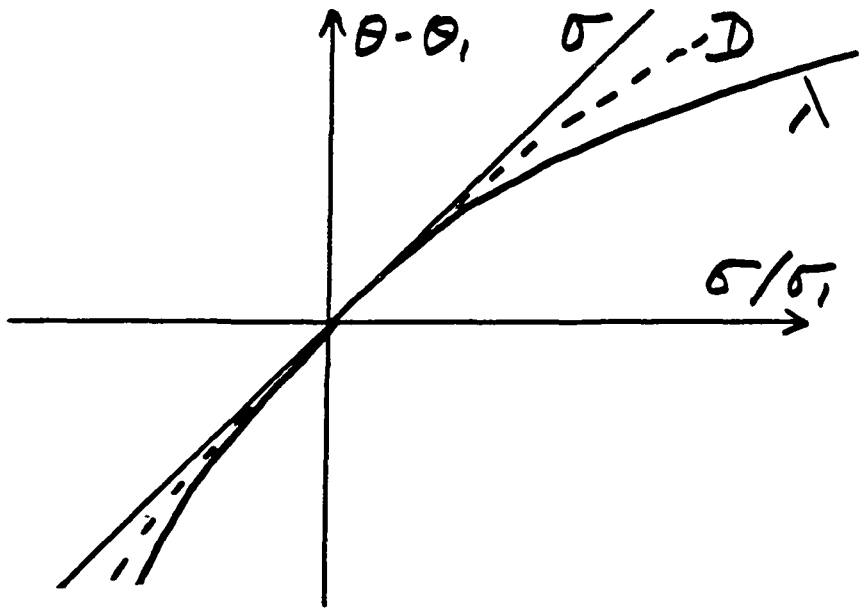

Figure 11.- Three different types of dispersion curves $\theta-\theta_1$ as a function of wavenumber. σ is a wavenumber-normal (straight line), λ, a wavelength-normal (hyperbola), and D, a Doppler-normal (logarithmic). If a wavelength scale is used instead, σ and λ are interchanged but D stays the same.

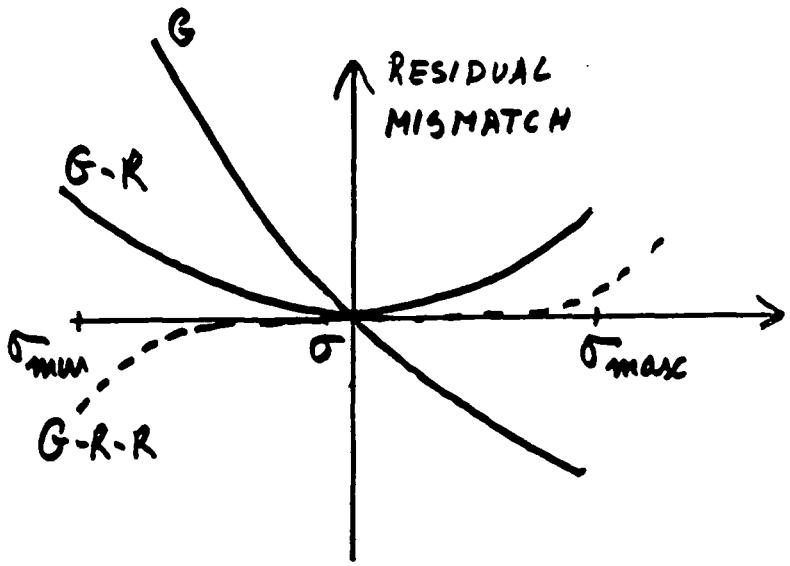

Figure 12.- General appearance of residual mismatch between spectrum and mask. With a grating alone, the mismatch is zero at one selected line σ_1 and the variation approximately linear (G). By adding one suitably oriented refracting surface, one may get G-R and with two surfaces, G-R-R.

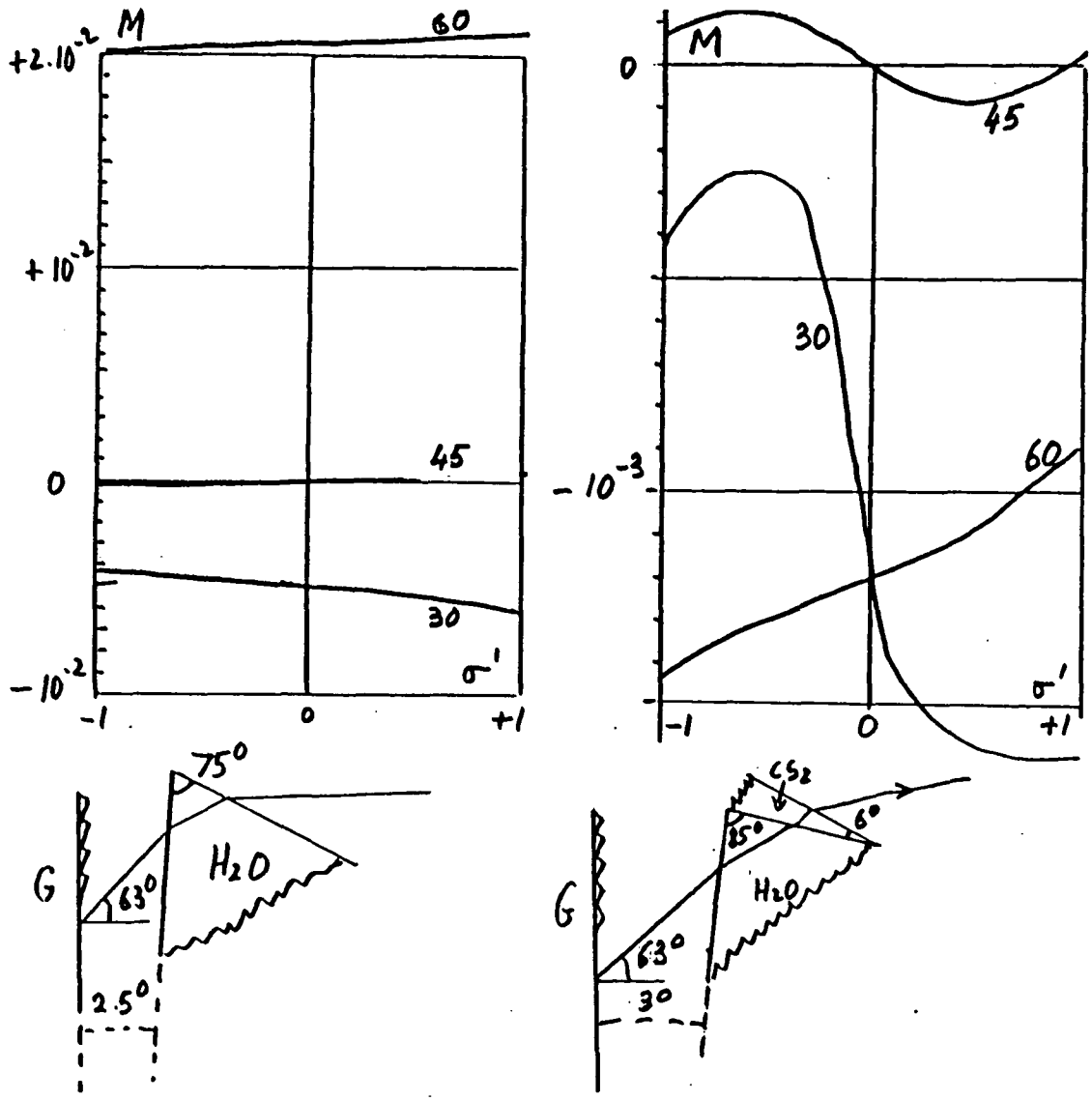

Figure 13.- Residual relative mismatch (i.e., relative radial velocity difference for different mask portions) as a function of reduce wavenumber $\sigma' = 2(\theta-\theta_1)/\Sigma$ where Σ is the free echelle spectral range. One has $\sigma' = 0$ at the center of each echelle order and ± 1 at the extremities. Results are plotted for orders 30, 45, and 60 of our 63°, 73 grooves per mm echelle with 411 cm^{-1} free spectral range. The single pass non-Littrow case is illustrated; actually, the prism would have to be quite far from the echelle. Left - H_2O prism; Right - compound H_2O-CS_2 prism. Water absorption would be quite acceptable down to 3500 Å, but the one of carbon disulfide is not.

For large echelles the thickness of low resolution material becomes too large unless one takes for the smaller prism high dispersio· liquids like CS_2 or ethylcinnamate ; an example is shown in fig. 13. In principle this is quite practical ; we have had excellent experience with a 60° angle, 30 cm base thickness ethylcinnamate prism (built by A. Couder) which did show the theoretical resolving power, of the order of 250 000 in the blue, in Littrow mount. However the absorption becomes unacceptably large in the near UV. These solutions are no good for solar type stars- i.e. the most interesting ones -since one could not match the 3600 - 5200 A° range of CORAVEL. For cool stars and a range of perhaps 5000 - 9000 A° (and Ga - As detectors) theybecome reasonable, particularly for a non Littrow spectrograph.

c) Compensator system

The main point in favor of Doppler-normal dispersers is simplicity of operation, merely one translation (of the mask) being needed. The rest of the system is passive. The Fellgett-Walraven solution requires two motions and accurate synchronization. We propose here a compensator system which needs only one but, unlike b) involves no additional thick absorbing elements. We note actual translation of the entrance slit seems easy when the output end of a fiber is used as spectrometer input ; however the presence of the image slicer complicates things. Rotation of the grating with the degree of accuracy required here, is difficult. With a long focal length, high f number spectrograph it is better to use relatively large translation of compensating elements in the vicinity of slit or mask. With a Littrow system these are rather close together and it is feasible to translate just one small platform carrying elements which simultaneously move the images of the slit and of the mask as seen by the grating. For a 63° echelle in Littrow mount the motion of the slit has to be 8 times greater than the one of the mask, and in the opposite direction ; residual mismatch is presented in fig. 13. For our proposed 6 m focal length spectrometer and a maximum ± 60 km/s radial velocity, we need ± 0.6 mm (apparent) motion for the mask and ± 5 mm for the slit.

Fig. 14 presents two solutions. The first involves two large plane mirrors M2 M'2 in front of the mask forming a low angle wedge, and two small ones M1, M'1 in front of the slit, all four of them on a single carriage with longitudinal translation T. Magnitude of translation would be a few cm and may be selected by adjusting the mirror angles. Two small additional fixed plane mirrors M3 M4 are needed . These can be total reflexion prisms and M1 M'1 was replaced by one small prism P with two total reflexions. The main difficulty is high sensitivity to rotations in the figureplane ; this would have to be checked permanently. Compensation for rotation appears cumbersome.

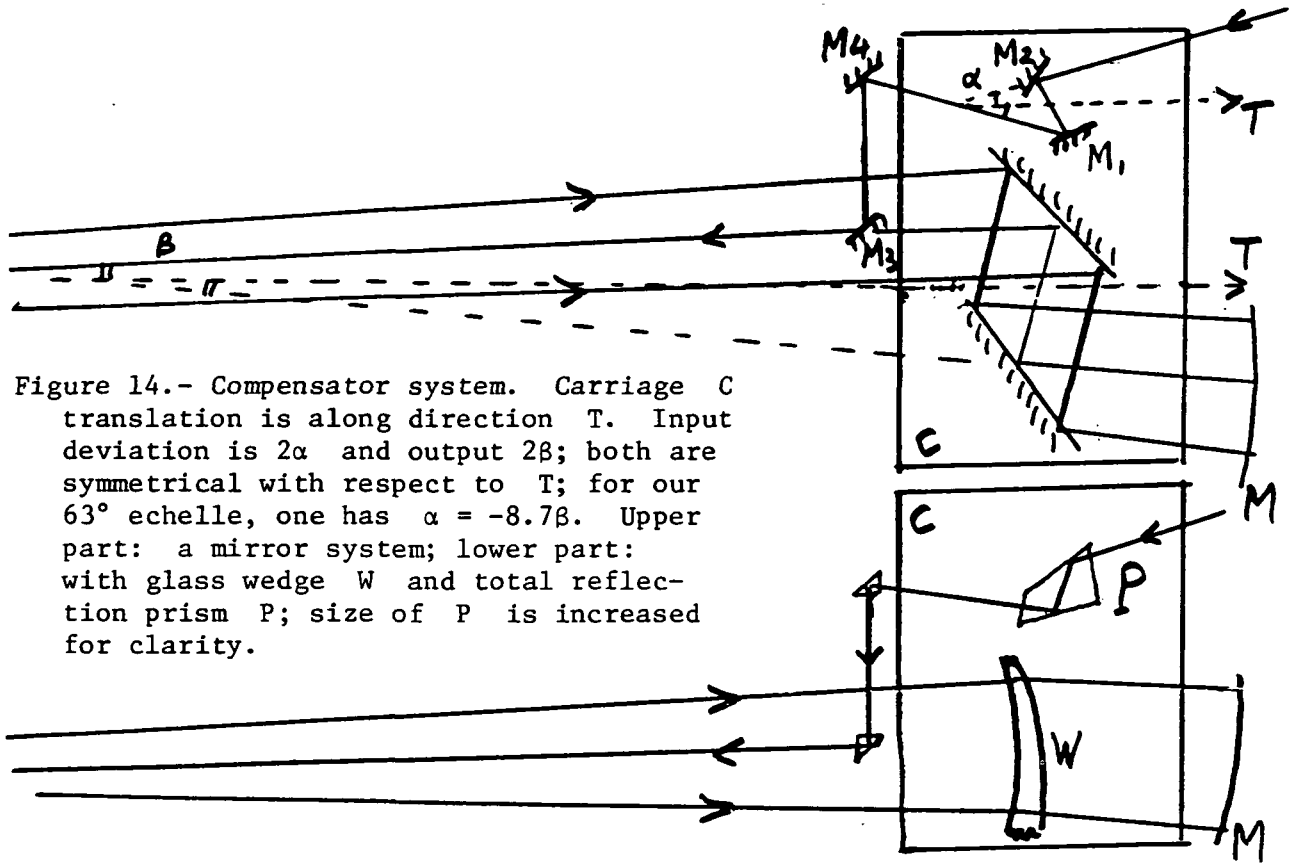

Figure 14.- Compensator system. Carriage C translation is along direction T. Input deviation is 2α and output 2β; both are symmetrical with respect to T; for our 63° echelle, one has $\alpha = -8.7\beta$. Upper part: a mirror system; lower part: with glass wedge W and total reflection prism P; size of P is increased for clarity.

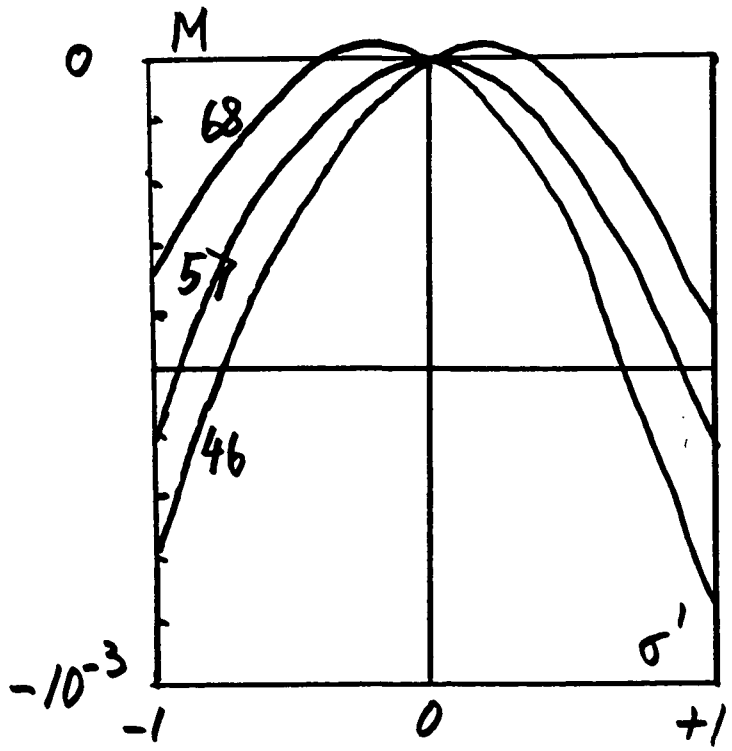

Figure 15.- Residual mismatch of figure 14 compensator (using BI664 crown glass). The three echelle orders indicated correspond approximately to the 3600-5200 Å CORAVEL range. All calculations are done in the principal plane; consideration of cross-dispersion and lens effects from the lens introduces other terms of comparable magnitude.

The other solution replaces the two large mirrors by a low angle wedge. Fused silica or crown glass being used, absorption is negligible. To minimize aberrations faces may be spherical with radius of curvature equal to spectrometer focal length. However some dispersion is re-introduced. The major effect (a small distortion of the spectrum) is irrelevant, since it is taken care of during mask construction while a first order mismatch also appears, rather like the one in fig. 12 but considerably smaller. However compensation is now easy. One may achromatize the wedge, which is feasible with standard materials. With the above parameters we have found at least one solution with a 18 mm maximum thickness of crown, and 12 mm of light flint (with good near UV transmission). Another solution is obtained if one introduces a small similar but opposite sense dispersion at the input, by either adding a small prism or (better) changing slightly one angle in P. Fig. 15 gives the computed mismatch and we now have a satisfactory solution - on paper.

However other factors have to be taken care of. One must consider the (necessary) cross dispersion, sagittal and tangential curvatures and lens chromatic aberration : the lens-disperser system has to be treated as a whole. This study has been undertaken with the help of Pencialelli at Institut d'Optique. Some preliminary results may be given : a light flint-calcium fluoride lens would be suitable to cover the CORAVEL range and we believe mismatch from all computed causes may be kept below 10^{-3}.

This means contributions from all mask portions changing differentially by less than ±30 m/s. Then with reasonable care in keeping or checking uniformity of illumination on mask etc... the final velocity (integrated over mask) might be stable to ±3 m/s.

3) Reference problems -

We are not interested in an absolute zero velocity reference since we search for fluctuations in radial velocities only, but we must incorporate the best possible local standards. These must be a) if not uniformly spread over the range, at least sufficiently numerous and scattered to check both translation and rotation of the (two dimensional) mask. b) sufficiently bright to make photon noise negligible i.e. a setting accuracy somewhat better than on the stellar spectrum must be realized in a time short compared to the observations, hopefully in a few seconds. c) have intrinsic stability of the order of 10^{-8} or better, or be easily checked with another source having that kind of stability. All possible solutions have been proposed, if not demonstrated in the past.

a) Absorption lines -

Telluric lines are not ideal because too few are suitable and they may well be affected by shifts of a few tens m/s. The use of an absorption cell in the beam, discussed by Griffin [22] seemed very attractive to reduce guiding-seeing errors ; however that was for spectrographs, and the method did not appear suitable with the radial velocity meter (11).

We present on fig.16 the situation that arises if the iodine spectrum - a good choice - is simply superimposed on the solar spectrum. If instrumental resolution is adequate to resolve fully the I_2 lines many of them shall be usable within the small microwindows between solar lines ; however the solar lines themselves become useless. A simple optical system like the one on fig.17 solves the problem ; the 'stellar' photomultiplier PMS observes stellar lines only -uncontaminated by I_2- while on the reference channel I_2 lines are used merely in selected regions where the stellar background is observable, i.e. they are only slightly contaminated by stellar lines. There are several difficulties. I_2 gives negligible absorption below 5000 A° so is inadequate for checking the CORAVEL range. With cool stars the background tends to disappear, and even with solar types it is more accessible at longer wavelengths. Other molecules might of course be used, in particular NO_2 (we have not been able so far to obtain a comparable resolution spectrum). So far it is not certain we might fully realize the desirable interlacing between the stellar and reference spectra. A very accurate reference at one side of the mask only would clearly be no good.

For optimum operation of a correlation spectrometer a modulation in velocity of the order of the line half width must be introduced. Since reference lines are much sharper than stellar ones, two different amplitudes are needed for zero checking (on I_2 lines) or when working on stars. This is not necessarily a drawback. However I_2 lines are well resolved only with a FTS, and even then are not fully symetrical because of hyperfine structure. With the resolution accessible to a large grating even with an image slicer, the situation will be rather worse because of blends ; then the correlation peak position becomes dependent on instrumental resolution and modulation amplitude, which is undesirable.

A F.P. etalon in the beam solves some of the problems and introduces others. Lines are in principale symetrical, uniformly spread and the width is adjustable at will. A confocal etalon is particularly suitable, because fringe position will be totally independant of small variations in beam shape or incidences. Of course long term stability should be checked with either standard Kr^{86} lines or stabilized lasers.

However, unlike absorption cells the etalon cannot be introduced after the mask because of beam spreading. Then it has to be located in front of entrance slit (unless compensating de-dispersion was added, which would be complex and wasteful of light). This means stellar lines are not accessible. The zero checking operation must be a separate one, with the white light source and the etalon taken off for the stellar observations. Then one important point in favor of absorption standards (elimination of small geometrical differences between stellar and reference beams) is lost. On the other hand a F.P. etalon seems ideal for preliminary checking of mask, spectrometer and scanning system actual performance.

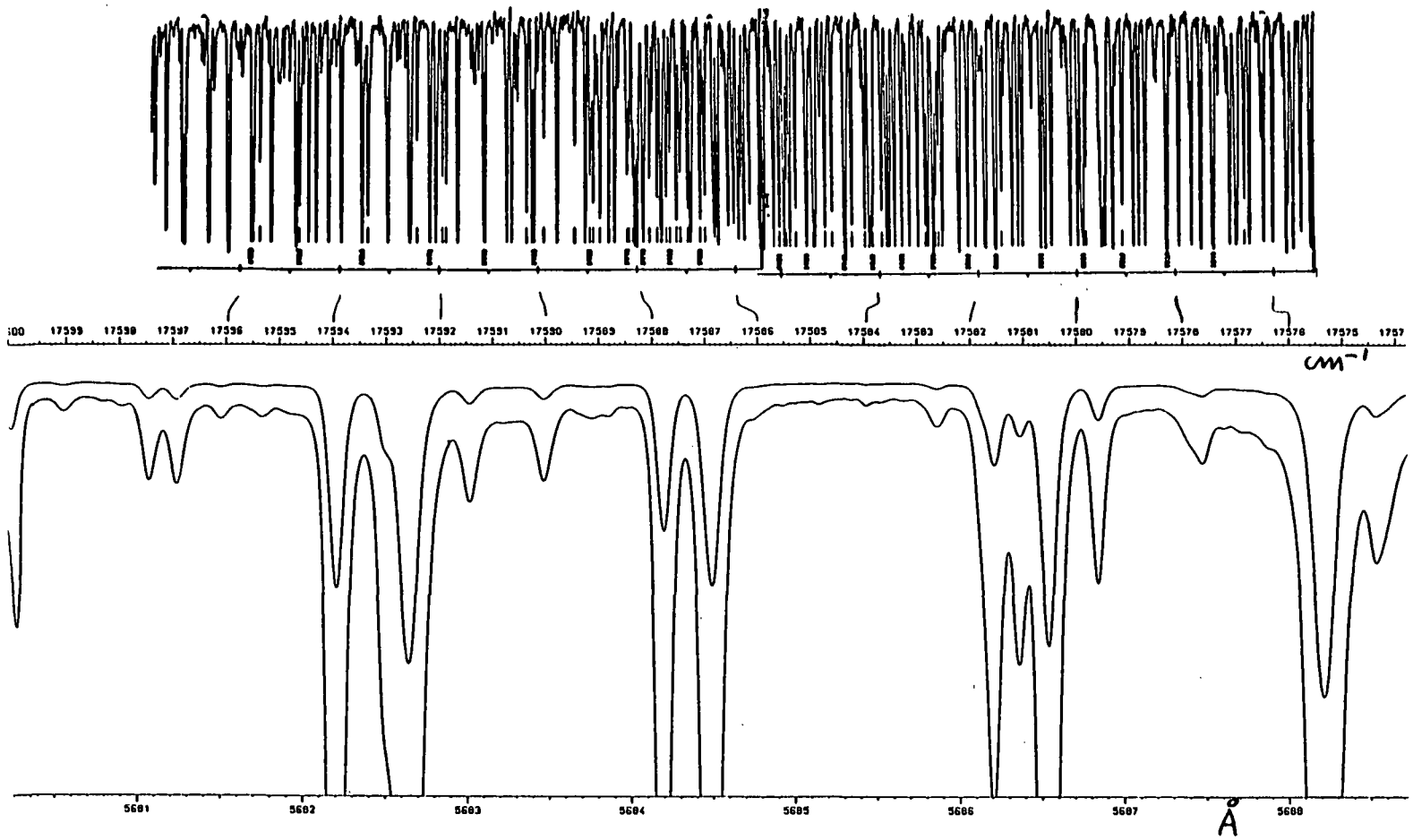

Figure 16.- Upper: Iodine absorption spectrum from a FTS (ref. 6) with enough resolution to show the line profiles, but plotted here on a totally inadequate scale. Lower: Solar spectrum from the Delbuille-Roland atlas. The scales are only approximately equal.

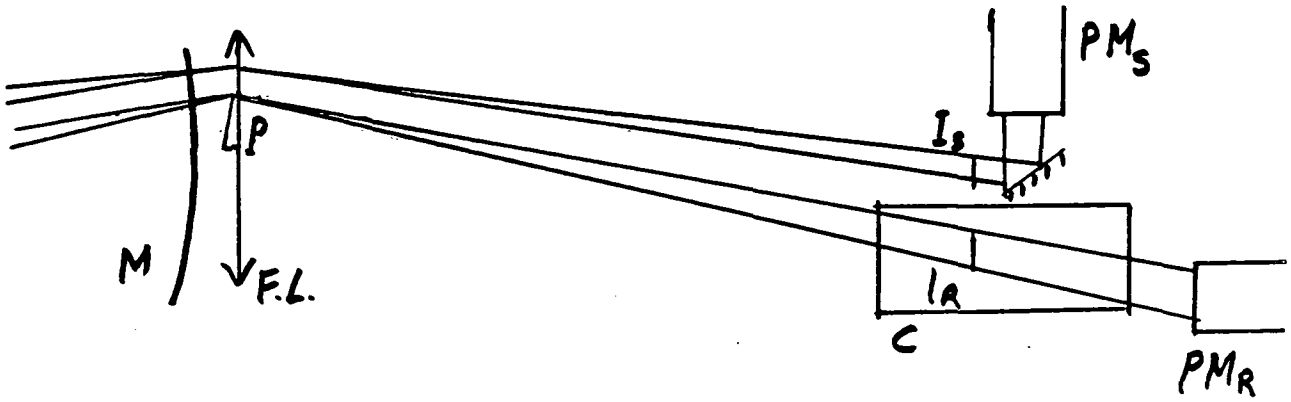

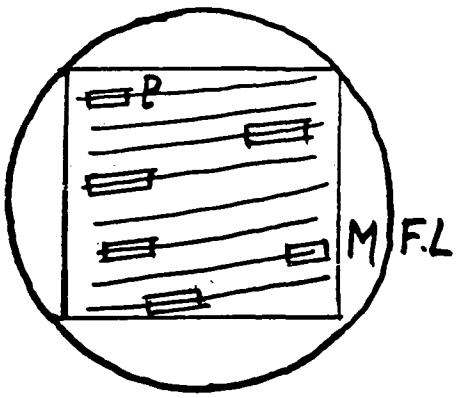

Figure 17.- Use of absorption lines as standards. Behind the square mask M, field lens FL produces an image of I_S of the grating on photomultiplier PM_S which looks at stellar lines only. Several small prisms P scattered behind M select low stellar absorption regions and send the corresponding light through an absorption cell C to PM_R; I_R is the second stellar grating image.

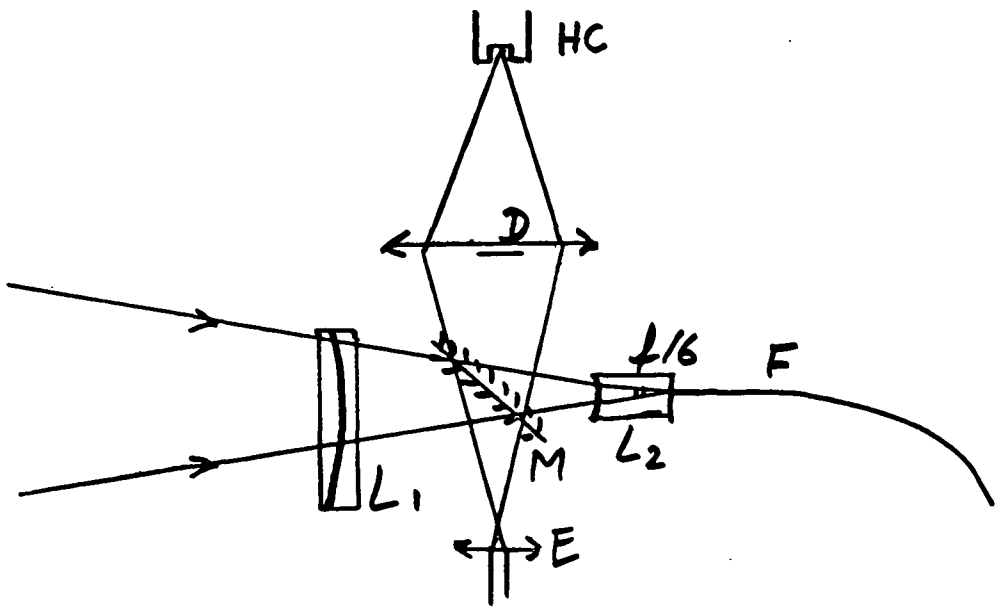

Figure 18.- Optical system at fiber input. E is a finding eyepiece; the guiding system is not represented. HC is the reference hollow cathode giving the Fe spectrum, D a central occulting disk.

b) Emission lines -

The technique is standard ; for instance the CORAVEL mask contains a set of slits for iron lines (from a hollow cathode) spread over the spectral range.

So far the velocity stability obtained in this way is poor, but our scrambler removes the main objection. If the hollow cathode light is fed to the fiber input as a cone of light simulating the one from the telescope mirror (and incorporating a central obstruction) all the geometrical difficulties disappear. Of course the hollow cathode may be located in the laboratory, and its output sent to the telescope through another fiber.

If a few additional slits corresponding to the Kr^{86} lines are available in the mask, the mean of the Fe lines may be checked -at infrequent intervals- in an absolute manner. Use of the Kr^{86} standard only is probably inadvisable : with too few lines one could not fully check all possible effects. A difficulty we should not minimize with the correlation spectrometer is the physical separation of spectral lines in the vicinity of the mask (while interformeters are free of this problem). The best we can do is to spread the reference points over the whole mask.

Altogether we hope Fe lines will prove adequate, while keeping open the use of an absorption spectrum. Also it is conceivable bright reference stars observed several times per night should finally prove even better-at the cost of course of a non negligible loss in observing time.

V - PROPOSED SPECTROMETER

1) Description

We describe here the general outlook of a version suitable for a 1 m telescope with either a prime, Newtonian or Cassegrain focus.

a) Fiber input. Fig. 18 presents the system. L_1 is a hyperchromatic lens with zero power in the center of the spectral range ; by moving it transversely one compensates for atmospheric dispersion. A thick fused silica lens L_2 (either converging or diverging) adapts the beam to f/6 ; the fiber input is cemented to the rear surface. Flipping mirror M is used on one side for finding the star, on the other for feeding light from the Fe hollow cathode. Guiding may be done in two ways. One may take the fraction of the light spilling over from the 5 arc sec region -possibly with other fibers. Alternately one might add a filter-beams plitter taking a fraction of the full beam from an unused spectral region, for instance the red with a solar type star.

b) Fiber and slicer. The output of the 150 μ fiber would be collected with about 95% efficiency within a $\beta = 0.18$ cone ; then $U_L = 28\ \mu \times \text{rad}$.

We propose to use an (available) échelle with $\beta = 63°$ and 208 x 102 mm size. Theoretical resolving power is 926 000 at 4000 Å. If no image slicer was used the actual resolving power computed from U_L would be merely 13 200. We propose a slicer with N = 15 ; thus we get R = 200 000. The velocity half width of the ILS is 1.5 km/s (5 times less than with CORAVEL) while the acceptance angle on sky would be 5 times more. All these choices are of course rather arbitrary.

The orders of magnitude for the N = 15 slicer are R = 1200 mm, D = 25 mm ; the slices would be approximately 1.5 mm wide on both mirrors. Two small spherical fused silica lenses (one in immersion) are needed for adaptation at fiber output. They magnify the end face 10 times to 1.5 mm, while reducing beam divergence by the same amount. One cylindrical lens is needed at spectrometer input ; no actual slit is required. Chromatic aberration from these lenses is negligible.

If we ask for stabilities of the order of 1.5 m/s with an ILS width of 1.5 km/s we need the photocenter at fiber end to remain stable within 1/1000 of the fiber diameter. We must admit our photographic tests do not reach that degre of accuracy. Should photoelectric ones reveal some residual shift from varying conditions at fiber input, we would simply add a rotating prism (after the magnifying lenses). It would induce no additional spreading and negligible losses. The requirement for the axis of rotation to remain stable within 1.5 mm/1000 = 1.5 μ (merely during the interval between zero check and stellar observations) does not seem severe. Overall spectrometer stability - even over a few minutes - should be a greater problem.

c) Spectrometer. This would be a Littrow type with f = 6 m, and a CaF_2 - lightflint nearly apochromatic lens - Pupil size is 102 x 94 mm (for $\beta = 63°$) and lens diameter 150 mm (corresponding to f/40. The square pupil is filled from the slicer output. Spherical aberration and coma are negligible and astigmatism irrelevant. Within the 0.05 x 0.05 rad field (300 x 300 mm mask) cylindrical curvature with about 1.6 m radius is needed to fit the tangential focal surface ; maximum flexure is 7 mm and poses no problems. In the plane perpendicular to dispersion residual chromatic aberration and sagittal curvature almost cancel.

Cross dispersion would be from either a fused silica or an (available) water prism with crown glass windows. In either case absorption is almost negligible down to 3600 Å. The angle would be of the order of 60°, and selected to fill approximately the square mask. Actual spectral range would be at least the CORAVEL 3600 - 5200 Å range (i.e. 8500 cm^{-1}, or 20 orders for the 73 grooves/mm, 411 cm^{-1} free spectral range echelle selected : other choices are possible). If lens performance proves adequate it might be extended towards the red.

The compensator system needs a 300 x 300 glass wedge but this is not a particularly high accuracy element. Maximum translation would be 100 mm and measured with a commercial moiré grating device giving 1 μ accuracy. Selecting the wedge angle to cover for instance a ± 75 km/s velocity range the error from the moiré reading is 1.5 m/s.

d) Mask. The selected size (300 x 300 mm) is the maximum one permissible with the Optronic digitizer-synthesizer available at CERN where the CORAVEL mask was made. To start with one would simply copy this mask with greatly increased size (the original one is 70 x 13 mm). Use of a low material dispersion prism means vertical dispersion is almost proportional to wavenumber. Hence the vertical order separation is nearly constant, which means optimum use of mask vertical dimension.

e) Measuring procedure. The carriage is servo controled from the moiré system digital output in the same marmer as our interferometer carriages for FTS (4). Normal procedure is a nearly square wave carriage oscillation with amplitude of the order of 15 km/s (i.e. 10 mm) on the stellar lines, or about 10 times less on the reference ones. Modulation frequency might be 2 to 5 Hz.

Mean carriage position is precomputed from previous observations of the same star ; the PM signal is demodulated and integrated for no more than a few minutes (on the equator we get about 2 m/s velocity change per minute). To take care of scintillation etc... the total stellar flux in the same range is measured simultaneously by a second PM, for instance from the grating zero order through a filter, and used to normalize results.

The small difference between anticipated and actual radial velocity gives rise to a slight unbalance from which the velocity error is computed. A small desk calculator with digital input should easily handle the calculations in real time.

2) Test program

Before spectrometer construction we need more and better tests on more fibers. From the results we will decide whether the image rotator is needed or not ; but no other impact on spectrometer design must be expected.

After spectrometer assembly the first mask should be made from an in situ photograph of a FP channeled spectrum. Then the mask errors, dispersion law errors and compensator errors can all be determined by pressure scanning the FP and looking for the correlation peak from either small mask portions or the entire mask.

The second mask would be derived from the CORAVEL one which was computed from the α Boo spectrum (but is perfectly suitable for the sun : Optimal work on much cooler stars will require a different mask, a different PM and possibly a different lens). Then extensive testing on the sun should be undertaken. Integrated solar light may be realized by producing a solar image smaller than 150 μ at the fiber input, or through other means. With a fast reflecting wheel at the input one may introduce at will velocities up to a few tens of m/s (we happen to have such a wheel, on loan from Dr Nieuwenhuijzen from Utrecht Observatory) ; of course the Earth rotation is also usable. With suitable attenuators the flux from any solar type star can be simulated.

In this way the sensitivity and long term stability of the system might be fully checked. One should try to accumulate at least a year's experience on the Sun, and might possibly detect integrated solar light phenomena. It would be desirable to make these tests near a solar maximum. One might also work on smaller plages and compare results with the standard techniques for detecting solar oscillations which do reach sensitivities of a few m/s.

The last remaining factor - linearity - may be fully tested only by going to a telescope. Neddless to say the first part of the program should be calibration and study of systematic errors on a few selected bright stars.

VI - CONCLUSION -

Experience with the development of FTS has given us the feeling that fundamental limits are finally reached in these kinds of problems - after much hard work. While the principle has been clearly formulated by Fellgett in 1950 it took about 15 years to produce stellar, planetary or for that matter laboratory spectra clearly better that existing ones. With the correlation spectrometer, also proposed by Fellgett (1955) we now have many excellent results and the method is gaining wide acceptance. However, so far, nobody has made a real push for low velocity errors. In view of the fundamental importance of extrasolar planetary detection, we believe an all out attempt should be made. Undoubtedly the solution is far simpler than any other of comparable efficiency based on interferometers, and while not competing with astrometric attempts it should provide quicker returns in the form of shorter periods binairies detection.

REFERENCES

1) Connes P. : - A Proposed Astrometric System for the measurement of parallaxes, and detection of dark companions (1977, unpublished).

- Opt. Tel. of the Future, Conf. Proceed, p. 351 (ESO - CERN, 1978).

- Eur. Conf. on Space Astrometry (Padova, 1978, in print).

- IAU Coll. 50 (Un. of Maryland, 1978, in print).

- IAU Coll. 48 (Vienna, 1978, in print).

- Should we go to Space for Parallaxes ? (To be published, 1978).

2) Duchesne, M., Guinot, B : C.R. Ac. Sc. 268B, 1594 (1969).

3) Connes P, Connes S., Kaplan L.P., Benedict W. : Ap. J. 152, 731 (1968).

4) Connes P., Michel G. : App. Opt. 14, 2067 (1975).

5) Connes P. et al. : Nouv. Rev. Opt. App. 1, 3 (1971).

6) Luc P., Gerstenkorn S. : - Nouv. Rev. Opt. App. 7, 149 (1976)
- App. Opt. 17, 1327 (1978)
- Atlas du Spectre d'Absorption de la molécule d'Iode (Ed. CNRS, 1977).

7) Bopp B., Edmonds F. : Pub. As. Soc. Poc. 82 (1970).

8) Guelachvili G. : Opt. Comm. 8, 171 (1973); App. Opt. 17, 1322 (1978).

9) Valentin A. : Thèse, University of Paris VI (1976).

10) Fellgett P. : Opt. Act. 2, 9 (1955).

11) Griffin R., Gunn S. : Ap. J. 191, 545 (1974).

12) - Baranne A., Mayor M., Poncet J. : CRAC Sc., 285B, 117 (1976).

Poncet J. Thèse, Université de Genève, 1978, (in print)

13) Serkowsky K. : Icarus 27, 13 (1976).

14) Griffin R. : Atlas of the Arcturus spectrum.

15) Edmonds F. et al. : Ap. J. Supp. 19, 1 (1969).

16) Connes P., Connes J. : JOSA, 56, 896 (1966).

17) Angel J. : Opt. Tel of the Future Conf. Proceed, p. 227 (ESO-CERN, 1978). Ap. J.,218,776, 1977)

18) Bowen I. : Ap. J. 81, 113 (1938).

19) Richardson E. : Aux. Inst. for Large Telescopes, Conf. Proceed., p. 275 (ESO-CERN, 1972).

20) Walraven T.: Aux. Inst. for Large Telescopes, Conf. Proceed., p. 175 (ESO-CERN, 1972).

21) Hulthen E., Neuhaus H. : Arkiv fur Phys. 8, 343 (1954).

22) Griffin R. : MNRAS 162, 243 (1973).

23) Pinnow D. et al. : App. Phys. Lett. 22, 527 (1973).

PAPER 10

SITES FOR FUTURE DEDICATED TELESCOPES

M. F. Walker
Lick Observatory
University of California, Santa Cruz, California

It appears likely that, in order to conduct a proper search for planetary systems, special dedicated telescopes must eventually be constructed. To use these instruments at their greatest efficiency and to maximize their capability of detecting planetary systems, it is essential that they be located where the prevailing observing conditions do not degrade the performance of the systems. Even though the construction of these dedicated telescopes may be some time off, it is important to begin now to characterize and identify potential observing sites because:

(1) On-site tests may be required to ascertain the quality of a particular site, and the process of setting up and carrying out such a program is a lengthy one. On-site observations must cover *at least* a period of 1 yr to assess seasonal effects and *should* cover 2 yr to allow an assessment of the variability of conditions from one year to another.

(2) The number of promising locations is small and ever-decreasing because of increasing light and atmospheric pollution, environmental restrictions, and by other installations or activities.

Thus, an early decision on the site(s) to be acquired is needed to make possible the initiation of procedures to forestall site pollution and preemption and to allow time for the lengthy procedures now required by environmental legislation. That is, the preparation of an Environmental Import Report is required before any new site can be developed (within U.S. territories) (see, e.g., the Draft Environmental Impact Report on the Proposed Dark Sky Optical Observatory at Junipero Serra Peak, University of California, Santa Cruz, June 1977).

The site characteristics required by the various types of detection systems discussed at this workshop, as specified by the system proponents, are listed in table 1. This table indicates that the constraints on sites for the radial velocity instruments are not severe; instruments of this type can apparently be located at any reasonably good location, away from cities and their atmospheric pollution, that has a high percentage of clear (though not necessarily "photometric") weather. For the astrometric detectors, conditions are much more restrictive. Here, except for speckle interferometry, the best possible seeing is required and a dark sky is essential for the photoelectric scanning and imaging systems. All systems require minimum cloud cover, although only photoelectric imaging requires photometric transparency. Most of the astrometric systems appear to require low to moderate wind velocities, and it seems desirable to avoid nighttime temperatures below perhaps -15° to

-20° F to minimize mechanical problems. In no case do these systems require a high altitude. Thus, sites should be at as low an altitude as possible consistent with the other required characteristics to avoid the problems associated with high-altitude locations, that is, observer acclimatization and working efficiency, low temperatures, high wind velocities, and snow accumulation.

Generally speaking, regions with minimum cloud cover can be identified from the Global Atlas of Relative Cloud Cover 1967-70. These are shown in figure 1 where the unshaded areas have no more than 0-2 Octas of cloud cover at least half of the year. The figure shows that there are two zones of minimum cloud cover, extending from about +10° to +35° to 40° N latitude and -10° to -35° to -40° S latitude. Thus, in general, sites should be chosen between these latitude limits, but since considerable variations in the latitude extent of the cloudy regions occur, this cannot be taken as a general rule, and the location of each proposed site must be carefully compared with the map. Additionally, sites should be restricted to latitudes less than ±40° (indicated by the dashed lines in figure 1) to avoid the very short nights near the summer solstice.

The largest body of data on the seeing at different sites as measured on a uniform system is that which has resulted from the Polar star trail measurements on the Lick system (Harlan and Walker, 1965; Walker, 1970; Walker, 1971; McInnes and Walker, 1974; and McInnes and Walker (unpublished data)). The sites investigated by this method are listed in table 2, and the percentages of nights with different qualities of seeing are shown in table 3. This material suggests that, while reasonably good seeing conditions can be found on interior mountain peaks, the very best locations occur on islands or on peaks along the coasts of continents where one has maritime tropical stable air masses. The eastern edges of these air masses are associated with cold ocean currents and are characterized by subsidence of the air mass and a low inversion layer so that stable laminar air flow is encountered at moderate altitude.

The observations also show that the effects of local topography are extremely important, as in the case of Izaña Tenerife (McInnes and Walker, 1974) and Fogo (McInnes and Walker (unpublished data)), so that, to assure the quality of a site, seeing measurements at the site must be made.

Of those sites so far tested on the Lick system, the best are the island and coastal sites, Fuente Nueva, Encumeada Alta, Junipero Serra, Cerro Tololo, and Mauna Kea. These sites typically have average nightly seeing of $\leq 1''.0$ on 21 to 35% of the nights, compared to about 15% for the interior sites at Kitt Peak and San Pedro Martin, and 19% for the high-altitude site at White Mountain.

As indicated above, in addition to seeing, the percentage of clear hours and the wind velocity must be considered. The yearly averages of these quantities for the sites with better seeing are listed in table 4, which shows the percentage of photometric hours (defined as hours with zero cloud cover above 10° to 15° altitude, depending on the site) and spectroscopic hours (defined as hours with $\leq 60\%$ cloud cover above the same altitude limit) and the percentage of nights on which the wind velocity was constantly ≥ 25 mph during the entire night. Combining the data in tables 3 and 4, we find Encumeada Alta

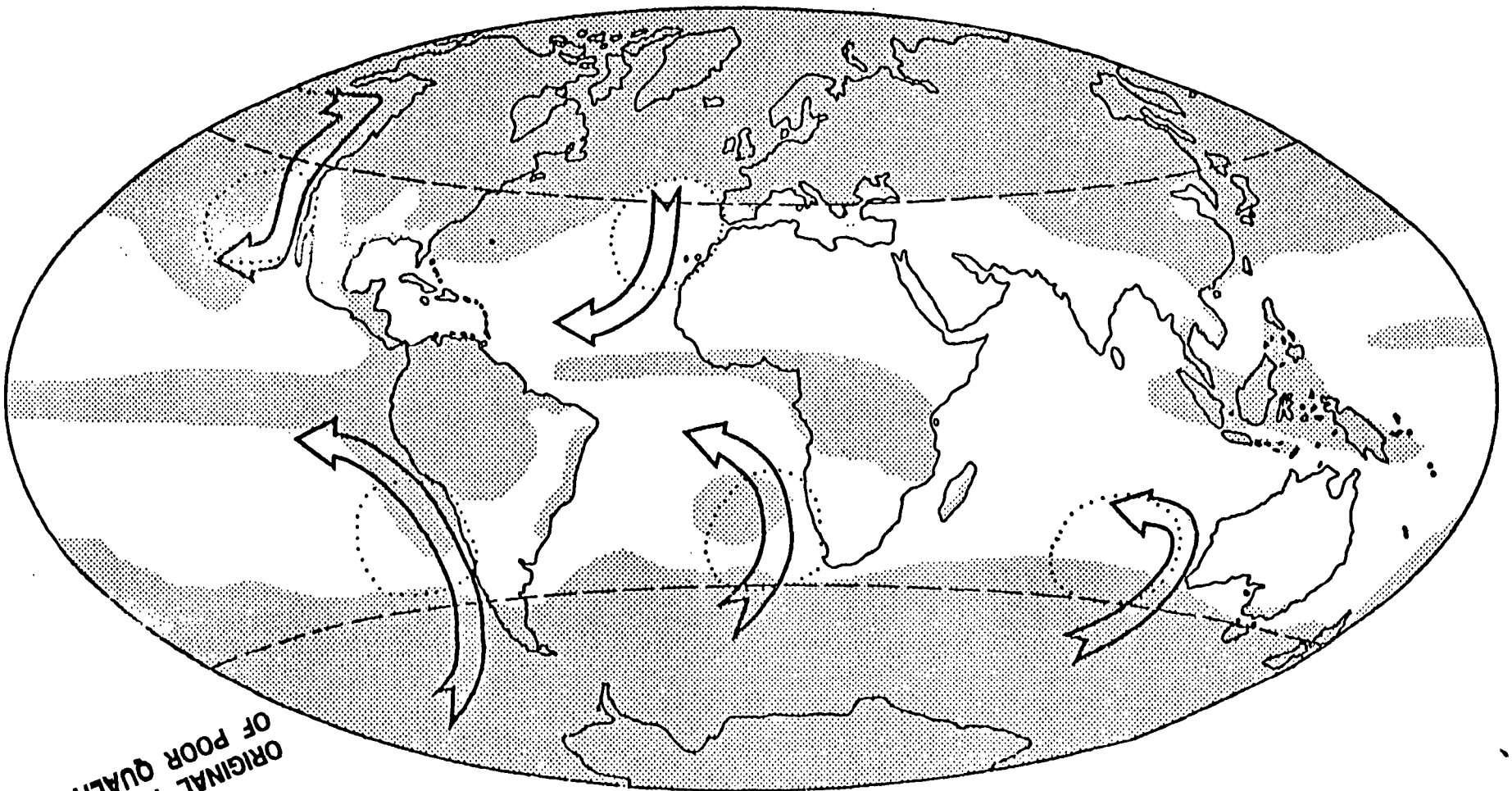

Figure 1.- Regions with minimum cloud cover (unshaded areas).

has the best seeing (in the sense of the highest percentage of observed nights with $\leq 1''.0$) the percentage of photometric nights with $\leq 1''.0$ seeing is nearly the same (15 and 17%, respectively) at Encumeada Alta and Fuente Nueva, and is only slightly lower (12%) for Junipero Serra and Mauna Kea. These yearly summaries average out the seasonal variations in seeing and cloud cover.

Minimum nighttime temperatures at these sites range down (in winter months) to: Encumeada Alta, -2° C; Fuente Nueva, -4° C; Junipero Serra, -9° C; Mauna Kea, -9° C; White Mountain, -20° C; Tololo, -1° C. To summarize, the available seeing and weather data for those sites observed on a uniform system suggest that the best locations we are presently aware of are Encumeada Alta, Fuente Nueva, Junipero Serra, Mauna Kea, and Tololo — these locations should be considered first.

The present status of these sites is as follows:

(1) Encumeada Alta, Madeira — This site is owned by Portugal and is presently undeveloped. It appears likely that the Portuguese would be cooperative if this site were selected.

(2) Fuente Nueva, La Palma — This site was chosen by the British for their Northern Hemisphere Observatory on the basis of their site survey which included also Izaña, Encumeada Alta, Fogo, and Mauna Kea. Fuente Nueva has the best combination of seeing and cloud cover, and the wind velocities, although slightly higher, would not be a problem. The site is being developed by a consortium of European nations in collaboration with the Spanish authorities and an international observatory will soon be completed there, somewhat like the European Southern Observatory in Chile, although the Spanish authorities and astronomers will play a decisive role in its operations, in contrast to the arrangements in Chile. It seems certain that permission would be granted to install U.S. instruments at this site; space would not be a problem. It would, however, probably be necessary to grant some fraction of the observing time to the Spanish astronomers.

(3) Junipero Serra Peak — The Lick Observatory is presently attempting to acquire this site as a new dark-sky station to overcome the increasing light-pollution at Mt. Hamilton. An Environmental Impact Report has been prepared, but permission to use the site has not yet been obtained. The main issue yet to be resolved is the interest of the local Indian community in this peak as a former Indian religious site. To meet environmental objections by the Sierra Club, the Observatory has agreed to limit the scope of the installation at the site to two 60- to 100-in. class telescopes on the summit and the Carnegie 20-in. double astrograph and a 24-in. reflector on a lower ridge. Thus, even with successful completion of negotiations for the site, it appears there is not sufficient space available for the type of dedicated telescopes considered here. This site is therefore not feasible.

(4) Mauna Kea — As indicated earlier, the dedicated instruments considered here need not be located at high altitude. Thus, Mauna Kea is to some degree unsuitable because of its high altitude and resulting problems of

observer acclimation and efficiency. Further, the seeing observations reported here refer to the summit of the cinder cone where the University of Hawaii's 88-in. reflector is located. Essentially all the space on this ridge has now been used or committed. However, observations on the lower ridge to the north, where the National Infrared Telescope is being installed, indicate that the seeing is as good or better than on the summit.

In addition, there is considerable doubt whether environmental approval can be obtained to install additional instruments on the tops of the cinder cones where the present or planned telescopes are located, or on the tops of other adjacent cinder cones. Ample space is available below the cinder cones on the summit of the shield volcano on which these cones sit. However, we do not have adequate information regarding seeing on the shield volcano plateau. It is possible that conditions may be poorer there, at least with some wind directions, because of shadowing by the higher cinder cones. Also, the fact that the summit of the shield volcano is nearly flat and is very irregular in surface may cause local seeing problems because air cooled by contact with the surface collects in pools and is then picked up and blown over the observing site by gusts of wind.

On the other hand, if seeing conditions are good on the shield, then any number of telescopes or long-baseline interferometers could be installed, and could be kept out of sight of residents living elsewhere on the island, thereby meeting one objection to the present installations on the cinder cones — their high visibility from locations such as Hilo.

Thus, if Mauna Kea is to be considered as a site, seeing tests on the shield volcano are mandatory. Such a program should be carried out in any case since the data presented here suggest such island sites have the best conditions, and this is the only such site (and particularly the only high-altitude site) in the U.S., and thus represents a limited and nonrenewable national resource that should be carefully managed and conserved.

(5) Tololo — The seeing observations refer to the summit where the present telescopes are located (except the Lowell 24-in.). If additional instruments are built, they would have to be placed on a lower ridge or on Cerro Morado. These areas have not been tested by the polar star trail method, and it is uncertain how good the seeing conditions are there. In particular, Morado is downwind from Tololo and, when the cloud level is at the proper height, one can see that the Tololo peak divides the air flow into two streams, one on either side of Tololo, that reconverge just in front of Morado. Morado presents a long sheer face toward this air flow so that the recombined stream, which has by now acquired some turbulence, is forced up and over the cliff face and then flows rather turbulently across the Morado plateau. Thus, it is likely that the seeing there will not be as good as on Tololo. Seeing tests *at the desired location* are mandatory before dedicated telescopes can be installed at this site.

Finally, the amount of good seeing obtained at White Mountain suggests that if an island or coastal site cannot be used, an inland site with 15 to

19% of the nights with average seeing $\leq 1''.0$ may be found. The exact percentage probably depends on the shape of the peak, the altitude of the peak, and the location of the peak in relation to other mountains and the direction of the prevailing wind.

If an inland site is to be considered, a testing program should be set up to determine whether a location more favorable than Kitt Peak or White Mountain can be located; the number of inland sites tested by the trail method is as yet too small to permit us to determine how favorable a combination of altitude, seeing, wind velocity, and cloud cover might be found.

Clearly, whatever choice is made, considerable work is required, including a program of site testing unless one goes to Encumeada Alta or Fuente Nueva. Thus, it is important to begin work on the site problem immediately, without waiting for the development and funding of the instruments themselves.

REFERENCES

Harlan, E. A.; and Walker, M. F.: Publications of the Astronomical Soc. of the Pacific, vol. 77, 1965, p. 246.

McInnes, B.; and Walker, M. F.: Publications of the Astronomical Soc. of the Pacific, vol. 86, 1974, p. 529.

Walker, M. F.: Publications of the Astronomical Soc. of the Pacific, vol. 82, 1970, p. 672.

Walker, M. F.: Publications of the Astronomical Soc. of the Pacific, vol. 83, 1971, p. 401.

TABLE 1.- SITE REQUIREMENTS

System	Seeing	Transparency	Sky brightness	Cloud cover	Wind velocity	Temperature	Humidity	Others
Radial velocity								
1. Fabry-Perot spectrometer	Reasonably good	Clear, non-photometric	---	Minimum cloud	---	---	---	---
2. Correlation-type grating spectrometer	Not important	Clear, non-photometric	Not important	Minimum cloud	---	---	---	---
Astrometry								
1. Photoelectric scanning refractor	Important Image ≤1".5 Motion ≤2".0	Clear, non-photometric	Dark sky needed	Minimum cloud	≤25 mph	>-15° F	---	---
2. Connes-type system	Important, also small image motion	Clear, non-photometric	Dark sky needed	Minimum cloud	≤40-50 mph	---	---	---
3. Photoelectric imaging (CCD)	Important	Clear, photometric	Dark sky needed	---	---	---	Low humidity desirable	---
4. Long baseline 2-color interferometer	Very important	Moderately important	Not important	Minimum cloud	≤10 mph	Not very important	---	Need enough area for 50-m baseline in 2 orthogonal directions
5. Spectral interferometer	Not important if ≤6"	Clear, non-photometric	Not important	Need constant conditions during ~5 min intervals	Need ≤6" telescope motion	---	---	---

TABLE 2.- SITES AT WHICH POLAR STAR TRAIL SEEING MEASUREMENTS HAVE BEEN MADE

Location	Altitude, ft (m)	Coordinates	
		Longitude	Latitude
Island and coastal sites			
Fuente Nueva La Palma, Canary Islands	7762 (2366)	17° 52!1 W	28° 45!2 N
Encumeada Alta Madeira	5853 (1784)	16° 56' W	32° 46' N
Junipero Serra California	5862 (1787)	121° 25!1 W	36° 08!7 N
Cerro Tololo Chile	7871 (2399)	70° 49!2 W	30° 10!2 S
Mauna Kea Hawaii	13796 (4205)	155° 28' W	19° 49' N
Izaña Tenerife Canary Islands	7844 (2391)	16° 30' W	28° 18' N
Monte Liso, Fogo Cape Verde Islands	8858 (2700)	24° 25' W	14° 50' N
Inland sites			
Barcroft Peak White Mountain, California	13040 (3975)	118° 15' W	37° 34' N
Kitt Peak Arizona	6772 (2064)	111° 35!7 W	31° 57!5 N
San Pedro Martir Baja California	9252 (2826)	115° 27' W	31° 03' N
Piper Mountain California	7703 (2348)	117° 57' W	37° 27' N
Mt. McKinley Australia	3442 (1049)	139° 06' E	30° 31' S
Flagstaff Arizona	7579 (2310)	111° 44!4 W	35° 11!0 N

TABLE 3.- COMPARISON OF POLAR STAR TRAIL SEEING AT VARIOUS SITES

Location	Percentage of nights with indicated average seeing in seconds of arc				No. of months observed	Interval	No. nights w/observations	Remarks
	≤1.0	1.1-1.5	1.6-2.0	>2.0				
Island and Coastal Sites								
Fuente Nueva La Palma, Canary Islands	26	26	15	33	12	12/74-11/75	245	
Encumeada Alta, Madeira	25 36	29 24	15 7	32 32	11 12	1/74-11/74 5/74-6/75	167 176	Top mount north slope
Junipero Serra California	26	38	13	23	26	8/65-9/67	558	
Cerro Tololo, Chile	24	32	22	22	23	10/68-8/70	509	
Mauna Kea, Hawaii	21	29	19	30	12	2/74-1/75	217	88" ridge except 6/74 & 7/74= North cone
Izaña Tenerife Canary Islands	13	33	18	35	20	1/72-11/72; 1/75-9/75	367	
Monte Liso, Fogo Cape Verde Islands	0	19	12	69	1.6	5/28/73-7/18/73	16	
Inland Sites								
Barcroft Peak White Mountain, California	19	30	8	44	10	11/16/78-8/31/78	115	Summit mount only
Kitt Peak Arizona	15	30	16	39	29	6/68-10/70	253	
San Pedro Martir Baja California	15	25	17	42	4	4/70-7/70	52	
Piper Mountain, California	9	30	20	42	8		164	
Mt. McKinley Australia	2	32	20	46	4	4/66-9/66	50	
Flagstaff Arizona	1	5	29	65	6	12/66-10/68	80	Observed in: 12/66, 1/67, 5/67, 6/67, 9/68, 10/68

TABLE 4.- AVERAGES OVER THE ENTIRE YEAR OF CLOUD COVER AND WIND VELOCITY

Location	Hours		Nights with wind velocity constantly >0.25 mph, %	Interval covered
	Photometric, %	Spectroscopic, %		
Encumeada Alta	41.8	53.9	1.3	Jan-Dec 74
Fuente Nueva	65.5	81.0	16.9	Jan-Nov 75
Junipero Serra	47.5	72.9	5.8	Oct 65-Sep 67
Mauna Kea	55.8	74.9	11.3	Feb-Dec 74
Izaña	65.3	78.6	12.6	Jan-Nov 72
White Mountain	Incomplete		19.9	Jan-Aug 78